UNIVERSITÀ
DEGLI STUDI
DI PADOVA

Sede Amministrativa: Università degli Studi di Padova

Dipartimento di Fisica e Astronomia "Galileo Galilei"

SCUOLA DI DOTTORATO DI RICERCA IN FISICA
CICLO XXX

Observables from inflation: gravitational waves and magnetic fields

Tesi redatta con il contributo finanziario di Fondazione Cariparo

Coordinatore: Ch.mo Prof. Gianguido Dall'Agata

Supervisore: Ch.mo Prof. Nicola Bartolo

Co-Supervisore: Ch.mo Prof. Sabino Matarrese

Dottorando: Maria Chiara Guzzetti

To my dear friends Stefano, Paolo, Davide A. and Davide M.

"... ma nondimeno il non potere essere soddisfatto da alcuna cosa terrena, né, per dir così, dalla terra intera; considerare l'ampiezza inestimabile dello spazio, il numero e la mole maravigliosa dei mondi, e trovare che tutto è poco e piccino alla capacità dell'animo proprio; immaginarsi il numero dei mondi infinito, e l'universo infinito, e sentire che l'animo e il desiderio nostro sarebbe ancora più grande che sì fatto universo;"

Giacomo Leopardi, Pensieri LXVIII

Abstract

The inflationary paradigm represents a fascinating and elegant way of explaining crucial cosmological phenomena; moreover it is remarkably in agreement with current cosmological observations. However we are still blind to many aspects of the physics encoded in such a process and an unequivocal probe of such a mechanism is still lacking. On the other hand inflation suggests the solution to current open cosmological questions, as the observation of magnetic fields in the intergalactic medium.

In order to investigate in depth the inflationary mechanism, one possibility is offered by the new era of gravitational wave detectors. In the first part of the thesis we focus on this aspect of the inflationary epoch.
Any inflationary model predicts the production of a stochastic gravitational wave background (tensor modes) due to quantum fluctuations of the gravitational field. Moreover, in some scenarios, the presence of additional fields besides the inflaton and the gravitational field gives rise to efficient sources of gravitational waves, activating the so-called classical production. Inflationary gravitational wave signals turn out to represent a unique and exciting window on the origin and evolution of the universe, and a possibility of investigating the underlying theory of gravity.
We point out the significant role of primordial gravitational waves in testing the inflationary mechanism itself and in constraining many aspects of the inflationary physics, exploiting the validity/violation of an inflationary consistency relation.
Being inflationary gravitational waves a promising way of exploring many aspects of the physics of the early universe, we provide an updated picture of the current status and the observational prospects of inflationary tensor modes, with a particular focus on the possibility of a direct gravitational wave detection offered by current and upcoming laser interferometer detectors.
Then we perform a dedicated forecast analysis of the capabilities of the LISA (Laser Interferometer Space Antenna) experiment in probing the inflationary physics. In particular, the capabilities of LISA in measuring a stochastic gravitational wave background are presented. Furthermore, we calculate the gravitational wave signal expected at the LISA frequencies for a number of selected inflationary models. We collect and re-elaborate current limits on the present time gravitational wave spectral energy density, and the sensitivity curves of LISA and other experiments, in order to outline current and expected constraints on the parameter space of the selected inflationary models. The results we find show the efficiency of the method, suggesting an exciting direction in order to investigate inflationary physics and a validation of the significant science

that can be done by an experiment as LISA.

In the second part of the thesis another interesting aspect of the inflationary mechanism is considered, i.e. the possibility of a significant magnetogenesis. Gamma-ray observations from blazars point out the presence of magnetic fields in the intergalactic medium, where no charged plasma are present. This fact suggests a primordial origin of such fields. Interestingly, the inflationary mechanism provides a fascinating way of explaining the presence of magnetic fields at cosmological scales. In a dedicated section, the main models of inflationary magnetogenesis are outlined. A common aspect of these models is the associated overproduction of curvature and tensor perturbations with respect to single-field slow-roll inflation. In general, observational constraints obtained by CMB measurements on such quantities lead to relevant restrictions on the associated production of magnetic fields. Other limits are provided by keeping under control the backreaction of the electromagnetic fields.
In particular, we consider the case proposed in [1], where a magnetogenesis mechanism able to explain current gamma-ray observations and to start the galactic dynamo takes place. We calculate the correction to the scalar spectrum and bispectrum (the latter related to primordial non-gaussianities) with respect to single-field slow-roll inflation generated in such a scenario. We find that the strongest constraints on the model originate from the non-observation of a scalar bispectrum of CMB anisotropies. Nevertheless, we found that even when those stringent constraints are taken into consideration, that scenario provides a robust explanation of the observed magnetic fields for a reasonably high energy scale of inflation.

List of Papers

- C. Caprini, M.C. Guzzetti, L. Sorbo, *Inflationary magnetogenesis with added helicity: constraints from non-gaussianities.*
  Submitted to *Classical and Quantum Gravity*
  Preprint: arXiv:1707.09750 [astro-ph.CO].

- N. Bartolo et al., *Science with space-based interferometer LISA. IV: Probing inflation with gravitational waves*, JCAP **1612**, 026 (2016).
  arXiv:1610.06481 [astro-ph.CO].
  DOI: 10.1088/1475-7516/2016/12/026.

- Prepared as invited review: M.C. Guzzetti, N. Bartolo, M. Liguori and S. Matarrese, *Gravitational waves form inflation*, Riv. Nuovo Cim. **39** (2016) no.9, 399-495.
  arXiv:1605.01615 [astro-ph.CO].
  DOI: 10.1393/ncr/i2016-10127-1.

Contents

Introduction

Over the last decades, huge steps towards understanding the physics of the early universe has been made, both from a theoretical and an observational point of view. Current cosmological observations are in remarkably agreement with the inflationary model for the early universe, as the results of the Plank mission show [2]. Moreover, the inflationary mechanism provides an explanation for several cosmological observations that we are not able to explain in other elegant ways, such as the presence of matter structures and anisotropies of the Cosmic Microwave Background (CMB). Up to now, inflationary scalar perturbations are well constrained by CMB measurements and provide impressive information about the physics of the early universe.
However, several questions about the physics of such a crucial period of the universe are still unsolved, e.g. did actually a primordial inflationary period take place? In case, which are the fields involved and at which energy scale? What is the theory of gravity underlying such a mechanism? Different ways can be carried out in order to address such questions. One possibility is the analysis of higher-order correlators besides the power spectrum, as a measurement of primordial non-gaussianity, another one is the investigation of the gravitational wave (GW) signal associated to the inflationary mechanism.

Interestingly, with the success of the GW detectors LIGO-Virgo [3], a new promising way of investigating the history of the universe has arisen. Indeed, several primordial processes are expected to generate a GW signal [4–6] which permeates the universe up to the present time, offering an exciting window on the origin and evolution of the universe. The inflationary mechanism predicts the production of a stochastic GW background as well. In such a direction, especially the project of the Laser Interferometer Space Antenna (LISA) [7] for GW detection, is expected to provide a new fascinating way of probing cosmology [8–10].
During inflation, the stretching of quantum fluctuations of the gravitational field generates a stochastic GW background [4] whose spectrum covers a wide range of frequencies, from $f \simeq 10^{-17}$Hz up to $f \simeq 10^{3}$Hz, while its amplitude depends on the energy scale of inflation. Any inflationary model predicts the generation of such a signal.
Interestingly, inflationary GWs permeate the whole universe propagating almost freely from their generation up to the present time, thus representing an exciting and unexplored window on the origin and evolution of the universe.
In light of the massive importance of searching for primordial GWs, in this thesis we overview in details the production processes of gravitational radiation during inflation,

especially taking into account for the new era of direct GW detection opened by laser interferometer experiments. In particular we investigate the capabilities of the space-borne laser interferometer LISA [7] as a fascinating way of probing inflationary physics.

On the other hand, besides providing an elegant solution for the main issue of standard cosmology, the inflationary paradigm offers an explanation for some cosmological observations whose origin is still under debate.
Gamma-ray measurements from blazars [11–13] point out the presence of non-vanishing magnetic fields in the intergalactic medium, where processes of magnetogenesis are difficult to be implemented. Moreover, current observations provide a measurement of the magnetic field amplitude at galactic scales [14]. Especially, the lack of charged plasmas in cosmic voids rises the question about the origin of magnetic fields observed in the intergalactic medium. The presence of the initial seeds of magnetic fields is still an open issue. Interestingly, the inflationary mechanism turns out to be able of accounting for the presence of magnetic fields at cosmological scales and, in some cases, also for primordial seeds required to start the galactic dynamo. These aspects make even more fascinating the inflationary mechanism. However, primordial scenarios where a relevant magnetogenesis takes place, require a detailed study of the associated processes, such as the generation of extra curvature perturbations and GWs, since the latter are strictly constrained by CMB observations. In the present thesis we consider a specific inflationary model [1] able to account for current observations of magnetic fields at cosmological scales and we studied in details the associated processes of curvature perturbation and GW production.

The thesis is organized as follows: in chapter 1 we introduce the basic notions of the inflationary paradigm. Then the first part of the work is dedicated to inflationary GWs. In chapter 2 we make a deep overview of the GW generation taking place during inflation, presenting the possible mechanisms of production, the results for the GW amount for a few specific inflationary models and the evolution of a primordial GW background up to the present time. In chapter 3 we give an updated picture of current status and observational prospects for inflationary GW signal, with a particular focus on the possibility of a direct GW detection. In chapter 4 the so-called inflationary consistency relation is provided and an overview of its possible violations is given. Then in chapter 5 we present the LISA project showing the expected capabilities of such an experiment in detecting a stochastic GW background and we perform a forecast analysis for LISA with respect to the GW signal associated to a number of selected inflationary models.
In the second part of the thesis, i.e. in chapters 6-7, we present the observations related to magnetic fields at cosmological scales and how such fields evolve along the history of the universe. Then we consider an inflationary model in which a significant magnetogenesis takes place and we analyse the counterpart production of curvature perturbations and GWs. Finally we conclude with part IV.
Throughout the thesis we will use natural units $c = \hbar = 1$, the reduced Mass Planck $M_{\rm pl}^{-2} = 8\pi G$, and the metric signature $(-,+,+,+)$.

Part I

Introduction to inflation

Chapter 1

The physics of Inflation

According to the Standard Big Bang theory, the universe behaviour at large scale is well described by a homogeneous and isotropic background whose evolution is governed by Einstein equations. More precisely, at some epoch well before primordial nucleosynthesis, the universe consists of a hot gas which cools because of cosmic expansion. Such a model successfully explains many cosmological observations, as the presence of a cosmic microwave background (CMB) and the observed abundance of particle relics. However the Standard Big Bang theory presents a number of issues, as the well-known horizon and flatness problems (see for example [15]). Originally inflation has been introduced in order to solve such problems [16] but, amazingly, combined with quantum aspects, it turns out to provide an elegant explanation for the formation of cosmic structures too. The inflationary model of the early universe does not replace the standard theory, but rather it is an additional piece of the overall picture related to the early stages of the cosmic evolution. Moreover, current cosmological observations widely support that the universe underwent an inflationary period in its early stages [2, 17].

1.1 Inflationary paradigm

In early eighties, it has been noted that the horizon and flatness problem can be eliminated assuming the early universe underwent a brief but intense period of *accelerated* expansion, i.e. inflating by a factor of at least 10^{26} within less than 10^{-34} seconds [16]. The immediate question is in which situation such a dynamics can take place.

Assuming the hypothesis of homogeneity and isotropy, the universe turns out to be described by a Friedman-Robertson-Walker (FRW) metric:

$$\mathrm{d}s^2 = -\mathrm{d}t^2 + a^2(t)\left[\frac{\mathrm{d}r^2}{1-Kr^2} + r^2(\mathrm{d}\theta^2 + \sin^2\theta \mathrm{d}\varphi^2)\right], \tag{1.1}$$

where r, θ, φ are comoving spherical coordinates and K the curvature of the three-dimensional spatial hyper-surfaces. The evolution of the metric is enclosed in the time dependence of the function $a(t)$, i.e. the scale factor.

The metric (1.1) corresponds to an energy content of the universe dominated by a perfect fluid. The stress-energy tensor of the latter as the form:

$$T_{\mu\nu} = (\rho + P)\mathrm{u}_\mu \mathrm{u}_\nu + P g_{\mu\nu}\,, \tag{1.2}$$

where ρ is the density, P the pressure, u_μ the 4-velocity of fluid elements and $g_{\mu\nu}$ the metric tensor. From eq.(1.2) and eq.(1.1), Einstein equations lead to the following relations:

$$H^2 = \frac{8\pi G}{3}\rho - \frac{K}{a^2}\,, \qquad \frac{\ddot{a}}{a} = -\frac{4\pi G}{3}(\rho + 3P)\,, \tag{1.3}$$

where H is the Hubble parameter defined as $H \equiv \dot{a}/a$.
Hereafter we will set $K = 0$, in agreement with observational constraints which point out negligible spatial curvature [17]. From the second equation in (1.3), the condition for an accelerated expansion taking place, results

$$P < -\frac{\rho}{3}\,. \tag{1.4}$$

From this relation, it is clear that ordinary radiation nor matter cannot drive an inflationary dynamics.
For the specific case $P = -\rho$, the scale-factor evolves as

$$a(t) = a_{\mathrm{I}} e^{H_{\mathrm{i}}(t-t_{\mathrm{i}})}\,, \tag{1.5}$$

with the Hubble parameter nearly constant in time $H = H_i \simeq$ const; where the subscript i indicates the beginning of the inflationary process. A period characterized by this evolution of the scale-factor is called *de Sitter stage*.

It is now useful to introduce a quantity called Hubble radius (or Hubble horizon), defined as $R_{\mathrm{H}}(t) \equiv 1/H(t)$. For a non-exotic content of the Universe $R_{\mathrm{H}} \propto ct$, so it sets the size of causally connected regions at each time. During a de Sitter stage, the physical Hubble radius is constant in time, while physical lengths continue to grow, thus being able to exit the Hubble radius at some "horizon-crossing" time. This phenomenon is a consequence of requiring an accelerated expansion, and it is the processes that actually we were looking for in order to fix the horizon and flatness problem of the standard cosmology. In order to all scales relevant for cosmological observations were able to exceed the Hubble radius during inflation, a sufficiently long inflation is required.

Interestingly, it turns out that the condition (1.4) can be satisfied when the universe content is dominated by the vacuum energy density of a scalar field associated to a potential $V(\varphi)$, i.e.:

$$\mathcal{L} = \frac{1}{2}\partial_\mu\varphi\partial^\mu\varphi - V(\varphi)\,. \tag{1.6}$$

Varying the lagrangian with respect to the filed φ, Klein-Gordon equation $\Box\varphi = \partial V/\partial\varphi$ is obtained. Assuming a FRW background, and the homogeneity of φ, it reads

$$\ddot{\varphi} + 3H\dot{\varphi} + V_\varphi = 0\,, \tag{1.7}$$

where $V_\varphi = dV/d\varphi$. Notice that the rolling of the field suffers a friction due to the expansion of the universe. The stress-energy tensor associated to (1.6) has the same form of that of a perfect fluid with the pressure and the energy density given by:

$$\rho_\varphi = \frac{\dot{\varphi}^2}{2} + V(\varphi)\,, \qquad P_\varphi = \frac{\dot{\varphi}^2}{2} - V(\varphi)\,. \tag{1.8}$$

The request (1.4) turns out to be $V(\varphi) > \dot{\varphi}^2$. In particular, to obtain a quasi-de Sitter stage, i.e. $P \simeq -\rho$, the following condition is required:

$$V(\varphi) \gg \dot{\varphi}^2\,, \tag{1.9}$$

so that $P \simeq V(\varphi)$ and $\rho \simeq (\varphi)$. It is now clear that a scalar field whose energy density is dominant in the Universe and whose potential energy dominates over the kinetic one, gives rise to an inflationary stage. The simplest way to satisfy eq.(1.9) is to introduce a scalar field slowly rolling towards the minimum of its potential, a shown in figure 1.1.

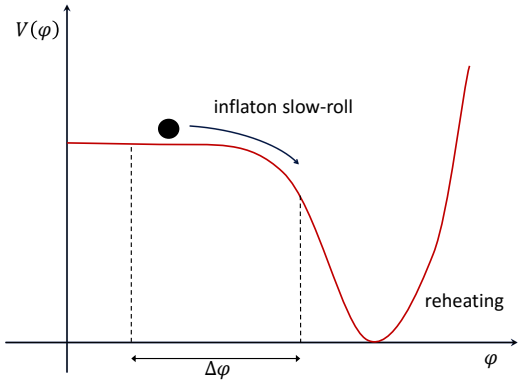

Figure 1.1: Example of inflationary potential with a "flat" region. The inflaton φ slowly rolls towards the minimum of its potential giving rise to an inflationary stage. Taken from [18].

1.1.1 Slow-roll parameters

Usefully, the required conditions for the inflaton potential energy to dominate over the kinetic one can be expressed by suited quantities which encode the key information on the inflaton potential, called *slow-roll* parameters [19–21]. The simplest way to satisfy eq.(1.9) is to require that there exist regions of the field-configuration space where the potential is sufficiently flat. In such a situation, for sufficiently late times the evolution of the scalar field is driven by the friction term, that is we can consider

$$\ddot{\varphi} \ll 3H\dot{\varphi} \tag{1.10}$$

in eq.(1.7), so that the equation of motion of the inflaton results:

$$3H\dot{\varphi} + V_\varphi = 0\,. \tag{1.11}$$

Equation (1.11) gives $\dot{\varphi}$ as a function of V_φ, then the slow-roll condition (1.9) and the condition on the friction term (1.10) turn out to be written as, respectively:

$$\frac{(V_\varphi)^2}{V} \ll H^2\,, \qquad\qquad V_{\varphi\varphi} \ll H^2\,. \tag{1.12}$$

On the other hand, form the condition (1.9), the first equation in (1.3) becomes:

$$H^2 \simeq \frac{8\pi G}{3} V(\varphi)\,, \tag{1.13}$$

so that, the conditions in eq.(1.12), implies:

$$\epsilon \equiv \frac{M_{\rm pl}^2}{2}\left(\frac{V_\varphi}{V}\right)^2 \ll 1 \qquad\qquad \eta \equiv M_{\rm pl}^2\,\frac{V_{\varphi\varphi}}{V} \ll 1\,, \tag{1.14}$$

where ϵ and η are the so-called *slow-roll parameters*. Notice that we can also write the parameter ϵ in terms of the Hubble parameter and its derivative as $\epsilon = -\dot{H}/H^2$. During inflation, the slow-roll parameters can be considered constant in time at first order, since, as it is easy to show, $\dot{\epsilon}, \dot{\eta} = O\left(\epsilon^2, \eta^2\right)$. Once constraints (1.14) are satisfied, the inflationary process happens generically for a wide class of models $V(\varphi)$. As soon as these conditions fail, inflation ends.

1.2 Quantum aspects of inflation

Considering quantum aspects, besides solving the horizon and flatness problem, the inflationary mechanism provides also an elegant way of explaining the presence of the matter structure and of the CMB anisotropies we observe today [4, 22, 23].
Current understanding of structure formation and of CMB anisotropies, requires the presence of small fluctuations of matter and radiation fields during the radiation and matter dominated eras. Standard cosmology cannot explain the presence of such seeds. The introduction of quantum aspects to the inflationary scenario, provides a fascinating and surprisingly elegant way of generating such primordial seeds.

According to quantum field theory, each field involved in a theory is characterized by quantum fluctuations with all possible wavelengths and whose average amplitude vanishes on a sufficient large amount of time. The fields involved in the inflationary dynamics are characterized by these fluctuations too. The accelerated expansion stretches the wavelengths of quantum fluctuations up to cross the causal region, while their amplitude continues to be small. Interestingly, fluctuations well outside the horizon turns out to be almost frozen, so that their amplitude does not evolve up to the time in which they re-enter the horizon in the radiation or matter dominated epoch. Along with the growing of the radius of the causal region, the perturbations which have been pushed out of the horizon during inflation, re-enter the causal region with a non-zero amplitude; the process is shown in figure 1.2. Scalar perturbations re-enter the horizon with sufficient large wavelengths to allow matter clustering and to form large

scale structures, and to generate to temperature and polarization CMB anisotropies at the time of recombination.
The same mechanism takes place also for the gravitational field. Its quantum fluctuations which re-enter the causal region give rise to a stochastic GW background. Therefore, quantum fluctuations of the fields involved in the inflationary mechanism, are supposed to be the early origin of cosmological perturbations, which finally give rise to several physical observables. The latter, therefore, include extremely significant information about the inflationary dynamics, making cosmological perturbations a crucial aspect in order to understand and investigate inflationary physics.

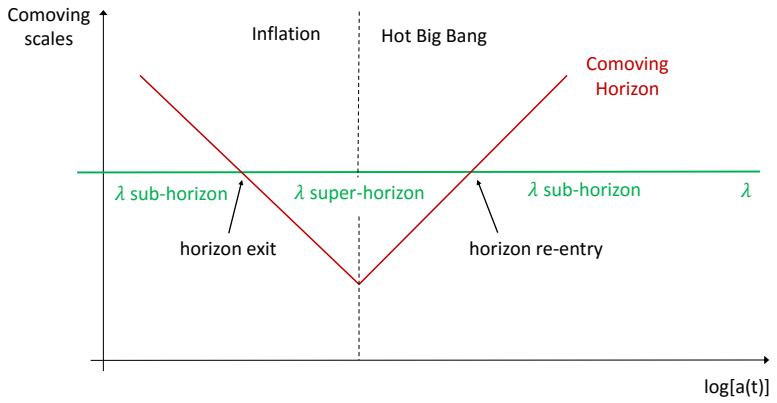

Figure 1.2: Evolution of the comoving horizon (red) and of a comoving wavelength λ (green), during the inflationary epoch and the subsequent radiation dominated era. Taken from [18].

According to this picture, the seeds of cosmological perturbations that give rise to large scale structures, CMB anisotropies and the stochastic GW background, are quantum fluctuations of the fields involved during inflation. This makes the inflationary physics a unique context where General Relativity and quantum mechanics are exploited simultaneously to obtain theoretical predictions testable by observations. This fact opened several intriguing issues about fundamental physics behind the theory of cosmological perturbations [24]. For example, looking at CMB anisotropies, we are observing the result of a measurement corresponding to a specific observable. According to the Copenhagen interpretation, in obtaining CMB maps we are making a measurement which leads the quantum state of the CMB radiation falling into an eigenvalue of the related observable. The collapse is supposed to happen at the time of observation. In light of this interpretation, CMB perturbations get the value of the eigenvalue only at the present time when we are making the measurement, since no observers existed before us. This seems in contrast with our current understanding of structure formation from the same seeds which give rise to CMB anisotropies. Several steps have been made in order to face this issue [25–27], however, how a single outcome is produced still continues to be an open question, that in cosmology takes the name of *macro-objectivation* problem. A way of solving such an issue which presents discriminatory predictions comparable, in principle, with experimental data, has been proposed: the collapse models [26, 27]. In this scenarios the Schrodinger equation which drives the

evolution of quantum fluctuations, and then of cosmological perturbations, presents deviations from the standard predictions of quantum mechanics, leading to deviations in the theoretical predictions for scalar and tensor modes in the inflationary context. In this sense, cosmological perturbations, including GWs, could also carry interesting and unique information about fundamental physics behind the inflationary paradigm.

1.2.1 Power spectrum definition

The most useful way of studying inflationary perturbations is to characterize them with a power spectrum and eventually higher-order correlation functions, as the bispectrum and trispectrum.
According to quantum field theory the mean value of these fluctuations is expected to vanish, i.e. $\langle \hat{\phi}(\mathbf{x},t)\rangle = 0$, on the other hand, the mean value of the quadratic fluctuations in general is expect to be different from zero, i.e. $\langle \left[\hat{\phi}(\mathbf{x},t)\right]^2\rangle \neq 0$. Then an efficient way to describe these fluctuations is the power spectrum.
We define the Fourier transform of a generic random field as:

$$g(\mathbf{x},t) = \int \frac{d^3\mathbf{k}}{(2\pi)^{3/2}} e^{i\mathbf{k}\cdot\mathbf{x}} g_{\mathbf{k}}(t) \ . \tag{1.15}$$

Working in the real space, the ensemble average then reads:

$$\langle g(\mathbf{x},t)\, g(\mathbf{x},t)\rangle = \int \frac{d^3\mathbf{k}}{(2\pi)^{3/2}} \int \frac{d^3\mathbf{k}'}{(2\pi)^{3/2}} e^{i\mathbf{x}\left(\mathbf{k}-\mathbf{k}'\right)} \langle g_{\mathbf{k}}(t)\, g^*_{\mathbf{k}'}(t)\rangle \, . \tag{1.16}$$

The power spectrum $P_{\rm g}$ is then defined by the following relation:

$$\langle g_{\mathbf{k}}(t)\, g_{\mathbf{k}'}(t)\rangle = \frac{2\pi^2}{k^3} P_{\rm g}(k)\, \delta\left(\mathbf{k}-\mathbf{k}'\right) \ . \tag{1.17}$$

Form eq.(1.16) and eq.(1.17), one can also see that

$$\langle g(\mathbf{x},t)\, g(\mathbf{x},t)\rangle = \int \frac{dk}{k} P_g \, , \tag{1.18}$$

i.e. the power spectrum is the contribution to the variance per unit logarithmic interval in k. Moreover, one can also define a spectral index, i.e. a parameter which quantifies the slope of the power spectrum with respect to the scale:

$$n_{\rm g} \equiv \frac{d\,\ln P_{\rm g}}{d\,\ln k} \, . \tag{1.19}$$

In general $n_{\rm g}$ is a function of the scale k, and the variation with respect to k of $n_{\rm g}$ is usually denoted as *running* of the spectral index.

For a quantized field, the power spectrum assumes a specific form in terms of the its perturbation modes. We define the conformal time as $\tau \equiv \int {\rm d}t/a(t)$ and we consider quantum fluctuations of a generic scalar field: $\chi(\mathbf{x},\tau) = \chi(t) + \delta\chi(\mathbf{x},\tau)$. It is useful to

perform the redefinition $\widetilde{\delta\chi} = a\,\delta\chi$. We promote $\widetilde{\delta\chi}$ to an operator and we decompose it on the two ladder operators $a_{\mathbf{k}}$ and $a^{\dagger}_{\mathbf{k}}$:

$$\widetilde{\delta\chi}(\mathbf{x},\tau) = \int \frac{\mathrm{d}^3\mathbf{k}}{(2\pi)^{3/2}} \left[u_k(\tau) a_{\mathbf{k}} e^{i\mathbf{k}\cdot\mathbf{x}} + u^*_k(\tau) a^{\dagger}_{\mathbf{k}} e^{-i\mathbf{k}\cdot\mathbf{x}}\right] , \tag{1.20}$$

where

$$[a_{\mathbf{k}}, a_{\mathbf{k}'}] = 0\,, \qquad [a_{\mathbf{k}}, a^{\dagger}_{\mathbf{k}'}] = \delta(\mathbf{k}-\mathbf{k}')\,. \tag{1.21}$$

Notice that here and elsewhere k is a comoving scale. From the above relations and from the quantization rule it follows that $u_{\mathbf{k}}$ and $u^*_{\mathbf{k}}$ satisfy the canonical commutation relation $u^*_k u_k - \dot{u}_k \dot{u}_k{}^* = -i$. From eqs.(1.20)-(1.21) then we can calculate the ensemble average on the vacuum state:

$$\langle \delta\chi_{\mathbf{k}} \delta\chi_{\mathbf{k}'} \rangle = \frac{|u_k|^2}{a^2} \delta(\mathbf{k}-\mathbf{k}')\,, \tag{1.22}$$

so that the power spectrum results:

$$P_{\delta\chi}(k) = \frac{k^3}{2\pi^2} |\delta\chi_k|^2 \ , \tag{1.23}$$

where $\delta\chi_k \equiv u_k/a$. Exploiting this relation, in the next sections we will calculate the power spectrum of the quantum fluctuations of the fields involved during inflation. More precisely, we will be interested in the power spectrum of fluctuations in the super-horizon regime, i.e. to those which re-enter the horizon at radiation and matter dominated epochs.

Bispectrum definition. If cosmological perturbations are gaussian distributed, the power spectrum includes all the statistical information about them, since higher-order correlation functions vanish or can be written in terms of the two-point correlation function. This is not more true for a perturbation field which is not gaussian distributed. In such a case, higher-order correlation functions include different information with respect to the power spectrum. In this sense, higher-order correlation functions provides a way to distinguish gaussian distributed perturbations to those which are not. The bispectrum, i.e. the three-point correlation function, is the lowest-order correlation function which can be exploited in such a direction. The bispectrum and higher-order correlation functions, i.e. non-gaussianities, turn out to include extremely significant information in order to understand the physics that generate the perturbations, in particular about field self-interactions and interactions with other fields. For this reason, non-gaussianities of inflationary perturbations are widely studied.
The bispectrum, usually indicated by $B_{\delta\varphi}(k_1,k_2,k_3)$, is defined as:

$$\langle \delta\varphi_{\mathbf{k}_1} \delta\varphi_{\mathbf{k}_2} \delta\varphi_{\mathbf{k}_3} \rangle = (2\pi)^3\, \delta(\mathbf{k}_1+\mathbf{k}_2+\mathbf{k}_3)\, B_{\delta\varphi}(k_1,k_2,k_3)\ , \tag{1.24}$$

where the triplet k_1, k_2, k_3 forms a closed triangle configuration. Fixing a shape for the latter, specific models for the bispectrum can be constructed. Usually, constraints

on a specific model of the bispectrum are expressed by bounds on a related amplitude parameter $f_{\rm NL}$ defined by:

$$B_{\delta\varphi}\left(k_1,k_2,k_3\right)=f_{\rm NL}F\left(k_1,k_2,k_3\right)\ , \tag{1.25}$$

where $F\left(k_1,k_2,k_3\right)$ expresses the functional dependence of the bispectrum on the chosen shape.
Several configurations of the triangular combination have been widely studied, in particular the *local* or *squeezed* configurations, the *equilateral* and the *orthogonal* ones. In the case of the squeezed configuration, one of the three scales is assumed to go to zero, in the equilateral configuration the threes scales are supposed to be the same, while the latter model is the configuration orthogonal to the equilateral and squeezed templates.
In many cases it turns out that $f_{\rm NL}\sim B_{\delta\varphi}\left(k_1,k_2,k_3\right)/P^2_{\delta\varphi}$.

In this chapter we outline the theory of scalar perturbations, then in chapter 2 we will present in details that related to tensor perturbations.

1.2.2 Curvature perturbations in Quasi de-Sitter spacetime

We want to calculate the power spectrum of cosmological perturbations assuming a quasi de-Sitter spacetime for the background. We consider quantum fluctuations of the fields involved in the inflationary dynamics, that is the inflaton φ and the gravitational field $g_{\mu\nu}$:

$$\varphi\left(t,\mathbf{x}\right)\to\varphi\left(t\right)+\delta\varphi\left(t,\mathbf{x}\right)\ , \tag{1.26}$$

$$g_{\mu\nu}\left(t,\mathbf{x}\right)\to g_{\mu\nu}\left(t\right)+\delta g_{\mu\nu}\left(t,\mathbf{x}\right)\ . \tag{1.27}$$

where $\varphi\left(t\right)$ and $g_{\mu\nu}\left(t\right)$ are the homogeneous and classical values of the fields. Perturbing the action of the system in this way, the equations of motion for the fluctuations are obtained. However, before proceeding in such a direction, introducing the theory of perturbed tensor objects is required.

Perturbing tensor objects. The most useful way of perturbing tensors is to decompose such perturbations into objects with definite transformation properties with respect to the underling three-dimensional space, since their dynamics reveals to be uncoupled at first order. Following this reasoning, perturbations of the metric tensor can be decomposed as follows [28–30]:

$$g_{00}=-a^2\left(\tau\right)\left(1+2\sum_{r=1}^{+\infty}\frac{1}{r!}\Psi^{(r)}\right) \tag{1.28}$$

$$g_{0i}=a^2\left(\tau\right)\sum_{r=1}^{+\infty}\frac{1}{r!}\omega_i^{(r)} \tag{1.29}$$

$$g_{ij}=a^2\left(\tau\right)\left\{\left[1-2\left(\sum_{r=1}^{+\infty}\frac{1}{r!}\Phi^{(r)}\right)\right]\delta_{ij}+\sum_{r=1}^{+\infty}\frac{1}{r!}h_{ij}^{(r)}\right\}\ , \tag{1.30}$$

where the functions $\Phi^{(r)}$, $\omega_i^{(r)}$, $\Psi^{(r)}$, $h_{ij}^{(r)}$ represent the rth-order perturbations of the metric. We decompose these quantities in objects with well-defined transformation under spatial rotations [31, 32]. Exploiting Helmholtz theorem, we can split each vector object into a solenoidal and a longitudinal part, respectively called *vector part* and *scalar part*:

$$\omega_i = \partial_i \omega^{\parallel} + \omega_i^{\perp} \,, \tag{1.31}$$

where $\omega_i^{\perp}$ is a solenoidal vector, *i.e.* $\partial^i \omega_i^{\perp} = 0$ and $\omega^{\parallel}$ the longitudinal object. Similarly, the off-diagonal part of the spatial metric can be written as

$$h_{ij} = D_{ij} h^{\parallel} + \partial_i h_j^{\perp} + \partial_j h_i^{\perp} + h_{ij}^{\mathrm{TT}} \,, \tag{1.32}$$

where $h^{\parallel}$ is a suitable scalar function, $h_i^{\perp}$ is a solenoidal vector field, and the *tensor part* h_{ij}^{TT} is symmetric, transverse ($\partial^i h_{ij} = 0$) and trace-less ($h_i^i = 0$), i.e. the tensor degrees of freedom (see appendix A). We have used the traceless operator $D_{ij} := \partial_i \partial_j - \delta_{ij} \nabla^2 / 3$, and we omitted the apex (r) for simplicity. Hereafter, where we neglect such an apex we mean a perturbation of first order.

In this chapter we study perturbation theory at first order. Later we will present the theory at second order and we will see that for several inflationary models it is also relevant going beyond the first order. We will also do not consider vector perturbations since they are found to decay and then to be substantially irrelevant in this context. At linear order in perturbation theory, what we called *scalar* and *tensor parts*, i.e. those objects with a defined transformation properties with respect to the underling three-dimensional space, turn out to be independent. This fact does not hold at higher order.

Due to Einstein equations, we have to consider perturbations of the energy content of the universe and of the metric tensor at the same time. This fact leads to the so-called gauge problem [31]: perturbations of the energy content of the universe are perturbations of fields living on the space-time variety, which is perturbed itself. To define a perturbation of a field we need a background value of the field in order to make a comparison with the perturbed quantity. The perturbed field is defined on the perturbed space-time variety, while the background value is defined on the background variety. Therefore, before defining a field perturbation, the choice of a one-to-one connection between the background and the perturbed variety, is required. This is the gauge choice. Changing this connection, keeping the same coordinate system on the background variety is a gauge transformation. The usual way to proceed is then to build up quantities which do not vary under a gauge transformation, i.e. gauge-invariant objects, which describes the physical quantities.

Curvature power spectrum. We consider single-field slow-roll inflation:

$$S = \int \mathrm{d}^4 x \sqrt{-g} \left[\frac{1}{2} M_{\mathrm{pl}}^2 R - \frac{1}{2} g^{\mu\nu} \partial_\mu \varphi \partial_\nu \varphi - V(\varphi) \right] , \tag{1.33}$$

where we suppose the feature of the inflaton potential to be so that the evolution of the scale factor is that of a quasi de-Sitter space. Moreover we consider a massless

inflaton field φ.
We perturb the inflaton and the metric field at the linear order as we explained. At such an order, the action for scalar perturbations is independent from that of tensor perturbations, so that we can consider the respective equation of motion separately.

The usual way to proceed is to refer to the so-called Mukhanov variables [33]:

$$Q_\varphi \equiv \delta\varphi + \frac{\varphi'}{\mathcal{H}}\Phi\,, \tag{1.34}$$

which turn out to be gauge-invariant. Perturbing the action (1.33), and varying it with respect to the inflaton field, one obtains the equation of motions of inflaton perturbations:

$$\delta\varphi'' + 2\mathcal{H}\delta\varphi' - \nabla^2\delta\varphi + a^2\delta\varphi\frac{\partial^2 V}{\partial\varphi^2}a^2 + 2\Psi\frac{\partial V}{\partial\varphi} - \varphi_0'\left(\Psi' + 3\Phi' + \nabla^2\omega^{\parallel}\right) = 0\,. \tag{1.35}$$

In terms of the gauge-invariant variable $\tilde{Q}_\varphi = aQ_\varphi$, such an equation turns out to be [34]:

$$\tilde{Q_\varphi}'' + \left(k^2 - \frac{a''}{a} + \mathscr{M}_\varphi^2 a^2\right)\tilde{Q}_\varphi = 0\,, \quad \text{where} \quad \mathscr{M}_\varphi^2 = \frac{\partial^2 V}{\partial\varphi^2} - \frac{8\pi G\varphi^2}{H}\,. \tag{1.36}$$

In slow-roll approximation the expression of $\mathscr{M}_\varphi^2$, reduces to $\mathscr{M}_\varphi^2/H^2 = 3\eta - 6\epsilon$. The solution on super-horizon scales at lowest order in the slow-roll parameters, are approximated by:

$$|Q_\varphi(k)| = \frac{H}{\sqrt{2k^3}}\left(\frac{k}{aH}\right)^{3/2-\nu_\varphi}\,, \tag{1.37}$$

where $\nu_\varphi \simeq \frac{3}{2} + 3\epsilon - \eta$.
We need a gauge-invariant quantity which unequivocally describes scalar perturbations. The intrinsic spatial curvature on hyper-surfaces of constant conformal time at linear order, reads

$${}^{(3)}R = \frac{4}{a^2}\nabla^2\hat{\Phi} \qquad \text{where} \qquad \hat{\Phi} \equiv \Phi + \frac{1}{6}\nabla^2\chi^{\parallel}\,. \tag{1.38}$$

$\hat{\Phi}$ is usually referred to as the *curvature perturbation*, however it is not a gauge-invariant quantity, since under a transformation on constant time hyper-surfaces $\tau \to \tau + \alpha$ we have: $\hat{\Phi} \to \tilde{\hat{\Phi}} = \hat{\Phi} - \mathcal{H}\alpha$, where $\mathcal{H} \equiv a'/a$ is the Hubble parameter in conformal time and the prime denote differentiation with respect to it. We need a gauge-invariant combination that reduces to the curvature perturbation choosing a particular gauge. Consider the following expression [31, 35]:

$$-\zeta \equiv \hat{\Phi} + \mathcal{H}\frac{\delta\rho}{\rho'}\,. \tag{1.39}$$

Accounting for the $\hat{\Phi}$ transformation and the gauge transformation for scalars, the quantity (1.39) results gauge-invariant and it is referred to as *gauge-invariant curvature*

perturbation of the uniform energy-density hyper-surfaces. We are interested in the power spectrum of ζ. An analogous gauge-invariant quantity is defined on comoving hypersurfaces, i.e.:

$$\mathcal{R} \equiv \hat{\Phi} + \frac{\mathcal{H}}{\varphi'}\delta\varphi \,. \tag{1.40}$$

which is related to the Mukanhov-Sasaki variables by:

$$\mathcal{R} = \frac{\mathcal{H}}{\varphi'}Q_\varphi \,. \tag{1.41}$$

On large scales we have $\mathcal{R} = -\zeta$. Quantum fluctuations which give rise to structure formation and CMB anisotropies, are those which are stretched on super-horizon scales during inflation and that are frozen there up to the horizon re-entering during radiation and matter dominated eras, therefore we evaluate the curvature power spectrum at large scales. The power spectrum of ζ in such a regime, turns out to be:

$$P_\zeta(k) = \left(\frac{H^2}{2\pi\dot{\varphi}}\right)^2 \left(\frac{k}{aH}\right)^{3-2\nu_\varphi} \simeq \left(\frac{H_*^2}{2\pi\dot{\varphi}}\right)^2 , \tag{1.42}$$

where in the first expression H and $\dot{\varphi}$ are evaluated at the horizon exit of the scale k, while in the second one, $*$ denotes quantities evaluated at the time a given perturbation mode leaves the horizon during inflation, i.e. the power spectrum is almost scale invariant.

Scalar power spectrum parametrization. In order to compare these theoretical predictions with observational data, it is useful to introduce a phenomenological parametrization of the power-spectrum [2], that is:

$$P_{\rm S} = A_{\rm S}(k_*)\left(\frac{k}{k_*}\right)^{n_{\rm S}-1+\frac{1}{2}\frac{{\rm d}n_{\rm S}}{{\rm d}\ln k}\ln(k/k_*)+\ldots} , \tag{1.43}$$

where $A_{\rm S}$ is the amplitude of the perturbations to a fixed pivot scale k_* and $n_{\rm S}-1$ is the spectral index defined in eq.(1.19). Following this parametrization, the amplitude of scalar perturbations power spectrum is:

$$A_{\rm S}(k_*) = \left(\frac{H_*^2}{2\pi\dot{\varphi}}\right)^2 \simeq \frac{1}{2\epsilon M_{pl}^2}\left(\frac{H_*}{2\pi}\right)^2 , \tag{1.44}$$

while the spectral index at the lowest order in slow-roll parameters reads:

$$n_{\rm S}(k_*) - 1 = 3 - 2\nu_\varphi = -6\epsilon + 2\eta \,. \tag{1.45}$$

1.3 Duration and end of inflation

In order to solve the horizon and flatness problems, inflation has to last a sufficiently long period. On the other side, in order to recover standard cosmology, the inflationary

expansion has to end.
The duration of inflation is usually expressed by the number of e-folds, i.e. [20]:

$$N \equiv \int_{t_\mathrm{i}}^{t_\mathrm{f}} H \, \mathrm{d}t \ , \tag{1.46}$$

where t_i and t_f are the starting and ending time of inflation. If the evolution of the scale factor is given by (1.5), the previous expression turns out to be:

$$N = \ln\left(a_\mathrm{f}/a_\mathrm{i}\right) \tag{1.47}$$

where $a_\lambda = a\left(t\left(\lambda\right)\right)$. The lower bound required to solve the horizon problem, for an Hubble parameter of the order of $H \sim 10^{12}\mathrm{GeV}$ is $N \gtrsim \ln 10^{26} \sim 60$ [2].

Reheating. The greatest successes of the Standard Big Bang model, such as primordial nucleosynthesis and the formation of the CMB, requires an evolutionary progression from radiation to a matter domination era. In particular, we know that the Universe must be repopulated by hot radiation in order to initiate the hot Big Bang phase. In most inflationary models, at the end of the accelerated expansion, the inflaton field oscillates around the minimum of its potential. The main requirement for the developing of the hot Big Bang is a radiation dominated Universe at $T \simeq 1\mathrm{MeV}$. Therefore it is required to suppose that the energy density stored in the inflaton field decays into radiation before such a temperature of the universe is reached. This era of transition is called reheating [36–39]. Such an epoch of the universe is widely unknown. This is because the mechanism itself washes away the initial conditions that initiate it, thermalizing the energy content of the universe.
Many models have been proposed to describe this transition, some of which include the perturbative decay of the inflaton field while others involve non-perturbative mechanisms. If the fluctuations are sufficiently small, inflaton quanta could decay into relativistic products. This happens as soon as the inflaton decay rate Γ becomes comparable to the Hubble constant. Usually each decay product is supposed to thermalize quickly so that their energy distribution can be described by a black-body function and the reheating temperature for a sudden process is $T_\mathrm{reh} \sim \sqrt{M_\mathrm{pl}\Gamma}$. Then a mechanism is supposed to take place that leads to energy transfer of the decay products into radiation.

Part II

Inflationary gravitational waves

Chapter 2

Gravitational wave production during inflation

According to quantum field theory, each field involved in the inflationary mechanism is characterized by quantum fluctuations. In the basic inflationary model, the fields involved are the inflaton, which drives the dynamics, and the gravitational field. In section 1.2.2 we saw the dynamics of inflationary scalar perturbations generated by the presence of the inflaton and by the *scalar part* of metric perturbations. Here we are interested into the *tensor part* of the gravitational field perturbations. As we anticipated, the latter give rise to a stochastic GW background which permeates the universe up to the present time [40].
But the stretching of quantum fluctuations is not the only mechanism by which GWs can be generated during inflation. We will see that also a *classical* production of gravitational radiation is possible: the fields involved in the inflationary dynamics can give rise to anisotropic transverse and traceless components of the stress-energy tensor of the universe, playing the role of a GW source. Moreover, inflationary models built on a theory of modified gravity, instead of GR, in general leads to a non-standard GW production.
Inflationary GWs, besides being a stringent probe for inflation itself, then represent a possible discriminant among the variety of inflationary models, over than being an interesting signal in order to understand the theory of gravity itself.

In this chapter we present the GW production processes that can take place during inflation and we study the evolution of the generated GW background from the end of inflation up to the present time.
Most of the content of this chapter is presented in the review [18].

2.1 Gravitational wave production from quantum fluctuations

We calculate the power spectra of tensor fluctuations for a system described by the action (1.33) [4, 41]. We perturb the inflaton and the metric field at the linear order

following the decomposition described in section 1.2.2. At such an order the action for scalar perturbations is independent from that of tensor perturbations, then we can consider separately the evolution of the *tensor part*. Tensor perturbations appearing in the following sections all refer to this quantity, in particular we will use denomination h_{ij} in substitution of h_{ij}^{TT}.
For tensor perturbations the action is found to be:

$$S_{\mathrm{T}}^{(2)} = \frac{M_{pl}^2}{8} \int \mathrm{d}\tau \ \mathrm{d}^3\mathbf{x} \ a^2(\tau) \, \eta^{\mu\nu} \partial_\mu h_{ij} \partial_\nu h_{ij} \tag{2.1}$$

where $\eta^{\mu\nu}$ is the Minkowski metric. Remember that h_{ij} is a gauge-invariant object. Varying the action with respect to h_{ij}, the equation of motion reads:

$$\boxed{h_{ij}'' + 2\mathcal{H} h_{ij}' - \nabla^2 h_{ij} = 0 \, .} \tag{2.2}$$

It turns out that tensor perturbations solve a wave equation. Recalling that h_{ij} is symmetric, transverse and traceless, the solutions of eq.(2.2) present the following form

$$h_{ij}(\mathbf{x}, \tau) = h(\tau) \, \mathsf{e}_{ij}^{(+,\times)}(\mathbf{x}) \ , \tag{2.3}$$

where $\mathsf{e}_{ij}^{(+,\times)}$ are the polarization tensors, with $+, \times$ the two GW polarization states [42]. In Fourier space, the polarization tensors $\mathsf{e}_{ij}^{(+)}$, $\mathsf{e}_{ij}^{(\times)}$ can be expressed by two polarization vectors $\mathsf{e}_i(\mathbf{k})$, $\bar{\mathsf{e}}_i(\mathbf{k})$ orthogonal to the propagation vector $\mathbf{k}$ as

$$\mathsf{e}_{ij}^{(+)}(\mathbf{k}) \equiv \frac{1}{\sqrt{2}} \left[\mathsf{e}_i(\mathbf{k}) \, \mathsf{e}_j(\mathbf{k}) - \bar{\mathsf{e}}_i(\mathbf{k}) \, \bar{\mathsf{e}}_j(\mathbf{k}) \right] \ , \tag{2.4}$$

$$\mathsf{e}_{ij}^{(\times)}(\mathbf{k}) \equiv \frac{1}{\sqrt{2}} \left[\mathsf{e}_i(\mathbf{k}) \, \bar{\mathsf{e}}_j(\mathbf{k}) - \bar{\mathsf{e}}_i(\mathbf{k}) \, \mathsf{e}_j(\mathbf{k}) \right] \ . \tag{2.5}$$

$\mathsf{e}_{ij}^{(+)}$ and $\mathsf{e}_{ij}^{(\times)}$ satisfy the conditions $\mathsf{e}_{ij} = \mathsf{e}_{ji}$, $k^i \mathsf{e}_{ij} = 0$, $\mathsf{e}_{ii} = 0$.
Equation (2.3) reflects the fact that tensor modes are left with two physical degrees of freedom: starting from six of the symmetric tensor h_{ij}, four constraints are given by the requirement of being traceless and transverse. In summary, the most general solution of eq.(2.2) reads

$$h_{ij}(\mathbf{x}, \tau) = \sum_{\lambda=(+,\times)} h^{(\lambda)}(\tau) \, \mathsf{e}_{ij}^{(\lambda)}(\mathbf{x}) \ . \tag{2.6}$$

To get the shape of $h(\tau)$ from (2.2), it is useful to perform the transformation

$$v_{ij} \equiv \frac{a M_{\mathrm{pl}}}{\sqrt{2}} h_{ij} \, . \tag{2.7}$$

In terms of v_{ij} the action (2.1) reads

$$S_{\mathrm{T}}^{(2)} = \frac{1}{2}\int \mathrm{d}\tau \mathrm{d}^3\mathbf{x}\left[v'_{ij}v'_{ij} - (\nabla v_{ij})^2 + \frac{a''}{a}v_{ij}v_{ij}\right], \tag{2.8}$$

which can be interpreted as the action for two scalar fields in Minkowski space-time, with effective mass squared equal to a''/a. Moving to Fourier space:

$$v_{ij}(\mathbf{x},\tau) = \int \frac{\mathrm{d}^3\mathbf{k}}{(2\pi)^{3/2}} e^{i\mathbf{k}\cdot\mathbf{x}}\left[v_{\mathbf{k}}^{(+)}(\tau)\,\mathsf{e}_{ij}^{(+)}(\mathbf{k}) + v_{\mathbf{k}}^{(\times)}(\tau)\,\mathsf{e}_{ij}^{(\times)}(\mathbf{k})\right]. \tag{2.9}$$

where $v_{\mathbf{k}}^{(\lambda)}$ are the Fourier modes of the scalar amplitude, and the same for $\mathsf{e}_{ij}^{(\lambda)}(\mathbf{k})$. The equation of motion for each mode $v_{\mathbf{k}}^{(\lambda)}$, then reads:

$$v_{\mathbf{k}}^{(\lambda)\,\prime\prime} + \left(k^2 - \frac{a''}{a}\right)v_{\mathbf{k}}^{(\lambda)} = 0\,, \tag{2.10}$$

which is the equation of motion of an harmonic oscillator with a time dependent frequency $\omega_k^2(\tau) = k^2 - a''/a$. Notice that eq.(2.10) has the same structure of the equation of motion of $\tilde{Q}_\varphi$, i.e. eq.(1.36). Let us study the qualitative behaviour of its solutions. We can identify two main regimes depending on the relative magnitude of the second and third term. First, consider the case in which $a''/a \ll k^2$. Ignoring the second term in parenthesis, the equation becomes that of a free harmonic oscillator, so that tensor perturbations v_{ij} oscillate without any damping of their amplitude. This approximation corresponds to overlook the effect of the expansion of the Universe. To make explicit the physical condition corresponding to this regime, notice that, since $a''/a \sim (a'/a)^2$, $a''/a \ll k^2$ corresponds to $k \gg aH$, i.e. to the *sub-horizon* behaviour (check for example the case of a de Sitter space-time where $a(\tau) \sim 1/\tau$). Keeping in this regime, the solution of (2.10) reads

$$v_k(\tau) = Ae^{ik\tau}\,, \tag{2.11}$$

which means that the amplitude of the modes of the original field h_{ij} decreases in time with the inverse of the scale factor as an effect of the cosmic expansion. Consider now the regime in which the second term is negligible with respect to the third one: $k^2 \ll a''/a$. There are two possible solutions of the eq.(2.10):

$$v_k(\tau) \propto a\,, \qquad \text{and} \qquad v_k(\tau) \propto 1/a^2\,, \tag{2.12}$$

which corresponds to $h \propto$ const and a decreasing in time solution, respectively. This situation clearly corresponds to the *super-horizon* regime. In particular we are interested in the $h(\tau)$ solutions with constant amplitude.

Now we calculate more accurately the power spectrum of tensor perturbations, solving in details (2.10). We quantize the field v_{ij}, by the standard rules:

$$\begin{aligned}
&\left[\hat{v}^{(\lambda)}(\mathbf{x},\tau), \hat{v}'^{(\gamma)}(\mathbf{x}',\tau)\right] = i\delta^{(3)}_{\lambda\gamma}(\mathbf{x}-\mathbf{x}')\,,\\
&\left[\hat{v}^{(\lambda)}(\mathbf{x},\tau), \hat{v}^{(\gamma)}(\mathbf{x}',\tau)\right] = \left[\hat{v}'^{(\lambda)}(\mathbf{x},\tau), \hat{v}'^{(\gamma)}(\mathbf{x}',\tau)\right] = 0\,.
\end{aligned} \tag{2.13}$$

and decomposing the field as:

$$v_{\mathbf{k}}^{(\lambda)} = v_k(\tau)\,\hat{a}_{\mathbf{k}}^{(\lambda)} + v_k^*(\tau)\,\hat{a}_{-\mathbf{k}}^{(\lambda)\dagger}\,, \tag{2.14}$$

where the ladder operators $\hat{a}$ and $\hat{a}^\dagger$ satisfy:

$$\left[\hat{a}_{\mathbf{k},\lambda}, \hat{a}^\dagger_{\mathbf{k'},\lambda}\right] = \delta_{\lambda\lambda'}\delta^{(3)}(\mathbf{k}-\mathbf{k'})\,. \tag{2.15}$$

From the latter relation, joined to the quantization rules (2.13), it follows that the modes are normalized by $v_k^* v_k' - v_k v_k'^* = -i$.
In order to proceed, the choice of the vacuum state is required. Defining the vacuum as an eigenstate of the hamiltonian operator and as the state with the lowest energy, for an harmonic oscillator with a constant frequency, the vacuum state turns out to be unique. Here the frequency is time dependent. However in the limit of small scales, i.e. $k \gg Ha$, our system reduces to an harmonic oscillator with a constant frequency given by k, so that we can safely say that the vacuum is unique. For an harmonic oscillator with $\omega^2 = k^2$, the vacuum state turns out to be given by:

$$v_k = \frac{e^{-ik\tau}}{\sqrt{2k}}\,. \tag{2.16}$$

This is the so-called Bunch-Davies vacuum choice [43]. The generic solution of (2.10) has to match (2.16) in the limit of sub-horizon scales.
For a quasi de-Sitter spacetime the term a''/a in the eq.(2.10), can be written in terms of the slow-roll parameter ϵ as:

$$\frac{a''}{a} \simeq \frac{1}{\tau^2}(2+3\epsilon)\,. \tag{2.17}$$

Defining the ν as $\nu \equiv \epsilon + 3/2$, the equation of motion (2.10), results:

$$v_k'' + \left[k^2 - \frac{1}{\tau^2}\left(\nu^2 - \frac{1}{4}\right)\right] v_k = 0\,. \tag{2.18}$$

The exact solution of the Bessel equation (2.18), is given by [44]:

$$v_k(\tau) = \sqrt{-\tau}\left[C_1 H_\nu^{(1)}(-k\tau) + C_2 H_\nu^{(2)}(-k\tau)\right]\,, \tag{2.19}$$

where C_1, C_2 are integration constants and $H_\nu^{(1)}, H_\nu^{(2)}$ are Hankel functions of first and second order. To determine C_1 and C_2, we impose that on the sub-horizon scales, the solution matches the plane-wave solution (2.16). The asymptotic shape of Hankel functions is given by:

$$H_\nu^{(1)}(x \gg 1) \sim \sqrt{\frac{2}{\pi x}} e^{i\left(x - \frac{\pi}{2}\nu - \frac{\pi}{4}\right)}\,, \qquad H_\nu^{(2)}(x \gg 1) \sim \sqrt{\frac{2}{\pi x}} e^{-i\left(x - \frac{\pi}{2}\nu - \frac{\pi}{4}\right)}\,. \tag{2.20}$$

Due to the behaviour of the exponent, we need to put $C_2 = 0$, while matching the asymptotic solution to a plane wave leads to

$$C_1 = \frac{\sqrt{\pi}}{2} e^{i\left(\nu + \frac{1}{2}\right)\frac{\pi}{2}}\,. \tag{2.21}$$

Therefore, the exact solution turns out to be:

$$v_{\mathbf{k}} = \frac{\sqrt{\pi}}{2} e^{i\left(\nu+\frac{1}{2}\right)\frac{\pi}{2}} \sqrt{-\tau} H_{\nu}^{(1)}\left(-k\tau\right) . \tag{2.22}$$

In the super-horizon regime, the Hankel function reads

$$H_{\nu}^{(1)}\left(x \ll 1\right) \sim \sqrt{2/\pi} e^{-i\frac{\pi}{2}} 2^{\nu-\frac{3}{2}} \left[\Gamma\left(\nu\right)/\Gamma\left(3/2\right)\right] x^{-\nu} , \tag{2.23}$$

so that in such a limit, Fuorier modes of the solution result:

$$v_k = e^{i\left(\nu-\frac{1}{2}\right)\frac{\pi}{2}} 2^{\left(\nu-\frac{3}{2}\right)} \frac{\Gamma\left(\nu\right)}{\Gamma\left(3/2\right)} \frac{1}{\sqrt{2k}} \left(-k\tau\right)^{\frac{1}{2}-\nu} , \tag{2.24}$$

where Γ is the Euler function.
From the generic expression of the power spectrum (1.17), the tensor power spectrum on super-horizon scales reads:

$$\left\langle h\left(\mathbf{x},t\right) h\left(\mathbf{x},t\right)\right\rangle = \int \frac{dk}{k} P_T . \tag{2.25}$$

Taking into account for the two independent polarizations, from eq.(1.23), we have:

$$P_{\mathrm{T}}\left(k\right) = \frac{k^3}{2\pi^2} \sum_{\lambda} \left|h_{\mathbf{k}}^{(\lambda)}\right|^2 , \tag{2.26}$$

so that on super-horizon scales the following power spectrum holds:

$$\boxed{P_{\mathrm{T}}\left(k\right) = \frac{8}{M_{\mathrm{pl}}^2} \left(\frac{H}{2\pi}\right)^2 \left(\frac{k}{aH}\right)^{-2\epsilon} \simeq \frac{8}{M_{\mathrm{pl}}^2} \left(\frac{H_*}{2\pi}\right)^2 ,} \tag{2.27}$$

where the asterisk denotes quantities evaluated at the epoch a given perturbation mode leaves the horizon during inflation. The result shows that tensor perturbations on super-horizon scales are time independent, which means that the solution obtained at the time of inflation, is valid throughout the different evolution eras of the Universe until the modes remain super-horizon. The latter is a crucial behaviour which allows to access to early times of the universe exploiting current cosmological observations. Moreover, the tensor power spectrum turns out to be almost scale-invariant, i.e. all modes frozen on super-horizon scales have all almost the same amplitude. More precisely, from the definition of spectral index (1.19), we have $n_{\mathrm{T}} = -2\epsilon$. For $n_{\mathrm{T}} < 0$ the power-spectrum is called *red*, while in the opposite case it is indicated as *blue* [45] (we will call *scale-invariant* the case in which $n_{\mathrm{T}} = 0$).

Inflation stretches tensor perturbation wavelengths to super-horizon scales, making their amplitude almost frozen. When the inflationary expansion ends and the radiation epoch starts, cosmological perturbations which are frozen outside the horizon, start entering the causal region sequentially, due to the growth of the comoving horizon. This process proceeds during the matter domination era. When this happens the decaying solution has substantially disappeared, so what re-enters the causally connected space is the almost scale-invariant power-spectrum at the time of first horizon crossing, which occurred during inflation. When primordial tensor modes enter the horizon, they start evolving giving rise to a stochastic GW background which permeates the universe. More precisely, their evolution is driven by the equation of motion (2.2), where now the scale factor is determined by the radiation or matter domination.

Tensor power spectrum parametrization. For a comparison with observations, the tensor power spectrum is usually parametrized in the following manner [46]

$$P_{\mathrm{T}}(k) = A_{\mathrm{T}}(k_*) \left(\frac{k}{k_*}\right)^{n_{\mathrm{T}} + \frac{1}{2}\frac{\mathrm{d}n_{\mathrm{T}}}{\mathrm{dln}k}\ln(k/k_*)+\ldots}, \tag{2.28}$$

where A_{T} is the tensor amplitude at some pivot scale k_*, n_{T} is the tensor spectral index, and $\frac{1}{2}\frac{\mathrm{d}n_{\mathrm{T}}}{\mathrm{dln}k}$ the running of the spectral index. Following this parametrization, the tensor amplitude corresponds to:

$$A_{\mathrm{T}}(*) = \frac{8}{M_{\mathrm{pl}}^2}\left(\frac{H_*}{2\pi}\right)^2, \tag{2.29}$$

and the spectral index to be

$$n_{\mathrm{T}} = -2\epsilon\,. \tag{2.30}$$

People usually refer also to another quantity, i.e. the ratio between the tensor and scalar amplitude of inflationary perturbations:

$$r(k_*) \equiv \frac{A_{\mathrm{T}}(k_*)}{A_{\mathrm{S}}(k_*)}, \tag{2.31}$$

which, in case of single-field slow-roll inflation, from equations (2.27)-(1.42) turns out to be:

$$r = \frac{8}{M_{\mathrm{pl}}^2}\left(\frac{\dot{\varphi}}{H}\right)^2 = 16\epsilon\,. \tag{2.32}$$

The proportionality to the slow-roll parameter ϵ unveils that r is predicted to be a very small quantity, which means that the GW amplitude is expected to be several order of magnitude smaller that scalar one.
From the expression of the tensor spectral index in eq.(2.27) and the equation above, the following relation holds at first-order in slow-roll parameters:

$$r = -8n_{\mathrm{T}}\,. \tag{2.33}$$

This equality turns out to be a consistency check of the inflationary paradigm itself, therefore we will study it in a dedicated chapter 4.

2.2 Classical gravitational wave production

Quantum fluctuations of the gravitational field is not the only way by which GWs can be produced during inflation. Up to now we have considered only perturbation theory at the first order, where scalar, vector and tensor perturbations are independent to each other. This is not true at higher order in perturbation theory. More precisely, different kinds of perturbations of order n are independent to each other, but they are not uncoupled with perturbations of lower orders. Therefore, the dynamics of second-order tensor perturbations is coupled to that of first order scalar, vector and tensor perturbations [29, 47]. As we will see soon, in general, the equation of motion of second-order tensor perturbations present a source term, provided by combinations of first-order perturbations. Such a source leads to a further contribution to the GW production, besides that due to quantum fluctuations of the gravitational field. This kind of GW production is denoted as *classical*.
During inflation, such a source term is always not vanishing, but in general is negligible. However, in several well-motivated inflationary scenarios the source in the tensor equation of motion can be significantly efficient so that the amount of GWs produced by the classical mechanism exceeds that generated by quantum fluctuations of the gravitational field.

2.2.1 Gravitational wave equation of motion at second order

In order to find the equation of motion of second-order GWs, in principle, we have to consider scalar, vector and tensor perturbations of first and second order. For simplicity, we neglect tensor and vector perturbations of the first order. Combinations of two first-order scalar perturbations turns out to be a source for GWs at second order [29, 47]. This means that, when scalar perturbations are present, we always have generation of GWs, even if tensor perturbations at first order are absent.
We start considering the generic perturbation theory, then we will specify the results for several inflationary scenarios.

In order to extract the equation of motion of GWs, we project Einstein equations on the transverse and traceless part with a proper projector $\hat{\Pi}_{ij}^{lm}$:

$$\hat{\Pi}_{ij}^{lm} G_{lm}^{(2)} = \frac{1}{2M_{pl}^2} \hat{\Pi}_{ij}^{lm} T_{lm}^{(2)} \,, \tag{2.34}$$

where $\hat{\Pi}_{ij,lm} = \Pi_{il}\Pi_{jm} - \frac{1}{2}\Pi_{ij}\Pi_{lm}$ with $\Pi_{ij} = \delta_{ij} - \partial_i\partial_j/\Delta$ [48], and $T_{lm}^{(2)}$ is the second-order term of a generic stress-energy tensor, defined by:

$$T_{\mu\nu} = T_{\mu\nu}^{(0)} + T_{\mu\nu}^{(1)} + \frac{1}{2} T_{\mu\nu}^{(2)} \,. \tag{2.35}$$

From the perturbed metric (1.28), ignoring first-order vector and tensor perturbations,

the second-order term of the Einstein tensor results [30]:

$$\begin{aligned} G_j^{(2)i} =& a^{-2}\left[\frac{1}{4}\left(h_j^{\prime\prime i}+2\mathcal{H}h_j^{\prime i}-\nabla^2 h_j^i\right)+2\Psi^{(1)}\partial^i\partial_j\Psi^{(1)}-2\Phi^{(1)}\partial^i\partial_j\Psi^{(1)}\right. \\ &+4\Phi^{(1)}\partial^i\partial_j\Phi^{(1)}+\partial^i\Psi^{(1)}\partial_j\Psi^{(1)}-\partial^i\Psi^{(1)}\partial_j\Phi^{(1)}-\partial^i\Phi^{(1)}\partial_j\Psi^{(1)} \\ &\left.+3\partial^i\Phi^{(1)}\partial_j\Phi^{(1)}+\left(\Psi^{(2)},\Psi^{(2)},\omega_i^{(2)}\text{term}\right)+(\text{diagonal part})\,\delta^i_j\right]\,, \end{aligned} \tag{2.36}$$

where here h_{ij} is the second order, transverse and traceless, *tensor part* (as before, we omit the TT apex). In order to extract the equation of motion for tensor modes, from the previous expression we write the LHS of eq.(2.34) as:

$$\begin{aligned} \hat{\Pi}_{ij}^{lm}G_{lm}^{(2)} =& \frac{1}{4}\left(h^{\prime\prime ij}+2\mathcal{H}h_{ij}^{\prime}-\nabla^2 h_{ij}\right)+ \\ &+\hat{\Pi}_{ij}^{lm}\left[\left(2\Psi^{(1)}\partial_l\partial_m\Psi^{(1)}-2\Phi^{(1)}\partial_l\partial_m\Psi^{(1)}+4\Phi^{(1)}\partial_l\partial_m\Phi^{(1)}+\right.\right. \\ &\left.\left.+\partial_l\Psi^{(1)}\partial_m\Psi^{(1)}-\partial_l\Psi^{(1)}\partial_m\Phi^{(1)}-\partial_l\Phi^{(1)}\partial_m\Psi^{(1)}+3\partial_l\Phi^{(1)}\partial_m\Phi^{(1)}\right)\right]\,, \end{aligned} \tag{2.37}$$

where notice that the pure second-order terms and the diagonal part of $G_{lm}^{(2)}$ are dropped away by the projector, and the factor a^{-2} disappeared because of the lowering of the index. We define the second contribution as:

$$\begin{aligned} \mathscr{S}_{lm}(\mathbf{x},\tau) \equiv& 2\Psi\partial_l\partial_m\Psi-2\Phi\partial_l\partial_m\Psi+4\Phi\partial_l\partial_m\Phi+4\Psi\partial_l\partial_m\Psi+ \\ &+\partial_l\Psi\partial_m\Psi-\partial_l\Psi\partial_m\Phi-\partial_l\Phi\partial_m\Psi+3\partial_l\Phi\partial_m\Phi\,, \end{aligned} \tag{2.38}$$

so that:

$$\hat{\Pi}_{ij}^{lm}G_{lm}^{(2)}=\frac{1}{4}\left(h_{ij}^{\prime\prime}+2\mathcal{H}h_{ij}^{\prime}-\nabla^2 h_{ij}\right)+\hat{\Pi}_{ij}^{lm}\mathscr{S}_{lm}(\mathbf{x},\tau)\,. \tag{2.39}$$

The equation (2.34), then takes the following general form:

$$\boxed{h_{ij}^{\prime\prime}+2\mathcal{H}h_{ij}^{\prime}-\nabla^2 h_{ij}=\hat{\Pi}_{ij}^{lm}\left[-4\mathscr{S}_{lm}+\frac{2}{M_{\rm pl}^2}T_{lm}^{(2)}\right]\,.} \tag{2.40}$$

The general source of second-order GWs can be identified into two parts, one due to the perturbed terms of the Einstein tensor, i.e. $-4\mathscr{S}_{lm}$, and the other one due to contributions directly coming from the stress-energy tensor of the system, i.e. $2T_{\mu\nu}^{(2)}/M_{pl}^2$. The projector eliminates terms of pure second order in the stress-energy tensor, leaving only combinations of first-order scalar perturbations.
In order to write the solution of eq.(2.40), we Fourier transform the tensor perturbations, according to what we did in (2.9), as:

$$h_{ij}(\mathbf{x},\tau)=\int\frac{\mathrm{d}^3\mathbf{k}}{(2\pi)^{3/2}}e^{i\mathbf{k}\cdot\mathbf{x}}\left[h_{\mathbf{k}}^{(+)}(\tau)\,\mathsf{e}_{ij}^{(+)}(\mathbf{k})+h_{\mathbf{k}}^{(\times)}(\tau)\,\mathsf{e}_{ij}^{(\times)}(\mathbf{k})\right]\,, \tag{2.41}$$

where the polarization tensors are those defined in (2.4). In order to write the equation of motion in the Fourier space we need to write the RHS of eq.(2.40) in terms of the polarization tensors, we have:

$$\hat{\Pi}_{ij}^{lm}\left[-4\mathscr{S}_{lm}+\frac{2}{M_{\rm pl}^2}T_{lm}^{(2)}\right]=\int\frac{\mathrm{d}^3\mathbf{k}}{(2\pi)^{3/2}}e^{i\mathbf{k}\cdot\mathbf{x}}\left[\mathsf{e}_{ij}^{(+)}(\mathbf{k})\,\mathsf{e}^{(+)\,lm}(\mathbf{k})+\mathsf{e}_{ij}^{(\times)}(\mathbf{k})\,\mathsf{e}^{(\times)\,lm}(\mathbf{k})\right]\cdot \\ \cdot\left[-4\tilde{\mathscr{S}}_{lm}(\mathbf{k},\tau)+\frac{2}{M_{\rm pl}^2}\tilde{T}_{lm}^{(2)}(\mathbf{k},\tau)\right], \quad (2.42)$$

where $\tilde{T}_{lm}^{(2)}(\mathbf{k},\tau)$ and $\tilde{\mathscr{S}}_{lm}(\mathbf{k},\tau)$ are the Fourier transform of $T_{lm}^{(2)}(\mathbf{x},\tau)$ and $\mathscr{S}_{lm}(\mathbf{x},\tau)$, respectively, and we have expressed the projector in terms of the polarization tensors. In particular $\tilde{\mathscr{S}}_{lm}(\mathbf{k},\tau)$ is the convolution of pairs of first-order scalar perturbations. We consider now one polarization once a time, then for each of them the equation of motion of the related modes reads:

$$h_{\mathbf{k}}^{\prime\prime(\lambda)}+2\mathcal{H}h_{\mathbf{k}}^{\prime(\lambda)}+k^2h_{\mathbf{k}}^{(\lambda)}=\mathsf{e}^{(\lambda)\,lm}(\mathbf{k})\left[-4\tilde{\mathscr{S}}_{lm}(\mathbf{k})+\frac{2}{M_{\rm pl}^2}\tilde{T}_{lm}^{(2)}(\mathbf{k},\tau)\right]. \quad (2.43)$$

For compactness of notation we define:

$$\mathscr{T}_{\mathbf{k}}^{(\lambda)}(\tau)=\mathsf{e}^{(\lambda)\,lm}(\mathbf{k})\left[-4\tilde{\mathscr{S}}_{lm}(\mathbf{k})+\frac{2}{M_{\rm pl}^2}\tilde{T}_{lm}^{(2)}(\mathbf{k},\tau)\right]. \quad (2.44)$$

It is now convenient to refer to $\gamma_{\mathbf{k}}=ah_{\mathbf{k}}$, so that:

$$\gamma_{\mathbf{k}}^{\prime\prime(\lambda)}+\left(k^2-\frac{a^{\prime\prime}}{a}\right)\gamma_{\mathbf{k}}^{(\lambda)}=a(\tau)\,\mathscr{T}_{\mathbf{k}}^{(\lambda)}(\tau). \quad (2.45)$$

The equality (2.43) is a wave equation with a source, whose solution reads

$$\boxed{h_{\mathbf{k}}^{(\lambda)}(\tau)=\frac{1}{a(\tau)}\int\mathrm{d}\tilde{\tau}\,G_{\mathbf{k}}(\tau;\tilde{\tau})\left[a(\tilde{\tau})\,\mathscr{T}(\mathbf{k},\tilde{\tau})\right],} \quad (2.46)$$

where the Green function $G_{\mathbf{k}}$ solves eq.(2.45) with the source given by $\delta(\tau-\tilde{\tau})$, so that it depends only on the evolution of the scale factor. Given eq.(2.46), the expression for the GW correlator can be written in terms of that of the source as

$$\left\langle h_{\mathbf{k}}^{(\lambda)}(\tau)\,h_{\mathbf{k}'}^{(\lambda)}(\tau)\right\rangle=\frac{1}{a^2(\tau)}\int_{\tau_0}^{\tau}\mathrm{d}\tilde{\tau}_1\int_{\tau_0}^{\tau}\mathrm{d}\tilde{\tau}_2\,a(\tilde{\tau}_1)\,a(\tilde{\tau}_2)\,G_{\mathbf{k}}(\tau;\tilde{\tau}_1)\,G_{\mathbf{k}'}(\tau;\tilde{\tau}_2)\cdot \\ \cdot\left\langle\mathscr{T}_{\mathbf{k}}^{(\lambda)}(\tilde{\tau}_1)\,\mathscr{T}_{\mathbf{k}'}^{(\lambda)}(\tilde{\tau}_2)\right\rangle, \quad (2.47)$$

where τ_0 is the time at which the source switches on. Equation (2.47) represents the general expression for the GW power spectrum due to tensor modes which solve

eq.(2.40).
The Green function relative to a De Sitter spacetime reads:

$$G_{\mathbf{k}}\left(\tilde{\tau},\tau\right)=\frac{1}{k^{3}\tau\tilde{\tau}}\left[k\tilde{\tau}\cos\left(k\tilde{\tau}\right)-\sin\left(k\tilde{\tau}\right)\right]\Theta\left(\tau-\tilde{\tau}\right)\,, \tag{2.48}$$

in slow-roll approximation, while for a radiation dominated era is:

$$G_{\mathbf{k}}\left(\tilde{\tau},\tau\right)=\frac{1}{k}\left[\sin\left(k\tau\right)\cos\left(k\tilde{\tau}\right)-\sin\left(k\tilde{\tau}\right)\cos\left(k\tau\right)\right]\Theta\left(\tau-\tilde{\tau}\right)\,. \tag{2.49}$$

When people study eq.(2.40) in the context of inflation, usually set to zero scalar and vector perturbations in the Einstein tensor, i.e. they neglect $\mathscr{S}_{lm}$, since such sources gives rise to negligible contributions to tensor modes with respect to the first-order GW amount. Then the second-order GW equation of motion turns out to be simplified as:

$$\boxed{h_{ij}''+2\mathcal{H}h_{ij}'-\nabla^{2}h_{ij}=\frac{2}{M_{\mathrm{pl}}^{2}}\hat{\Pi}_{ij}^{lm}T_{lm}^{(2)}} \tag{2.50}$$

From this equation, it is clear that *any transverse and traceless contribution to the an anisotropic stress-energy tensor turns out to be a source of GWs*. For a perfect fluid such a term vanishes, while in presence of other fields besides the inflaton, as for many inflationary scenarios, such a source reveals to be significantly efficient.

Possible efficient sources. As anticipated, in some inflationary scenarios, the contribution due to a second-order source to tensor perturbations can be relevant as those of the first order, making a second-order analysis not negligible. The presence itself of the inflaton, provides a second-order source of GWs. Indeed, the combination of perturbations of the inflaton field $\delta\varphi$ constitute a source in eq.(2.50):

$$h_{ij}''+2\mathcal{H}h_{ij}'-\nabla^{2}h_{ij}=-\frac{4}{M_{\mathrm{pl}}^{2}}\hat{\Pi}_{ij}^{lm}\partial_{l}\delta\varphi\partial_{m}\delta\varphi\,. \tag{2.51}$$

This source is present in all the inflationary models driven by a scalar field, but it turns out to be negligible during inflation (later we will see that they act as a source after inflation too).
However, adding new degrees of freedom to the system, the source in (2.50) receives extra contributions. In such a direction, the main possibilities are:

- gauge field coupled or minimally coupled to the inflaton;
- light scalar fields minimally coupled to the inflaton;

- massive scalar field coupled to the inflaton.

In the following section we are going to present in details a specific example for each of these categories. As a common aspect, we will see that a significant classical production of GWs is in general followed by a relevant second-order production of curvature perturbations. Since the latter are well constrained by CMB measurements, usually such bounds put a limit also on the classical GW production.
Then we will see also that a second-order GW production due to inflationary perturbations, takes place also during the post-inflationary period, when curvature perturbations re-enter the horizon.

2.2.2 Inflationary models with gauge particle production

Several models of the so-called Axion inflation [49] have been proposed in literature. The underlying idea of these scenarios is to preserve the slow-roll phase from UV corrections. Here we study a specific model among this class, where a significant GW production takes place.
We consider a system described by the Lagrangian [50, 51]:

$$\mathscr{L} = -\frac{1}{2}\partial_\mu\varphi\partial^\mu\varphi - V(\varphi) - \frac{1}{4}F_{\mu\nu}F^{\mu\nu} - \frac{\varphi}{4f}F_{\mu\nu}\tilde{F}^{\mu\nu}\,, \tag{2.52}$$

where the potential $V(\varphi)$ drives the slow-roll evolution, f is the measure of the coupling between the pseudo-scalar inflaton φ and the gauge field A_μ, $F_{\mu\nu} = \partial_\mu A_\nu - \partial_\nu A_\mu$ is the field strength associated to the gauge field and $\tilde{F}^{\mu\nu} = \tau^{\mu\nu\beta}F_{\alpha\beta}/2$ its dual.
The coupling between the two fields leads to two main phenomena [51–54]: the presence of an efficient source in the GW equation of motion, and the presence of extra source terms in the equation of motion of the inflaton perturbations. The extra amount of tensor modes is then associated to an extra production of scalar perturbations.
More precisely, the equation (2.50) turns out to be:

$$h_{ij}'' + 2\mathcal{H}h_{ij}' - \nabla^2 h_{ij} = -\frac{2}{M_{\rm pl}^2}\hat{\Pi}_{ij}^{lm}\left[-a^2\left(E_iE_j + B_iB_j\right)\right]\,, \tag{2.53}$$

where $E_i \equiv -A_i'/a^2$ and $B_i \equiv (\nabla\times\mathbf{A})_i/a^2$. In this kind of models the gauge field is considered a perturbation of the order $\mathcal{O}(1/2)$, so that the source term in eq.(2.53) is of the first-order in perturbation theory.
In order the background to be well described by a FRW metric, the energy density of the gauge field has to be kept under control, i.e. the backreaction of the gauge field has to be negligible. This issue is discussed in details in [55], where the authors conclude that, in the regime of large scales, current CMB measurements put stronger constraints than the constraint required by keeping under control the backreaction. On the other hand, at small scales, a slow down of the gauge coupling has to supposed in order to avoid a relevant backreaction. The same considerations holds with respect to the perturbative regime of the inflaton and of the gauge field.

In order to solve the equation of motion (2.53), we need to track the evolution of the source, i.e. of the gauge field. Quantizing the gauge field as usual, and working in the Coulomb gauge, i.e. $A_0 = \partial_i A_i = 0$, we have:

$$A_i(\mathbf{x},\tau) = \sum_{\lambda=\pm} \int \frac{d^3\mathbf{k}}{(2\pi)^{3/2}} \varepsilon_i^\lambda(\mathbf{k})\, e^{i\mathbf{k}\cdot\mathbf{x}} \left[A_\lambda(\mathbf{k},\tau)\,\hat{a}_\lambda(\mathbf{k}) + A_\lambda^*(-\mathbf{k},\tau)\,\hat{a}_\lambda^\dagger(-\mathbf{k})\right], \quad (2.54)$$

where $\varepsilon_i^\lambda(\mathbf{k})$ is the helicity vector, and $\lambda = \pm$ indicates the helicity state. The equation of motion of the gauge field modes turns out to be [56]:

$$\frac{d^2 A_\pm(\mathbf{k},\,\tau)}{d\tau^2} + \left[k^2 \pm 2\,\xi\,\frac{k}{\tau}\right] A_\pm(\mathbf{k},\,\tau) = 0\,, \quad (2.55)$$

where

$$\xi \equiv \frac{\dot{\varphi}}{2\,f\,H}\,. \quad (2.56)$$

Notice that the sign of the third term in the equation of motion (2.55) depends on the helicity of the gauge mode. From the equation of motion of the gauge field, it turns out that for positive values of ξ, the + mode is exponentially amplified by a factor $\sim e^{\pi\,\xi}$ for $\xi \gtrsim \mathcal{O}(1)$ [50], while the other is suppressed. From now on we assume, without loss of generality, $\xi > 0$. The amplified modes make efficient the source term in the GW. A_μ in the source can be approximated by the enhanced modes.

The solution of (2.55), for $k\tau \ll \xi$ turns out to be well approximated by:

$$A_+(k,\tau) = \frac{1}{\sqrt{2k}} \left(\frac{k}{2\xi aH}\right)^{1/4} e^{\pi\xi - 2\sqrt{2\xi k/aH}}\,. \quad (2.57)$$

From this expression one can solve the equation of motion (2.53) by (2.46) and then calculate the corresponding GW power spectrum. The results is [51]:

$$P_{\rm T}^{(s)}(k) \simeq 8.6\times 10^{-7} \frac{H^4}{\pi^2 M_{\rm pl}^4} \frac{e^{4\pi\xi}}{\xi^6}\,, \quad (2.58)$$

where the apex (s) means that we are referring to the GW amount due to the classical production only.
Notice that, since not only the inflaton is involved in the inflationary dynamics, an extra production of curvature perturbations is expected with respect to single-field slow-roll inflation.

Chirality and non-gaussianities of scalar and tensor modes. Interestingly, this kind of inflationary scenarios presents peculiar features in some observables, which trace this kind of models and at the same time provide constraints from current observations, i.e. the chiarlity of GWs and the non-gaussianity level of scalar and tensor modes.

The enhancement of only one of the two helicity modes of the gauge field, unveils the parity-violation of the system, which in turn reflects on a non-vanishing chirality of the GW signal. Instead of considering the usual polarization (+) and (×), one can consider another polarization basis, i.e. left and right handed modes, indicated by (+) and (−). This basis reflects the parity/parity-violation of a system. Decomposing the GWs produced by the classical mechanism on such circularly polarized modes, it turns out that the cross-correlation for each of those polarization differs for a large amount. More precisely we have [57]:

$$\left\langle h_+\left(\mathbf{k}\right) h_+(\mathbf{k}')\right\rangle \simeq 8.6\times 10^{-7}\,\frac{H^4}{M_{\rm pl}^4}\,\frac{e^{4\pi\xi}}{\xi^6}\,\frac{\delta^{(3)}\left(\mathbf{k}+\mathbf{k}'\right)}{k^3}\,, \tag{2.59}$$

$$\left\langle h_-\left(\mathbf{k}\right) h_-(\mathbf{k}')\right\rangle \simeq 1.8\times 10^{-9}\,\frac{H^4}{M_{\rm pl}^4}\,\frac{e^{4\pi\xi}}{\xi^6}\,\frac{\delta^{(3)}\left(\mathbf{k}+\mathbf{k}'\right)}{k^3}\,. \tag{2.60}$$

The two contributions differ for about three orders of magnitude. Adding the GW amount due to the vacuum fluctuations of the gravitational field, the overall power spectrum turns out to be:

$$P_{\rm T}^{+} = \frac{H^2}{\pi^2 M_{\rm pl}^2}\left(1+8.6\times 10^{-7}\,\frac{H^2}{M_{\rm pl}^2}\,\frac{e^{4\pi\xi}}{\xi^6}\right)\,, \tag{2.61}$$

$$P_{\rm T}^{-} = \frac{H^2}{\pi^2 M_{\rm pl}^2}\left(1+1.8\times 10^{-9}\,\frac{H^2}{M_{\rm pl}^2}\,\frac{e^{4\pi\xi}}{\xi^6}\right)\,. \tag{2.62}$$

The parity violation is well identified by the following parameter [50]:

$$\Delta\chi = \frac{P_{\rm T}^{+}-P_{\rm T}^{-}}{P_{\rm T}^{+}+P_{\rm T}^{-}} \simeq \frac{8.6\times 10^{-7}\,\frac{e^{4\pi\xi}}{\xi^6}\,\frac{H^2}{M_{\rm pl}^2}}{1+8.6\times 10^{-7}\,\frac{e^{4\pi\xi}}{\xi^6}\,\frac{H^2}{M_{\rm pl}^2}}\,. \tag{2.63}$$

For small ξ, vacuum oscillations dominate the tensor power spectrum and $\Delta\chi\to 0$, while for large values of ξ, i.e. when sourced GW constitute the main contribution, $\Delta\chi\to 1$. The departure of $\Delta\chi$ from zero represents a peculiar feature of this kind of models. In this direction cross-correlations of CMB temperature and polarization could carry significant information [52, 58–61].

Another interesting feature is the non-gaussianity of sourced scalar and tensor modes. The scalar bispectrum has an approximate equilateral shape, more precisely the related non-linear parameter $f_{\rm NL}$ reads [51]:

$$f_{NL}^{\rm equil} \simeq 7.1\times 10^{5}\,\frac{H^6}{|\dot\varphi|^3}\,\frac{e^{6\,\pi\,\xi}}{\xi^9}\,. \tag{2.64}$$

Current bounds on non-gaussianities provided by Planck implies $\xi\lesssim 2.5$ at 95% C.L. at CMB scales [2, 46]. The shape of the three point function for tensor modes has been calculated too in the case of constant ξ. It is found to be close to the equilateral one [59]. The constraints from tensor non-gaussianities, obtained by Planck [46] put a limit on the parameter ξ on CMB scales in agreement with the one obtained from the measurements of CMB scalar bispectrum (2.64).

Adding a minimally coupled pseudo-scalar field. The inflationary parameters which determine the amount of extra GWs, are the same which identify the extra amount of scalar perturbations. Therefore, current observational estimations and bounds on the scalar sector, puts constraints on the GW production too. As we said, the estimated amplitude and the upper bound of non-gaussianities of scalar perturbations at large scales, constrain the parameters ξ. Notice that such a limit is related to CMB scales. More generally one can consider the parameter ξ as evolving in time during inflation. In particular on small scales, current observations allow the presence of scalar perturbations with an amplitude several order of magnitude larger than that on CMB scales. Then, at small scales, larger values of ξ are allowed and a significant amount of second-order GWs, on such scales, can be supposed. Interestingly, with respect to experiments which are sensitive to GWs at small scales, the absence of strict bounds on ξ at small scales, allows a GW signal with an enhancement of the amplitude at such scales. On the other hand, in this regime the backreaction control provides the most stringent constraints (as we will see in section 5.4.2).
These considerations leaded to the idea of introducing a further field in the lagrangian (2.52), i.e. [62]:

$$\mathscr{L} = \frac{1}{2}\partial_\mu\varphi\partial^\mu\varphi - V(\varphi) - \frac{1}{2}\partial_\mu\sigma\partial^\mu\sigma - U(\sigma) - \frac{1}{4}F_{\mu\nu}F^{\mu\nu} - \frac{\sigma}{4f}F_{\mu\nu}\tilde{F}^{\mu\nu}\,, \tag{2.65}$$

with φ the inflaton field, and σ a pseudo-scalar; see also [63, 64]. Now the gauge field is minimally coupled to the main source of curvature perturbations, the inflaton. The background dynamics is still supposed to be driven only by φ. In such a way, the overproduction of curvature perturbations due to the presence of the gauge field is suppressed by the gravitational coupling, while the GW production is the same as the previous model. The lower production of curvature perturbations leads to weak constraints of the parameter ξ due to current cosmological observations. Moreover, the production of scalar perturbations takes place only on those scales for which $\dot{\sigma} \neq 0$, so that limits from CMB measurements can be easily evaded [64].

2.2.3 Inflationary models with scalar particle production

One can consider also inflationary models in which scalar particles are produced [65]. Let us study a system described by the following Lagrangian [65]:

$$\mathscr{L} = -\frac{1}{2}\partial_\mu\varphi\partial^\mu\varphi - V(\varphi) - \frac{1}{2}\partial_\mu\chi\partial^\mu\chi - \frac{g^2}{2}(\varphi-\varphi_0)^2\chi^2\,, \tag{2.66}$$

where φ is the inflaton, $V(\varphi)$ is the potential that drives the dynamics of the inflationary period, χ is an extra scalar field, and, for simplicity, the self-interaction of the field χ is neglected. The mass of the secondary field, m_χ, depends on time, being related to the value of the inflaton field, which is rolling down its potential. When the inflaton φ reaches the value φ_0, m_χ vanishes and the production of χ quanta becomes energetically favoured. During the period around which the inflaton is equal to φ_0, a non-perturbative production of such particles takes place (non-adiabatic period).

After this interval of time the Universe is filled with χ particles besides the inflaton ones (adiabatic period).
The presence of χ quanta gives rise to a contribution to the transverse and traceless term in the stress-energy tensor of the system, which plays the role of a source in the equation of motion of tensor modes. More precisely, the related spatial part which gives rise to the source $T_{ij} = \partial_i\chi\partial_j\chi + \delta_{ij}(...)$, where the factor proportional to the Kronecker delta is projected away by $\hat{\Pi}_{ij}^{lm}$.
The GW production takes place into two different regimes: the phase of non-adiabatic production of the χ quanta and the subsequent period, when the previously produced χ quanta fills the universe. In both cases a GW production takes place.

In order to find the generated amount of GWs, we have to track the evolution of the source in the GW equation of motion. Quantizing χ as usual, its equation of motion is find to be [65]:

$$\chi''(\mathbf{k},\tau) + \omega(\mathbf{k},\tau)^2\chi(\mathbf{k},\tau) = 0\,, \tag{2.67}$$

where

$$\omega(\mathbf{k},\tau)^2 \equiv k^2 + g^2a(\tau)^2\left[\varphi(\tau) - \varphi_0\right]^2 - \frac{a''}{a}\,. \tag{2.68}$$

This expression can be approximated in different ways depending on the system regime.

In order to find the amount of GW generated during the adiabatic phase, when the produced χ quanta fill the universe, we have to track the evolution of χ and to find the initial amount of such field quanta left by the previous non-adiabatic phase. Performing few approximations, the generated amount of GWs for such a phase is find to be [65]:

$$P_{\mathrm{T}}^{(s)}(k) = \left(4.8\times10^{-4}\right)\frac{2H^4}{\pi^2M_{\mathrm{pl}}^4}\left(\frac{g\dot{\varphi}_0}{H^2}\right)^{3/2}\ln^2\left(\frac{\sqrt{g\dot{\varphi}_0}}{H}\right)\left[\frac{(k\tau_0\cos k\tau_0 - \sin k\tau_0)}{|k\tau_0|^3}\right]^2, \tag{2.69}$$

where $\varphi(t=0) = \varphi(\tau=\tau_0) = \varphi_0$. The last factor shows a peculiar scale dependence of this GW amount. However, estimating the values of the physical quantities involved, it turns out that such a contribution evaluated at the scale of its maximum value is several order of magnitude smaller than the GW amount due to vacuum fluctuations of the gravitational field. Therefore we conclude that the presence of a gas of scalar particles evolving adiabatically, generate a negligible correction to the overall inflationary GW amount.

Let us now consider the non-adiabatic period, when χ quanta are rapidly produced. Such a phase is so rapid that the expansion of the universe can be neglected. Under the condition of non-adiabaticity and the approximation of linear evolution of the inflaton, eq.(2.67) takes the form

$$\ddot{\chi} + \left(k^2H^2\tau_0^2 + g^2\dot{\varphi}_0^2t^2\right)\chi = 0\,. \tag{2.70}$$

Solving this equation and calculating the tensor power spectrum by (2.47), one finds that the contribution to the GW amount due to this stage is of the same order of

magnitude of (2.69), modulo a logarithmic term [65]. Therefore, again the GW power spectrum produced in such a phase is negligible with respect to the scale invariant contribution generated by vacuum fluctuations.

It has been noted that also if several bursts of scalar particles production develop during the rolling down of the inflaton (*trapped inflation*; see for example [66]), the generated amount of GW is still several orders of magnitude smaller than the contribution from vacuum oscillations [65].
In summary, the production of a scalar field quanta, due to a coupling to the inflaton as described by eq.(2.66), does not lead to a significant overproduction of GWs.

2.2.4 Inflationary models with extra scalar fields

People proposed inflationary models in which beside the inflaton, other scalar fields are present. The latter is supposed to do not influence the background dynamics and then to do not give rise to isocurvature perturbations. For this reason the are called *spectator* fields. People studied specific scenarios in which such kind of fields are present during inflation. The perturbations of the spectator fields give rise to a second-order source term in the equation of motion of tensor perturbations. Depending on the features of the spectator fields, such a source can be so efficient to generate a significant extra amount of GWs.

Here we present the specific model considered by [67], however similar cases has been studied by [68, 69]. We consider an inflationary scenario described by the following lagrangian:

$$\mathcal{L} = \frac{1}{2}M_{Pl}^2 R + \frac{1}{2}\partial_\mu\varphi\partial^\mu\varphi - V(\varphi) + P(X,\sigma)\ , \tag{2.71}$$

where φ is the inflaton, σ is the spectator field, $X = \frac{1}{2}\partial_\mu\sigma\partial^\mu\sigma$ and P is a generic function of X and σ. The inflaton φ is supposed to drive the background dynamics and to be responsible for curvature perturbations. The spectator field σ is assumed to do not influence the background dynamics, but its perturbations are supposed to induce a second-order production of GWs and of curvature perturbations. The evolution of the spectator field is described by a non-standard dynamics, but by a generic function of the canonical kinetic term and of the fields itself. As usual, we define the propagation speed of sound as $c_s^2 \equiv \partial P/\partial\rho$. From such a lagrangian, it turns out that the propagation speed of σ perturbations is equal to $c_s \equiv P_X/(P_X + P_{XX}\dot{\sigma}_0^2)$ (where σ_0 is the background value). In general, c_s can be different from the speed of light, and we can suppose that it varies with time during the inflationary stage. Therefore we introduce the following parameter:

$$s \equiv \dot{c}_s/Hc_s \neq 0\,. \tag{2.72}$$

We will see that s plays an interesting role in determining the spectral index of second-order GWs. We consider $|s|$ as a small quantity.

Sourced GW. Perturbing the action of the system at third order, a term of the form $\sim h_{ij}\delta\sigma\delta\sigma$ appears. The latter is responsible for the generation of second-order GWs. More precisely, the equation of motion for tensor modes up to second-order, turns out to be [67]:

$$h''_{ij} + 2\mathcal{H}h'_{ij} - \partial_k^2 h_{ij} = \frac{2P_{\rm X}}{M_{Pl}^2}\hat{\Pi}_{ij}^{lm}\partial_l\delta\sigma\partial_m\delta\sigma\,, \tag{2.73}$$

where $P_{\rm X}$ is the derivative of P with respect to X and $\hat{\Pi}_{ij}^{lm}$ is the projector tensor we defined in section 2.2.1. Solving this equation, the power spectrum amplitude of such tensor modes, at a chosen pivot scale, turns out to be well approximated by:

$$A_T^{(s)} \simeq \frac{8}{15\pi c_s^3}\frac{H^4}{M_{Pl}^4}\,, \tag{2.74}$$

where H and c_s are evaluated at the pivot scale. Considering the scale dependence of the latter, the related spectral index is found to be:

$$n_{\rm T}^{(s)} = -4\epsilon - 3s\,, \tag{2.75}$$

where quantities denoted by (s) refers to GWs produced by the classical mechanism. Now it is clear that the propagation speed $c_{\rm s}$ plays a significant role in determining the amount of produced GWs. In particular, for $c_{\rm s} \ll 1$ the source becomes more efficient than in the case of $c_{\rm s} = 1$, and a relevant GW production takes place. Moreover, for negative value of the parameter s, the spectral index of the second-order GWs can reach positive values, i.e. the sourced GW power spectrum can be blue.
The overall amount of produced GWs is given by the sum of two contributions: one due to quantum fluctuations of the gravitational field, and one which corresponds to the second-order production due to the presence of the spectator field σ. Considering the usual results for tensor perturbations from quantum fluctuations of the gravitational field, see eq.(2.27), the whole power spectrum for GWs results:

$$P_{\rm T}(k) \simeq \frac{2H^2}{M_{Pl}^2}\left(\frac{k}{k_*}\right)^{-2\epsilon} + \frac{8}{15\pi c_s^3}\frac{H^4}{M_{Pl}^4}\left(\frac{k}{k_*}\right)^{-4\epsilon-3s}\,, \tag{2.76}$$

where H and c_s are evaluated at $k = k_*$.
Equation (2.76) shows that for sufficiently small values of the propagation speed $c_{\rm s}$ the amplitude of sourced GWs can reach significant values and in principle, it can exceed the amplitude of GWs generated by quantum fluctuations of the gravitational field. Moreover, if $c_{\rm s}$ is getting smaller during inflation, the related spectral index can be positive, so that the sourced GWs can reach a significantly large amplitude at the scale of laser interferometer experiments [9].

On the other hand, the overproduction of scalar perturbations is relevant. Perturbations of the spectator field play the role of a source in the equation of motion of curvature perturbations too. The inflationary parameters which describe the sourced curvature perturbations are the same which determine the GW amount produced classically. Therefore, bounds on the curvature power spectrum provide limits on the same inflationary parameters which determines the amount of GWs (for more details see section 5.4.1).

Gravitational-wave production during reheating. As seen in section 2.2.1, the presence of large, time-dependent inhomogeneities in the distribution of the energy-density of the Universe leads to a classical GW production. Such a situation could also occur during the reheating stage.

The production of gravitational radiation during reheating was first pointed out by Khlebnikov and Tkachev in [6]. The GW signal generated at that time, in principle, represents a source of information on the inflationary physics and the reheating period itself. Gravitational waves remain decoupled since the moment of their production and therefore the features of their spectrum represent a very interesting probe of the physics that generate them, such as the coupling between the inflaton and other fields ([70] and refs. therein). In this sense, the GW signal produced during reheating as a particular relevance since the others physical observables generated in the same period are washed away by the subsequent thermalization, thus representing a unique way of investigating such a phase of the universe.
At the end of inflation, the field that has driven the accelerated expansion starts oscillating around the minimum of its potential. In such a way it produces elementary particles which interact to each other, eventually leading to a state of thermal equilibrium. In many scenarios, oscillations are large and coherent and lead to a non-perturbative process, in which the inflaton energy is explosively moved to a coupled-energy sector [71–73]. In such a case a perturbative description does not work, being the process violent and rapidly efficient. People call it *preheating*. After such an explosive stage the produced particles are not in thermal equilibrium, contrary to the case of the perturbative mechanism; so, another phase is needed to get thermalized radiation.

The preheating is a scenario of gravitational radiation generation [74–76], since it is dominated by a production of highly inhomogeneous, non-thermal fluctuations of the inflaton and other fields coupled to it. Right after preheating, turbulent interactions between scalar waves take place, providing another phase of GW production. Then the system settles into thermal equilibrium.
The gravitational radiation generated by this process is strictly peaked on frequency, which it turns out to be around $\sim 10^5 - 10^8$Hz, with an amplitude that can reach $\Omega_{\rm GW} \simeq 10^{-7}$ (see section 2.5 for the definition of $\Omega_{\rm GW}$). Unfortunately, this kind of signal is outside of the range of frequencies to which current and planned experiments for GW detection are sensitive.

2.3 Gravitational waves from inflation built on modified gravity theories

The tensor power spectrum obtained in eq.(2.27) corresponds to the GW amount we expect from quantum fluctuations of gravitational field, where the calculations are based on General Relativity (GR). If this is not the case, the gravitational field could present features which in turn could appear in the tensor power spectrum and not only.

Several inflationary models built on modified gravity theories have been studied, and for many of them the predictions for the related tensor modes have been calculated. The mechanism of tensor modes production is the same as for inflationary scenarios built on GR, i.e. the amplification of quantum fluctuations of the gravitational field. The most basic way to modify GR is to introduce a new scalar degree of freedom in the Hilbert-Einstein action, i.e. building up a scalar-tensor theory. One can also add more then one degrees of freedom, as for example assigning a non-vanishing mass to the graviton. Scalar-tensor theories have been widely studied. The most general Lagrangian of a tensor-to-scalar theory in a four dimensional space-time, which leads to second-order equations of motion for the fields, albeit starting from higher order derivative terms, is the Horndeski one [77–80]. Inside of this class, several theories have been investigated also in relation to inflation, such as for example the *kinetically driven G-inflation* and a the *potential-driven slow-roll inflation* [81].

In the context of inflationary perturbations, the main signature of modification of GR are the deviation from the speed of light of the propagation velocity of tensor modes [81, 82] and the possible appearing of further polarization states besides the two predicted by GR.

Notice that gravitons decouple when the temperature of the universe is about $T_{\rm dec} \simeq M_{\rm pl}$, then inflationary GWs carry information about the state of the universe at an extremely high energy, where the main physics theories are still not understood, in particular the theory of gravity at so high energy could differ significantly from GR. Therefore, it is allowed to consider that GWs generated during the inflationary process can present different features from those that we observe at low energy scales, as for example GWs generated by the merger of compact objects. As a consequence, current limits on modified gravity theories obtained by compact object merger [83–85], do not exclude that, at the energy scales of inflation, the theory of gravity, and then GWs, significantly deviates from GR. For this reason, in the inflationary context, we can elude current limits on the graviton mass and the speed of propagation of GWs obtained by observing the GW signals of compact objects mergers.

A non-vanishing graviton mass in general enters in the spectral index of the tensor power spectrum, while a deviation of the propagation speed leaves a signature in the amplitude of tensor perturbations. Furthermore, in these kinds of scenarios, often the scalar sector presents features which deviate from the predictions of single-field slow-roll inflation [81]. Imprints of an inflationary scenario built on a modified gravity theory, can be included also in the higher-order correlation function (also between scalar and tensor modes) [86–88].

Reasoning form another point of view, one can build up an inflationary model starting from the symmetries that one want to preserve, this is the approach of Effective Field Theory of inflation (EFT) [89]. Proceeding in such a way and breaking the temporal diffeomorphism, preserving the spatial ones, new parameters describing the gravitational field turn out. Moreover, when also broken spatial diffeomorphism are

considered over than the usual broken temporal symmetry [90, 90], new relevant features of tensor modes appear. Notice that at the end of inflation, the inflaton can arrange itself to recover space-reparametrization symmetry.
Considering such broken symmetries, the most general action at second order for the tensor sector turns out to be [91]:

$$S^{(2)} = \frac{M_{\rm pl}^2}{8} \int dt\, d^3\mathbf{x}\; \alpha a^3\left(t\right) n\left(t\right) \left[\dot{h}_{ij}^2 - \frac{c_{\rm T}^2\left(t\right)}{a^t}\left(\partial_l h_{ij}\right)^2 - m_{\rm T}^2\left(t\right) h_{ij}^2\right] \tag{2.77}$$

where $c_{\rm T}$ plays the role of the propagation speed of tensor modes, $m_{\rm T}$ of the graviton mass and α is a constant, which here we put equal to one. The appearing of the graviton mass is a signature of the broken spatial diffeomorphism. With an analogous procedure of what we did in section 2.1, for a pure de Sitter spacetime, and for $c_{\rm T}$ and $m_{\rm T}$ constant in time, the tensor power spectrum following from the lagrangian (2.77), reads:

$$P_{\rm T} = \frac{H^2}{4\pi M_{pl}^2}\left(\frac{k}{k_*}\right)^3 \left|H_\nu^{(1)}\left(\frac{c_{\rm T}k}{k_*}\right)\right|^2 , \tag{2.78}$$

where $H_\nu^{(1)}$ is the Hankel function of fist kind and

$$\nu = \frac{3}{2}\sqrt{1 - \frac{4m_{\rm T}^2}{9H^2}}\,. \tag{2.79}$$

In the limit of $|m_{\rm T}/H| \ll 1$, the tensor mode power spectrum is found to be well parametrized by a power-law and it reads:

$$P_{\rm T} = \frac{H^2}{2\pi^2 M_{\rm pl}^2 c_{\rm T}^3}\left(\frac{k}{k_*}\right)^{n_{\rm T}} \qquad \text{with} \qquad n_{\rm T} = \frac{2}{3}\frac{m_{\rm T}^2}{H^2}\,. \tag{2.80}$$

As visible, the propagation speed $c_{\rm T}$ influences the amplitude of tensor mode power spectrum, while the graviton mass enters the related spectral index. Notice that in general $c_{\rm T}$ and $m_{\rm T}$ are functions of the scale. For positive values of the mass, the spectral index turns out to be blue, i.e. in this context vacuum fluctuations of the gravitational field can lead to an enhancement of the tensor amplitude at small scales. Notice that such a behaviour is forbidden for inflationary models built on GR due to the Null Energy Condition.
The possibility of a blue power spectrum makes this kind of inflationary scenario interesting for experiments of GW detection sensitive to small scales; see section 5.1.

2.4 Information carried by inflationary gravitational waves

The GW signal produced by the inflationary mechanism represents the possibility of deepen the physics of the inflationary paradigm, to test such a theory itself and to unveil new details about the underline theory of gravity. Inflationary GWs then represent an amazing source of cosmological information.

A direct or indirect detection of a primordial GW background, is usually considered as a *smoking gun* probe of the inflationary paradigm. This fact is the main motivation which leaded many people to search for a probe of the presence of inflationary GWs. However, to be precise, the production of a primordial GW background is not predicted only by the inflationary model of the early universe. Alternative to inflation have been proposed in last decades [92–95], and for many of them a production of a stochastic GW background is expected. Notice however that the inflationary model still remains the most elegant to explain current cosmological observations. In the direction of testing the inflationary paradigm itself, the validation of the consistency relation (2.33) is widely considered the strongest way. This fact makes the search for primordial GWs of massive importance in order to clarify the physics of the early universe.
Moreover, an estimation of the amplitude of inflationary GWs, would provide an estimation of the energy scale V of the inflationary process. The latter is related to the Hubble parameter by the Friedman equation as: $V = 3M_{pl}^2 H^2$. A measurement of the amplitude of scalar perturbations, provides an estimation of the combination H^2/ϵ at the corresponding scale, see eq.(1.44), so that it is not enough in order to extract the Hubble scale. On the other hand, the amplitude of tensor perturbations, i.e. (2.29), can provides the value of H and then V could be extracted. Usually such a relation is expressed in terms of the tensor-to-scalar ratio, it reads [96]:

$$V = \left(1.88 \times 10^{16}\text{GeV}\right)^4 \frac{r}{0.10}\,. \tag{2.81}$$

Up to now we have only un upper bound on r, i.e. $r_{0.05} < 0.09$ at 95% C.L. [97] at a pivot scale of $k_* = 0.05\text{Mpc}^{-1}$, and then on the energy scale of inflation $H\left(k_*\right) \lesssim 10^{13}\text{GeV}$ [2].

An estimation of the tensor-to-scalar ratio would provide also the amount of the inflaton excursion, that is the variation on the expectation value of φ from the horizon crossing of the large scales to the end of inflation. Restoring the definition of the e-foldings N, we can express the evolution in time of the field via such a quantity:

$$r = \frac{8}{M_{\text{pl}}}\left(\frac{\mathrm{d}\varphi}{\mathrm{d}N}\right)^2\,. \tag{2.82}$$

Integrating $\mathrm{d}\varphi$ from the horizon crossing of a pivot scale to the end of inflation and making explicit the dependence of r on N, we have

$$\frac{\Delta\varphi}{M_{\text{pl}}} = \left(\frac{r\left(\varphi_{\text{cross}}\right)}{8}\right)^{1/2} \int_{N(\varphi_{\text{cross}})}^{N(\varphi_{\text{end}})} \left(\frac{r\left(N\right)}{r\left(\varphi_{\text{cross}}\right)}\right)^{1/2} \mathrm{d}N\,. \tag{2.83}$$

One can consider the second factor as the effective number of e-foldings

$$N_{\text{e}} \equiv \int_{N(\varphi_{\text{cross}})}^{N(\varphi_{\text{end}})} \left(\frac{r\left(N\right)}{r\left(\varphi_{\text{cross}}\right)}\right)^{1/2} \mathrm{d}N\,, \tag{2.84}$$

so that

$$\frac{\Delta\varphi}{M_{\rm pl}} = \left(\frac{r\left(\varphi_{\rm cross}\right)}{8}\right)^{1/2} N_{\rm e}\,. \tag{2.85}$$

$N_{\rm e}$ depends on the evolution of the tensor-to-scalar ratio during inflation and so it is model-dependent. In particular for the single-field slow-roll model, r is constant up to the second order, then the integral (2.84) becomes simply the number of e-foldings. Keeping this approximation, in agreement with the chosen pivot scale, one can find a lower bound for the field excursion. The first evaluation of this bound was given by Lyth [98], putting $N_{\rm e} \simeq 30$ we obtain [99, 100]

$$\frac{\Delta\varphi}{M_{\rm pl}} \gtrsim 1.06 \left(\frac{r\left(\varphi_{\rm cross}\right)}{0.01}\right)^{1/2}\,. \tag{2.86}$$

From this relation we can conclude that a model producing a large amount of GWs would involve a field excursion of the order of the Planck mass. This constraint leads to a classification of inflationary models according to the field excursion: *small field* and *large field* models, where the discriminating value is the Planck mass. Being this inflationary feature strictly related to the UV completion of gravity, constraining the inflaton excursion could provide useful information about the correct quantum gravity theory [100–104].

Information about inflationary GWs would also open the chance of investigating the theory of gravity at high energy scales. In fact, as we saw, inflationary models built on modified gravity theories in general predicts a tensor power spectrum with different features with respect to inflationary scenarios built on GR.

Moreover, we saw that GWs can be produced by two main kinds of mechanism during inflation. Interestingly, the features of GWs produced by the *classical* process, are determined by the physics of other possible fields involved in the accelerated dynamics, such as the nature of such fields and their coupling with the other degrees of freedom involved in the process. In light of this, inflationary GWs represent also the opportunity of discriminating among the variety of inflationary models and of putting constraints on several inflationary scenarios. In table 2.1, we summarized several representative inflationary models, highlighting the features related to the associated GW production.

2.5 Stress-energy tensor and energy-density of gravitational waves

Consider the weak-field limit, where GWs can be described as spacetime ripples propagating on a *fixed* background.
Vacuum field equations read $G_{\mu\nu} = 0$, which is equivalent to $R_{\mu\nu} = 0$. Making explicit the Ricci tensor as a sum of a background term and perturbative terms up to second

GW PRODUCTION	Discriminant	Specific discriminant	Examples of specific models	Produced GW
Vacuum oscillations quantum fluctuations of the gravitational field stretched by the accelerated expansion	**theory of gravity**	General Relativity	*single-field slow-roll*	*broad spectrum*
			all other models in GR	broad spectrum
		MG/EFT approach	G-Inflation	broad spectrum
			Potential-driven G-Inflation	broad spectrum
			EFT approach	broad spectrum
Classical production second-order GW generated by the presence of a source term in GW equation of motion	**source term**	vacuum inflaton fluctuations	*all models*	*broad spectrum*
		fluctuations of extra scalar fields	inflaton+spectator fields	broad spectrum
			curvaton	broad spectrum
		gauge particle production	pseudoscalar inflaton+gauge field	broad spectrum
			scalar infl.+pseudoscalar+gauge	broad spectrum
		scalar particle production	scalar inflaton+ scalar field	peaked
		particle production during preheating	chaotic inflation	peaked
			hybrid inflation	peaked

Table 2.1: Main mechanisms of GW production during inflation. In the fourth column, some examples for each of the mentioned case are reported. Some of them are discussed in the following sections: *"single-field slow-roll"* section 2.1, *"G-Inflation"* and *"EFT approach"* section 2.3, *"spectator fields"* section 2.2.4, *"curvaton"* section 2.7, *"pseudoscalar inflaton+gauge field"* and *"scalar infl.+pseudoscalar+gauge"* section 2.2.1, *"scalar inflaton+scalar field"* section 2.2.3. For other model see for example [18]. To clarify the notation: *"EFT approach"* refers to all models encoded in the generic action used in the EFT approach to inflation. *"Broad spectrum"* means that a power spectrum, broad on a large range of scales is expected, while *"peaked"* indicates a signal peaked on a narrow range of frequencies.

order, $R_{\mu\nu} = \bar{R}_{\mu\nu} + R^{(1)}_{\mu\nu}(h) + R^{(2)}_{\mu\nu}(h) + \mathcal{O}(h^3)$, one can deduce from the vacuum equations, how the presence of the GWs affects the background $\bar{R}_{\mu\nu}$ (where, for example, $R^{(2)}_{\mu\nu}(h)$ indicates the contribution to the Ricci tensor which contains terms as $\sim h \cdot h$). The terms that play this role then can be interpreted as a stress-energy tensor $t_{\mu\nu}$ due to the presence of GWs. In this direction it is useful to note that $R_{\mu\nu}$ can be written as a sum of two kinds of terms, those representing a smooth contribution and others which encode the fluctuating part. Each of the two contributions vanishes on its own [42]. The background term $\bar{R}_{\mu\nu}$ varies only on large scales with respect to some coarse-graining scale, therefore we are interested in the equation for the smooth contributions. The only linear term $R^{(1)}_{\mu\nu}(h)$ solves by itself $R^{(1)}_{\mu\nu}(h) = 0$[1]. Then, the

[1]More precisely, the perturbation $h_{\mu\nu}$ may contain non-linear corrections $j_{\mu\nu}$, which lead to a non-linear term, that we call $R^{(1)\mathrm{NL}}_{\mu\nu}(j)$. The latter contributes to the fluctuating part of the Ricci tensor, but, being non-linear, is not constrained by the equation just shown in the text. In fact, in general, smoothed parts can be obtained only from combinations $\sim h_{\mu\nu}h_{\rho\sigma}$, where the two high frequencies of each perturbation $h_{\mu\nu}$ can cancel each other, leading to a smooth contribution [48].

remaining equation for the smooth part of the vacuum equation reads [42, 48]:

$$\bar{R}_{\mu\nu} + \langle R^{(2)}_{\mu\nu} \rangle = 0 \,, \tag{2.87}$$

where $\langle ... \rangle$ indicates the average over several wavelengths which extracts the smooth contribution with respect to the coarse-graining scale. An analogous reasoning can be enlarged to the Einstein tensor, so that one gets the following Einstein equations, in vacuum:

$$\bar{G}_{\mu\nu} = \bar{R}_{\mu\nu} - \frac{1}{2}\bar{R}\bar{g}_{\mu\nu} = \langle R^{(2)}_{\mu\nu} \rangle - \frac{1}{2}\bar{g}_{\mu\nu}\langle R^{(2)} \rangle \,. \tag{2.88}$$

The terms on the RHS tell how the presence of GW affects the background metric, then they can be interpreted as the GW stress-energy tensor $t_{\mu\nu}$, apart from a factor 8πG. In terms of the tensor perturbations of the metric it reads [42]:

$$t_{\mu\nu} = \frac{1}{32\pi G}\langle \partial_\mu h_{ij} \partial_\nu h^{ij} \rangle \,; \tag{2.89}$$

see also [48, 105]. From the previous equation, the GW energy-density, on a FRW background, reads

$$\rho_{\rm GW}(\tau) = \frac{1}{32\pi G a^2}\langle h'_{ij}(\mathbf{x}, \tau)\, h'^{ij}(\mathbf{x}, \tau) \rangle \,. \tag{2.90}$$

However, more often people refer to the GW energy-density per logarithmic frequency interval, normalized to the critical density $\rho_{\rm c} \equiv 3H^2/8\pi G$,

$$\Omega_{\rm GW}(k, \tau) \equiv \frac{1}{\rho_{\rm c}} \frac{{\rm d}\rho_{\rm gw}}{{\rm d}\ln k} \,. \tag{2.91}$$

People usually refer also to $h^2\Omega_{\rm GW}$, where $h \equiv H_0/100$, in order to take a part observations uncertainties on the value of the Hubble parameter.

2.6 Post inflationary evolution

Obtained the predictions for the tensor power spectrum produced by the inflationary mechanism, now we want to calculate the related present time GW spectral-energy density. This is interesting in light of the current and upcoming experiments of direct GW detection. Primordial tensor modes are stretched outside the causal region by the accelerated expansion, in such a regime their amplitude is frozen. After inflation, they re-enter subsequently the horizon starting evolving and giving rise to a stochastic GW background which permeates the universe.

Being super-horizon tensor modes frozen, independently on the evolution of the scale factor, the general solution of eq.(2.2) in terms of Fourier modes can be written as:

$$h_k(\tau) \equiv h_{k,\rm prim} T_{\rm h}(\tau, k) \,, \tag{2.92}$$

where $h_{k,\rm prim}$ is the amplitude at horizon crossing, and the transfer function $T_{\rm h}(\tau, k)$ describes the evolution of the GW mode after the time they enter the horizon during

later stages after inflation. The transfer function is normalized such that $T_{\rm h}(\tau, k) \to 1$ as $k \to 0$.
Modes that are inside the horizon, start oscillating with the amplitude damped by a factor $1/a$. In particular, during radiation and matter dominance the scale-factor evolves as $a \sim \tau$ and $a \sim \tau^2$ respectively, so that eq.(2.2) becomes a Bessel equation with the following solutions respectively:

$$h_k(\tau) = h_{k,\rm prim} j_0(k\tau) \ , \qquad h_k(\tau) = h_{k,\rm prim}\left(\frac{3j_1(k\tau)}{k\tau}\right) , \tag{2.93}$$

where j_0 and j_1 are the Bessel functions. Notice that the damping factor depends on the frequency of the GW. During an era of pure dominance of the cosmological constant, the spacetime assumes a de Sitter metric so that the scale factor evolves in a exponential way, as during inflation in case of $\epsilon = 0$. Then, in such an epoch, the form of the solution of the GW equation of motion (2.2) is given by eq.(2.19).

The transfer function. In light of the behaviour of the GW solutions along the history of the universe, one can calculate the GW spectral energy density at a generic time τ. In terms of the transfer function $T_{\rm h}(k, \tau)$ defined in (2.92), for modes well inside the horizon, it turns out to be well approximated by [105]:

$$\Omega_{\rm GW}(k, \tau) = \frac{1}{12}\left(\frac{k}{aH}\right)^2 T_{\rm h}^2(k, \tau) P_T(k) \ , \tag{2.94}$$

where $P_{\rm T}$ is the primordial power spectrum defined in (2.25) and it refers to the primordial amplitude $h_{k,\rm prim}$. Calculations to obtain this expression are performed in appendix B.
Solving the GW equation of motion for radiation and matter dominated eras, one finds that in both cases the amplitude depends on the wavenumber and is modulated by the inverse of the scale factor with the corresponding time dependence (while the oscillatory behaviour is described by Bessel functions). This damping factor is what we are interested in. Notice that the present GW amount is a superposition of tensor modes that re-entered the horizon in different epochs of the history of the Universe, so that we have to take into account that each mode k undergoes a different damping, depending on the time it evolves sub horizon and on the specific time dependence of the scale-factor during such an evolution.
Well inside the matter dominated epoch, the solution of eq.(2.2) for all modes is

$$h_k(\tau) = h_{k,\rm prim}\left(\frac{3j_1(k\tau)}{k\tau}\right) , \tag{2.95}$$

where $j_1(k\tau_0) \to 1/\left(\sqrt{2}k\tau_0\right)$ in the limit $k\tau_0 \to 0$. Here the subscript 0 denotes the present time. Averaging over time the previous solution to extract the amplitude behaviour, one finds the factor $1/a$ mentioned above. Then the GW spectral energy density spectrum today turns out to be:

$$\Omega_{\rm GW}(k, \tau_0) = \frac{1}{12}\left(\frac{k}{aH}\right)^2 P_{\rm T}(k)\left(\overline{\frac{3j_1(k\tau_0)}{k\tau_0}}\right)^2 (\ldots) \ , \tag{2.96}$$

where the last factor embodies all terms arising from the change of the scale factor from the horizon re-entry to the present time, for a given mode k, and it will be specified now.
A first damping factor comes from the change of the relativistic degrees of freedom [105, 106]:

$$\left(\frac{g_*\left(T_{\rm in}\right)}{g_{*0}}\right)\left(\frac{g_{*\rm s0}}{g_{*\rm s}\left(T_{\rm in}\right)}\right)^{4/3}\,, \tag{2.97}$$

where g_* are the relativistic degrees of freedom, $g_{*\rm s}$ its counterpart for the entropy, *in* denotes the time when a considered mode enters the horizon, and $T_{\rm in}$ is given by [107]

$$T_{\rm in}\left(k\right) \simeq 5.8\times 10^6{\rm GeV}\left(\frac{g_{*\rm s}\left(T_{\rm in}\right)}{106.75}\right)^{-1/6}\left(\frac{k}{10^{14}{\rm Mpc}^{-1}}\right)\,. \tag{2.98}$$

Another function is needed in order to connect GWs that enter the horizon before and after matter-radiation equality at $t = t_{\rm eq}$ [108]:

$$T_1^2\left(x_{\rm eq}\right) = \left(1 + 1.57x_{\rm eq} + 3.42x_{\rm eq}^2\right)\,, \tag{2.99}$$

where $x_{\rm eq} = k/k_{\rm eq}$ and $k_{\rm eq} \equiv a\left(t_{\rm eq}\right)H\left(t_{\rm eq}\right) = 7.1\times 10^{-2}\Omega_{\rm m}h^2{\rm Mpc}^{-1}$, where $\Omega_{\rm m}$ is the matter energy density. Analogously, a transfer function is needed to describe the change in the expansion rate at the end of reheating $t = t_{\rm R}$, when the Universe moves from being inflaton-dominated to radiation-dominated [107]:

$$T_2^2\left(x_{\rm R}\right) = \left(1 - 0.32x_{\rm R} + 0.99x_{\rm R}^2\right)^{-1}\,, \tag{2.100}$$

where $x_{\rm R} = k/k_{\rm R}$ and $k_{\rm R} \simeq 1.7\times 10^{14}{\rm Mpc}^{-1}\left(g_{*\rm s}\left(T_{\rm R}\right)/106.75\right)^{1/6}\left(T_{\rm R}/10^7{\rm GeV}\right)$. In terms of frequency it corresponds to

$$f_{\rm R} \simeq 0.026\,{\rm Hz}\left(\frac{g_{*\rm s}\left(T_{\rm R}\right)}{106.75}\right)^{1/6}\left(\frac{T_{\rm R}}{10^6{\rm GeV}}\right)\,, \tag{2.101}$$

which is the frequency at which the change in the frequency dependence of the spectrum due to the reheating stage appears. In summary, the whole transfer function $T_{\rm h}^2\left(k\right)$ reads

$$T_{\rm h}^2\left(k\right) = \Omega_{\rm m}^2\left(\frac{g_*\left(T_{\rm in}\right)}{g_{*0}}\right)\left(\frac{g_{*\rm s0}}{g_{*\rm s}\left(T_{\rm in}\right)}\right)^{4/3}\left(\frac{\overline{3j_1\left(k\tau_0\right)}}{k\tau_0}\right)^2 T_1^2\left(x_{\rm eq}\right)T_2^2\left(x_{\rm R}\right)\,. \tag{2.102}$$

This expression tells that, once the values for the degrees of freedom evaluated at various epochs and $\Omega_{\rm m}$ are given, the GW spectral energy density is a function of the tensor-to-scalar ratio r and of the reheating temperature $T_{\rm R}$; see also [109]. The so-obtained GW spectral energy density at the present time, is shown in fig.2.1 for different primordial parameters. The whole expression for the GW spectral-energy density at the present time is then given by (2.94), where $T_{\rm h}\left(k,\tau\right)$ is given by (2.102). Notice that the behaviour of the Bessel function j_1 with respect to k, makes the scale

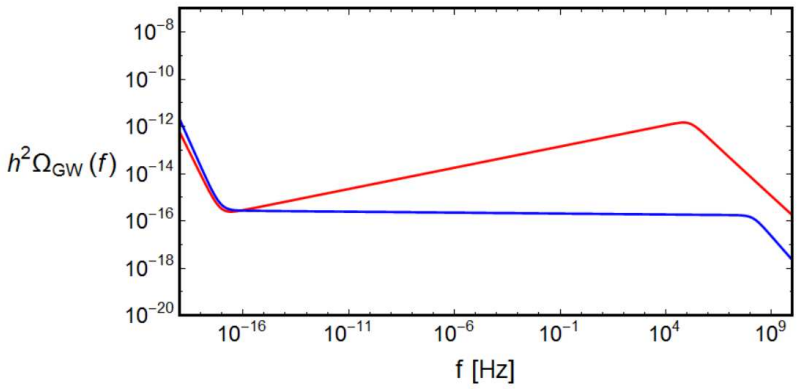

Figure 2.1: GW spectral energy density due to an inflationary GW production evaluated at the present time. Each curve corresponds to the following primordial parameter values: $r = 0.07$ at $f = 10^{-17}$Hz, $n_{\rm T} = 0.18$, $T_{\rm reh} = 10^5$GeV (red) and $r = 0.07$ at $f = 10^{-17}$Hz $n_{\rm T} = -0.008$, $T_{\rm reh} = 10^8$GeV (blue).

dependence of the transfer function T_h well approximated by $1/k$. Therefore, finally the GW spectral energy density reflects the same scale dependence of the primordial GW signal.
It has been studied also the fact that the neutrino free-streaming when the universe is at a temperature of about 1MeV left an imprint on the present time GW spectral energy density [105]. However, with respect to current and planned observational capabilities it is a phenomenon which can be safely neglected.

2.7 Second-order gravitational waves produced after inflation

Second-order primordial GWs are produced not only during inflation. After the accelerated expansion, scalar perturbations start entering the horizon, constituting a source for GWs. More in general, if we explain the growth of structures by the presence of initial scalar perturbations, without specifying the origin of the latter, the second-order production of GWs due to such scalar perturbations, takes place [110–112]. The features of this gravitational radiation only depends on the details of the scalar perturbations at the time of their horizon crossing, independently on their origin mechanisms. These second-order GWs clearly contributes to the present time GW spectral energy density and to the tensor power spectrum which left its imprint on the CMB at the time of photon decoupling. From a certain viewpoint, this contribution to the GW energy density is a contaminant with respect to the signal of inflationary origin [110]. Moreover, for low energy scale of inflation, the amplitude of the second-order GWs generated after inflation, can be comparable with the inflationary signal, making it an interesting phenomenon to be studied.

Primordial scalar perturbations re-enter the causal region during the post-inflationary

radiation and matter dominated eras. At that time the universe is described by a FRW perturbed metric with an energy-momentum tensor of a fluid to be specified as radiation or matter. In this context we consider the full second-order equation (2.34). The stress-energy tensor of a general perfect fluid perturbed at second order reads [30]:

$$T^{(2)i}_{\ j} = \left(\rho^{(0)} + P^{(0)}\right) v^{(1)i} v^{(1)}_j + P^{(0)} \pi^{(2)i}_{\ j} + P^{(1)} \pi^{(1)i}_{\ j} + P^{(2)} \delta^i_{\ j} \,, \tag{2.103}$$

where in order ρ, P, v and Π are the energy density, the pressure, the velocity and the anisotropic stress, to be specified in case of radiation or matter dominance. Using first-order Einstein constraint equations, the first-order perturbations of the stress-energy tensor can be written in terms of the linear metric perturbations and of background quantities, so that the second contribution in (2.34) becomes:

$$\begin{aligned} \hat{\Pi}^{lm}_{ij} \frac{2}{M^2_{\rm pl}} T^{(2)}_{lm} = &- \frac{4}{3\left(1+\omega\right)\mathcal{H}^2} \partial_l \left(\Phi' + 3\mathcal{H}\Psi\right) \partial_m \left(\Phi' + 3\mathcal{H}\Psi\right) \\ &- \frac{2c^2_{\rm S}}{3\omega\mathcal{H}^2} \left[3\mathcal{H}\left(\mathcal{H}\Psi - \Phi'\right) + \nabla^2\Phi\right] \partial_l\partial_m \left(\Psi - \Phi\right) \,, \end{aligned} \tag{2.104}$$

where $\omega \equiv P^{(0)}/\rho^{(0)}$, $\Psi \equiv \Psi^{(1)}$, $\Phi \equiv \Phi^{(1)}$ and $c_{\rm S} = P^{(1)}/\rho^{(1)}$. The whole source term in (2.40) then reads:

$$\begin{aligned} \hat{\Pi}^{lm}_{ij} \left[-4\mathscr{I}_{lm} + \frac{2}{M^2_{\rm pl}} T^{(2)}_{lm}\right] = &2\Psi\partial_l\partial_m\Psi - 2\Phi\partial_l\partial_m\Psi + 4\Phi\partial_l\partial_m\Phi + 4\Psi\partial_l\partial_m\Psi + \\ &+ \partial_l\Psi\partial_m\Psi - \partial_l\Psi\partial_m\Phi - \partial^l\Phi\partial_m\Psi + 3\partial_l\Phi\partial_m\Phi + \\ &- \frac{4}{3\left(1+\omega\right)\mathcal{H}^2} \partial_l \left(\Phi' + 3\mathcal{H}\Psi\right) \partial_m \left(\Phi' + 3\mathcal{H}\Psi\right) + \\ &- \frac{2c^2_{\rm S}}{3\omega\mathcal{H}^2} \left[3\mathcal{H}\left(\mathcal{H}\Psi - \Phi'\right) + \nabla^2\Phi\right] \partial_l\partial_m \left(\Psi - \Phi\right) = \\ &\equiv \mathcal{S}_{ij}\left(\mathbf{x}, \tau\right) \,, \end{aligned} \tag{2.105}$$

In order to solve the equation of motion, we move to the Fourier space analogously of what we did in eq.(2.43):

$$h^{\prime\prime(\lambda)}_{\mathbf{k}} + 2\mathcal{H} h^{\prime(\lambda)}_{\mathbf{k}} + k^2 h^{(\lambda)}_{\mathbf{k}} = \mathsf{e}^{(\lambda)\, ij}\left(\mathbf{k}\right) \tilde{\mathcal{S}}_{ij}\left(\mathbf{k}, \tau\right) \,. \tag{2.106}$$

Scalar perturbations present in the source are those appearing in the perturbed metric (1.28), where we did not specify any gauge. However, deriving eq.(2.40), we neglected vector perturbations and we considered only the tensor part of the h_{ij} perturbations in (1.28). Proceeding in such a way is equivalent of working in the longitudinal gauge. Therefore, the scalar perturbations Φ and Ψ appearing in the expression (2.105), coincide with the Bardeen potentials and then are gauge-invariant variables. Moreover, neglecting anisotropic stress, $\Psi = \Phi$ holds (this simplification it is found to do not alter significantly the final result [112]). The evolution of such scalar modes appearing in the source can be specified by a transfer function and the amplitude at the horizon crossing:

$$\Psi_{\mathbf{k}}\left(\tau\right) = t_\Psi\left(k\tau\right) \psi_{\mathbf{k}} \,, \tag{2.107}$$

where ψ_k are the scalar perturbations evaluated at their horizon crossing and t_Ψ the transfer functions. We define the power spectrum of ψ_k evaluated at the horizon crossing, following the usual definition:

$$\langle \psi_{\mathbf{k}} \psi_{\mathbf{k}'} \rangle = \frac{2\pi^2}{k^3} P_\psi (k)\, \delta^{(3)} \left(\mathbf{k} + \mathbf{k}' \right) . \tag{2.108}$$

In terms of the primordial scalar power spectrum, the source in (2.106), can be written in the following form [112]:

$$\mathsf{e}^{(\lambda)\, ij} (\mathbf{k})\, \tilde{\mathcal{S}}_{ij} (\mathbf{k}, \tau) = \int d^3\mathbf{k'} \mathsf{e}^{ij} (k)\, k'_i k'_j f (\mathbf{k}, \mathbf{k'}, \tau)\, \tilde{\psi}_{\mathbf{k-k'}} \tilde{\psi}_{\mathbf{k}} , \tag{2.109}$$

where $f (\mathbf{k}, \mathbf{k'}, \tau)$ encodes the transfer function, and the convolution between the scalar perturbations is visible. The GW correlation function amount is given by (2.47), with the appropriate source, therefore, from (2.109), it will be a function of the squared power spectrum P_ψ.

In order to obtain the amount of GWs at a certain time τ, the evolution of the source from the horizon-crossing up to the chosen time has to be tracked. The features of scalar perturbations at the time of the horizon crossing, are constrained by CMB observations, in particular we know their amplitude and spectral index. Supposing that scalar perturbations $\psi_{\mathbf{k}}$ are generated by single-field slow-roll inflation, we know that the power spectrum of curvature perturbations on comoving hypersurfaces is given by (1.42). The Bardeen potential and the gauge-invariant curvature perturbations on comoving hypersurfaces, for modes out-side the horizon during radiation matter dominance, are related by:

$$\Psi = -\frac{2}{3} \zeta , \tag{2.110}$$

and then:

$$P_\psi (k) = \frac{4}{9} P_S (k) , \tag{2.111}$$

whose amplitude and spectral index are constrained by CMB observations. Moreover, at the time of the entering of the horizon, as initial conditions, we have: $h_{ij} = 0$ and $h'_{ij} = 0$ (remember that if tensor perturbations of the first order are present, they are uncoupled to the second-order ones, so that these initial conditions hold also in the case in which an inflationary GW background due to vacuum fluctuations is present). Depending on the time we want to evaluate the amount of GWs, we need to consider the evolution of the source for a radiation and eventually matter dominated era.
With the parametrization introduced in (1.43), solving (2.106) for radiation dominated era, the following results is obtained [111]:

$$P_{\mathrm{T}} (k, \tau) = \frac{32\,(216)^2}{81\pi^4} \frac{A_S^2 (k_*)}{\tau^2} \left(\frac{k}{k_*} \right)^{2n_S - 2} \mathcal{F} (n_S, k\tau) , \tag{2.112}$$

where $\mathcal{F}$ is a function presented in fig.5 of [111].
For $A_{\mathrm{S}} = 2 \cdot 10^{-9}$ and $n_{\mathrm{S}} = 0.95$, the present time GW spectral-energy density, turns

out to be of the order of $\Omega_{\rm GW} \simeq 10^{-22}$. Strictly, in doing this estimation we supposed that CMB constraints on scalar perturbations can be extended on the overall range of scales, which is not obvious. Furthermore, notice that this amount is not related one-to-one with the energy scale of inflation as it is for first-order GWs generated by quantum fluctuations of the gravitational field. The amplitude of second-order GWs is fixed by the observed amount of primordial scalar perturbations. Therefore, for a low energy scale of inflation, the amplitude of first-order GWs can be comparable or even lower of the second-order GWs considered here. This fact has to be taken into account if future experiments will put upper bound on the tensor-to-scalar ratio comparable with the amount of second-order GWs, indeed they represent the second important contaminant of B-modes after B-modes lensing. Secondary tensor modes becomes comparable at low multipoles ℓ with GWs due to quantum fluctuations during inflation, for $r \simeq 10^{-6}$.
People considered also the GW production that could take place in a possible early matter dominated epoch [113].

Chapter 3

Current status and observational prospects for inflationary gravitational waves

Stimulating by the first detection of a GW signal by LIGO-VIRGO Collaboration [3], a great interest has been grown with respect to the possibility of directly or indirectly searching for primordial GWs too. A new attention developed about different ways of probing the presence of a primordial GW background with respect to CMB physics and at different frequencies. The prospects of detection at scales smaller than CMB also make attractive those scenarios in which a blue power spectrum of primordial GWs is expected.
Established that the inflationary mechanism predicts the production of a stochastic GW background, in this section we want to give a picture of the present status from the observational point of view.

After the inflationary process, tensor modes start re-entering the causal region sequentially. Such tensor modes start evolving following the solutions (2.93). Then the universe turns out to be populated by propagating GWs, which constitute a stochastic background. As we saw in section 2.6, the features of such background turns out to be strictly related to the primordial mechanism that generate them. Interestingly, the presence of such a gravitational radiation has several effects on the phenomena that happened along the history of the universe, and also on the evolution of the universe background itself.
The inflationary GWs spectrum covers a wide range of frequencies: from $f \simeq 10^{-17}$ Hz, which corresponds to the present time observable universe, up to a frequency which depends on the reheating temperature, for example for $T_{\rm reh} = 10^{13}$GeV the GW spectral energy density has a strong decrease at $f \simeq 10^4$ Hz. For lower reheating temperatures such a frequency gets higher. This rapid decreasing of the GW spectral energy density marks the end of inflation, i.e. the smallest length scale which is pulled outside the horizon by the accelerated expansion. The inflationary gravitational radiation therefore covers a wide range of frequencies, which spans more than two decades. The frequency f is related to the scale k as $f = k/2\pi a$. On the other hand, notice that

a physical phenomenon happening at a certain time of the history of the universe, is sensitive to those primordial GWs which have already entered the causal region.

3.1 Imprints of inflationary gravitational waves on physical observables

A GW background generated in the early stages left several imprints along the history of the universe, providing the possibility of getting information about it by indirect observations. Here we present the most significant signatures.

Modification of the expansion rate. Inflationary GWs contributes to the total energy density of the universe as relativistic degrees of freedom. The presence of such a contribution to the energy density of the universe influences the evolution of the scale factor [114,115]. In particular, it leads to a faster expansion of the universe background and a deviation of the matter-radiation equality epoch. Interestingly, this fact reflects on the primordial nucleosynthesis (BBN) physics. More precisely, the faster expansion of the universe background means that, at the time of nucleosynthesis, neutrons have less time to decay before reaching the freeze out temperature of weak interactions. As a consequence, an Helium over production is expected [116, 117]. An estimation of the Deuterium abundance combined with Planck and BAO data provides an integral upper bound of $\Omega_{\rm GW} < 3.8 \cdot 10^{-6}$ at 95% C.L. [118] for $f \gtrsim 10^{-10}$ Hz, i.e. for those GWs which have already entered the causal region at that time. The limit is shown in figure 3.1.

Influence on CMB physics. The presence of inflationary GWs affects also the physics at the recombination epoch, when CMB is generated [15, 119–121]. In particular, the presence of tensor perturbations at the time of the photon decoupling, leads to the production of temperature and polarization anisotropies in the photon distribution. Therefore CMB features carry information about the GW background filling the universe at the time of recombination. Actually, only a certain range of frequencies of such a gravitational radiation really left an imprint on CMB. Moreover, also scalar perturbations induce temperature and polarization anisotropies and other phenomena along the subsequently history of the universe can modify the signal generated at last scattering, introducing a degeneracy between contributions due to primordial perturbations and more recent effects. CMB temperature and polarization anisotropies are usually described by angular power spectra. Gravitational waves contribute to the temperature angular power spectrum only for multipoles $\ell \lesssim 60$, since on smaller scales tensor perturbations are damped by the cosmic expansion. However, temperature anisotropies due to scalar perturbations largely dominates those due to GWs. At low multipoles the cosmic variance prevents the possibility of extracting stringent information about the source of the signal at those scales, moreover the uncertainty on the scalar spectral index leads to a degeneracy between the amplitude of tensor and scalar modes. The possible presence of isocurvature perturbations is another source of

degeneracy between scalar and tensor modes. Therefore, from the temperature power spectrum it is not possible to extract distinct information about GWs present at last scattering surface.
A more efficient observable, is the angular power spectrum of CMB polarization anisotropies. CMB photons get linearly polarized by Thomson scattering if a quadrupolar anisotropy in the temperature field is present at last scattering [122–124]. Actually, only a few percent of CMB photons get polarized since Thomson scattering washes away temperature anisotropies on small scales. This makes the amplitude of the polarization angular power spectrum smaller than the temperature one. However, GWs leave a peculiar imprint on the CMB polarization anisotropies. The latter can be decomposed in two independent modes, the so-called E and B modes, depending on the rotational properties of the pattern. Interestingly, B modes, i.e. curly-like modes, can be generated in the observed CMB pattern only by tensor perturbations (locally, at the last scattering surface, only E modes can be produced). This fact makes observation of B modes an unequivocal probe of the presence of primordial GWs at the moment of recombination. Notice that, on the other hand, B modes in the CMB power spectra can be generated also by late time mechanisms, such as by lensing and galactic foregrounds. This makes the search for primordial B modes more complicated. The contribution to the B modes from primordial GWs is mainly at $\ell \lesssim 150$. For these multipoles, contaminations from foregrounds and for late time phenomena, could be larger than the primordial signal of more than an order of magnitude.
Current observation provide an upper bound on the amplitude of tensor modes, expressed in terms of the tensor-to-scalar ratio equals to $r_{0.05} < 0.09$ at 95% C.L. [97] at a pivot scale of $k_* = 0.05\text{Mpc}^{-1}$.
Primordial GWs leave other minor imprints on CMB physics, such as the alteration of the time of radiation-matter equality which reflects also on the CMB power spectra [115, 125]. Moreover, also the CMB energy spectrum includes the imprint of possible presence of GWs. More precisely, the integrated GW energy density in the frequency range $10^{-12} - 10^{-9}$Hz leads to spectral distortions in the CMB energy spectrum [126, 127].

Imprint on large scale structure. The presence of primordial GWs affects the mass distribution of the universe. Early and late time effects can be identified. A primordial GW background modifies the power spectrum of curvature perturbations, more precisely it leads to a non-vanishing off-diagonal terms in the two-point correlation function of primordial curvature perturbations (which is expected to vanish for statistically isotropic and Gaussian perturbations). Moreover a quadrupolar anisotropy in the local galaxy power spectrum is expected if GW long wave modes are present.
Moreover, GWs present when matter cluster in order to form structures, lead to a tidal effect because of long wavelength modes [128–131]. But tensor modes modifies also the background in which photons emitted by structures propagate towards us, i.e. lensing effect. This effects leads to distortions of the galaxy shapes, with correlation between the ellepticity of galaxies, and a projection effect [129, 132–134, 134]. This kind of observations are particularly sensitive to GWs of frequencies $f \sim 10^{-9} - 10^{-7}$

Hz [135]. However in order to obtain significant bounds on the primordial GW background by this kind of observations, galaxy surveys with best capabilities with respect to the current ones are required [136, 137].

Inflationary gravitational waves and primordial black holes. It is known that curvature perturbations which re-enter the horizon during the radiation dominated epoch with an amplitude larger than a certain threshold, leads to the collapse into a black hole [138]. A number of inflationary scenarios predict a significant production of these kind of objects. People also hypothesize that primordial black holes (PBH) could constitute dark matter [139, 140]. Up to now we have no evidence of the production of PBH. From non-observation of these objects, an upper bound on the scalar perturbation amplitude can be obtained. For our purposes, the interesting fact is that second-order combinations of tensor perturbations act as a source term for scalar perturbations. An upper bound on scalar perturbations can be translated into an upper limit on their sources [141, 142]. In the end, non-observations of primordial black holes correspond to an upper limit on primordial tensor modes. It results: $\Omega_{\rm GW} < 10^{-5} - 10^{-4}$ for the frequency range $f \sim 10^{-12} - 10^{4}$ Hz [142] (see figure 5 of [142] to find out the accurate scale-dependence). Notice that this upper bound on the GW amplitude is completely model-independent.
Moreover it is interesting to note that PBH, if present, carry also other information about the inflationary physics, in particular about the possible mechanism that generate them during inflation. The possible presence of PBH gives rise to several signatures in physical observables (for a review see [143]). PBH could produce also a GW signal because of their merger during their dynamical evolution or soon after the recombination. Moreover the gravitational collapse which forms PBH at the horizon re-entry should generate a stochastic GW background. These GW signals could be captured by current and upcoming laser interferometer experiments. Information obtained in such a way should provide new constraints on the inflationary mechanisms that lead to the generation of such objects, such as the hybrid inflationary scenario, single-field models with an inflection point in the potential or specific scenarios in which the inflaton is coupled with a gauge field. It is not excluded that the first GW observation by the LIGO detectors could be due to a PBH merger [144].

Imprint on the pulsar signals. The presence of a GW background affects light signals which propagates from astrophysical objects towards us. The distortion effect for close astrophysical objects is clearly small. However ultra-stable millisecond pulsars are characterized by an extremely precise signal modulation. If a GW background is present, a non-vanishing and significant correlation between perturbations of pulsar signals is expected. This phenomenon is exploited by pulsar timing array experiments which collect and analyse the correlation of the signals coming from a set of these astrophysical objects. In such a way a GW background of frequency around $f \sim 10^{-8}$Hz can be captured [135, 145]. Considering $H_0 = 70 \mathrm{Kms}^{-1}\mathrm{Mpc}^{-1}$, at a reference frequency of $f = 10^{-8}$Hz, and parametrizing $\Omega_{\rm GW}$ as a power law with spectral index equal to 2/3, current upper bound provided by PPTA is $\Omega_{\rm GW} < 6.0 \cdot 10^{-10}$ [146].

Constraints from associate scalar perturbation production. According to some inflationary models, constraints on primordial GWs can be also obtained indirectly exploiting limits on the associated overproduction of scalar perturbations. For example, in scenarios as those described in section 2.2.1, primordial parameters which establishes the features of tensor perturbations, are involved also in determining the second-order production of scalar perturbations. Current estimation of the scalar power spectrum amplitude provided by Planck [2], and even more efficiently the upper bound on scalar non-gaussianities [46], in general, limit the parameter space of the inflationary models [46]. Moreover, also the non-observation of primordial black holes puts constraints on the scalar perturbations amplitude at small scales. Form these limits on the scalar sector also the associated GWs production results constrained. Notice that such bounds on GWs are model-dependent.
Non-gaussianities represent a clear example where information coming from features of scalar perturbations can provide constraints on tensor perturbation properties, and viceversa.

Imprints on gravitational waves. We have seen the main signatures that a primordial GW background leaves on physical observables along the history of the universe. Clearly also the contrary happens, i.e. the propagating GWs are themselves influenced by the spacetime they travel through. Indeed, for example, GWs memorize the expansion history of the universe. In particular the GW spectral energy density is affected by a dumping effect due to the decoupling of particles such as neutrinos, and by the change in the number of relativistic degrees of freedom [105]. Moreover, GW anisotropies could form along the travel of the signal throughout the universe due to the local anisotropy and non-homogeneity of the universe [147,148], i.e. matter structures.

3.2 The possibility of direct gravitational wave detection

Up to now we have no direct (nor indirect) detection of primordial GWs. However with the new era of laser interferometer experiments disclosed by LIGO, new encouraging prospects have been opened also for the observation of primordial signals.
Notice that experiments of direct GW detection are clearly sensitive to the present time GWs amplitude, while CMB measurements are sensitive directly to the primordial amplitude of tensor modes, so that cosmological GWs eventually detected by laser interferometer experiments would include the imprints of the whole history of the universe they have pass through.

Laser interferometer detectors are sensitive to completely different waveband with respect to CMB experiments. In particular, terrestrial observatories, such as the LIGO and Virgo detectors, work at $f \sim 10^2 - 10^3$Hz [149], while space-born experiments are expected to be sensitive to $f \sim 10^{-2}$Hz [7]. Some studies are in development in order

to investigate the possibility of realizing direct GW detectors sensitive to frequencies $f \sim 10^7$Hz and based on electromagnetic cavity resonator [150], Bose-Einstein condensates [151], resonant mass detectors [152], microwave cavity resonators coupled to superfluid Helium [153] and atomic interferometry [154]. Experiments sensitive to such scales would be relevant in particular for the GW signals expected to be generated in some reheating scenarios.
Current and upcoming direct GW detectors are based on Michelson interferometry, i.e. they measure the phase shift of laser beams which propagates in different directions. Indeed GWs distort spacetime is such a way that the light path on different directions is modified in different ways. Ground-based and space-borne laser interferometer experiments, are substantially based on this idea, while its actualization is partially different for the two situations. For example, in the case of space-borne experiments, each laser beam cannot be reflected at the end of its path in order to go back and be compared with the other beam, since only few photons of the original laser signal get to the receiver because of the huge armlength. In such a situation, the comparison between the laser beams cannot be done, while it has to be made virtually by comparing data. Another main difference between terrestrial and space-based experiments, is the amount and the signal length of GW events that is expected to be recorded. An experiment as LISA (see section 5.1) is predicted to detect a huge quantity of long-duration GW events, differently from LIGO detectors. For the latter, the crucial point is to distinguish a GW signal from the noise, while for an experiment as LISA, a superposition of a lot of events is expected, so that the challenge will be to distinguish them among each other.

Differently from the GW signals captured by LIGO-Virgo detectors, inflationary GWs constitute a persistent background. There are two significant issue related to the detection of such a kind of signal. Firstly, it is not trivial distinguishing a background GW signal from a background noise, in particular for space-borne experiments [155, 156]. In order to distinguish them, the expected correlation among GW signals is exploited, in contrary of the uncorrelation expected for a noise signal. Secondly, there are several cosmological and astrophysical phenomena which predict the production of a stochastic GW background. In order to disentangle them among each other, recognizing the scale dependence or eventual features in such signal would be crucial.
This kind of experiment unveil to be interesting also with respect to search for new constraints on primordial GWs. The fact that GW detectors are sensitive to extremely different frequencies with respect to CMB experiments, leads to the possibility of estimating or putting significant constraints on the scale dependence of primordial signals since the latter are expected to cover a wide range of frequencies [157–159]. In particular, parametrizing the inflationary GW by a power low, exploiting the long lever arm between CMB scales and small scales, interesting constraints on the tensor spectral index can be obtained. As a consequence tests on the consistency relation (4.1) can be performed.

The updated LIGO detectors, that is aLIGO [160], have already collected data in two observational run. The most recent upper limit provided by LIGO and Virgo

Collaboration is shown in fig.5 of [161], it is of around $\Omega_{\rm GW} < \times 10^{-7}$ at 95% C.L. at $f \simeq 5 \cdot 10$Hz Hz, and it is the result of the first observational run. On August 2017 Virgo detector has joined LIGO observatories in the second observational run.

3.3 Current bounds from joint analysis

Parametrizing the primordial GW power spectrum as in eq.(2.28), current cosmological data provide bounds on its amplitude and spectral tilt.
CMB data gives an upper bound on the GW amplitude at frequencies around $f \simeq 10^{-17}$ Hz, which is abundantly the most stringent constraint we have at any scale. Other physical observables alone give upper limits on the GW amplitude weaker than this, but at different scales. Combinations of constraints obtained on several wavebands are exploited to put limits on the GW spectral index. In this direction a number of data analysis has been performed:

- The joint analysis of Planck and external data (named as *Planck TT+lowP+lensing +ext* in [162]), BICEP2 and Keck Array data, provided an upper bound of $r_{0.05} < 0.07$ at 95% C.L. [97], assuming the consistency relation (4.1). A less model-dependent constraint was obtained assuming a scale-invariant power spectrum: from BICEP2 and Keck Array data, Planck data only for polarization and WMAP9 23 GHZ and 33 GHZ maps, the bound becomes $r_{0.05} < 0.09$ at 95% C.L. [97].

Other works [157, 158, 163–165] extended this analysis taking into account for a non-vanishing spectral index and the measurements by LIGO [149].

- Considering data coming from CMB, LIGO (notice that they use the LIGO-Virgo upper bound provided in [166], which now has been updated) and the Parker Pulsar Timing Array (PPTA) [167], and fitting data allowing the tensor spectral index to vary, [157] found that a blue power-spectrum and $r > 0.12$ are preferred (this value of r refers to the previous constraint on such a quantity provided by [162]). Constraints on $n_{\rm T}$ have been obtained combining BICEP2/Keck Array, temperature Planck data 2013, WMAP low ℓ polarization, a prior on H_0 from HST data, BAO measurements from SDSS and the upper limit on the intensity of a stochastic GW background from LIGO: $n_{\rm T,0.01} = 0.06^{+0.63}_{-0.89}$ at 95% C.L. [157], in correspondence of a best-fit for the tensor-to-scalar ratio of $r_{0.01} = 0.02$. Admitting the spectral index to vary leads to a weaker bound on the tensor-to-scalar ratio r.

- [163] provides other results which take into account the data release of Keck Array at 95 GHz [97] and one by one the bounds coming from the Helium abundance, μ-distortions of the CMB and the LIGO-Virgo experiment (as before, they use the LIGO-Virgo upper bound provided in [166], which now has been updated). The limits resulting from the analysis with LIGO-Virgo bounds are $n_{\rm T} = 0.04^{+0.61}_{-0.85}$ at 95% C.L. with $r < 0.085$, found putting a prior lower bound on the tensor-to-scalar ratio of $r > 0.001$.

- [158] makes a further analysis which takes into account CMB data from Planck, BICEP and SPTpol, current bounds form PPTA, LIGO-Virgo (referring to the results shown in [166], which now have been updated) and BAO and BBN indirect constraints, providing an upper bound on the tensor spectral index of $n_{\rm T} < 0.36$ at 95% C.L. in correspondence of $r_{0.05} = 0.11$.

- An updated joint data analysis has been done by [165]. In particular bounds on the tensor spectral index is obtained performing a combined analysis of Planck 2015, HST, BAO and BK14 data with the most recent upper limit provided by aLIGO O1[1] [149]. They obtain: $n_{\rm T} = 0.016^{+0.614}_{-0.989}$ and $r < 0.066$ at 95% of CL.

Notice that in the mentioned works the primordial power spectrum of GWs is always parametrized as a power law. This assumption could be not appropriate for a waveband extended over several orders of magnitudes. In particular, at the end of inflation, the slow-roll conditions are no longer satisfied and then the GW power spectrum is expected to deviate form a pure power law. In this direction, [157] parametrized the power spectrum also taking into account a scale dependence of the tensor spectral index, concluding that with available data no significant constraints can be obtained.

3.4 Observational prospects for the next future

Several experiments are planned to improve the mentioned bounds and hopefully detect a primordial GW background. In figure 3.1 the power-law sensitivity curve of main current and future detectors are shown, together with current upper bounds on the GW spectral energy density for a power-law GW power spectrum. For the explanation on how to obtain the power-law sensitivity curve of an experiment, see section 5.2. Gravitational wave signals passing above a power-law sensitivity curve is in principle detectable by such an experiment, and analogously for current upper limits shown.
For what concerns CMB polarization experiments, several ground-based, balloon and space-borne experiments are under construction or have been proposed:

- Ground-based and balloon experiments, such as the Atacama Cosmology Telescope Polarization Experiment (ACTPol) [175] and Polarbear [176] (which are already underway), the Cosmology Large Angular Scale Surveyor (CLASS) [177], the Primordial Inflation Polarization ExploreR (Piper) [178] and Spider [179], are designed to improve the sensitivity over a restricted range of multipoles of the polarization power-spectra related to one or two frequency channels. Recently another project has been proposed, the CMB-S4 experiment, consisting of a number of ground-based telescopes operating in different areas of the Earth [180].

[1] LIGO-Virgo upper limits on stochastic background have been updated in last years. The older one is *initial LIGO-Virgo* [166], then in [168] the expected sensitivity of *aLIGO O1* for a stochastic GW background was provided, while in [161] the upper limit provided by data of *aLIGO O1* are presented (and does not differ to much from that forecast in [168]). *aLIGO-Virgo O2* is under way. The designed sensitivity for *aLIGO-Virgo O5* is reported in [161].

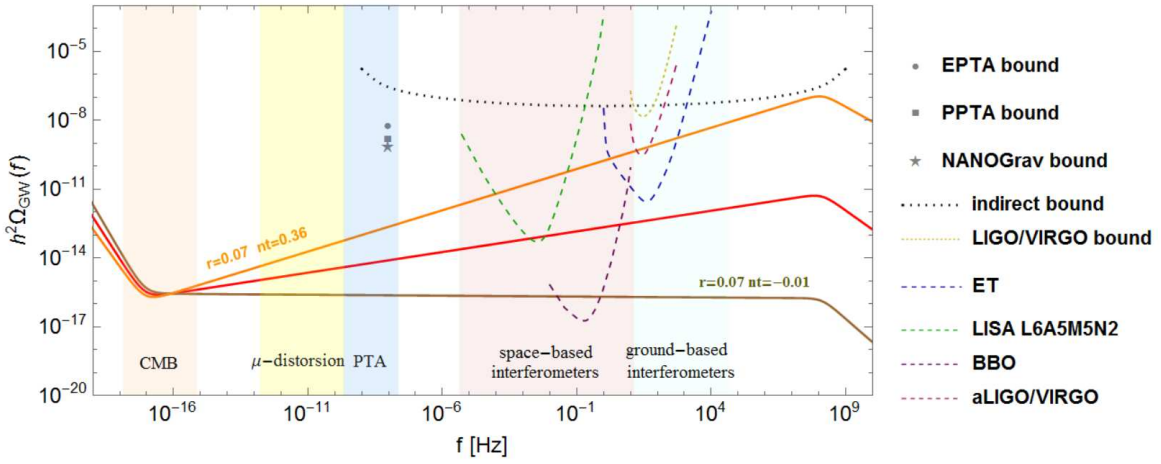

Figure 3.1: GW spectral energy-density for different values of $n_{\rm T}$ are shown with solid lines: $n_{\rm T} = -r/8$ (brown), $n_{\rm T} = 0.18$ (red) and $n_{\rm T} = 0.36$ (orange). The r value is fixed at $r_{0.05} = 0.07$. It is assumed also $T_{\rm R} = 10^{16}$ GeV. The coloured bands highlight the waveband to which each physical observable or experiment is sensitive. Current bounds: combined analysis of Planck data, BAO and BBN measurements which provides an integral bound $\Omega_{\rm GW} < 3.8 \times 10^{-6}$ (black) [118]. The grey dot corresponds to the bound provided by EPTA [169], the star by the NANOGrav [170] and the square by PPTA [146], assuming $n_T = 2/3$. The aLIGO O1:2015-16 power-law sensitivity curve of the first observing run (yellow) is also shown [168]. The collected data show a slight worsening of such forecast. Long-dashed lines are expected power-law sensitivity curves for the following experiments: BBO (violet) [171,172], LISA configuration L6A5M5N2 (green) [173], aLIGO-adVirgo, O5:2020-22 observing run (magenta) [168], Einstein Telescope (blue) [174]. Plotted upper bounds and expected sensitivity curves are obtained by the method provided by [172] (see section 5.2), assuming a power-law signal. See also section 5.1 for the mentioned LISA configurations. All the bounds and sensitivity curves refer to a confidence level of 95%, a part from the LISA curves which refer to a signal-to-noise ratio of 10 (see 5.2 to clarify this point).

Such a kind of observatory is planned to reach a sensitivity on the tensor-to-scalar ratio of about 10^{-3}. People are also organizing comities and communities in order to optimize the work that is developing in such directions, such as the ASI/COSMOS project [181].

- Space-borne experiments have been proposed in order to span a larger multipoles range and to get data related to several frequency channels to improve the control of systematic errors and the component separation analysis. We mention, for example, the Cosmic Origins Explorer mission (COrE) [182], the Polarized Radiation Imaging and Spectroscopy Mission (PRISM) [183] and LiteBIRD [184].

But not only CMB telescopes are under consideration for an improvement of our current knowledge of primordial GWs, also experiments sensitive to smaller scales are in development:

- Pulsar timing array experiments are under way, such as PPTA [167], the Euro-

pean Pulsar Timing Array (EPTA) [169], and the North American Nanohertz Observatory for Gravitational Waves (NANOGrav) [185], and others are planned, such as the Square Kilometre Array (SKA) [186]. Considering $H_0 = 70\text{Kms}^{-1}\text{Mpc}^{-1}$, at a reference frequency of $f = 10^{-8}\text{Hz}$, and parametrizing Ω_{GW} as a power law with spectral index equal to 2/3, current upper bounds provided by pulsar timing array experiments are the following [187]: $\Omega_{\text{GW}} < 5.4 \cdot 10^{-9}$ for EPTA, $\Omega_{\text{GW}} < 1.3 \cdot 10^{-9}$ for NANOGrav [170] and $\Omega_{\text{GW}} < 6.0 \cdot 10^{-10}$ for PPTA [146]; see figure 3.1. The nominal SKA experiment is expected to put poorer constraints on inflationary GWs with respect to space-based laser interferometer experiments, while in an optimal case, with more than twenty years of collecting data, the capabilities of SKA in constraining a primordial power-law GW background would be comparable with those of LISA [188].

- Also for what concerns direct GW detection by ground-based experiments, several efforts are under way. The aLIGO detectors [160], have already collected data in the first and second of its five expected observation runs. From the O1 observation run, LIGO-Virgo Collaboration provided an upper limit of around $\Omega_{\text{GW}} < \times 10^{-7}$ at 95% C.L. at $f \simeq 5 \cdot 10\text{Hz}$ Hz [161] (for the curve see fig.5 of [161]). The Virgo detector has recently joined LIGO observatories in the second observational run. Further upgrades are planned for aLIGO and for Virgo, and a sequence of observing runs are expected for the more and more improved configurations of such laser interferometers (see for example [168], table I). In fig.3.1 the expected power-law sensitivity curves of the O1 and O5 observation run [168] are shown. The curve expected for the first run it is found to do not differ significantly form the final upper bound obtained form the data.
  A number of ground-based experiments have also been proposed for the next future, such as LIGO India (IndIGO) [189] (that will be included in the network aLIGO-adVirgo), the Kamioka Gravitational Wave Detector (KAGRA) [190] and the Einstein Telescope (ET) [174].

- With respect to observatories in space, the space-born experiment LISA [7] is planned. See figure 3.1 for the expected sensitivity curves and section 5.1 for more details on this observatory. [165] provided forecasts for a combined data analysis of Planck 2015, HST, BAO and BK14 data with the upper limit provided by LISA telescope in case of a non-detection, they found: $n_{\text{T}} = -0.050^{+0.612}_{-0.992}$ and $r < 0.062$ at 95% of CL. For a possible detection of a scale-invariant inflationary power-spectrum, bold experiments, such as the DECI-Hertz Interferometer Gravitational wave Observatory (DECIGO) [191] and BBO [171] have been proposed too. The expected power-law sensitivity curve for BBO is reported in figure 3.1.

For next future experiments based on laser interferometry, such as upgraded aLIGO-Virgo and LISA, a direct detection of primordial GWs might be possible only in case of a blue inflationary power spectrum, that is, in case of an inflationary scenario different from single-field slow-roll model; see figure 3.1. Therefore, a detection of inflationary GWs by such experiments would rule out single-field slow-roll inflation and all those

inflationary scenarios which predict a red GW power-spectrum. On the other hand, a non-detection of primordial tensor modes by next future laser interferometer experiments, would represent the possibility to put significant limits on the tensor spectral index and then to obtain new constraints on the inflationary physics for those primordial scenarios which predict an enhancements of the GW amplitude at small scales, as those presented in section 2.2.1. Moreover, constraints on the tensor spectral index would provide the opportunity of testing the consistency relation eq.(4.1). For example, a non-detection by an experiment with upgraded aLIGO capabilities would put a constraint on the tensor spectral index of $n_{\rm T} < 0.34$ at the 95% C.L. for $r = 0.11$ on CMB scales [163], and analogously LISA would put an upper limit of $n_{\rm T} \simeq 0.2$; see section 4.
Then next future laser interferometer experiments represent an exciting chance of improving our knowledge on the inflationary physics.

Current pulsar timing array experiments, as NANOGrav and PPTA, do not significantly contribute to constrain the inflationary GW background features, in particular in case of a power-law signal, as one infers from figure 3.1. Future pulsar timing array experiments as SKA, might provide more interesting constraints in this direction, even though poorer than LISA ones. In any case, they provide information of a frequency range that is not accessible by laser interferometer experiments.

For the far future, it could be possible to obtain information about the inflationary physics also from the features of GWs, such as their level of non-gaussianity and chirality. The latter would provide interesting bounds on parameters of those inflationary models which present events of particle production, such as the parameter ξ defined in (2.56) [57,65]. Also the tensor bispectrum could provide constraints on inflationary physics. An example is given by the inflationary scenario associated with a pseudo-scalar coupling to a gauge field, where $f_{\rm NL}^{\rm tens}$ can provide upper bounds for the model parameter ξ, complementary to those coming from the scalar bispectrum [59, 60].

Chapter 4

The inflationary consistency relation

Interestingly, the theory of single-field slow-roll inflation predicts an equality which involves tensor modes. More precisely, in such an inflationary scenario the tensor-to-scalar ratio r and the tensor spectral index $n_{\rm T}$, are expected to be connected by the following relation at first order in slow-roll parameters, and at each scale k [121]:

$$r = -8n_{\rm T}\,, \tag{4.1}$$

see eqs. (2.32)-(2.30). Notice that, in general, r and $n_{\rm T}$ are scale dependent quantities. We will refer to the equality (4.1) as consistency relation. Others similar equalities which involve higher order parameters, such as the running of tensor power spectrum, exist [19]. However, since the tensor spectral index is a small quantity, its running is expected to be even smaller, so that such relations are still far from being relevant for current and planned observational capabilities.

Interestingly, eq.(4.1) strictly characterizes single-field slow-roll inflation. Other inflationary models predict a violation of the consistency relation, making it a strict test for single-field slow-roll scenario. The evidence of a violation of the consistency relation would rule out such an inflationary model. Moreover, primordial scenarios proposed as an alternative to the inflationary mechanism, in general, predict a violation of the consistency relation, such as string gas cosmology [192] and matter bounce cosmology [193, 194].
Notice also that the link between r and $n_{\rm T}$ expressed by the consistency relation, is the results of the strict connection of each of those quantities to the slow-roll parameter ϵ, i.e. to the energy scale of inflation. Therefore, a deviation from the standard expressions of r and $n_{\rm T}$ means loosing such a specific link.

Current cosmological observations are remarkably in agreement with an inflationary period in the early universe, however they are not sufficient to unequivocally probe the development of such a stage. Some alternative scenarios are still allowed by current cosmological observations [92–95]. In such a direction, testing the consistency relation is considered the stricter way of unequivocally probing the inflationary mechanism, since

eq.(4.1) provides a extremely peculiar relation between two primordial parameters. It would be also a validation test for single-field slow-roll inflation model. Furthermore, testing the consistency relation would help in constraining some features of the inflationary physics. For these reasons, we consider testing the inflationary consistency relation, a key step towards best understanding the physics of the early universe and the inflationary mechanism.

4.1 Possible violations of the consistency relation

There are several ways by which the consistency relation can be violated.
Firstly, a blue tensor power spectrum, i.e. a positive tensor spectral index, is clearly not compatible with eq.(4.1). In general, inflationary models predict the tensor power spectrum due to vacuum fluctuations to be red, as a consequence of the non-violation of the null energy condition. On the other hand, for certain inflationary scenarios built on modified gravity theories, a blue tensor power spectrum is expected, preserving at the same time such a condition. Furthermore GWs produced by the classical mechanism can present a blue spectral index, or a more general enhancement of the tensor amplitude at small scales.
A violation of the consistency relation can turn out also because of a deviation from the standard expression of the tensor-to-scalar ratio r. Both a deviation of scalar and tensor amplitude can induce such a situation. For example, if a significant classical production of GWs takes place, the overall amount of tensor modes deviates from the predictions of single-field slow-roll inflation. Also an extra production of scalar perturbations can happen, for example because of the presence of extra fields beside the inflaton.

Notice that, in some scenarios, the violation of the consistency relation is significant only on a certain range of scales, i.e. where a substantial deviation from the standard scalar and/or tensor modes takes place, and it is non-relevant on other scales. In light of this fact, investigations on cosmological perturbations at several scales becomes particularly significant.

At the end of the section we summarized in table 4.1, main examples of inflationary models in which the violation of the consistency relation is due to a deviation from the GW amount predicted in single-field slow-roll inflation.

4.1.1 Single-field slow-roll inflation with adding features

The consistency relation can be violated due to the presence of extra sources of scalar and/or tensor modes, which lead to a larger amount of the respective power spectrum. Furthermore, non-standard features of the inflaton can reflect on the amplitude of scalar perturbations, such as an anomalous propagation speed of its perturbations.

Inflationary scenarios with extra-sources of gravitational waves. We showed in section 2.2.1 that, besides quantum fluctuations of the gravitational field, GWs can be produced classically because of the presence of a source. If the latter is efficient, GWs generated in such a way can introduce a significant deviation of the tensor-to-scalar ratio from that expected in single-field slow-roll inflation. In this case, also the spectral index can be different from the standard value. Furthermore, if a relevant classical production of GWs takes place, the strict relation between the amplitude of tensor modes and the energy scale of inflation is lost.
Notice that the violation could be significant only for a certain range of scales, more precisely on those scales on which the second-order production of GWs is relevant. For example, the consistency relation could be significantly violated at small scales, and at the same time presenting a unmeasurable deviation on CMB scales. Most relevant models in which such a situation occurs, are scenarios in which a spectator field or a gauge field is coupled to the inflaton dynamics, as we show in section 2.2.1.

Inflation driven by multi-fields. If the background dynamics during inflation is driven by more than one field, as in multi-field inflation, besides adiabatic scalar modes, isocurvature perturbations are produced too. The latter acts as a source in the equation of motion of curvature perturbations leading to a deviation in the denominator of r with respect to the predictions of single-field slow-roll inflation. On the other side, tensor modes are expected to be the standard ones. In this scenario eq.(4.1) turns out to be [195]:

$$r = -8 n_{\rm T} \sin^2 \Delta \,, \tag{4.2}$$

where $\cos\Delta$ parametrizes the correlation between curvature and isocurvature perturbations at horizon exit (the Planck Collaboration provided constraints on isocurvature perturbations which can be translated into constraints on $\cos\Delta$ [2]). Furthermore, if inflation is driven by more than two scalar fields, an additional isocurvature mode could contribute to the non-adiabatic perturbations. In such case (4.2) then becomes [195]:

$$r \leq -8 n_{\rm T} \sin^2 \Delta \,. \tag{4.3}$$

General single field inflation. Scenarios in which the inflationary expansion is driven by a scalar field with a Lagrangian of the form $P(X, \varphi)$ where X is the canonical kinetic term, and P a generic function, are usually called models of *general single field*. DBI inflation and k-inflation are examples of this class of models [196, 197]. In such scenarios, scalar perturbations have a non-canonical dynamics and then a deviation from the standard scalar power spectrum is predicted, which finally results in a violation of the consistency relation. More precisely, the inflaton sound speed turns out to be $c_{\rm S}^2 \equiv dP/d\rho = P_{,X} \,/\, (P_{,X} + 2X P_{,XX})$, where ρ is the energy-density of the inflaton, and then in general different from the standard unitary value [196]. The amplitude of scalar power spectrum results enhanced by a factor $1/c_{\rm S}$ with respect to single-field slow-roll case, and the consistency relation turns out to be:

$$r = -8 c_{\rm S} n_{\rm T} \,. \tag{4.4}$$

Exploiting CMB data, significant constraints on the parameter $c_{\rm S}$ have been provided [46], in particular exploiting limits on non-gaussianities.

Inflationary models with spatial and time variation of the inflaton decay rate. Usually the decay rate of the inflaton into ordinary particles during reheating is assumed to be constant. However, the decay rate depends on the vacuum expectation value of the field χ into which the inflaton decays. Actually, the field χ can fluctuate during the accelerated expansion and leave the imprints of the variations on super-horizon scales. In such a scenario the inflaton decay rate cannot be considered constant. The variations of the decay rate leads to a shift of the curvature perturbations on super-horizon scales, which finally leads to a deviation of the amplitude of scalar perturbations, and then to a violation of the consistency relation [198]:

$$r = -8\left(1 - 2\Delta\right) n_{\rm T}\,, \tag{4.5}$$

where $\Delta \equiv \left(\zeta_{\rm f} - \zeta_{\rm i}\right)/\zeta_{\rm i}$, and i and f indicate the initial and final times of the reheating stage.

4.1.2 Inflationary models with modifications in fundamental physics

A violation of the consistency relation could be also due to non-standard features in the fundamental physics on which inflation is based. We outline some examples.

Inflation with collapse model for quantum fluctuations. In order to solve the problem of quantum to classical transition [25] of inflationary perturbations, people proposed to modify the evolution equation of primordial perturbations, i.e. the Schrodinger equation. As a consequence, scalar and tensor power spectra deviate from standard predictions, leading to a violation of the consistency relation of the following form [199]:

$$r = -8 n_{\rm T} + 8\delta\,, \tag{4.6}$$

where δ encodes the parameters that modify the Schrodinger equation.

Inflation with general initial conditions for quantum fluctuations. In order to obtain the amplitude of scalar and tensor perturbations in section 2.1, we assumed as initial condition for such modes, the so-called Bunch-Davies vacuum, which corresponds to choice the lowest energy state. Actually, this could be not the case. There are several motivations to question about the initial vacuum conditions of quantum fluctuations at so high energy scales as in the inflationary scenario. Considering general initial conditions, additional factors turn out in the expressions of the field power spectra [200, 201], and then a violation of the consistency relation appears [200]. The analogous of eq.(2.19), for general initial conditions for the gravitational field, becomes:

$$v_k = C_+\left(k\right)\frac{H}{\sqrt{2k^3}}\left(1 + ik\tau\right)e^{-ik\tau} + C_-\left(k\right)\frac{H}{\sqrt{2k^3}}\left(1 - ik\tau\right)e^{ik\tau}\,, \tag{4.7}$$

where $|C_+(k)|^2 - |C_-(k)|^2 = 1$. In particular, the scale dependence of $C_\pm(k)$ can lead to a blue tensor power spectrum.

Inflation with non-commutative phase space. People considered the possibility of non-standard commutative relations for quantum fields involved during inflation [202], in particular in the context of quantum gravity. The consequence of such a choice are non-standard equations of motion for tensor perturbations. In particular, the tensor spectral index vanishes at small scales and becomes blue at large scales. Therefore a significant violation of the consistency relation is expected at large scales.

4.1.3 Inflation with spatial broken diffeomorphisms

In section 2.3 we introduced the EFT approach to inflation, and we saw that if spatial diffeomorphisms are supposed to be broken during inflation, besides the temporal one, tensor perturbations can admit a non-vanishing mass $m_{\rm T}$ and a speed of sound $c_{\rm T}$ different form unity [91]. In particular $m_{\rm T}$ influences the spectral index, which in some cases can be blue, while the propagation speed appears in the amplitude of tensor modes as a factor $1/c_{\rm T}$, see eq.(2.80). Therefore, in such a scenario, in general, the consistency relation is predicted to be violated.

4.1.4 Inflationary models built on modified gravity

When the inflationary mechanism is built on a modified gravity theory, a different dynamics of scalar and tensor perturbations with respect to the canonical one is usually expected. As a consequence, in general, a deviation from standard scalar and tensor power spectra is predicted. We give as an example, one of the most significant case.

G-Inflation. In G-Inflation scenario [79], the accelerated expansion is described by the Horndeski Lagrangian. The dynamics of tensor perturbations is not modified with respect to GR, however, even if the tensor spectral index reads as in the standard case $n_{\rm T} \simeq -2\epsilon$, it can assume positive values since negative values of the slow-roll parameter ϵ are allowed (in general the null energy condition is not guaranteed to be satisfied). On the other side, the scalar power spectrum deviates from predictions of single-filed slow-roll inflation. In the particular case of potential-driven G-Inflation considered by [203], a consistency relation can be written:

$$r \simeq -\frac{32\sqrt{6}}{9} n_{\rm T} \,. \tag{4.8}$$

G-inflation model can be generalized by adding new terms in the Lagrangian, keeping equation of motion of the second order [81]. In such a case the dynamics of tensor modes is no more the standard one, and the new amplitude and spectral index, in general violate the standard consistency relation [204].

	Model	Tensor power-spectrum	Tensor spectral index		Consistency relation
Background	Standard infl.	$P_{\rm T} = \frac{8}{M_{\rm pl}^2}\left(\frac{H}{2\pi}\right)^2$	$n_{\rm T} = -2\epsilon$	red	$r = -8n_{\rm T}$
	EFT inflation[(a)]	$P_{\rm T} = \frac{8}{c_{\rm T} M_{\rm pl}^2}\left(\frac{H}{2\pi}\right)^2$	$n_{\rm T} = -2\epsilon + \frac{2}{3}\frac{m_{\rm T}^2}{\alpha H^2}\left(1+\frac{4}{3}\epsilon\right)$	r/b	-
	EFT inflation[(b)]	$P_{\rm T} = \frac{8}{c_{\rm T} M_{\rm pl}^2}\frac{2^{\frac{-p}{1+p}}}{\pi}\Gamma^2\left(\frac{1}{2(1+p)}\right)\left(\frac{H}{2\pi}\right)^2$	$n_{\rm T} = \frac{p}{1+p}$	blue	violation
	Gen. G-Infl.	$P_{\rm T} = \frac{8}{M_{\rm pl}^2}\gamma_{\rm T}\frac{\mathscr{G}_{\rm T}^{1/2}}{\mathscr{F}_{\rm T}^{3/2}}\left(\frac{H}{2\pi}\right)^2$	$n_{\rm T} = 3 - 2\nu_{\rm T}$	r/b	-
	Pot.-driv. G-Infl.	$P_{\rm T} = \frac{8}{M_{\rm pl}^2}\left(\frac{H}{2\pi}\right)^2$	$n_{\rm T} = -2\epsilon$	r/b	$r \simeq -\frac{32\sqrt{6}}{9}n_{\rm T}$
Extra background	Particle prod.	$P_{\rm T}^{(s)} = 8.6\times10^{-7}\frac{4H^2}{M_{\rm pl}^2}\left(\frac{H}{2\pi}\right)^2\frac{e^{4\pi\xi}}{\xi^6}$	-	blue	violation
	Spectator field	$P_{\rm T}^{(s)} = \frac{8}{15\pi c_s^3}\frac{H^4}{M_{Pl}^4}$	$n_{\rm T} \simeq -4\epsilon - 3s$	r/b	violation

Table 4.1: GW features for selected inflationary models. We show the prediction for the amplitude of the tensor power spectrum at the horizon crossing and the related spectral index, as functions of the model parameters. In the next column we indicate if the tensor spectral index is expected to be red, $n_{\rm T} < 0$, or blue $n_{\rm T} > 0$, or if both possibilities are admitted r/b. In last column we point out the consistency relation, where it is significant, and denote *violation* the cases in which, due to an extra background of GWs, a violation of the standard consistency relation can be expected on some ranges of scales (see discussion in section 4.1). *Standard Inflation*: Lagrangian of eq.(1.6); see section 2.1. *EFT inflation*[(a)]: Lagrangian of eq.(2.77), $c_{\rm T}$ GW propagation speed, $m_{\rm T}$ graviton mass; see section 2.3. *EFT inflation*[(b)]: Lagrangian of the same form of eq.(2.77) with $\alpha = c_{\rm T}^{-2}/2$, $m = 0$, $c_{\rm T}$ a time-dependent parameter and $p \equiv -\dot{c}_{\rm T}/c_{\rm T}H_*$ a positive quantity; for more details see [82]. *Generalized G-Inflation*: see section 2.3, $\gamma_{\rm T}$, $\mathscr{G}_{\rm T}$, $\mathscr{G}_{\rm T}$ and $\nu_{\rm T}$ defined in [203]. *Potential-driven G-Inflation*: see [79, 203]. *Particle production*: Lagrangian of eq.(2.52), ξ defined in (2.56); see section 2.2.1. *Spectator field*: Lagrangian of eq.(2.71), $c_{\rm S}$ and s defined in section 2.2.4.

4.2 Observational test of the consistency relation

In order to test the consistency relation eq.(4.1), an estimation of the scalar and tensor amplitude, and a measure of the tensor spectral index are required. The most difficult task is the estimation of the parameters related to GWs. Notice that a detection of inflationary GWs on different scales is required in order to constrain $n_{\rm T}$.
At the present time, the stricter upper bound on the tensor perturbation amplitude is provided by CMB measurements. However, such observations cannot put strong constraints on the spectral index being them limited to a small range of scales. In this direction, experiments of direct GW detection and measurements related to BBN physics, give a substantial contribution, because of their sensitivity to small scales. In particular, due to the weaker sensitivity on the GW amplitude of detectors at small scales with respect to the CMB experiments, the former lead to significant constraints on blue tensor spectral indexes.

Current measurements provide only an upper bound on the tensor-to-scalar ratio $r_{0.05} < 0.09$ at 95% C.L. [97], and of the tensor spectral index $n_{\rm T} = 0.016^{+0.614}_{-0.989}$ at 95% of CL [165]. Notice that, often, data analysis are made assuming the validity of the consistency relation. Admitting a prior on the tensor spectral index which violates eq.(4.1), leads to non-irrelevant deviations in the parameter estimations [157].

The prospects of constraining a possible deviation of the inflationary consistency relation are shown in figure 4.1, together with current upper limits provided by several experiments (for details on each experiment and the related limits see section 3). The plot shows the parameter space given by the tensor-to-scalar ratio r and tensor spectral index n_{T}, referred to CMB scales. The curves are obtained assuming a power-law parametrization of the inflationary GW signal on the whole range of frequencies, from CMB up to laser interferometer scales. The range of the spectral index shown in the plot is all allowed by current CMB measurements [2, 157]. Each point on the curves corresponds to a GW signal which is tangent to the power-law sensitivity curve of the associated detector or it is tangent to the upper limit curve provided by the related data. As visible, space-borne GW detectors are expected to widely improve current constraints in such a parameter-space, in particular providing stricter constraints on the tensor spectral index for fixed values of the tensor-to-scalar ratio. In some limit cases, such kind of experiments could be able of capturing a GW signal which violates the inflationary consistency relation, that would be undetectable for planned experiments on CMB scales.

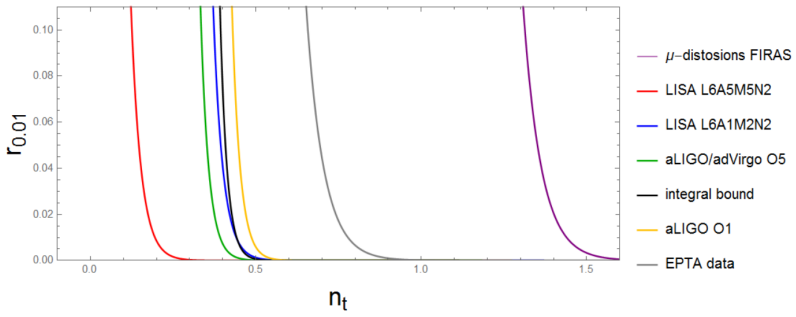

Figure 4.1: Parameter space of tensor-to-scalar ratio r and tensor spectral index n_{T} at the pivot scale of $k = 0.01\mathrm{Mpc}^{-1}$. The plot is obtained assuming a GW signal parametrized by a power-law. The region on the left of each curve is that allowed by the related data or that admitted by eventual non-observation of primordial GWs by the associated experiment. Curves are obtained from those shown in 3.1, then refer to current data or planned experiment capabilities at 95% of CL, a part from the LISA curves which refer to a signal-to-noise ratio of 10 (see 5.2 to clarify this point).

Chapter 5

Forecast for detection of inflationary gravitational waves, the case of LISA

The space-based interferometer LISA [7] for detection of GWs, is feasible to be launched in 2030. In light of the expected sensitivity to a stochastic GW background, it is interesting to study which information on inflationary physics could be probed by such an experiment. In [9], me and other collaborators of the LISA Cosmology Working Group, we made a deep investigation in this direction, considering a general inflationary GW signal and the stochastic GW background predicted by a number of specific inflationary scenarios. We found that LISA should provide new exciting information about such a physics.

The main results shown in this chapter are published in [9].

5.1 The LISA mission

LISA (Laser Interferometer Space Antenna) is the project for a space-borne laser interferometer detector of GWs. On June 20th 2017, ESA Science Programme Committee has selected LISA as the third large-class mission (L3) in its Cosmic Vision future science program. At the moment, the LISA project is approaching the end of Phase-0, i.e the mission analysis and identification. The flight is planned for 2030.

LISA is a laser interferometer composed by three spacecraft arranged in an equilateral triangle scheme. The distance between two spacecraft is planned to be 1.5 million Kilometers. This configuration will fly at a distance of about 50 million Kilometers from the Earth and will follow our planet in the revolution around the Sun; see figure 5.1. Surprisingly, three equilibrium orbits exist around the Sun and at a distance of about 50 Million Kilometers form the Earth which naturally creates the orbits for the three spacecraft, so that the path of each spacecraft has to be corrected in a minimal part each year. The proposed mission lifetime is 4 years, extendible to 10 years.

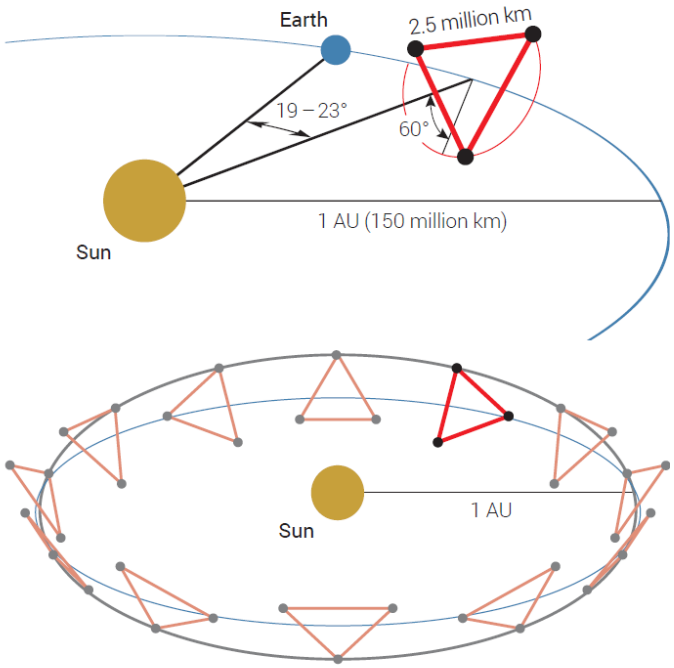

Figure 5.1: Configuration of the LISA experiment. Above, the triangular configuration with the specified position with respect to the Earth and the Sun. Below, orbit of the triangular configuration around the Sun along one year. Pictures taken from [7].

From each satellite two laser beams are emitted towards the other observatories, and two test masses are positioned in each of them, one for each incoming beam. As for terrestrial experiments, the GW signals are searched looking for the variation of the travel of laser light between two masses. However, in the case of LISA, the spacecraft are too far away from each other in order to reflect the laser signal as in a proper Michelson interferometer, then the comparison between the laser beams cannot be done concretely, while it is made virtually comparing data of incoming beams in two different spacecraft. LISA can be view as a combination of two independent interferometer (plus a null channel). The situation is complicated by the fact that a position and acceleration local disturbance of the masses are expected to be produced by several phenomena.

The robustness of the LISA project is supported by the success of the LISA Pathfinder [205], i.e. an ESA mission with the aim of studying a prototype of the LISA experiment. A single satellite has been launched on December 2015, equipped by an optical bench and two test masses, in order to test the possibility of controlling a free falling mass in such an environment, to study the related low frequency and local noise and to probe the operation of the optical bench. The exciting results of LISA Pathfinder show that the required noise for the mission have been widely achieved [206].
It has to be noticed that LISA Pathfinder tested the *local* physics, while LISA is composed by test masses separated by millions of Kilometers. However, most of the

noise in LISA is generated inside each spacecraft independently to each other, since the disturbance forces are local, then most of the expected disturbance can be well tested within a single spacecraft. This fact makes LISA Pathfinder results even more significant and promising.

The expected energy-density sensitivity of LISA is shown in fig.5.2 (in a cosmological context people usually refer to the energy-density sensitivity which is the re-expression of the more common strain sensitivity). The observatory should capture GWs with frequencies $f \in (10^{-5}, 10^{-1})$ Hz. Actually, several configurations have been proposed for LISA, according to different specifications of the experiment, in particular the number of links, the arm length, the noise at low frequencies and the mission duration. In the plot we show the curves corresponding to the configurations usually denoted as L6A1M2N2 (6 links, 1 MKm arm-length, 2 year mission, $N2$ noise level at low frequency) and L6A5M5N2 (6 links, 5 MKm arm-length, 5 year mission, $N2$ noise level at low frequency).

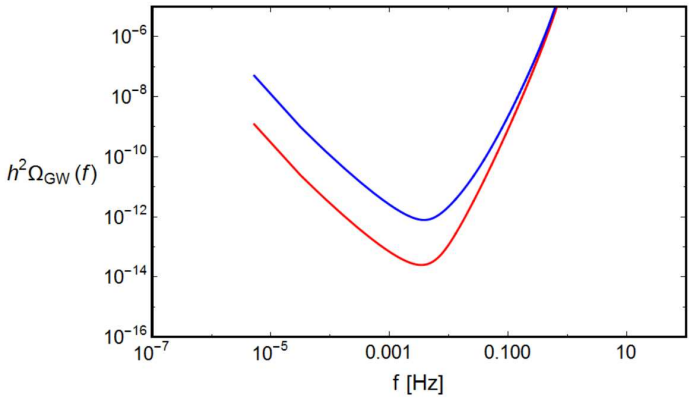

Figure 5.2: LISA energy-density sensitivity curves Ω_{sens} [173] related to the configurations L6A1M2N2 (blue) and L6A5M5N2 (red); see main text for the specifications. We will refer to the shown configurations as the *best* and the *worst* configurations.

Actually, the proposal accepted by ESA does not correspond to any of the configurations shown in figure 5.2. The planned experiment has a sensitivity which is intermediate between the two displayed curves. In the next sections we will consider the two configurations of the plot 5.2 since the presented analysis has been done before the proposal acceptance. In any case, the results we are going to present do not suffer to any relevant modification. We will refer to the shown configurations as the *best* and the *worst* configurations.

Fascinatingly, the GW waveband to which LISA is sensitive, is unexplored up to now. For this reason, LISA is expected to give a new and impressive progress in the physics of GWs. Differently from current ground-based detectors, LISA should collect a huge amount of GW signals with a large signal-to-noise ratio[1]. The main targets

[1]Contrary to terrestrial laser interferometer detector, in the case of LISA, one of the main challenge is developing tools able to disentangle and identify the huge amount of superposed GW signals.

are the GWs produced by massive black holes binaries [207], which are expected to be detected with a large signal-to-noise ratio and up to high redshifts. Moreover, solar mass black holes binaries (such as those detected by LIGO detectors) far from their merger[2] should produce a GW radiation within the LISA waveband [209], as well as galactic binaries and extreme mass ratio inspirales [210]. Astrophysical and possible cosmological backgrounds should be observed too.

5.2 Constraining power of LISA for a stochastic GW background

Claiming a detection of an extra-galactic stochastic GW background by planned laser interferometer experiments is not an easy task [155,156]. In such a direction, the main challenge is implementing a method able to disentangle a possible cosmological GW signal from instrumental noise and foregrounds.

Two main tools can be exploited in order to separate the instrumental noise from a stochastic GW signal [155]. Firstly, the cross-correlation between multiple detectors, secondly, the different transfer function and spectral shape of the noise and of the GW signals. Moreover, interestingly, one of the combinations of the three detector responses turns out to be un-sensitive to GW signals. Such a combination is usually called null channel. Actually, the latter is completely un-sensitive only in the zero-frequency limit, elsewhere a weak response is expected because of the finite arm-length of the detectors. The null channel is crucial to search for un-modelled background signals and to distinguish them from the instrumental noise. In the LISA studies performed up to now, a perfectly stationary, Gaussian and completely well understood noise is assumed. In such a case, the special role of the null channel is not relevant. When departures from such hypothesis are considered, then the null channel acquires its significance. Clearly, an improvement in this direction is required for future investigations.

Furthermore, in the LISA waveband, galactic background signals are expected, in particular galactic white dwarf binaries should constitute the most relevant one. Many galactic white dwarf should be individually resolvable, while the rest will generate a stochastic background signals which could be significantly larger than possible cosmological gravitational radiation. In order to distinguish the galactic signal from the cosmological one, their different spectral shape can be exploited [156]. On the over hand, from the solvable white dwarf GW signals, constraints on the parameters which describes their contribution can be extracted. Furthermore, the galactic GW foreground is expected to be modulated with a one-year period due to the motion of LISA around the Sun. Modelling these features, it is found that a cosmological GW background should be detectable by LISA even if its amplitude is strongly below that of

[2]People found out that such a kind of sources could be visible in the LISA window and after a certain period of time, the same source could be visible in the LIGO-Virgo detectors [208].

the galactic foreground [156].
Notice that, moreover, also extra-galactic background of astrophysical origin constitute a foreground for cosmological signals. In particular, unsolved signals from black hole - black hole and neutron star - neutron star mergers may have a significant impact on the identification of a stochastic background of cosmological origin.

5.2.1 Signal-to-noise ratio and signal detectability of a detector network

From the instrumental specifications of an observatory and with a simulator of the experiment, the sensitivity curve, i.e. the ratio between the response of the detector to the noise and the response of the detector to the GW signal, can be obtained [211,212]:

$$h^2\Omega_{sens}\left(f\right) \equiv \frac{2\pi^2}{3H_0^2} f^3 \left[\frac{P_{\rm n}\left(f\right)}{R_{\rm h}\left(f\right)}\right] , \tag{5.1}$$

where $P_{\rm h}$ is the noise spectral power density, while $R_{\rm h}$ is the response to a GW signal, i.e. the antenna pattern averaged over polarizations and direction on the sky. The latter is obtained by simulations. For a network of detectors, the previous expression is generalized as [212]:

$$h^2\Omega_{sens}\left(f\right) \equiv \frac{2\pi^2}{3H_0^2} f^3 \left[\sum_{I=1}^{N}\sum_{J>1}^{N} \frac{\Gamma_{IJ}^2\left(f\right)}{P_{\rm nI}\left(f\right) P_{\rm nJ}\left(f\right)}\right]^{-1/2} , \tag{5.2}$$

where I and J denotes the detectors, N is their number and Γ_{IJ} is the overlap reduction function which expresses the cross-correlation between detector I and detector J (Γ_{IJ} reduces to $R_{\rm h}$ for $I = J$). The sensitivity curve $h^2\Omega_{sens}\left(f\right)$ provides the frequency band and an *indication* of the required spectral energy density of a GW signal in order to be detectable by the associated experiment.
However, in order to claim a GW detection, referring to a proper statistic is required. Once a threshold value of the latter is established, signals corresponding to a statistic value above the threshold are considered as a GW detection. In this context, people usually refer to the signal-to-noise ratio (SNR) statistic.

In general, the collected signal of each detector I is given by the sum of a GW input and the intrinsic noise, that is:

$$s_I = h_I\left(t\right) + n_I\left(t\right) , \tag{5.3}$$

where h_I is the GW strain and n_I is the intrinsic noise. Considering the simple case of a network composed by two coincident and coaligned detectors, we can define the following quantity:

$$S \equiv \int_{T/2}^{T/2} dt\, s_1\left(t\right) s_2\left(t\right) \tag{5.4}$$

where T is the detection time. Then the SNR statistic is defined as:

$$\mathrm{SNR} \equiv \frac{\langle S\rangle}{\sigma} , \tag{5.5}$$

where σ^2 is the cross correlation variance of the signal s. In terms of the spectral energy density, the expression for $\langle S \rangle$ turns out to be (calculation are performed in appendix C):

$$\langle S \rangle = \int_{-T/2}^{+T/2} dt \, \langle h\,(t)\, h\,(t) \rangle = T \langle h^2\,(t) \rangle = \frac{3H_0^2}{20\pi^2} T \int_{-\infty}^{+\infty} df \, \frac{\Omega_{\rm GW}\,(f)}{f^3}\,. \tag{5.6}$$

Generalizing S for a network of detectors and modelling the noise n_I in terms of P_n, the definition (5.5) turns out to be [212]:

$$\mathrm{SNR} = \left[2T \int_{f_{min}}^{f_{max}} df \, \sum_{I=1}^{N} \sum_{J>1}^{N} \left(\frac{3H_0^2}{2\pi^2} \frac{\Omega_{\rm GW}}{f^3} \right)^2 \frac{\Gamma_{IJ}^2\,(f)}{P_{\rm nI}\,(f)\, P_{\rm nJ}\,(f)} \right]^{1/2}, \tag{5.7}$$

where a vanishing correlation between noise and signal is assumed, and f_{min}, f_{max} are the extreme frequencies to which the experiment is sensitive (and a numerical factor has been included in the overlap reduction function). From the definition (5.2), the SNR can be expressed also in terms of the sensitivity curve $\Omega_{\rm sens}$:

$$\mathrm{SNR} = \left[T \int_{f_{min}}^{f_{max}} df \, \frac{\left[h^2 \Omega_{\rm GW}\,(f) \right]^2}{\left[h^2 \Omega_{sens}\,(f) \right]^2} \right]^{1/2}. \tag{5.8}$$

In order to claim or not a detection, referring to a threshold value of the statistic SNR is required. To establish such a value, in the case of LISA, a bayesian method has been employed. More precisely, the procedure is based on the evaluation of the Bayes factors for several GW signals with respect to the hypothesis of noise only. Varying the parameters which determine the GW signal, when the Bayes factor gets a reasonably large value, the associated parameters of the GW signal are taken as the threshold values. By the latter, the corresponding threshold value of the SNR, i.e. SNR_{th} is calculated by (5.8). Notice that, for each parametrization of GW signal, a proper analysis has to be done, and a specific value of SNR_{th} is found. Then, in order to establish the detectability of a fixed GW signal, one calculates the corresponding SNR by (5.8), if the latter is larger than the threshold SNR value, then the GW signal can be considered as detectable.

5.2.2 Power-law sensitivity curves of LISA

In previous chapters we saw that the inflationary mechanism predicts the production of a stochastic GW background broaden on a wide range of frequencies. In particular, for several inflationary models the related GW power spectrum turns out to be well parametrized by a power law, i.e. by an amplitude and a spectral index. Moreover, in section 2.6, we found that the power-law shape is preserved in the associated present-time GW spectral energy density.

The SNR_{th} value for such a kind of signal has been obtained by [156]. More precisely, considering a power-law GW background, carrying out the Bayesian procedure, a threshold value of $\Omega_{\rm GW} \simeq 10^{-12}$ for a scale-invariant signal has been found. The corresponding value of the statistic threshold turns out to be $\mathrm{SNR}_{th} = 10$, for the

sensitivity of the LISA (configuration $L6A5M1N2$). Notice that this value has been obtained making several assumption, i.e. considering a gaussian and scale-invariant noise and a complete knowledge of the latter. On the other hand, it has been obtained taking into account for the expected galactic confusion foreground and assuming the GW signal amplitude to be well below the instrument noise. For the study of power-law inflationary GW signals we will refer to such a value of SNR_{th}.
Interestingly, established the SNR_{th} associated to a power-law GW signal, manipulating the sensitivity curve, it turns out that the comparison between the SNR of a candidate power-law signal and SNR_{th} can be done graphically by the construction of the so-called power-law sensitivity curves introduced by [172]. The underlying idea is to build up a curve which includes the calculation of SNR_{th}, i.e. taking into account the broad nature of the GW signal we are interested in. Clearly, this procedure can be performed for each experiment once the sensitivity curve $\Omega_{sens}(f)$ and the SNR_{th} value for power-law signals are provided.

Parametrizing the present-time GW spectral energy density by an amplitude $\Omega_\alpha(f_*)$ and a spectral index α, i.e.:

$$\Omega_{\mathrm{GW}}(f) = \Omega_\alpha(f_*)\left(\frac{f}{f_*}\right)^\alpha , \tag{5.9}$$

where $\Omega_\alpha(f_*)$ is a function of the primordial amplitude A_{T} (cf. eq.(2.94)), the expression of the SNR, results into a specific form. In particular, from (5.8), imposing the SNR to equal SNR_{th}, the following equality is obtained:

$$\Omega_\alpha = \frac{\mathrm{SNR}_{th}}{\sqrt{2T}}\left[\int_{f_{min}}^{f^{max}} df\,\frac{(f/f_*)^{2\alpha}}{\Omega^2_{sens}(f)}\right]^{-1/2} . \tag{5.10}$$

For each value of the parameter α, the Ω_α value which satisfy such an equation corresponds to a GW signal with $\mathrm{SNR} = \mathrm{SNR}_{th}$. Then, establishing a reasonable range of values E for the spectral index α, for each frequency f between f_{min} and f_{max}, we can calculate the following maximum:

$$\max_{\alpha\in E}\left[\Omega_\alpha\left(\frac{f}{f_*}\right)^\alpha\right] = \max_{\alpha\in E}\left[\frac{\mathrm{SNR}_{th}}{\sqrt{2T}}\left[\int_{f_{min}}^{f^{max}} df\,\frac{(f/f_*)^{2\alpha}}{\Omega^2_{sens}(f)}\right]^{-1/2}\left(\frac{f}{f_*}\right)^\alpha\right] \equiv \Omega_{sens,pl}(f) , \tag{5.11}$$

that is, we are selecting the "worst" case at each frequency. The pairs $f - \Omega_{\mathrm{GW}}$ obtained by eq.(5.11) constitute the power-law sensitivity curve $\Omega_{sens,pl}(f)$. By a simple reasoning, it is clear that the latter constitutes the curve above which each power-law GW signal has a SNR larger than SNR_{th}.
The interesting point is that for a signal to have $\mathrm{SNR} > \mathrm{SNR}_{th}$, is sufficient the corresponding Ω_{GW} to exceed the power-law sensitivity curve *somewhere*. Such a procedure does not hold for the sensitivity curve $\Omega_{sens}(f)$. Indeed, the latter does not take into account for the integration over frequencies required to calculate the SNR

for a broaden signal[3].
In figure 5.3 we show the result obtained from the LISA sensitivity curves presented in figure 5.2. Establishing the detectability of a GW power-law signal, now it is easy: we know that each curve that somewhere is above the power-law sensitivity curve corresponds to a SNR larger than the threshold value, and therefore that it is in principle detectable.

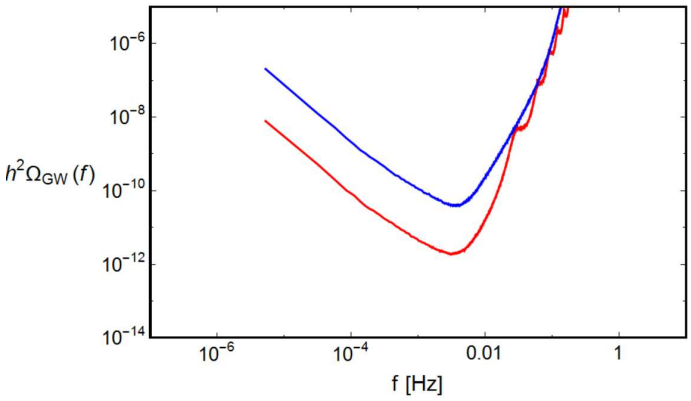

Figure 5.3: Power-law sensitivity curves of LISA $\Omega_{sens,pl}$ [173] related to the configurations presented in figure 5.2: L6A1M2N2 (blue) and L6A5M5N2 (red); see main text for the specifications.

In the next sections, in order to claim an expected detection of a primordial GW signal well described by a power-law, we will refer to the power-law sensitivity curve.

5.2.3 Constraints on the primordial parameters

In the following analysis we forecast the capabilities of LISA in probing inflationary physics. LISA is clearly sensitive to the *present time* GW spectral energy density, therefore in order to extract information on primordial parameters, modelling the evolution form their generation up to the present time is required.
We parametrize the *primordial* GW power spectrum by a power law:

$$P_{\mathrm{T}}(k) = A_{\mathrm{T}} \left(\frac{k}{k_*}\right)^{n_{\mathrm{T}}} . \tag{5.12}$$

In section 2.6, we presented how to calculate the present time GW spectral energy density starting from a primordial GW signal. We report such a result, evaluated at the present time:

$$h^2\Omega_{\mathrm{GW}}(k,\tau_0) = \frac{1}{12}\left(\frac{k}{a_0 H_0}\right)^2 P_{\mathrm{T}}(k)\, T_{\mathrm{h}}^2(k,\tau_0) , \tag{5.13}$$

[3]Notice that for each kind of a broaden GW signal, the SNR is given by an integration on frequencies, not only for power-law signals. Therefore a comparison of Ω_{GW} with the sensitivity curve $\Omega_{sens}(f)$ is, in principle, reasonable only for GW signal peaked on a single frequency. For broaden signal, with a more complicated shape than a power law, the related value of the SNR has to be calculated each time by (5.8) and then compared with the established threshold.

The combination of the transfer function $T_{\rm h}^2$ and the term proportional to k^2, gives an overall scale invariant factor, so that the present time GW spectral energy density reflects the same scale dependence of the primordial signal. Moreover, it has been noticed that the amplitude in (5.13) can be approximated by $\Omega_{\rm GW}(f_*) \simeq \Omega_{\rm R,0} A_{\rm T}(f_*)/24$ [53], where $\Omega_{\rm R,0} \simeq 10^{-5}$ is the present time radiation energy density. Such an approximation turns out to be safe in light of analysis we are going to perform. In summary, the present GW spectral energy density can be written as:

$$\Omega_{\rm GW}(f) \simeq \frac{\Omega_{\rm R,0}}{24} A_{\rm T}(f_*) \left(\frac{f}{f_*}\right)^{n_{\rm T}} . \tag{5.14}$$

Comparing $\Omega_{\rm GW}$ expressed as in eq.(5.14), with the LISA power-law sensitivity curves shown in figure 5.3, the pairs of values $A_{\rm T}$ and $n_{\rm T}$ corresponding to a signal tangent to $\Omega_{sens,pl}$ can be found. Such values identify the GW signals at the detection limit of LISA. In figure 5.4 we show the corresponding curves in term of the tensor-to-scalar ratio r and the tensor spectral index $n_{\rm T}$. The pivot scale is fixed at $k = 0.01{\rm Mpc}^{-1}$ and the scalar amplitude is fixed at the estimation provided by Planck, i.e. $A_{0.05} = 2.21 \cdot 10^{-9}$ at 68% C.L. at $k_* = 0.05{\rm Mpc}^{-1}$ [17]. In the next section, we will carry

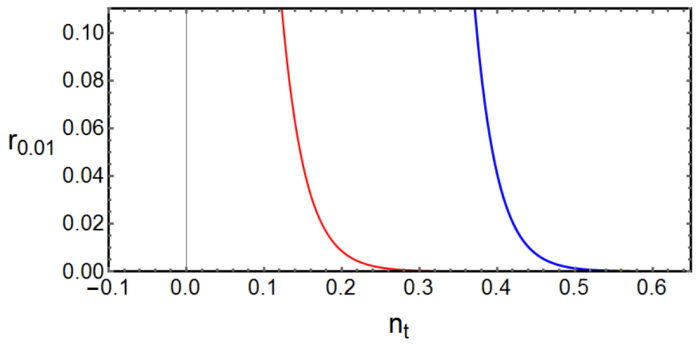

Figure 5.4: Constraining power of LISA on the parameter space given by the primordial tensor-to-scalar ratio r and the spectral index $n_{\rm T}$ at the scale $k = 0.01{\rm Mpc}$. the scalar amplitude is fixed at the estimation provided by Planck. Each curve refers to a specific LISA configuration: L6A1M2N2 (blue) and L6A5M5N2 (red); see main text for the specifications.

out the following procedure, to be adapted to each specific inflationary scenario: we explicit the primordial parameters $A_{\rm T}$ and $n_{\rm T}$ in eq.(5.14) in terms of the specific parameters of the selected inflationary model, we compare such a GW signal with the LISA power-law sensitivity, taking as a discriminant the GW signals tangent to such a curve and we extract the constraints on the GW parameters, and as a consequence on the inflationary quantities.

5.3 Constraints form other physical observables

Beside making forecasts for LISA capabilities in probing inflation, we would like to compare such results with other limits on the inflationary physics provided by several

observations. In the present section we outline those we are going to consider and how we will employ them, so that later we will refer to the procedures explained here.

Firstly, we consider current bounds on the present-time GW spectral energy density:

- The non-observation of B-modes of primordial origin in CMB polarization power spectra, provides un upper bound on the amplitude of the tensor power spectrum at large scales. Such a constraint is usually expressed by un upper limit on the tensor-to-scalar ratio r, obtained by fixing the amplitude of scalar power spectrum at the best fit value obtained by Planck observations. More precisely, the joint analysis of Planck and BICEP data provide un upper bound of $r_{0.05} < 0.09$ at 95% C.L. [97] at a pivot scale of $k_* = 0.05\text{Mpc}^{-1}$. From the expression (5.14), such a limit becomes $\Omega_{\text{GW}}(f_*) < 10^{-15}$ with $f_* \simeq 10^{-17}\text{Hz}$, at the present time.
  Assuming a power-law tensor modes, CMB data provides also constraints on the tensor spectral index n_{T}. However such constraints result weaker than other we are going to consider here.
  Where significant, we will also take into account for the upper bound on the tensor non-gaussianities provide by Planck observations [46].

- LIGO-Virgo Collaboration provided the power-law sensitivity curve of the LIGO detector for the expected five observational runs [168]. Here we consider the curve related to the aLIGO O1:2015-16 observation run which corresponds[4] to $\text{SNR}_{th} = 1$. In the next analysis we will use the aLIGO power-law sensitivity curve in the same manner we use the LISA power-law sensitivity curve, as explained in section 5.2.3.

- Another relevant constraint of the GW spectral energy density is provided by observations related to BBN physics (see section 3). More precisely, the latter is sensitive to the GW amount filling the universe at the time of BBN process. Notice that at the moment of BBN, only a certain range of scales have already entered the horizon, i.e. those corresponding to $f \gtrsim 10^{-10}\text{Hz}$. The combination of such a limit with CMB observations, BAO and primordial Deuterium abundance measurements leads to an upper bound on the integrated GW spectral-energy density of:
  $$\int_{f_m}^{f_M} \frac{\mathrm{d}f}{f} \Omega_{\text{GW}}(f) < 3.8 \cdot 10^{-6} \tag{5.15}$$
  at 95% C.L. [118]. The frequency f_m is fixed by the time of the BBN process, and it is found to be $f_m \simeq 10^{-10}\text{Hz}$, while f_M corresponds to the end of inflation, i.e. it depends on the reheating temperature. We fix the pivot frequency at CMB scales, i.e $f_* = 10^{-17}\text{Hz}$. Assuming that such an amount was given by

[4] After this analysis has been performed, LIGO-Virgo Collaboration published the upper bound on the GW spectral energy density for power-law signals, obtained by data of the O1 observation run [161]. Slightly worst limits have been found with respect to the proposed sensitivity curve [168]. However, such a difference turns out to be not relevant with respect to the results we are going to present.

GWs with a power spectrum described by a power law, the upper limit provided by [118], can be translated into an upper bound on the GW spectral energy density $\Omega_{\rm GW}(f)$. More precisely, writing $\Omega_{\rm GW}(f)$ as in (5.9), the bound (5.15) becomes:

$$\int_{f_m}^{f_M} \frac{\mathrm{d}f}{f} \Omega_\alpha(f_*) \left(\frac{f}{f_*}\right)^\alpha < 3.8 \cdot 10^{-6} \,. \tag{5.16}$$

The amplitude $\Omega_\alpha(f_*)$ turns out ot be:

$$\Omega_\alpha(f_*) < 3.8 \cdot 10^{-6} \frac{\alpha f_*^\alpha}{f_M^\alpha - f_m^\alpha} \,. \tag{5.17}$$

Then the GW spectral energy density which matches the integral limit (5.15), reads:

$$\Omega_{\rm GW}(f) = \left[3.8 \cdot 10^{-6} \frac{\alpha f_*^\alpha}{f_M^\alpha - f_m^\alpha}\right] \left(\frac{f}{f_*}\right)^\alpha \,. \tag{5.18}$$

This function is analogous to (5.10)-(5.11), i.e. in such a case the integral quantity equals a SNR_{th} value, here the integral quantity match the limits value provided by BBN observations. Therefore, varying α on a reasonable range of values, for each frequency we choose the maximum value of $\Omega_{\rm GW}(f)$. Such pairs $f - \Omega_{\rm GW}(f)$ constitute a sort of power-law "limit" curve. Indeed each $\Omega_{\rm GW}$ with a power-law shape which somewhere is above such a curve, corresponds to an integrated GW spectral energy density which exceed the limit provided by [118], and it is therefore excluded at the 95% of CL. The curve is shown in figure 3.1, black coloured. We will consider such a curve following the procedure explained in section 5.2.3.

Then we consider other constraints on inflationary physics provided by observations related to the scalar perturbations produced during inflation. Often, when a significant GW classical production happens during inflation, also a relevant second-order scalar production takes place. The latter and the classical GW production are usually described by the same parameters, so that, in many cases, constraints on the scalar perturbations corresponds to limits on the GW production. Clearly, these bounds will be relevant when the inflationary parameters involved in the scalar sector are the same that describe tensor perturbations.

- CMB measurements provides stringent constraints on inflationary scalar perturbations. Where significant, we will consider the current estimation of the scalar perturbation amplitude, i.e. $A_{0.05} = 2.21 \cdot 10^{-9}$ at 68% C.L. at $k_* = 0.05\mathrm{Mpc}^{-1}$ [213]. Notice that such limit refers only to CMB scales.

- Current non-observation of primordial black holes puts un upper bound on the amplitude of primordial scalar perturbations on a broad range of frequencies, see section 3.1. More precisely, they provide roughly un upper limit on the scalar perturbation amplitude of $A_{\rm S} \lesssim 10^{-10}$ for $f \in (10^{-2} - 10^2)\,\mathrm{Hz}$ at 95% of CL [142]. When relevant, we will consider such a bound, however, notice that it is obtained performing several assumptions which could compromise the value of such limits, therefore we will consider these bounds as uncertain.

Notice that all the constraints presented here refer to a 95% of CL, so that they are all comparable. On the other hand, the power-law sensitivity curve of LISA refers to a SNR_{th} value. The corresponding CL has not been calculated yet, even thought the value of the underlying Bayes factor is so large that we can surely refer to SNR_{th} to claim a detection. Then in the following analysis, we will compare anyhow the LISA curve with the others, being aware of this fact.

5.4 Forecast for specific inflationary models

We consider three specific inflationary models, that we have already presented in sections 2.2.1-2.3. In particular, we saw that in each of them a significant GW production takes place. Here we forecast the constraining power of LISA on the inflationary parameter space associated to such scenarios.

5.4.1 Inflation with a scalar spectator field

We study the specific model presented by [67] and that we have already discussed in section 2.2.4. Notice that we are investigating a specific model, in this sense our analysis is model-dependent. Consider an inflationary scenario described by:

$$\mathcal{L} = \frac{1}{2}M_{Pl}^2 R + \frac{1}{2}\partial_\mu\varphi\partial^\mu\varphi - V(\varphi) + P(X,\sigma) \ , \tag{5.19}$$

where φ is the inflaton, σ is the spectator field, $X = \frac{1}{2}\partial_\mu\sigma\partial^\mu\sigma$ and P is a generic function of X and σ. The propagation speed of σ perturbations is equal to $c_s \equiv P_X/(P_X + P_{XX}\dot{\sigma}_0^2)$. Perturbations of the spectator field give rise to a source term in the equation of motion of tensor modes. Here we are interest in the case in which $c_\mathrm{s} \ll 1$, since we will see that in such a situation the second-order production of GWs turns out to be significant. We also admit a time dependence of such a quantity. The whole amount of produced GWs is given by the sum of two contributions: one due to quantum fluctuations of the gravitational field, and one which corresponds to the second-order production due to the presence of the spectator field σ.

Gravitational wave production and second-order scalar perturbations. According to what we presented in section 2.2.4, the whole power spectrum for GWs, turns out to be:

$$P_\mathrm{T}(k) \simeq \frac{2H^2}{M_{Pl}^2}\left(\frac{k}{k_*}\right)^{-2\epsilon} + \frac{8}{15\pi c_s^3}\frac{H^4}{M_{Pl}^4}\left(\frac{k}{k_*}\right)^{-4\epsilon-3s} \ , \tag{5.20}$$

where H and c_s are evaluated at $k = k_*$, and s is defined in (2.72). For negative values of the parameter s, the spectral index of the second-order GWs can reach positive values, i.e. the sourced GW power spectrum can be blue.

In this scenario a relevant second-order scalar perturbation production takes place too. As for the tensor sector, scalar perturbations of the spectator field give rise to

a source term in the equation of motion of curvature perturbations, so that an extra contribution to the scalar power spectrum is produced.
The complete calculation of sourced curvature perturbations is quite complicated, since many terms of the form $\sim \delta\varphi\delta\sigma\delta\sigma$ appear in the action perturbed at third order. The authors of [67] claim that it is not clear which of those terms determines the main contribution to the curvature perturbations and they take into account only for the term of the form $\delta N \left(\partial_i \delta\sigma\right)^2$, where $\delta N \sim \delta\varphi$, which is enough for their aim. On the other hand it is not to be excluded that some term in the source could cancel to each other. Therefore we decided to proceed taking into account only the same term considered by [67]. The amplitude of scalar perturbations induced by such a source results:

$$A_S^{(s)} \simeq \frac{1}{32\pi c_s^7} \frac{H^4}{M_{Pl}^4}\,, \tag{5.21}$$

where H and c_s are evaluated at the pivot scale. Notice that also this amplitude is inversely proportional to the propagation speed c_s, therefore, an enhancement of the sourced GWs means at the same time an enhancement of sourced curvature perturbations. As before, considering a generic scale dependence of H and c_s, the sourced curvature perturbation power spectrum, is described by the following spectral index:

$$n_S^{(s)} - 1 = -4\epsilon - 7s\,. \tag{5.22}$$

Considering the result for curvature perturbations produced in the single-field slow-roll inflationary scenario, the whole amount of curvature power spectrum is given by the sum of two contributions described by a power-law respectively:

$$P_S\left(k\right) \simeq \frac{H^2}{4\epsilon M_{Pl}^2}\left(\frac{k}{k_*}\right)^{-6\epsilon+2\eta} + \frac{1}{32\pi c_s^7}\frac{H^4}{M_{Pl}^4}\left(\frac{k}{k_*}\right)^{-4\epsilon-7s}\,, \tag{5.23}$$

where H and c_s are evaluated at $k = k_*$.

Equation (5.20) shows that for sufficiently small values of the propagation speed c_s the amplitude of sourced GWs can reach significant values and in principle, it can exceed the amplitude of GWs generated by quantum fluctuations of the gravitational field. Moreover, if c_s is getting smaller during inflation, the related spectral index can be positive, so that the sourced GWs can reach a large amplitude at the scale of LISA.
On the other hand we have to consider the counterpart of scalar production. Current cosmological observations provide strict constraints on the amplitude and the spectral index of curvature perturbations at CMB scales [2]. From the expressions (5.20)-(5.23), it is clear that bounds on the curvature power spectrum provide limits on the same inflationary parameters which determines the amount of GWs. More precisely, they are both determined by the Hubble parameter H, the propagation sound speed c_s, the slow-roll parameters ϵ and s. Therefore in the following analysis, we will consider also the bound on the parameter space of the model obtained form current constraint on scalar perturbations.

We assume that the expressions (5.20)-(5.23) are valid on the range of frequencies from CMB scales up to the range of LISA frequencies. Notice that this not an obvious assumption, given the so large range of frequencies we are covering.
We consider the parameter space $c_s - s$ for fixed values of the Hubble parameter H and at the pivot scale $k = 0.05\text{Mpc}^{-1}$.

Current constraints from CMB observations. Consider the whole amount of curvature perturbations given by (5.23). Plank data provide un upper bound on the slow-roll parameter ϵ, i.e. $\epsilon < 0.0068$ at 95% C.L. [2] considering *Planck TT+lowP*, that is temperature and low ℓ polarization data. For a fixed value of H, the upper bound on the slow roll parameter ϵ provides a lower limit on the amplitude of scalar perturbations from vacuum fluctuations. As a consequence, an upper limit on the amplitude of the sourced curvature perturbations is found. Then from the expression (5.21), a lower bound on c_s is obtained. For values of c_s smaller than such a limit, in order to satisfy the estimation of the curvature amplitude, values of ϵ larger than the upper limit provided by Planck, are required.
In order to reach the LISA sensitivity we are interested in positive values of the spectral index of the sourced GWs. To obtain a blue tensor power spectrum a negative and sufficiently large value of s is required. However, at the same time, such values of s lead to a blue power spectrum for sourced curvature perturbations too. CMB measurements provide strict constraints on the scalar spectral index. Therefore we have to verify that on the whole range of frequencies to which CMB is sensitive, the amplitude of scalar perturbations agrees with such an estimation. In particular, we are looking for those cases in which the amplitude of the sourced scalar perturbations increases with the frequency, while current measurements point out a red value of the scalar spectral index at large scales. Therefore, in particular, we have to ensure that the sourced scalar contribution does not spoil current measurements at the smallest scale to which CMB measurements are sensitive. More precisely, we consider the parametrization of the scalar power spectrum made by [2], where a spectral index, a running of the spectral index and a running of the running are admitted. We calculate the scalar amplitude at $k = 0.1\text{Mpc}^{-1}$ with the parameter estimations provided by such analysis and we required the total amplitude of scalar power spectrum to not exceed it at the same scale. This requirement turns out to put a lower bound on c_s more stringent than the one found before (with same fixed value of H), providing a new upper bound on the sourced contribution to scalar perturbations. The same request points out also an upper bound on the spectral index, i.e. on $|s|$, for a given value of the sourced scalar amplitude. These bound are displayed in figure 5.5. Actually, the shown limits are sensitive to the choice of $k = 0.1\text{Mpc}^{-1}$ and to the related value of the amplitude imposed. However, as we will see soon the significance of the role of the LISA experiment does not suffer such changes, since it spits the parameter space in a completely different direction with respect to the bound shown up to now. Notice that the allowed parameter space, correspond to a sourced contribution to curvature perturbations on CMB scales, tiny with respect to that due to vacuum fluctuations of the inflaton. This fact also justify our choice of considering the upper limit of ϵ referred to a single-field model.

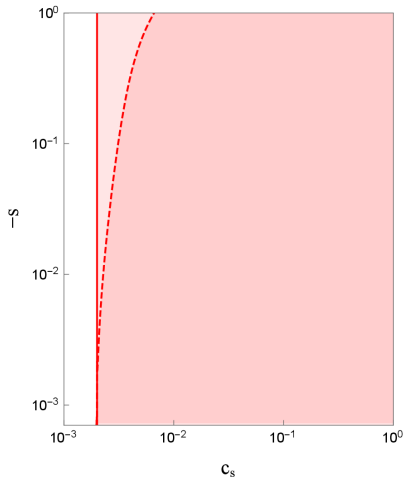

Figure 5.5: Parameter space of c_s-s at $k_* = 0.05\text{Mpc}^{-1}$. The lower bound on c_s obtained from the upper bound on ϵ and from the estimation of the scalar amplitude on CMB scales is reported. The red region is that allowed by such constraints. The red-dashed curve is the bound obtained from CMB data at small scales, as explained in the text. Taken form [9].

Moreover, in inflationary scenarios with spectator fields, a significant production of scalar non-gaussianities is, in general, expected. Current CMB observations provide upper bounds of the non-linear parameter f_{NL} defined in eq.(1.25), for different configurations of the bispectrum. In models where a spectator field is present, usually the amplitude of the parameter f_{NL} is inversely proportional to a power of the propagation speed of sound c_{s}. Therefore, un upper bound on non-gaussianities, in general, provides a lower bound on c_{s}. Also for the scenario we are considering here, we expect that the non-observation of a scalar bispectrum at CMB scales, implies a lower bound on c_{s}. Planck Collaboration provides the lower bound on the propagation speed only for a few specific models [46]. For our scenario, we expect that current bounds on f_{NL} implies a lower bound on c_{s}, but in order to find the exact value a complete calculation of the scalar bispectrum is required. Therefore, in principle, a complete calculation of non-gaussianities could point out a more stringent lower bound on c_{s} with respect to those reported before. However, the only estimation [68] we have about non-gaussianities in this kind of scenarios points out that scalar non-Gaussianities induced by the spectator field should be suppressed. In light of this consideration, LISA might turn out to be more powerful in constraining the parameter space than bounds on scalar non-gaussianities. On the other hand, in light of the dependence of this kind of estimations on the specific model considered, it should not be excluded that a complete computation of scalar non-gaussianities might reduce the allowed parameter space. In this direction, a complete calculation of the non-gaussianities of curvature perturbations related to this scenario could be an interesting improvement of the present analysis.
Notice that we are considering a region in the parameter space where the sourced scalar power spectrum can be significantly blue, therefore also the parameter f_{NL} could present a significant scale dependence. Current CMB observations do not pro-

vide constraints on the scale dependence of $f_{\rm NL}$ that could be applied in the scenario considered here. However, if significant constraints on the scale dependence of $f_{\rm NL}$ will be extracted from CMB data, these could provide a new bound in the parameter space.

Forecast for LISA. In the region of the parameter space for which the GW signal reaches the LISA power-law sensitivity curve, the amplitude of tensor modes due to quantum fluctuations of the gravitational field is negligible at LISA frequencies, then in order to establish for which parameter values the inflationary GWs are detectable by LISA, we can approximated (5.20) with the second term. At $k_* = 0.05{\rm Mpc}^{-1}$, the slow-roll parameter ϵ appearing in the spectral index of tensor modes can be written in terms of the parameters c_s by requiring the whole scalar amplitude at the pivot scale to be given by the value provided by Planck analysis, for a fixed value of H, see eq.(5.23). So, at the end $P_{\rm T}(k)$ turns out to be parametrized by c_s and s, for a fixed value of H. Then, by eq.(5.14), the present-time GW spectral energy density $\Omega_{\rm GW}$ is written as a function of c_s and s. Therefore, for each value of c_s, one can identify the smaller value of s for which $\Omega_{\rm GW}$ reaches the LISA sensitivity curve. These couples of values build up the curves represented in the right panel of figure 5.6, from which it is visible that LISA is expected to provide completely new information in the parameter space of this inflationary model. In this sense, the significance of the constraining power of LISA is not affect by the exact value of the lower bound on $c_{\rm s}$ due to constraints provided by the scalar sector.

Constraints from other observables. We consider also the power-law sensitivity curve provided by LIGO-Virgo Collaboration and by consideration on the BBN process introduced in section 5.3. Following th same procedure performed for LISA we obtain the related bounds in the parameter space $c_{\rm s} - s$. The results are shown in figure 5.7. For large values of $c_{\rm s}$, the LIGO-Virgo capabilities turns out to be the most stringent one with respect to other experiments at small scales.
For constraints from BBN physics, as range for the values of the spectral index, we chosen $n_{\rm T} \in (-1; 3)$. The final result does not depend significantly on the choice of such a range. On the other hand the limits found here significantly depend on $f_{\rm reh}$, i.e. on the reheating temperature, which determines the decay frequency of the GW spectral energy density. In the plot we show the situation in which the most stringent bounds are obtained, that is we supposed an instantaneous reheating at the end of inflation.
We also consider constraints obtained form non-observation of PBH. In most of the parameter region of our interest, the sourced scalar perturbations present a blue power spectrum. Therefore the constraints derived by PBH physics put strong bounds in such a region. In figure 5.7 on the right, the upper limit of the green region is obtained imposing an amplitude of the soured scalar amplitude of 10^{-2} at $\bar{f} = 10^6$Hz (where we fixed ϵ as explained above). The relevance of the bounds obtained does not vary significantly changing the value of $\bar{f}$ and the corresponding value of $\Omega_{\rm GW}$, of a few order of magnitude.

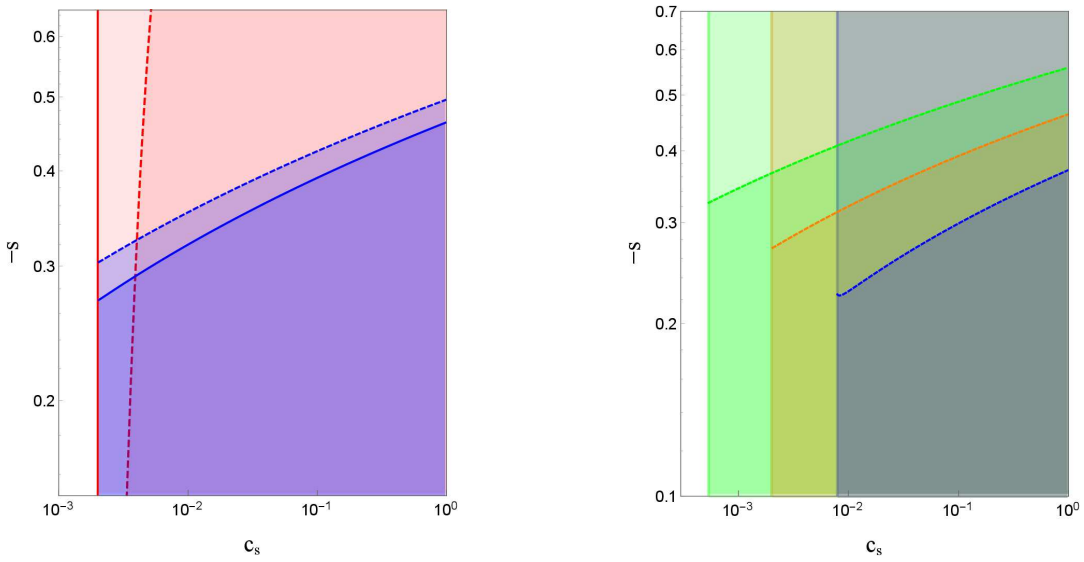

Figure 5.6: Parameter space of c_s-s at $k_* = 0.05\text{Mpc}^{-1}$. Plot on the right: blue curves represent the discriminant power of LISA, the dashed curve corresponds to worst LISA configuration, the solid one to the best one. The blue region is that left allowed by an eventual non-detection of the GW signal associated to this scenario by the respective LISA configuration. All the curves are obtained for $H = 10^{12}$ GeV. On the left: bounds obtained from CMB measurements (vertical lines) and LISA discriminant power, for different values of the energy scale of inflation, e.g. of H. Each colour corresponds to a fixed value of the Hubble parameter: $H = 10^{11}$ GeV (green), $H = 10^{12}$ GeV (orange), $H = 10^{13}$ GeV (blue). Taken form [9].

Assuming as valid the bounds we have from PBH physics, LISA is expected to be not able of detecting GWs produced in this kind of inflationary scenario. However, notice that we assumed that sourced scalar and tensor perturbations are described by a power-law for the whole range of frequencies from CMB scales up to the scales of laser interferometer experiments. If a running of the spectral index of scalar and/or tensor modes is assumed, the constraints form PBH observations would be widely revisited. In this sense, a non-detection of this kind of GWs by LISA would be a validation of the way we currently model PBH physics.
Notice that the possibility of testing the same parameter space by several observables or different experiments, is useful in order to discriminate among different inflationary models.

5.4.2 Inflation with gauge particle production

We now consider the inflationary model we discussed in 2.2.1, i.e. a scenario in which the inflaton is coupled to a gauge field as follows:

$$\mathscr{L} = -\frac{1}{2}\partial_\mu\varphi\partial^\mu\varphi - V(\varphi) - \frac{1}{4}F_{\mu\nu}F^{\mu\nu} - \frac{\varphi}{4f}F_{\mu\nu}\tilde{F}^{\mu\nu}\,, \tag{5.24}$$

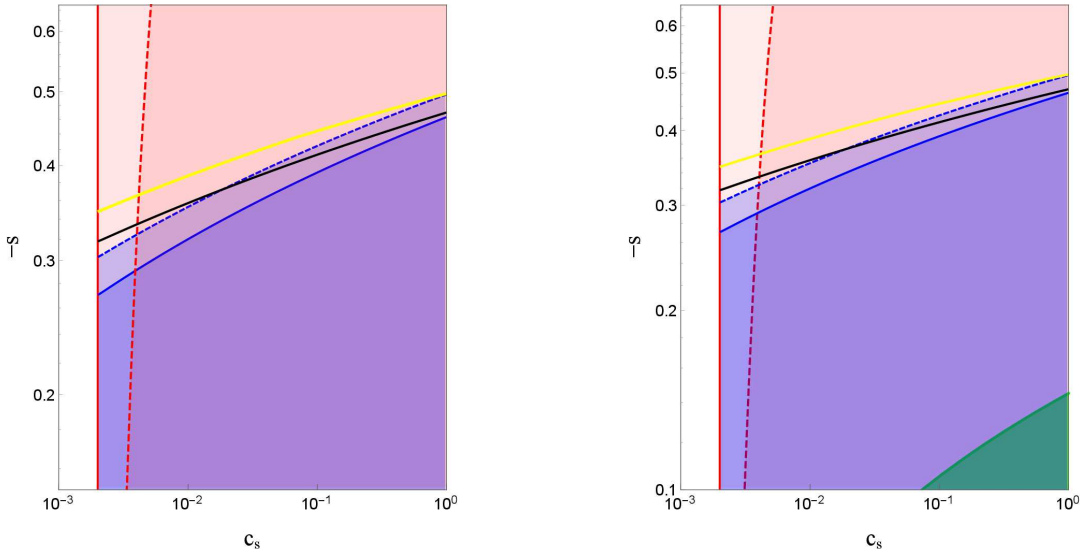

Figure 5.7: Parameter space of c_s-s at $k_* = 0.05\text{Mpc}^{-1}$. On the left: current bounds obtained from the limit provided by [118] for $T_{reh} = 10^{12}$ GeV (yellow) and those related to aLIGO O1:2015-16 observation run (black). The energy scale of inflation is fixed at $H = 10^{12}$ GeV. On the right: bounds obtained from considerations on PBH physics. The green region is that allowed by current considerations on such a physics. The energy scale of inflation is fixed at $H = 10^{12}$ GeV. Taken form [9].

where, $F_{\mu\nu} = \partial_\mu A_\nu - \partial_\nu A_\mu$, and $1/f$ is a coupling constant with the dimension of a length. We define $\xi \equiv \dot{\varphi}/2\,f\,H$ as in eq.(2.56). The gauge field A_μ gives rise to an anisotropic transverse and traceless component of the stress-energy tensor which acts as a source in the equation of motion of tensor modes, giving rise to a significant classical GW production.

Gravitational wave production. The whole amount of GWs is given by the sum of tensor modes produced by quantum fluctuations of the gravitational field and those generated by the classical mechanism. According to what we have already show in (2.61), for $\xi \gtrsim \mathcal{O}(1)$ the tensor modes power spectrum is well approximated by [51,57]:

$$P_{\rm T}\,(k_*) =\simeq \frac{2\,H^2}{\pi^2\,M_{Pl}^2} + 8.6\cdot 10^{-7}\frac{H^4}{\pi^2 M_{Pl}^4}\frac{e^{4\pi\xi}}{\xi^6}\,. \tag{5.25}$$

where H and ξ are evaluated at the horizon exit of the pivot scale. Quantities denoted by (v) refers to GWs produced by vacuum fluctuations of the inflaton.
The parameter ξ is in general time dependent [65], then the amplitude of the gauge field is scale dependent and consequently the amount of the sourced tensor modes too. The specific evolution of ξ as a function of the scale depends on the form of the inflaton potential. Interestingly, ξ si expected to grow with the frequency since $|\dot{\varphi}|$ increases and H decreases approaching the end of inflation. Such a behaviour leads to a blue power spectrum for the sourced tensor modes. The upper limit on ξ obtained by CMB measurements applies at large scales, therefore ξ could assume large values at

the frequencies of laser interferometer experiments, keeping a value compatible with current CMB measurements at the same time. On the other hand, it is also possible to suppose that ξ has a transient, so that the GW spectral energy density presents a bump [64, 214].

More precisely, three different regimes can be identified: at large scales, i.e. $f \lesssim 10^{-5}$ Hz the GW energy density is dominated by the contribution due to vacuum fluctuations of the gravitational field; for 10^{-5} Hz$\lesssim f \lesssim 1$ Hz, the sourced GWs dominate in (5.25) but the time-dependence of $\dot{\varphi}$ and H is determined by the standard slow-roll equations; at small scales, i.e. for $f \gtrsim 1$ Hz the backreaction of the gauge field cannot be neglected any more. Since the production of photons draws energy from the kinetic term of the inflaton, it has the effect of slowing down the increase of $|\dot{\varphi}|$, resulting into a flattening of $\Omega_{\rm GW}$ as a function of the frequency at smaller scales.

Interestingly, in this kind of scenario the sourced GWs have peculiar signatures: they are chiral and non-gaussian (see section 2.2.1). Also scalar perturbations present a high level of non-gaussianities. Current bounds on the latter provided by Planck, implies $\xi \lesssim 2.5$ at 95% C.L. at CMB scales [2, 46]. The shape of the three point function for tensor modes is close to be equilateral [59], and the related constraints obtained by Planck [46] put a limit on the parameter ξ in agreement with the one obtained from the scalar bispectrum, see eq.(2.64). In the next analysis we will consider such a bound on the parameter ξ.

Local parametrization of the GW spectral energy density. For large ξ the sourced GWs dominate over the vacuum ones, so that, at a fixed scale, we can consider

$$P_{\rm T}(k) \simeq 8.6 \cdot 10^{-7} \frac{H^4}{\pi^2 M_{Pl}^4} \frac{e^{4\pi\xi}}{\xi^6} \qquad \xi \gg 1\,. \tag{5.26}$$

Then, according to (5.14), at present time the GW spectral energy density reads:

$$h^2 \Omega_{\rm GW}(k) \simeq 1.5 \cdot 10^{-13} \frac{H^4}{M_{Pl}^4} \frac{e^{4\pi\xi}}{\xi^6} \qquad \xi \gg 1\,, \tag{5.27}$$

where H and ξ are evaluated at the scale k. Notice that in this case, $\Omega_{\rm GW}(f)$ cannot be well parametrized by a power law over an extended range of frequencies. Therefore, we proceed performing a local parametrization. We define a spectral index at each frequency by

$$n_{\rm T}(f) \equiv \frac{d \ln \Omega_{\rm GW} h^2}{d \ln f}\,. \tag{5.28}$$

We would like to write this expression in terms of the slow-roll parameters, therefore we need to express the differentiation with respect to the frequency appearing in (5.28), in terms of a differentiation of time. To do that we express the frequency in terms of the e-folds number N and then we use $\mathrm{d}N = -H\mathrm{d}t$. The frequency is related to the

number of e-folds by:

$$\begin{aligned} N &= N_{\rm CMB} + \ln\frac{k_{\rm CMB}}{0.002\,{\rm Mpc}^{-1}} - 40.3 - \ln\left(\frac{f}{\rm Hz}\right) + \ln\left(\frac{H_N}{H_{\rm CMB}}\right) \\ &\simeq 19.7 - \ln\left(\frac{f}{\rm Hz}\right) + \ln\left(\frac{H_N}{H_{60}}\right) \ , \end{aligned} \tag{5.29}$$

where in the second expression we have assumed that the Planck pivot scale $k_{\rm CMB} = 0.002\,{\rm Mpc}^{-1}$ exited the horizon at $N_{\rm CMB} = 60$. Then, differentiating eqs.(5.27) and (5.29), at first order in slow-roll we have:

$$n_T = -4\epsilon + (4\pi\xi - 6)\,(\epsilon - \eta) \ . \tag{5.30}$$

Choosing as a reference a quadratic inflaton potential, and fixing the coupling to $f = M_{Pl}/35$, gives $\xi_{N=60} \simeq 2.46$ at CMB scales. Moreover, in such a case, the expression for the spectral index can be further approximate by $n_{\rm T} \simeq (4\pi\xi - 6)\,(\epsilon - \eta)$. In figure 5.8, we show the results from a numerical computation and those obtained by the analytical formula just presented, in case of a quadratic potential. It is visible that the provided expression for $n_{\rm T}$ are both a good approximation of the behaviour.

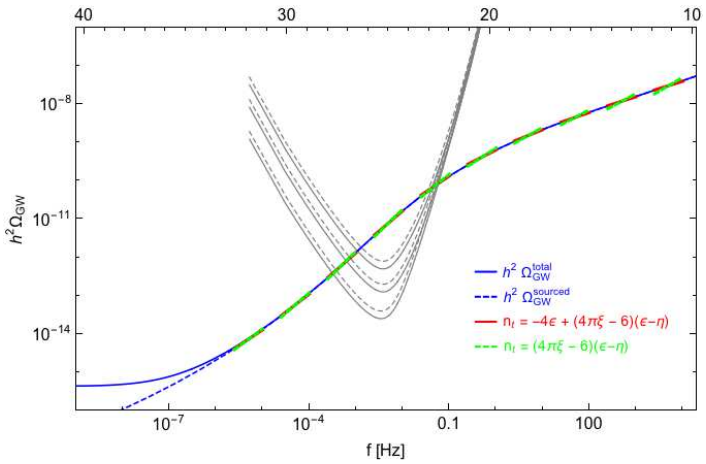

Figure 5.8: GW spectral energy density obtained from a numerical integration of the equations of motion (for quadratic inflaton potential, with $f = M_{Pl}/35$). Dashed-blue: contribution due to sourced GWs; solid-blue: total amount of GWs. Red and green coloured curves indicates the results form local parametrization $h^2\Omega_{\rm GW} \propto (f/f_*)^{n_{\rm T}}$, evaluated at various pivot frequencies f_* and with the spectral tilt $n_{\rm T}$ obtained by the analytic expressions as indicated. Taken form [9].

Forecast for LISA. Even if, the GW spectral energy density is not well described by a power-law for a broaden waveband, anyhow we refer to the LISA power-law sensitivity curves since the integrated amount is well approximated to that of a power-law.
We fix the pivot scale f_* in correspondence of the minimum of LISA sensitivity curve,

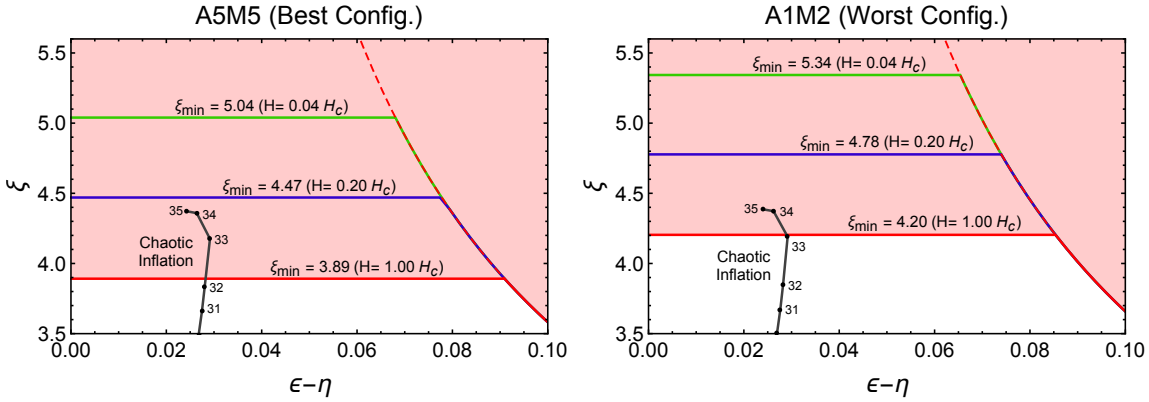

Figure 5.9: Region in the $(\xi, \epsilon - \eta)$ parameter space that LISA can probe, in the best configuration (left panel) and in the worst configuration (right panel). As a reference, we include the points corresponding to quadratic chaotic inflation for inflaton-gauge field coupling $M_{Pl}/f = 35, 34, 33, 32$ and 31. Note that the spectral index $n_{\rm T}$, not shown in the figures to avoid to overcrowd them, is well approximated by the simple formula $n_{\rm T} \simeq (4\pi\xi - 6)(\epsilon - \eta)$. Taken form [9].

i.e. $f_* \simeq 0.00346$Hz. Fixing the energy scale of inflation at the pivot scale, we calculate the minimum value of ξ required in order to have a detectable GWs signal by LISA. We consider as a reference, the Hubble rate in chaotic inflation with a quadratic potential at the e-fold $N_* = 25$ (corresponding to the frequencies f_*) which turns out to be $H_{\rm c} = 2.6 \cdot 10^{-5} M_{pl} = 6.4 \cdot 10^{13}$GeV.
For sufficiently small values of the slow-roll parameters, $(\epsilon - \eta) \ll 0.1$, such a value of ξ does not depend on the value of the spectral index and therefore it turns out to be independent on the slow-roll parameters. The corresponding values are shown as horizontal lines in figure 5.9.
On the other hand, when slow-roll parameters are sufficiently large, even if the GW signal is smaller than the LISA sensitivity at the pivot scale, thanks to a positive spectral index, the GW amplitude could be detectable at higher frequencies $f > f_*$. However large values of the slow roll parameters at $N_* \simeq 25$, i.e. in correspondence of f_* require a more complicated inflaton potential in order to sustain the final e-folds number of inflation and to keep under control the GW production in order to avoid BBN upper bounds at small scales. For simplicity, we consider $(\epsilon - \eta) \leq 0.1$ and we make a qualitative analysis. We consider the cases in which the GW amplitude does not reach the LISA sensitivity curve at the pivot frequency f_* and we find the minimum value of the spectra index in order to have a detectable signal at larger frequencies. Then the minimum value of the spectral index can be translated into a minimum value of the combination $(\epsilon - \eta)$. More precisely we required the spectral index of the GW signal to be larger than the slope of the LISA sensitivity curve at $f = 10 f_*$. This requirements turns out to be:

$$\xi \geq \frac{1}{4\pi} \left(\frac{n_{\rm T,LISA}}{(\epsilon - \eta)} + 6 \right) , \tag{5.31}$$

where $n_{\mathrm{T,LISA}}$ is the slope of the LISA power-law sensitivity curve. For $(\epsilon - \eta) = 0.1$, our limit case, and for a Hubble rate $H = H_{\mathrm{c}} = 2.6 \cdot 10^{-5} M_{pl} = 6.4 \cdot 10^{13}$GeV, we need $\xi \geq \xi_{\mathrm{min}}$, where the latter is the asymptotic value found in regime of small slow-roll parameters, as shown in the figure. At the qualitative level, equation (5.31) shows that for GW signals below the LISA sensitivity at the minimum of the curve, the minimum value of ξ required to detect the signal with LISA is slightly smaller than the asymptotic constant ξ_{min} values obtained for small $(\epsilon - \eta)$ values. The results are presented in figure 5.9.
In the same picture, we also depict the $(\xi, \epsilon - \eta)$ behaviour for a fiducial quadratic inflation model, evaluated numerically for $30 \lesssim M_{Pl}/f \leq 35$.
We present also the capabilities of LISA of constraining the parameter space $\xi - H$ for fixed values of $(\epsilon - \eta)$. We take as a reference chaotic inflation, i.e. the Hubble rate $H_c \simeq 6.4 \cdot 10^{13}$ GeV at the e-fold $N_* \sim 25$, considering the quantity H/H_c. For $(\epsilon - \eta)$ sufficiently small, we saw that $\xi > \xi_{\mathrm{min}}$ ensures a LISA detection. In figure 5.10 we show the region in the parameter space which corresponds to an expected LISA detection, for two different values of $(\epsilon - \eta)$ for which the asymptotic behaviour is ensured. It is visible how the capabilities of LISA get less significant for small values of the Hubble rate.

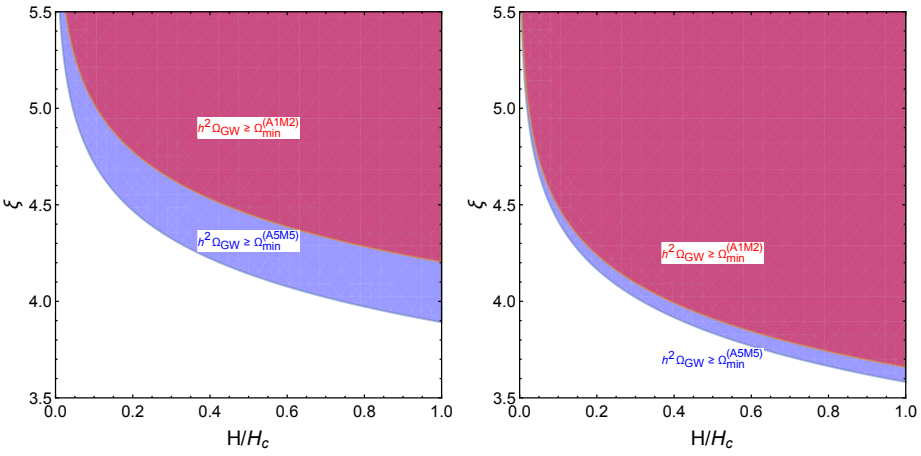

Figure 5.10: Regions in the $\xi - H$ parameter space which correspond to GW signals detectable by best (blue region) and worst (violet region) LISA configurations. Left panel corresponds to the parameter space for $(\epsilon - \eta) = 0.02$, right panel for $(\epsilon - \eta) = 0.1$. Taken form [9].

For a discussion about the constraints from PBH physics in this context see [9].

5.4.3 Inflation with broken spatial diffeomorthisms

We introduced in section 2.3 an inflationary model in which, besides temporal diffeomorphism, the spatial ones are broken too. In this kind of scenarios blue tensor power spectrum can be produced, then representing an interesting signal for LISA. Differently from the inflationary models we have investigated before, here the GW

amount produced by quantum fluctuations of the gravitational field, since it presents non-standard features. Then the overall amount of GW is given by a single term. Moreover, the produced tensor modes turn out to be well descried by a power law, therefore, also in this case we will refer to the power-law sensitivity curves.

Gravitational wave production. We consider a model described by the lagrangian (2.77), i.e. we are not considering a specific inflationary model, but the class of scenarios which satisfies the symmetries embedded in the previous lagrangian. In the limits of small graviton mass, i.e. $|m_{\mathrm{T}}/H| \ll 1$, at sufficiently large scales the amplitude and spectral index becomes, see eq.(2.80):

$$P_{\mathrm{T}}(k) = \frac{H^2}{2\pi^2 M_{\mathrm{pl}}^2 c_{\mathrm{T}}^3}\left(\frac{k}{k_*}\right)^{n_{\mathrm{T}}} \qquad \text{with} \qquad n_{\mathrm{T}} = \frac{2}{3}\frac{m_{\mathrm{T}}^2}{H^2}\,, \tag{5.32}$$

where c_{T} is the graviton propagation speed and m_{T} its mass[5]. Interestingly for the capabilities of LISA, in correspondence of positive values of the graviton squared mass, a blue tensor spectral index appears. In figure 5.11 we show the GW spectral energy density obtained by (5.14) for different values of the discussed parameters.

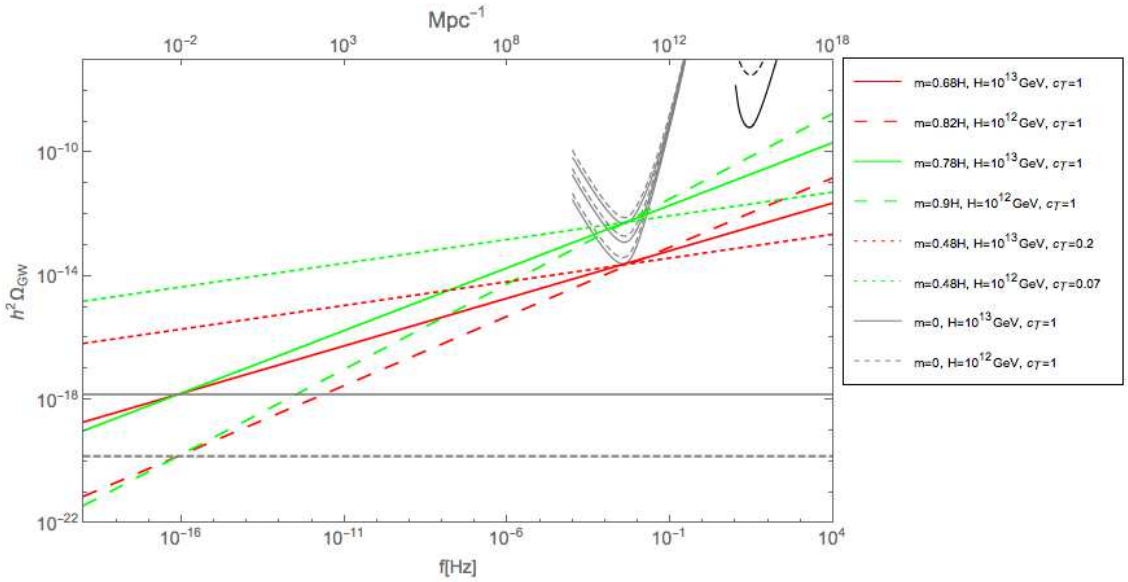

Figure 5.11: GW spectral energy density for different values of the effective mass of the graviton m_h, Hubble rate during inflation H, and tensor sound speed c_T, compared with the power-law sensitivity curves of LISA (grey) and the power-law sensitivity curves different observational runs of aLIGO (black) detectors. Parameter values refer to $k_* = 0.05$ Mpc^{-1}. Taken form [9].

[5]Remember, as we said in section 2.3, that current constraints obtained on GW features from the observations of compact object mergers, could be avoided at the energy scale of inflation.

Forecasts for LISA and bounds from other observables. The amplitude and spectral index of the tensor power spectrum are described by the Hubble parameter H, the graviton mass squared m_{T}^2 and its propagation speed c_{T}. Therefore, for a fixed value of H, we can forecast the capabilities of LISA in putting constraints on the parameter space given by $m_{\mathrm{T}}/H - c_{\mathrm{T}}$, where we decided to consider the dimensionless parameter m_{T}/H. As before, we refer to the parameter space evaluated at CMB scales, more precisely at $k_* = 0.05\mathrm{Mpc}^{-1}$.
Here we have to consider the current upper bound on tensor amplitude provided by CMB measurements, since the GWs we are dealing with have a relevant amplitude at such scales. More precisely, for a fixed value of H, we consider the values of the speed of sound c_{T} such that the amplitude at CMB scales does not exceed the current upper limit on the tensor-to-scalar ratio r.
A positive value of m_{T}^2 means an enhancement of the tensor amplitude at small scales, therefore for a fixed value of H, and for a fixed value of c_{T}, the minimum value of the graviton mass required in order to produce a signal detectable by LISA, can be found. The results are shown in the left panel of figure 5.12.

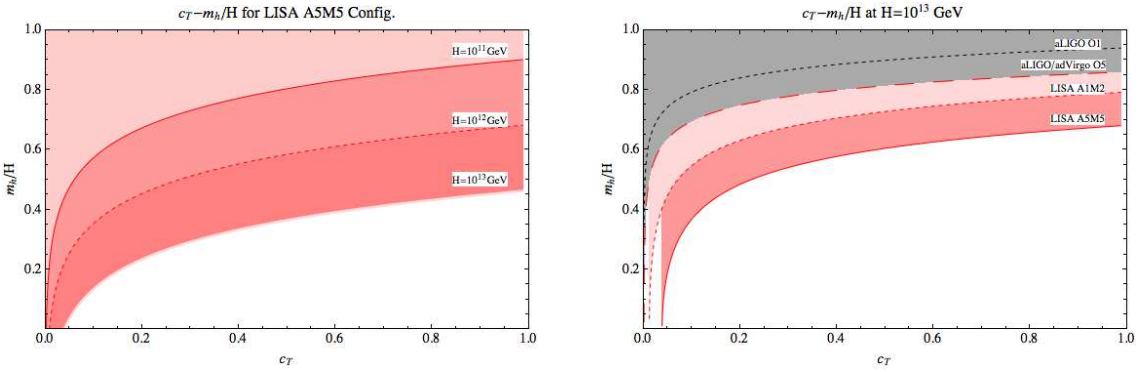

Figure 5.12: Parameter space of the model (2.77) at the pivot scale $k_* = 0.05\mathrm{Mpc}^{-1}$. The red region corresponds to signals detectable by the best configuration of LISA for different values of the Hubble parameter H. Grey region in the right panel is the analogous region for the aLIGO sensitivity curve of the first observational run. Taken form [9].

For example, for $H = 10^{13}$GeV, and $c_{\mathrm{T}} = 1$, a non-detection of this kind of signal will put un upper bound on the graviton mass equal to $m_{\mathrm{T}}/H \lesssim 0.68$. For smaller values of the energy scalar of inflation, LISA will be able to put stronger constraints.

We also compare the expected constraining power of LISA, with the power-law sensitivity curve of the first observation run of aLIGO. The results are shown in the right panel of figure 5.12. As visible, LISA is expected to put stronger bounds in such parameter space.
With respect to the situation shown for the parameter space of the inflationary model with a spectator field, here the bounds provided by LISA are stricter with respect to those provided by LIGO. This is due to the fact that in the inflationary scenario with

a spectator field, the bounds on the scalar sector at CMB scales, force the sourced tensor amplitude at the same scales to be much less than the admitted amount by current bound on the tensor-to-scalar ratio r.

Notice that the limits in the plane $m_{\rm T}/H - c_{\rm T}$, can be interpreted as constraints on the operators of the quadratic action of tensor modes; in this sense LISA could constrain symmetry braking inflationary scenarios on different scales with respect to CMB.
Moreover, models with spatial symmetry breaking are characterized by peculiar features other than the possibility of a blue tensor power spectrum. Especially, a significant amount of non-gaussianities can be produced (but not so large to exceed current upper bounds) [86, 88, 90]. Moreover, the latter can present peculiar features, as for example an enhancement of the tensor-scalar-scalar bispectrum which could be tested by future B-modes experiments.

5.5 Summary of the results

Considering an inflationary model where a spectator field is present as in (5.19), we conclude that, without considering PBH constraints, LISA is expected to significantly reduce the related parameter space, giving completely new information, in particular with respect to current constraints we have from CMB observations, while it should provide bounds comparable with current limits we have from LIGO detectors and from considerations on the BBN physics.
On the other hand, considering limits imposed on $c_{\rm s}$ and s by PBH, LISA is expected to be not able of detecting GWs produced in an inflationary scenario with spectator fields. At the same time LISA would still represent the possibility of validating our way of modelling PBH physics, in particular of the assumptions that are made to obtain such limits. Moreover, notice that admitting a running of the spectral index of the scalar and tensor power spectrum, the constraints obtained by PBH could be avoided.

For an inflationary scenario with a significant gauge particle production, second-order GW can reach the LISA sensitivity without violating current constraints we have from CMB measurements. Notice that no other planned experiments are expected to be able to detect such a kind of GW signal, providing to LISA a unique role in testing this kind of inflationary model. Moreover, in this case, interesting features such as the large chirality and non-gaussianity of the sourced GWs, could help in discriminating this kind of inflationary physics from other scenarios.

In the case of inflationary models with broken spatial diffeomorphisms we saw that LISA should be able of providing new constraints in the parameter space given by the graviton mass and speed of propagation. In the case considered in this work, LISA is found to have the capabilities of putting stricter constraints on such a space with respect to other current and planned experiments.

Furthermore, with respect to the inflationary models in which besides the significant GW production, a relevant scalar perturbations counterpart is generated, we noticed that the joint analysis of constraints coming from very different scales and physics, is useful in order to discriminate the origin of a possible detected signal, or to exclude some inflationary models. More precisely, in case of a detection by LISA of a signal in correspondence of a point of the parameter space excluded by CMB, this would rule out that the detected signal is originated by the mechanism under consideration. In this direction a complete calculation of the scalar power spectrum and the level of non-gaussianities produced in these kind of scenarios would be a significant improvement. On one hand, they could reveal a reduced significance of the LISA experiment in constraining this inflationary model on the other hand, they could point out that LISA could put stricter constraints than considerations on non-gaussianities.

We therefore conclude that LISA represent a promising experiment also for probing cosmology of the early universe, especially it would provide complementary information with respect to detectors sensitive to modes at large scales.

Part III

Inflationary magnetogenesis

Chapter 6

Magnetic fields at cosmological scales

The majesty of the inflationary paradigm does not end up with the solution of the standard cosmology problems and the explanation of CMB anisotropies and of the growth of large scale structures. The development of an inflationary period in the early stages of the universe is also studied as the possibility to account for the observed magnetic fields at cosmological scales. In this direction, successful inflationary scenarios have been proposed.

Current observations point out the presence of magnetic fields in astrophysical objects and on cosmological scales, surprisingly they are observed in voids of Large Scale Structure (LSS) too [215]. The presence of such fields on the scales of galaxies ($\sim 10^{-2}$Mpc) and cluster of galaxies ($\sim$ 1Mpc) is understood as the amplification by a dynamo mechanism of pre-existing weaker magnetic fields. The presence of magnetic fields in voids and in astrophysical object of any size, suggests that the initial seeds should had been there at least during structure formation. There are two main ideas in order to explain the presence of such seeds: they could have been produced in the early universe or they could have been formed in the same moment of gravitational collapse which leads to structure formation.
Interestingly, magnetic fields on large scales, i.e. on scales larger than cluster of galaxies, should evolve only because of the universe expansion. Therefore if magnetic fields in voids of LSS, are of primordial origin, they would provide a unique chance to investigate the original seeds. An alternative could be that they are formed by out flows of already formed galaxies. The evolution of magnetic fields on smaller scales is more complicated and uncertain, so that from a measure of magnetic fields on galaxy scales, it is not clear how to go back to the original seeds.
Supposing that magnetic fields in voids have been generated in the early universe, three main way of producing them have been proposed so far: they could have been generated during the inflationary period of the universe, during phase transitions or from second-order cosmological perturbation theory.

Here we are interested in the possible production of magnetic fields during the infla-

tionary stage of the universe. After an introduction of basic notions about magnetic field at cosmological scales and of the underlying idea of the inflationary magnetogenesis mechanism, in chapter 7 we will deepen a specific inflationary scenario in which a significant magnetic field production takes place.

Useful definitions. In agreement with [215], we define the power spectrum of the magnetic field $P_{\rm B}$ as:

$$\langle B_i(\mathbf{k})\, B_j^*(\mathbf{q})\rangle = \frac{1}{2}\,(2\pi)^3\,\frac{\delta(\mathbf{k}-\mathbf{q})}{k^3}\left[(\delta_{ij}-\hat{k}_i\hat{k}_j)\,P_B(k) - i\epsilon_{ijm}\hat{k}_m P_{aB}\,(k)\right] \tag{6.1}$$

where P_B and P_{aB} identifies the symmetric and antisymmetric part of the magnetic field power spectrum. For a symmetric power spectrum, the related spectral index is defined by $\sqrt{P_B(k)} \propto k^{n_B}$. We define ε^+ and ε^- the polarization vectors, as we did in section 2.2.2, which identifies right-handed and left-handed gauge field respectively. In general, the magnetic field can be decomposed as:

$$\mathbf{B}\,(\mathbf{k},t) = \mathbf{B}_{(+)}\,(k,t)\,\varepsilon^+ + \mathbf{B}_{(-)}\,(k,t)\,\varepsilon^-\,. \tag{6.2}$$

If one of the two helicity modes vanishes, the field is called totally helical. The intensity of the magnetic field is defined as

$$B^2 \equiv \langle B^2\rangle = \int \frac{d^3\mathbf{k}}{(2\pi)^3}\,|\mathbf{B}\,(k)|^2\,, \tag{6.3}$$

notice that it does not depend on the scale. Another useful quantity is the correlation length of the magnetic field, which is defined as

$$L = \frac{\int d^3\mathbf{k}\frac{2\pi}{k}\,|B\,(\mathbf{k})|^2}{\int d^3\mathbf{k}\,|B\,(\mathbf{k})|^2}\,. \tag{6.4}$$

Finally, we introduce the magnetic helicity, which is given by:

$$H\,(V) = \int_V \mathbf{A}\cdot\mathbf{B}\,dv\,, \tag{6.5}$$

where V is a volume whose boundary is not crossed by magnetic fields lines, and $\mathbf{A}$ is the magnetic vector potential.

6.1 Evolution after primordial magnetogenesis

After its generation, a primordial magnetic field evolves up to the present time. Firstly, due to the expansion of the universe, its intensity decreases with the redshift. Moreover, magnetic fields interact with charged particle plasmas. During the radiation dominated era before recombination and during the re-ionization phase, the universe is populated by a charged plasma, which couples with magnetic fields. On the other

hand, during matter dominated era the comoving intensity and correlation length of the magnetic field are constant, since no charged plasmas are present. The interaction between magnetic fields and charged plasma in an expanding universe are described by non-linear equations of the magnetoidrodynamics (MHD) [216] (for other references see [215]), obtained by the conservation of the whole stress energy tensor of the system. Solving analytically and numerically such equations is quite difficult, therefore people derived only a qualitative picture of the solutions (confirmed by numerical simulations). In determining the solutions, the kinetic viscosity of the plasma plays a significant role. Form MHD equations, it is found that the evolution of the magnetic fields when a charged plasma is present, is characterized by alternating phases of turbulence, viscous and free-streaming. The evolution during the radiation dominated era is described by such phases.
Usually magnetogenesis results in the production of magnetic fields and a regime of freely decaying turbulence, i.e a scenario in which the dissipation terms can be neglected. This regime is established for intermediate scales. Indeed, at very large scales turbulence does not have sufficient time to fully develop, while for very small scales the dissipative effects are not negligible and the turbulence energy is lost into heating the plasma. For very large scales then the initial slope of the power spectrum is conserved, while for intermediate scales, the effect is a transfer of power from large to small scales, with the final power-law spectrum described by a fixed spectral index, independently on the initial power spectrum slope.
At neutrino et photon decoupling. i.e. when the mean-free path of these particles increases, a regime of strong viscous damping is established. The dissipation scale depends on the mean-free path of the least coupled particles, therefore in such a moment it grows and becomes a significantly large scale. The coupling of the plasma with the magnetic field is removed, then the evolution of the comoving magnetic field intensity and correlation length stops. When the mean free path grows further, i.e. more than the typical scale of the system, the latter enters in the free streaming regime. In this situation the intensity of the magnetic field decreases and its correlation length grows. Then the turbulence regime is again established.
After photon decoupling and recombination, there is no more charged plasma coupled to the magnetic fields. The MHD evolution turns out to be active during the re-ionization phase. The qualitative evolution is the same of that of the radiation dominated era. The only difference is that the correlation length does not grow any more, due to the different evolution of the scale factor. From a practical point of view, it can be considered that B and L stays constant in this epoch.

For a totally helical magnetic field the inverse cascade mechanism [216–223] takes place, i.e. the comoving value of the magnetic field intensity decreases while the correlation length increases. Indeed form the conservation of the comoving helicity, we have the magnetic field intensity which scales as:

$$B \sim L^{-1/2}\,, \tag{6.6}$$

so that

$$B_f^2 L_f = B_i^2 L_i \left(\frac{a_i}{a_f}\right)^3 , \tag{6.7}$$

where i and f denotes two generic times. In general the evolution after the magnetogenesis leads to a power transfer from large to small scales. With such an evolution is difficult to explain the present time presence of magnetic fields on cosmological scales. The mechanism of inverse cascade therefore represents an interesting chance of providing significant magnetic power on large scales.

6.2 Observations and current bounds

There are many theoretical and observational constraints on cosmological magnetic fields [215]. Up to now we have not a direct detection on magnetic field in the intergalactic medium nor in the LSS voids, but we have many constraints coming from different kinds of observations. Here we will focus mainly on those we are interested in with respect to the next section. Notice that such limits refer to generic magnetic fields present on such scales, current bounds do not give any information about the origin of such fields.
The non-observation of Faraday rotation of the polarization plane of linearly polarized radio emission from quazars, puts upper bounds on the magnetic field strength in the intergalactic medium [11–13].
Other constraints come from CMB observations [224]. In fact CMB encode information about the state of the plasma at the epoch of recombination, which is influenced by the possible presence of magnetic fields. Several are the effects on CMB. Magnetic fields affect recombination and Silk damping, modifying the tail of CMB anisotropy power spectrum. Moreover, spectral distortions in the CMB energy spectrum can be introduced by magnetic fields. CMB constraints put upper limits on the magnetic field intensity of about nG. Interestingly, a helical magnetic field would introduce a peculiar signature in CMB power spectra, indeed it would lead to a non-vanishing correlation between temperature anisotropies and E and B polarization power spectrum, as an imprint of parity violation [225].
On the other hand, high-energy ($0.1 \div 10$GeV) and very high-energy ($10 \div 100$GeV) gamma-ray observations provide the possibility of establishing lower limits on the magnetic field strength in the intergalactic medium [11–13]. A gamma-ray which propagates through the intergalactic medium interacts with low-energy photons producing pairs of electron and positron. Then the latter interact with CMB photons by Compton scattering leading to an emission of a secondary gamma-ray. The latter carries information about positron and electrons from which it has been produced. The interesting fact is that those electron and positron, being charged particles, interact with magnetic fields if present. Therefore the final observations of the secondary gamma-rays include information about the possible presence of magnetic fields along the path of gamma-ray emissions. In modelling all this picture there are several uncertainties which reflect on the constraints on magnetic fields. In particular, non-observations by the Fermi telescope of secondary gamma-rays from blazars and AGN, put a lower

bound on the magnetic field in the intergalactic medium of the order of 10^{-18} G for $L \gtrsim D_e$, with D_e the electron/positron energy loss length for inverse Compton scattering, which is typically $D_e \simeq 80$ kpc [226]. If on the other hand $L < D_e$, the bound changes by a factor $\sqrt{D_e/L}\ \Pi^{-1}(D_e/L, n_B)$, where $\Pi(D_e/L, n_B)$ is a function presented in [227].
Also magnetic fields observed in galaxies provide lower bounds on the intensity of their possible primordial seeds. In galaxies, magnetic fields of the order of 10^6G are observed. It is believed that such magnetic fields are the result of the amplification by a dynamo mechanism of earlier seeds. There are large uncertainties on the evolution of such seeds after their generation, but estimations point out that the original magnetic fields should be at least of the order of $10^{-21} \div 10^{-23}$G at a comoving scale of 1Mpc [14]. Notice that this bound, differently from that obtained by gamma-ray observations, does not depend on the correlation length of the magnetic fields. Actually it is not excluded that the presence of a primordial magnetic field it is not required in order to explain the present time presence of magnetic fields in galaxies.

6.3 Inflationary magnetogenesis

As we anticipated, a possible way to explain the presumed presence of primordial magnetic field seeds, is to introduce a process of magnetogenesis during the inflationary stage of the universe.
In order to generate magnetic fields during inflation, a coupling between the electromagnetic field and some rolling field, or another coupling which breaks the conformally invariance of the electromagnetic field, is required [228]. In these models the gauge field is amplified by the rolling of the field to which is coupled.
In general, inflationary magnetogenesis leads to a blue power spectrum of the magnetic field, i.e. too small magnetic power at large scales in order to explain observations in the intergalactic medium. Furthermore, in general lowering the energy scale of inflation leads to larger amplitude of the magnetic fields.
Several inflationary models with a significant magnetogenesis have been proposed in last decades. In general, two issues can occur in the inflationary magnetogenesis models, which one has to keep under control. In these scenarios, the effective charge of the electron is determined by the coupling between the electromagnetic field and a rolling field. If this coupling decreases during inflation, in order to re-establish the standard charge of the electron at the end of inflation, a strong coupling of the electromagnetic field is required at the beginning of inflation [229]. In such a case, the perturbative quantum field theory calculations could be not proper any more. Moreover, the back-reaction on the background evolution of the electromagnetic energy has to be kept under control [230], in particular one has to ensure the electric and magnetic energy density to be negligible with respect to the inflationary expansion.
Usually both of these issues are kept under control limiting the parameter space of the model.
The most basic scenario of inflationary magnetogenesis was proposed by Ratra [231], in this case the gauge field is coupled to the inflaton by the following interaction

lagrangian:

$$\sim f(\varphi) F_{\mu\nu} F^{\mu\nu} \tag{6.8}$$

where $F_{\mu\nu} = \partial_\mu A_\nu - \partial_\nu A_\mu$. The case in which the inflaton is a pseudoscalar have been proposed too [232]. In such a scenario the amplitude and correlation length of the magnetic field are determined by the Hubble parameter. However, according to (6.8), in order to avoid problems of strong coupling and backreaction, the magnetic power spectrum turns out to be blue and to not be able to explain the observed amplitude of magnetic fields at large scales.
Another model proposed is an axion-like scenario [50, 232] where the dynamics of the electromagnetic field is described by:

$$-\frac{1}{4} F_{\mu\nu} F^{\mu\nu} - \frac{\varphi}{4f} F_{\mu\nu} \tilde{F}^{\mu\nu} , \tag{6.9}$$

where f is a constant and $\tilde{F}^{\mu\nu}$ is the dual of the electromagnetic strength. In this scenario, for values of the parameters which avoid the strong coupling and the back-reactions issues, the magnetic power spectrum results very blue. However the parity violation of the interaction term leads to the enhancement of only one of the two helicity modes of the gauge field and then to the production of a helical magnetic field [50]. The latter undergoes to the process of inverse cascade after inflation, which moves power from small to large scales. Moreover, in this case, the amplitude and the correlation length of the magnetic field are determined by a combination of the Hubble parameter and also by the strength of the coupling, so that one can find combinations of such parameters which lead to an amplitude of the magnetic field sufficient to explain current lower bound at cosmological scales.
A more general scenario has been proposed more recently, where the electromagnetic field dynamics is described by [1]:

$$I^2(\tau) \left(-\frac{1}{4} F_{\mu\nu} F^{\mu\nu} + \frac{\gamma}{4} F_{\mu\nu} \tilde{F}^{\rho\lambda} \right) , \tag{6.10}$$

with γ a constant. The model is a generalization of (6.9), here too a helical magnetic field is generated. Again, the strong coupling and the backreaction problems can be addressed by a suitable choice of the parameters. The interesting feature is that one can obtain a magnetic power spectrum which is less blue than in the case of (6.9).
In all these scenarios, at the end of inflation the electric field is dissipated by the high conductivity of the universe, while the magnetic field evolves as explained in section 6.1.
In particular we said that during the matter dominated era, the magnetic field intensity and correlation length can be considered as constant. Therefore, in order to compare the results of the inflationary magnetogenesis with current lower bounds at cosmological scales, to calculate how B and L evolve up to the recombination is required. For these calculations, usually instantaneous reheating is assumed.

6.3.1 Associated production of scalar and tensor perturbations

An important aspect of inflationary scenarios with an efficient magnetogenesis is the associated production of extra scalar and tensor perturbations. As we shown in section 2.2.1 the presence of further fields besides the inflaton, in this case the gauge field, leads to source terms in the equation of motion of scalar [233] and tensor modes [57]. Moreover, the sourced scalar and tensor modes turn out to be significantly non-gaussian [51, 59]. The presence of these extra amounts of perturbations and their non-gaussianity compared with current cosmological observations put strict constraints on the inflationary parameters of these scenarios [62, 234]. These limits become weaker, but still relevant, also in the case in which the gauge field is not directly coupled to the inflaton but to an auxiliary field [235].
Moreover, in scenarios in which helical magnetic fields are produced, as we saw in section 2.2.1, the related GWs produced by the classical mechanism turns out to be chiral [57]. This feature gives the possibility of distinguishing such a kind of scenario from others which preserve parity. The chirality of GWs, besides a direct measurement, can be traced by a non-vanishing cross-correlation between temperature and polarization modes of CMB anisotropies [225].

Chapter 7

Inflationary magnetogenesis with added helicity

One possibility to explain the presence of magnetic fields at cosmological scales, is to suppose a process of magnetogenesis during the inflationary period of the universe. In section 6.3 we outlined the main inflationary scenarios proposed in such a direction. In this chapter we study in details some crucial aspects of the model proposed in [1]. In particular, we investigate the extra production of scalar and tensor perturbations due to the presence of the gauge field. We calculate the bounds on the parameter space of the model, obtained from current constraints on scalar and tensor perturbations, and we establish if the allowed values leave open the chance of a magnetogenesis which could explain observations at cosmological scales, i.e. [11–13], and provide the primordial seeds required to start the galactic dynamo [14]. The stricter constraints turn out to be due to the current upper bound on scalar non-gaussianities. However we will find that the proposed inflationary model is able to explain current observations of magnetic fields at cosmological scales and at the same time to do not evade current bounds on cosmological perturbations, then representing an interesting possibility to explain the presence of magnetic fields in the intergalactic medium.

The results of this chapter are presented in [236].

7.1 The model

We consider an inflationary model described by the following Lagrangian [1]:

$$L = -\frac{1}{2}\partial_\mu\varphi\partial^\mu\varphi - V(\varphi) - \frac{1}{2}\partial_\mu\sigma\partial^\mu\sigma - U(\sigma) + I^2(\sigma)\left(-\frac{1}{4}F_{\mu\nu}F^{\mu\nu} + \frac{\gamma}{8}\eta_{\mu\nu\rho\lambda}F^{\mu\nu}F^{\rho\lambda}\right) \tag{7.1}$$

where φ is the inflaton, σ is an auxiliary field, $F_{\mu\nu} = \partial_\mu A_\nu - \partial_\nu A_\mu$, $\eta_{\mu\nu\rho\lambda}$ is the totally antisymmetric tensor and V and U are the potential of the inflaton and of the auxiliary field respectively. The function I is given by $I(\sigma(\tau)) = (-H\tau)^{-n}$, where $n < 0$ is a free parameter of the model, as the dimensionless constant γ. The function I encodes the coupling with the expanding universe. We consider the gauge field A_μ

a half order perturbation, so that quantities of the quadratic order in A_μ, such as the electromagnetic energy density, are of the first order in perturbation theory. The term $-\frac{I^2(\sigma)}{4}F_{\mu\nu}F^{\mu\nu}$, leads the spectral index of the magnetic field amplified by the rolling of σ depending on the parameter n. Interestingly, the magnetic field could be red. The other term $\frac{I^2(\sigma)}{8}\,\gamma\,\eta_{\mu\nu\rho\lambda}F^{\mu\nu}F^{\rho\lambda}$ leads to the amplification of one of the two helicity modes of the gauge field. As anticipated in 6.1, helical magnetic fields undergo to the process of the inverse cascade [217], which enhances the magnetic field amplitude at large scales during the subsequent epochs of the evolution of the universe. In order to avoid strong coupling during inflation [229], the parameter n is bounded to $n < 0$, while in order to prevent backreaction of the infrared modes of the gauge field on the background dynamics [230] (see also [237, 238]), $n > -2$ is required. Therefore we will consider$-2 < n < 0$ ($n = 0$ is excluded since in such a case there is no magnetic fields production).

The totally antisymmetric tensor $\eta_{\mu\nu\rho\lambda}$ is such that $\eta_{0123} = -\sqrt{-g}$. During inflation, $a(\tau) = 1/(-H\tau)^{1+\epsilon}$ with H the physical Hubble factor, while the comoving one is $\mathcal{H} = -(1+\epsilon)/\tau$, and $\epsilon = (\mathcal{H}^2 - \mathcal{H}')/\mathcal{H}^2$.

7.1.1 Production of helical magnetic fields

We describe the dynamics of the gauge field following from the lagrangian (7.1). We define $\tilde{A}_\mu = I\,A_\mu$ and we quantize such a field as usual:

$$\tilde{\mathbf{A}}_i\,(\mathbf{x}) = \sum_{\lambda=\pm}\int \frac{d^3\mathbf{k}}{(2\pi)^{3/2}}\varepsilon_i^\lambda\,(\mathbf{k})\,e^{i\mathbf{k}\cdot\mathbf{x}}\left[\tilde{A}_\lambda\,(\mathbf{k},\tau)\,\hat{a}_\lambda\,(\mathbf{k}) + \tilde{A}_\lambda^*\,(-\mathbf{k},\tau)\,\hat{a}_\lambda^\dagger\,(-\mathbf{k})\right], \qquad (7.2)$$

where ε_i^λ is the helicity vector, and $\lambda = \pm$ indicates the helicity state. We work in the Coulomb gauge, i.e. $\tilde{A}_0 = \partial_i\,\tilde{A}_i = 0$. Varying the Lagrangian (7.1), the equation of motion for $\tilde{A}_\lambda$ results:

$$\tilde{A}_\lambda'' + \left[-\frac{n\,(n+1)}{\tau^2} + 2\,\lambda\,\xi\,\frac{k}{\tau} + k^2\right]\,\tilde{A}_\lambda = 0\,. \qquad (7.3)$$

Notice that the equation of motion is different for the two helicity states.
The evolution of the field is characterized by three stages. For $\tau \to -\infty$ the term k^2 dominates and the photons are in the Bunch-Davies vacuum. When $|k\,\tau| \lesssim \xi$, the second term in the parenthesis becomes significant and then its sign turns out to determine the behaviour of the field. In particular, modes with a positive helicity are amplified while the others get damped by a friction term. This fact is what determines a final helical magnetic field. Moreover notice that the enhancement of the gauge modes is controlled by the parameter ξ; large values of ξ mean an efficient amplification of the gauge modes. Finally, for $\tau \to 0^-$, the first term in the parenthesis dominates.
The solution of the equation of motion, for $\tau \to -\infty$ is given by a combination of the Coulomb functions [1]:

$$\tilde{A}_+\,(k,\tau) \simeq \frac{1}{\sqrt{2k}}\left[G_{-n-1}\,(\xi;-k\tau) + iF_{-n-1}\,(\xi;-k\tau)\right]\,. \qquad (7.4)$$

For $|k\,\tau| \ll \xi$, that is for the regime in which the modes are outside of the Bunch-Davies vacuum, the Coulomb function F can be neglected and the solution of eq.(7.3) turns out to be well approximated by [1, 239]

$$\tilde{A}_+(k,\tau) \simeq \sqrt{-\frac{2\,\tau}{\pi}} e^{\pi\,\xi} K_{-2n-1}\left(\sqrt{-8\,\xi\,k\,\tau}\right), \tag{7.5}$$

where K_α is the modified Bessel function. Notice that $\tilde{A}_+(\mathbf{k},\tau) = \tilde{A}_+(k,\tau)$, so from now on we indicate only the dependence on the norm of $\mathbf{k}$. Moreover, for $|k\,\tau| \ll 1/\xi$ the above expression reduces to

$$\tilde{A}_+(k,\tau) \simeq \sqrt{-\frac{\tau}{2\,\pi}}\, e^{\pi\,\xi}\,\Gamma\left(|2n+1|\right)|2\,\xi\,k\,\tau|^{-|n+1/2|}\,. \tag{7.6}$$

Now it is clear that the amplification of the gauge field is exponential in the parameter ξ.
We define the electric and magnetic field in real space as

$$E_i(\mathbf{x}) \equiv -\frac{A_i'(\mathbf{x})}{a^2}\,, \qquad\qquad B_i(\mathbf{x}) = \epsilon_{ijl}\,\frac{\partial_j A_l(\mathbf{x})}{a^2}\,, \tag{7.7}$$

where ϵ_{ijl} is the totally antisymmetric tensor in flat space. For convenience we insert in these definitions an extra factor a^{-1} with respect to the standard definitions arising from the field tensor, that would read: $E_\mu = u^\nu F_{\mu\nu} = -\partial_0 A_\mu/a$ and $B_\mu = \eta_{\mu\nu\alpha\beta}\,u^\beta F^{\nu\alpha}/2 = \eta_{\mu\nu\alpha\beta}\,u^\beta(\partial^\nu A^\mu_\alpha - \partial^\alpha A^\nu)/2$.
Defining the spectral index of the magnetic field by $\sqrt{P_B(k)} \propto k^{n_B}$, from Eq. (7.6), we have $n_B = 5/2 - |n+1/2|$, i.e. the magnetic field power spectrum is blue.

7.1.2 Magnetic field evolution after inflation

As we said in section 6.1, during matter dominated era, we can consider B and L as constant. Therefore, in order to compare the magnetic fields produced during inflation with current lower bound, we need only to calculate B and L at the time of recombination.
We suppose instantaneous reheating, so that B and L calculated at the end of inflation are supposed to be the values at the beginning of the radiation dominated era. We will denote such values as $B_{\rm reh}$ and $L_{\rm reh}$. From the equation of motion of the gauge field, such values are found to be [1]:

$$B_{\rm reh} = H^2\frac{e^{\pi\xi}}{\xi^{5/2}}b_n\,, \qquad \text{where} \qquad b_n \equiv \sqrt{\frac{\Gamma\left(4-2n\right)\Gamma\left(6+2n\right)}{80640\,\pi^3}}\,, \tag{7.8}$$

$$L_{\rm reh} = \frac{\xi}{H}\,l_n\,, \qquad \text{where} \qquad l_n = \frac{18\pi}{(3-2n)\,(5+2n)}\,. \tag{7.9}$$

Interestingly, in case of helical magnetic field, the complicated evolution during the radiation dominated era can be approximated in a simply way exploiting the helicity

conservation.

Before doing that, we point out a useful relation. In general, not only for helical magnetic fields, an approximated relation which connects B and L can be obtained. At any time is found to be valid the following relation for the velocity v_L of the plasma on a scale L [216]:

$$v_L = HL\,. \tag{7.10}$$

From this relation it follows that, during the free-streaming of photons just before recombination, also the following relation approximately holds:

$$v_A = HL\,, \tag{7.11}$$

where $v_A \equiv B/\sqrt{\rho_{\rm em} + P_{\rm em}}$ (with the subscript em we indicate electromagnetic quantities). During the free-streaming of photons just before recombination, $v_L \simeq v_A^2 \lambda_\gamma / L$ [216], where $\lambda_\gamma \simeq 1/H_{\rm rec}$ is the mean-free path of photons. Exploiting these expressions, from (7.10), it follows that at the time of recombination $v_A \simeq H_{rec} L$.
From (7.11), expressing v_A in terms of B and L, a relation between $B_{\rm rec}$ and $L_{\rm rec}$ is obtained:

$$B_{\rm rec} \simeq 10^{-8}{\rm G} \left(\frac{L_{\rm rec}}{\rm Mpc}\right)\,. \tag{7.12}$$

Since B and L do not evolve during the matter dominated era, this relation holds also at the present time.

We now exploit the fact that in our model magnetic fields are helical, in order to have another equation which connects B and L and then finding their values. From the conservation of the helicity, we said that eq.(6.7) is valid. Therefore, the combination of (7.12) and (6.7) evaluated at the present time, i.e.

$$B_0 = 10^{-8}{\rm G}\,\frac{L_0}{\rm Mpc}\,, \qquad B_0^2\, L_0 = B_{\rm reh}^2\, L_{\rm reh} \left(\frac{a_{\rm reh}}{a_0}\right)^3\,, \tag{7.13}$$

provides the possibility to express the current values of the magnetic field B_0 and of the correlation length L_0 as a function of their values at the end of inflation:

$$\begin{aligned} \frac{L_0}{\rm Mpc} &= \left(\frac{a_{\rm reh}}{a_0}\right) \left(\frac{B_{\rm reh}}{10^{-8}{\rm G}}\right)^{2/3} \left(\frac{L_{\rm reh}}{\rm Mpc}\right)^{1/3}\,, \\ B_0 &= 10^{-8}{\rm G} \left(\frac{a_{\rm reh}}{a_0}\right) \left(\frac{B_{\rm reh}}{10^{-8}{\rm G}}\right)^{2/3} \left(\frac{L_{\rm reh}}{\rm Mpc}\right)^{1/3}\,. \end{aligned} \tag{7.14}$$

We will use these expressions in order to compare the magnetic field and its correlation length with the present time observational bounds.

7.2 Sourced perturbations

The gravitational coupling of the inflaton with the auxiliary field and the gauge field, gives rise to extra sources in the equation of motion of the inflaton perturbations. Being the latter the origin of curvature perturbations, we expect an extra contribution to

the curvature perturbations besides those due to vacuum fluctuations of the inflaton. Moreover, the presence of further fields besides the gravitational one, gives rise to a source term in the equation of motion of tensor modes, leading to an extra amount of GWs with respect to those generated by quantum fluctuations of the gravitational field (see section 2.2.1). The overproduction of scalar and tensor modes depends on the parameters of model (7.1). Therefore current observational constraints on scalar and tensor perturbations provide bounds on the parameters which describe the inflationary magnetogenesis (analogous studies for other models have been performed in [51, 62–64]).

Early it was believed that a minimal coupling between the gauge field and the inflaton, and then a non-minimal coupling between the gauge field and an auxiliary field, would lead to negligible extra production of scalar and tensor modes, in particular negligible non-gaussianities of second-order scalar perturbations. However, in [235] it has been shown that it not true, i.e. also in the case in which the gauge field is coupled to an auxiliary rolling field, the overproduction of scalar perturbations cannot be neglected with respect to current observational bounds. Indeed fluctuations of the auxiliary field sourced by the gauge field can oscillate into the observable curvature perturbations if such a field rolls for a sufficient number of e-folds. However the source term in the scalar perturbation equation of motion is reduced with respect to the case in which the gauge field is directly coupled to the inflaton, by a factor $\epsilon\, N_\sigma$, with N_σ the number of e-folds while the auxiliary field is rolling[1].

In light of this claim, in the next sections we calculate the amount of the sourced scalar and tensor modes as a function of the inflationary parameters. Then we will evaluate if current estimations and bounds on curvature and tensor modes allow a region in the parameter space which corresponds to a magnetogenesis able to justify gamma-ray observations.

7.2.1 Sourced tensor power spectrum

The gauge field turns out to act as a source term in the equation of motion of tensor modes [57, 62–64], therefore, besides vacuum fluctuations of the gravitational field, an extra amount of GWs is produced. Since in order to get an efficient magnetogenesis a low energy scale of inflation is required [1], in general, vacuum fluctuations of the gravitational field are expected to be less significant than those produced classically. Moreover notice that such GWs are expected to be chiral [57], and then to lead to non-vanishing cross-power spectra between temperature and polarization CMB anisotropies [225].
Current cosmological perturbations provide un upper bound on the GWs amount pro-

[1]Notice that the constraints from CMB are only valid if the gauge field was already excited when CMB scales were leaving the horizon. Since the coherence length L of the produced gauge field is well below the Mpc [1], one can think of a scenario where the auxiliary field starts rolling after CMB scales, but before L have left the horizon. In this (finely tuned) situation the constraints from CMB will not hold, and the mechanism can be effective even at higher energy scales for inflation.

duced during inflation, expressed by un upper limit on the tensor-to-scalar ratio.
The equation of motion of tensor modes is given by eq.(2.53), but notice that here the dynamics of A_μ is not the standard one. In [1] the amount of sourced GWs has been calculated as a function of the parameters of the model. More precisely, the tensor-to-scalar ratio is given in Eq. (3.6) of [1]:

$$r = p^t\,(n)\,\frac{H^4}{M_{pl}^4}\frac{e^{4\pi\xi}}{\xi^6}P_{\mathcal{R}}^{-1}\,, \tag{7.15}$$

where $p^t\,(n)$ is plotted in figure 1 of [1]. The tensor-to-scalar ratio is therefore a function of the Hubble parameter, ξ and n.

7.2.2 Sourced scalar modes

We calculate the sourced curvature power spectrum, generated by the presence of the extra fields beside the inflaton. We will find them to provide stricter limits on the parameter space of the model with respect to those due to tensor perturbations.

Equation of motion of inflaton perturbations. We perturb the inflaton and the auxiliary field as usual, $\varphi = \varphi_0 + \delta\varphi$ and $\sigma = \sigma_0 + \delta\sigma$, where $\delta\varphi$ and $\delta\sigma$ are first-order quantities while A_μ is half-order one. Here we identify the equation of motion of $\delta\varphi$ which is then required in order to evaluate curvature perturbations.
At zero-order in slow-roll expansion, the equation of motion of $\delta\varphi$ is the free Klein-Gordon equation. However it turns out that such an approximation is not sufficiently good in order to calculate curvature perturbations amount. Turning on the leading order in slow-roll leads to the appearing of a coupling between the inflaton perturbations $\delta\varphi$ and those of the auxiliary field $\delta\sigma$. Moreover, further sources due to the gravitational coupling between $\delta\varphi$ and the gauge fields appear too. Both of them gives a significant contribution to the final amount of $\delta\varphi$ perturbations.
We work in the flat gauge. From the Lagrangian (7.1), using Einstein equations to re-write metric perturbations [62], the equation of motion of $\delta\varphi$ in momentum space reads

$$\delta\varphi_{\rm flat}'' + 2\,\mathcal{H}\,\delta\varphi_{\rm flat}' + \left(k^2 + a^2\,V_{\varphi\varphi}\right)\,\delta\varphi_{\rm flat} - \left(\frac{a^2\,\varphi'^2}{\mathcal{H}}\right)'\,\frac{\delta\varphi_{\rm flat}}{M_{pl}^2 a^2} - \left(\frac{a^2\,\varphi'\,\sigma'}{\mathcal{H}}\right)'\,\frac{\delta\sigma_{\rm flat}}{M_{pl}^2\,a^2} = \\ = 2\,\varphi_0'\,S^{(3)} + \frac{\varphi_0'}{\mathcal{H}}\,S'^{(3)} + \frac{\varphi_0'}{\mathcal{H}}\,S^{(2)} \tag{7.16}$$

where $V_{\varphi\varphi}$ indicates the second derivative of the potential with respect to φ, and $\mathcal{H}$ is the comoving Hubble rate. The source terms depend on the gauge field and can be written in terms of the electromagnetic energy density and Poynting vector as follows

$$S^{(2)} = -\frac{a^2}{2\,M_{pl}^2}\,\rho_{\rm em}(\mathbf{k}) = -\frac{I^2\,a^2}{4\,M_{pl}^2}\,[E_i * E_i + B_i * B_i] \tag{7.17}$$

$$S^{(3)} = \frac{a}{2\,M_{pl}^2}\frac{i\,\hat{k}_j}{k}\,q_{{\rm em}j}(\mathbf{k}) = \frac{I^2\,a^2}{2\,M_{pl}^2}\frac{i\,\hat{k}_j}{k}\,\epsilon_{jlm}[E_l * B_m]\,, \tag{7.18}$$

where the convolution is defined as

$$[E_l * B_m](\mathbf{k}) = \int \frac{d^3\mathbf{q}}{(2\pi)^{3/2}} E_l(\mathbf{k}-\mathbf{q}) B_m(\mathbf{q})\,. \tag{7.19}$$

Notice that the term $\sim F_{\mu\nu}\tilde{F}^{\mu\nu}$ does not contribute to the electromagnetic stress energy tensor, and then it does not appear as a source in the Einstein equations. However, it clearly influences the sources in (7.16), being E_i and B_i depending on the solution of (7.3). Moreover notice that a term involving $\delta\sigma_{\rm flat}$ is present in the equation of motion of $\delta\varphi_{\rm flat}$. This term and the sources of the RHS of eq.(7.16) come from metric perturbations. Without accounting for those terms, one would find that $\delta\varphi_{\rm flat}$ satisfies the Klein-Gordon equation, since the inflaton φ is only minimally coupled to the other fields. Analogously, the equation of motion for $\delta\sigma_{\rm flat}$ reads

$$\begin{aligned}\delta\sigma''_{\rm flat} + 2\,\mathcal{H}\,\delta\sigma'_{\rm flat} + \left(k^2 + a^2\,V_{\sigma\sigma}\right)\,\delta\sigma_{\rm flat} - \left(\frac{a^2\sigma'^2}{\mathcal{H}}\right)'\frac{\delta\sigma_{\rm flat}}{M_{pl}^2\,a^2} - \left(\frac{a^2\,\varphi'\,\sigma'}{\mathcal{H}}\right)'\frac{\delta\varphi_{\rm flat}}{M_{pl}^2\,a^2} = \\ = S^{(1)} + 2\,\sigma'_0\,S^{(3)} + \frac{\sigma'_0}{\mathcal{H}}\,S'^{(3)} + \frac{\sigma'_0}{\mathcal{H}}\,S^{(2)}\,,\end{aligned} \tag{7.20}$$

where

$$S^{(1)} = a^2 I I_\sigma \left[E_i * E_i - B_i * B_i + 2\,\gamma\,\left(E_i * B_i\right)\right]\,, \tag{7.21}$$

and $I_\sigma \equiv \mathrm{d}I/\mathrm{d}\sigma$.
Equations (7.16) and (7.20) form a coupled system due to the mixing terms. We solve it by diagonalising the system. We account for both the mixing terms and the sources originated by the gravitational coupling between the inflaton and the other fields, i.e. we solve the exact equations at leading order in slow-roll. For compactness we denote S_φ the source on the RHS of eq. (7.16), and S_σ the source on the RHS of eq.(7.20). We express the system (7.16)-(7.20) with respect to $u_\varphi \equiv a\,\delta\varphi$ and $u_\sigma \equiv a\,\delta\sigma$. At first order in slow-roll we have

$$u''_\varphi + \left(k^2 - \frac{2}{\tau^2}\right)\,u_\varphi - \frac{3}{\tau^2}\,(3\,\epsilon - \eta_\varphi)\,u_\varphi - \frac{3}{\tau^2}\,(2\,\Theta\,\epsilon)\,u_\sigma = a\,(\tau)\,S_\varphi\,, \tag{7.22}$$

$$u''_\sigma + \left(k^2 - \frac{2}{\tau^2}\right)\,u_\sigma - \frac{3}{\tau^2}\,(\epsilon - \eta_\sigma)\,u_\sigma - \frac{3}{\tau^2}\,(2\,\Theta\,\epsilon)\,u_\varphi = a\,(\tau)\,S_\sigma\,, \tag{7.23}$$

where $\epsilon \equiv -\dot{H}/H^2$, $\eta_\varphi \equiv V_{\varphi\varphi}/V$ (and analogously for η_σ), and $\Theta \equiv \sigma'_0/\varphi'_0 \ll 1$, since only φ is supposed to drive the background dynamics. The mixing of u_φ with u_σ is described by the following matrix

$$M_{\varphi\sigma} = \begin{pmatrix} 2 + 9\,\epsilon - 3\,\eta_\varphi & 6\,\Theta\,\epsilon \\ 6\,\Theta\,\epsilon & 2 + 3\,\epsilon - 3\,\eta_\sigma \end{pmatrix} \tag{7.24}$$

which can be diagonalized by $U \cdot M \cdot U^T = \Lambda = \mathrm{diag}\,(\lambda_\varphi,\,\lambda_\sigma)$, with $U\,(\theta)$ a rotation matrix. We define $\mathbf{v} \equiv U^{-1}\mathbf{u}$, i.e. the eigenvectors of the Λ matrix. The diagonalized

system then reads

$$v_\varphi'' + \left(k^2 - \frac{\lambda_\varphi}{\tau^2}\right) v_\varphi = a(\tau)\left[\cos\theta\, S_\varphi + \sin\theta\, S_\sigma\right], \tag{7.25}$$

$$v_\sigma'' + \left(k^2 - \frac{\lambda_\sigma}{\tau^2}\right) v_\sigma = a(\tau)\left[-\sin\theta\, S_\varphi + \cos\theta\, S_\sigma\right]. \tag{7.26}$$

The solutions for v_φ and v_σ are given by

$$v_\varphi(\mathbf{k},\tau) = \int d\tau'\, G_k^{\lambda_\varphi}(\tau,\tau')\; a(\tau')\; \left[\cos\theta\, S_\varphi + \sin\theta\, S_\sigma\right], \tag{7.27}$$

$$v_\sigma(\mathbf{k},\tau) = \int d\tau'\, G_k^{\lambda_\sigma}(\tau,\tau')\; a(\tau')\; \left[-\sin\theta\, S_\varphi + \cos\theta\, S_\sigma\right], \tag{7.28}$$

where $G_k^{\lambda_{\sigma/\varphi}}$ are the Green functions of the equations (7.25) and (7.26) (note that the dependence on $\mathbf{k}$ and τ' is understood in the sources S_φ, S_σ). From the definition of v_φ, we can go back to the original function

$$\begin{aligned} u_\varphi(\mathbf{k},\,\tau) &= v_\varphi\,\cos\theta - v_\sigma\,\sin\theta = \\ &= \int d\tau'\, a(\tau')\,\left\{G_k^{\lambda_\varphi}(\tau,\,\tau')\,\left[\cos^2\theta\, S_\varphi + \sin\theta\,\cos\theta\, S_\sigma\right] + \right. \\ &\quad \left. + G_k^{\lambda_\sigma}(\tau,\,\tau')\left[\sin^2\theta\, S_\varphi - \sin\theta\,\cos\theta\, S_\sigma\right]\right\}. \end{aligned} \tag{7.29}$$

The Green function is given by

$$G_k^{\lambda_{\varphi/\sigma}}(\tau,\tau') = \frac{\pi}{2}\sqrt{\tau\tau'}\left[J_\mu(-k\tau)\; Y_\mu(-k\tau') - J_\mu(-k\tau')\; Y_\mu(-k\tau)\right]\Theta(\tau-\tau') \tag{7.30}$$

$$\text{with} \quad \mu = \frac{1}{2}\sqrt{1+4\,\lambda_{\varphi/\sigma}}\,,$$

where Θ here denotes the Heaviside step function. The relevant solution for the field perturbations concern modes outside the horizon, so that $|k\,\tau| \ll 1$. Furthermore, the solution for the gauge field (7.5) entering in the sources S_φ and S_σ is exponentially suppressed for $|k\,\tau'| \gtrsim 1/\xi \ll 1$, so that the biggest contribution to the above integral comes from modes well outside the horizon and we can set $|k\,\tau'| \ll 1$ in the Green function. Therefore, we can approximate (7.30) as

$$G_k^{\lambda_{\varphi/\sigma}}(\tau,\,\tau') \simeq \frac{\sqrt{\tau\,\tau'}}{2\,\mu}\left(\frac{\tau'}{\tau}\right)^{\mu}. \tag{7.31}$$

We next exploit the slow-roll expansion in order to simplify the solution. The system matrix given in (7.24) has the form

$$M_{\varphi\sigma} = \begin{pmatrix} 2+\delta M_{11} & \delta M_{12} \\ \\ \delta M_{12} & 2+\delta M_{22} \end{pmatrix}, \tag{7.32}$$

where $|\delta M_{\varphi\sigma}|$ are quantities that are first-order in slow-roll. The eigenvalues of $M_{\varphi\sigma}$ are

$$\lambda_{\varphi/\sigma} = 2 + \frac{1}{2}\left[\delta M_{11} + \delta M_{22} \pm \sqrt{4\,\delta M_{12}^2 + (\delta M_{11} - \delta M_{22})^2}\right], \tag{7.33}$$

so that we can define the quantities $\delta\lambda_{\sigma/\varphi}$, also first order in slow roll, by

$$\Lambda = \begin{pmatrix} \lambda_\varphi & 0 \\ 0 & \lambda_\sigma \end{pmatrix} = \begin{pmatrix} 2+\delta\lambda_\varphi & 0 \\ 0 & 2+\delta\lambda_\sigma \end{pmatrix}. \tag{7.34}$$

As a consequence one can also expand the Bessel function index of eq. (7.30) as $\mu \simeq 3/2 + \delta\lambda_{\varphi/\sigma}/3$, which, applied to eq. (7.31), leads to the following expansion for the Green function:

$$G_k^{\lambda_{\varphi/\sigma}} \simeq G_k^{(2)} + \delta\lambda_{\varphi/\sigma}\,\tilde{G}_k^{(2)} \equiv \frac{\sqrt{\tau\,\tau'}}{3}\left(\frac{\tau'}{\tau}\right)^{3/2}\left(1 - \frac{\delta\lambda_{\varphi/\sigma}}{3} + \frac{\delta\lambda_{\varphi/\sigma}}{3}\log\frac{\tau'}{\tau}\right). \tag{7.35}$$

The term proportional to the logarithm gives the dominant contribution between the last two terms, therefore we can use

$$G_k^{(2)}(\tau,\tau') = \frac{\sqrt{\tau\,\tau'}}{3}\left(\frac{\tau'}{\tau}\right)^{3/2}, \qquad \tilde{G}_k^{(2)} \simeq \frac{\sqrt{\tau\,\tau'}}{9}\left(\frac{\tau'}{\tau}\right)^{3/2}\log\left(\frac{\tau'}{\tau}\right), \tag{7.36}$$

which, applied to (7.29) finally leads to

$$u_\varphi(\mathbf{k},\tau) \simeq \sin\theta\,\cos\theta\,(\delta\lambda_\varphi - \delta\lambda_\sigma)\int d\tau'\,a(\tau')\,\tilde{G}_k^{(2)}(\tau,\,\tau')\,S_\sigma \tag{7.37}$$

$$+\int d\tau'\,a(\tau')\,G_k^{(2)}(\tau,\tau')\,S_\varphi\,. \tag{7.38}$$

Notice that, in the last term, we have neglected a term of order $\delta\lambda_{\varphi/\sigma}\,S_\varphi$, since, as we will see below, S_φ is higher order in slow roll with respect to S_σ. Now we can make a further simplification, which consists in approximating the logarithmic term $\log(\tau'/\tau)$ appearing in $\tilde{G}_k^{(2)}$ simply by a factor N_σ that we multiply outside of the time integral, where N_σ is the number of e-folds during which the field σ is rolling. This is possible because the integral in $d\tau'$ is dominated by $|\tau'| \sim (k\,\xi)^{-1}$, and greatly simplifies things, since the remaining part of the Green function actually corresponds to the one of eqs. (7.22) at zeroth order in slow roll. In summary, we can reduce the problem of determining the inflaton perturbation in the model under analysis to solve the following equation of motion for $u_\varphi = a\,\delta\varphi$:

$$u_\varphi'' + \left(k^2 - \frac{2}{\tau^2}\right)u_\varphi = \frac{N_\sigma}{3}\sin\theta\,\cos\theta\,(\delta\lambda_\varphi - \delta\lambda_\sigma)\,a(\tau)\,S_\sigma + a(\tau)\,S_\varphi\,. \tag{7.39}$$

This equation presents an effective source, combination of those for the fluctuations of the inflaton and of the auxiliary field (c.f. eqs. (7.16) and (7.20)), that we now proceed to estimate.

Estimation of the source. We want to evaluate the relative contribution of the source terms on the RHS of eq. (7.39). The exact relation

$$\sin\theta\,\cos\theta = \frac{\delta M_{12}}{\sqrt{4\,\delta M_{12}^2 + \left(\delta M_{11} - \delta M_{22}\right)^2}}\,, \tag{7.40}$$

implies that

$$\sin\theta\,\cos\theta\,\left(\delta\lambda_\varphi - \delta\lambda_\sigma\right) = \delta M_{12} = 6\,\Theta\,\epsilon\,. \tag{7.41}$$

Going back to the full expressions given in eqs. (7.16) and (7.20), the source in eq. (7.39), barring a overall factor $a\,(\tau)$, reads

$$2\,N_\sigma\,\Theta\,\epsilon\,\left[S^{(1)} + 2\,\sigma_0'\,S^{(3)} + \frac{\sigma_0'}{\mathcal{H}}\,S'^{(3)} + \frac{\sigma_0'}{\mathcal{H}}\,S^{(2)}\right] + 2\,\varphi_0'\,S^{(3)} + \frac{\varphi_0'}{\mathcal{H}}\,S'^{(3)} + \frac{\varphi_0'}{\mathcal{H}}\,S^{(2)}\,, \tag{7.42}$$

that, collecting terms and considering that $\Theta = \sigma_0'/\varphi_0' \ll 1$, can be approximated to

$$2\,N_\sigma\,\Theta\,\epsilon\,S^{(1)} + 2\,\varphi_0'\,S^{(3)} + \frac{\varphi_0'}{\mathcal{H}}\,S'^{(3)} + \frac{\varphi_0'}{\mathcal{H}}\,S^{(2)}\,, \tag{7.43}$$

which amounts to neglect the source due to the metric perturbations (as opposed to $S^{(1)}$, the one generated by the direct coupling between σ and the gauge field) in the equation of motion of $\delta\sigma$, eq. (7.20).
Let us now compare the term proportional to $S^{(1)}$ to the other terms in eq. (7.43). To do this we first need to estimate the amplitude of the fields E and B on which the sources depend, c.f. eqs. (7.17), (7.18) and (7.21). Let us go back to solution (7.5) for the gauge field, applying it in the regime relevant for particle creation, i.e. for $|k\,\tau| \ll \xi$ and $\xi \gg 1$. We can use it to approximate

$$B(k,\tau) \sim k\,A\,(k,\,\tau) \simeq k\,\left(-H\tau\right)^n\,\sqrt{-\frac{2\tau}{\pi}}\,e^{\pi\,\xi}\,K_{-2n-1}\left(\sqrt{-8\,\xi\,k\,\tau}\right)\,, \tag{7.44}$$

$$E(k,\tau) \sim -A\,(k,\,\tau)' \simeq -\left(-H\,\tau\right)^n\,\sqrt{\frac{4\,\xi\,k}{\pi}}\,e^{\pi\,\xi}\,K_{-2n}\left(\sqrt{-8\,\xi\,k\,\tau}\right)\,. \tag{7.45}$$

Moreover, the largest contribution to the above expressions comes from modes with $-k\tau \sim 1/\xi$, since the Bessel functions are exponentially suppressed for values of their arguments that are much larger than unity and the phase space suppresses contributions with small k. In this regime the Bessel functions take values that are of the order of the unity and

$$\frac{E}{B} \sim \sqrt{\frac{\xi}{-k\,\tau}} \sim \xi\,, \tag{7.46}$$

where in the last step we have used again $-k\,\tau \sim 1/\xi$. This means that the magnetic field is suppressed by a factor $1/\xi$ with respect to E (remember $\xi \gg 1$). Therefore we can conclude that in $S^{(1)}$ (eq. (7.21)) the term proportional to the convolution $E_i * E_i$ is dominant with respect to the one proportional to $B_i * B_i$.
Exploiting eq. (7.46), we can parametrically estimate the amplitude of the terms in

(7.43). Whenever there is a residual dependence on the momentum, we use the value corresponding to the peak of the electric and magnetic fields, i.e. $|k\,\tau| \sim 1/\xi$. Using $I_\sigma = n\,\mathcal{H}\,I/(\Theta\,\varphi_0')$ one gets

$$
\begin{aligned}
&2\,N_\sigma\,\Theta\,\epsilon\,S^{(1)} \sim 2\,N_\sigma\,\Theta\,\epsilon\,a^2\,n\,\mathcal{H}\,\frac{I^2}{\sigma_0'}(E*E) \simeq N_\sigma\,n\,\sqrt{2\epsilon}\left(\frac{a^2 I^2\,E*E}{M_{pl}}\right)\,,\\
&\varphi_0'\,S^{(3)} \sim \varphi_0'\,\frac{a^2\,I^2}{2\,M_{pl}^2}\,\frac{B*E}{k} \sim \sqrt{\frac{\epsilon}{2}}\left(\frac{a^2 I^2\,E*E}{M_{pl}}\right)\,,\\
&\frac{\varphi_0'}{\mathcal{H}}\,S'^{(3)} \sim \sqrt{\frac{\epsilon}{2}}\left(\frac{a^2\,I^2\,E*E}{M_{pl}}\right)\,,\\
&\frac{\varphi_0'}{\mathcal{H}}\,S^{(2)} \sim \sqrt{\frac{\epsilon}{8}}\left(\frac{a^2\,I^2\,E*E}{M_{pl}}\right)\,.
\end{aligned}
\tag{7.47}
$$

From the above estimations we conclude that all terms in eq. (7.43) are of the same order of magnitude, therefore we cannot neglect any of them a priori. In summary, to evaluate the inflaton perturbation (and therefore the curvature power spectrum), one has to solve the following equation:

$$
\delta\varphi_{\rm flat}'' + 2\,\mathcal{H}\,\delta\varphi_{\rm flat}' + k^2\,\delta\varphi_{\rm flat} = 2\,N_\sigma\,\Theta\,\epsilon\,S^{(1)} + 2\,\varphi_0'\,S^{(3)} + \frac{\varphi_0'}{\mathcal{H}}\,S'^{(3)} + \frac{\varphi_0'}{\mathcal{H}}\,S^{(2)}\,, \tag{7.48}
$$

resulting from eq. (7.39), going back to the variable $\delta\varphi_{\rm flat}$, and accounting only for the dominant term in the source S_σ. Note that, given (7.46), we can approximate

$$
S^{(1)} \simeq a^2 I\,I_\sigma\,(E_i * E_i + 2\,\gamma\,E_i * B_i) \tag{7.49}
$$

$$
S^{(2)} \simeq -\frac{I^2\,a^2}{4\,M_{pl}^2}\,E_i * E_i\,. \tag{7.50}
$$

7.3 The curvature perturbation $\mathcal{R}$

In this section we justify the use of an approximated expression for the curvature perturbation, i.e. $\mathcal{R} \simeq \frac{\mathcal{H}}{\dot\varphi}\delta\varphi_{\rm flat}$. When other fields are present beside the inflaton, it is not granted that the previous expression for $\mathcal{R}$ holds.
We follow the notations of [35]. In terms of the perturbations of the metric and of the content of the universe, uniform density curvature perturbations are defined by

$$
\zeta = -\frac{\mathcal{H}}{\rho_0'}\,\delta\rho_{\rm flat}\,. \tag{7.51}
$$

The derivative of the background energy density ρ_0 is given by:

$$
\rho_0' = -3\,\mathcal{H}\,(\rho_0 + P_0) \simeq -\frac{3\,\mathcal{H}}{a^2}\,{\varphi_0'}^2\,, \tag{7.52}
$$

where P_0 denotes the pressure. Remember that the energy density due to the gauge field is a quantity of the first order, then it does not contribute to the background

energy density. We have also assumed that the kinetic energy in σ is negligible: ${\sigma_0'}^2/{\varphi_0'}^2 \equiv \Theta^2 \ll 1$. In order to express $\delta\rho_{\rm flat}$ in terms of the fields, we use Einstein equations perturbed at the first order, in particular we use the $0-0$ and $0-i$ equations. Defining metric perturbations in the flat gauge by $\delta g_{00} = -2\,a^2\,\Phi_{\rm flat}$ and $\delta g_{0i} = a^2\,B_i$, we have:

$$3\,\mathcal{H}^2\,\Phi_{\rm flat} - \mathcal{H}\,k^2\,B_{\rm flat} = -4\pi\,G a^2\,\delta\rho_{\rm flat}\,, \tag{7.53}$$

$$\mathcal{H}\,\Phi_{\rm flat} - \frac{\varphi_0'}{2\,M_{pl}^2}\,\delta\varphi_{\rm flat} - \frac{\sigma_0'}{2\,M_{pl}^2}\,\delta\sigma_{\rm flat} = S^{(3)}\,. \tag{7.54}$$

At large scales the term $k^2\,B_{\rm flat}$ can be neglected, then from the second equation we get the expression of $\Phi_{\rm flat}$, we substitute it in the first equation, and then we get the sought expression for $\delta\rho_{\rm flat}$:

$$\delta\rho_{\rm flat} = -\frac{3\,\mathcal{H}}{a^2}\,\varphi_0'\,\delta\varphi_{\rm flat} - \frac{\mathcal{H}}{\varphi_0'}\,\Theta\,\delta\sigma_{\rm flat} - \frac{6\,\mathcal{H}\,M_{pl}^2}{a^2}\,S^{(3)}\,. \tag{7.55}$$

At large scales $\zeta = -\mathcal{R}$ [35], where $\mathcal{R}$ is the comoving curvature perturbation. From now on, we will refer to the curvature perturbations by $\mathcal{R}$. Combining (7.52) and (7.55), we obtain the expression of $\mathcal{R}$ in terms of the fields perturbations:

$$\mathcal{R} = \frac{\mathcal{H}}{\varphi_0'}\,\delta\varphi_{\rm flat} + \frac{S^{(3)}}{\mathcal{H}\,\epsilon} + \frac{\mathcal{H}}{\varphi_0'}\,\Theta\,\delta\sigma_{\rm flat}\,. \tag{7.56}$$

As expected, the comoving curvature perturbation $\mathcal{R}$ gets contributions directly from each field involved in the Lagrangian eq. (7.1).

Comparison of the terms in the expression of $\mathcal{R}$. With the prospect of calculating the curvature power spectrum, we make a comparison of the contributions to the expression of $\mathcal{R}$, in order to establish if some of them are negligible with respect to the others.
Notice that we are interested in calculating the curvature power spectrum at the end of inflation.
For what concerns the third term of eq.(7.56): we are supposing that at a certain time during inflation the field σ stops rolling, so that at the end of inflation σ_0' is vanishing. We can therefore neglect last term in equation (7.56).
The term proportional to $S^{(3)}$ in eq.(7.56) is expected to vanish at the end of inflation since at that time, σ has stopped rolling and does not source $S^{(3)}$ any more. To be conservative, however, in this section we will assume that σ is still rolling at the end of inflation so that the second term in eq.(7.56) is still present at that time.
On the other hand, notice that the factor $\delta\varphi_{\rm flat}$ evaluated at the end of inflation is anyway influenced by the gauge field even if at that time the electromagnetic source is switched off. In fact $\delta\varphi_{\rm flat}\,(t_{\rm end}, k)$ is obtained by the integration from the beginning of inflation up to the end, therefore it spans also the period in which the auxiliary field is rolling and then the electromagnetic source is active.

In order to compare the first and the second term of eq. (7.56), we estimate $\delta\varphi_{\rm flat}$ from its equation of motion (7.48). We only consider the first term of the source, given that they are all of the same order of magnitude, and we approximate $\delta\varphi'_{\rm flat} \simeq \mathcal{H}\,\delta\varphi_{\rm flat}$:

$$\delta\varphi_{\rm flat} \simeq N_\sigma\,\epsilon\,\Theta\,\frac{S^{(1)}}{\mathcal{H}^2} \simeq \sqrt{\frac{\epsilon}{2}}\frac{n\,N_\sigma}{\mathcal{H}^2}\,\frac{a^2\,I^2}{M_{pl}}\,E*E\,. \tag{7.57}$$

$S^{(3)}$ is taken from eq. (7.18):

$$\frac{S^{(3)}}{\mathcal{H}\epsilon} \simeq \frac{1}{\mathcal{H}\sqrt{\epsilon}}\frac{a^2 I^2}{\varphi'_0 M_{pl}}\,E*E\,. \tag{7.58}$$

Comparing the first two terms in (7.56), we have

$$\frac{\mathcal{H}\,\delta\varphi_{\rm flat}/\varphi'_0}{S^{(3)}/\mathcal{H}\,\epsilon} \sim n\,N_\sigma\epsilon\,, \tag{7.59}$$

showing that both terms should be retained when evaluating $\mathcal{R}$. From this result, we cannot make any conclusions about the respective importance of these two terms for the amount of the curvature power spectrum. Therefore, we decided to calculate the scale dependence of the curvature power spectrum due to the term proportional to $S^{(3)}$. As we will now see, the term proportional to $S^{(3)}$ has a blue spectrum, while the one proportional to $\delta\varphi_{\rm flat}$ is scale invariant. The former can therefore be safely neglected.

7.3.1 Contribution to the curvature power spectrum due to $S^{(3)}$

A we said before, at the end of inflation σ has stopped rolling and does not source $S^{(3)}$ any more. To be conservative, however, in this section we will assume that σ is still rolling at the end of inflation. As we will see, even in this case the term in $S^{(3)}$ will provide a blue and negligible contribution to the metric perturbation power spectrum. We want to calculate the scale dependence of the following contribution to the curvature power spectrum:

$$\left\langle \frac{S^{(3)}}{\mathcal{H}\,\epsilon}\left(\mathbf{k}_1,\tau\right)\frac{S^{(3)}}{\mathcal{H}\,\epsilon}\left(\mathbf{k}_2,\tau\right)\right\rangle, \tag{7.60}$$

with the aim of comparing it with the contribution due to the term $\mathcal{H}\,\delta\varphi_{\rm flat}/\varphi'_0$. We perform the quantization of the gauge field:

$$A_i\left(\mathbf{x},\tau\right) = \int \frac{\mathrm{d}^3\mathbf{p}}{\left(2\pi\right)^{3/2}} e^{i\mathbf{p}\cdot\mathbf{x}}\varepsilon_i^+\left(\mathbf{p}\right)\left[\hat{a}\left(\mathbf{p}\right)+\hat{a}^\dagger\left(-\mathbf{p}\right)\right]A_+\left(p,\tau\right), \tag{7.61}$$

where we have kept only the positive helicity mode and we have used the fact that the mode functions $A_+\left(p,\tau\right)$ are real in the regime $|p\,\tau| \lesssim \xi$ of interest. From eq. (7.18),

the expression of $S^{(3)}$ as a function of the gauge field reads

$$S^{(3)}(\mathbf{k}) = \frac{I^2}{2\,a^2\,M_{pl}^2}\int\frac{\mathrm{d}^3\mathbf{p}}{(2\pi)^{3/2}}\frac{1}{k^2}\left[\varepsilon_j^+(\mathbf{p})\,\varepsilon_j^+(\mathbf{k}-\mathbf{p})\;p_i\,k_i - p_j\,\varepsilon_j^+(\mathbf{k}-\mathbf{p})\,\varepsilon_i^+(\mathbf{p})\;k_i\right]\cdot \left[\hat{a}(\mathbf{p})+\hat{a}^\dagger(-\mathbf{p})\right]\left[\hat{a}(\mathbf{k}-\mathbf{p})+\hat{a}^\dagger(\mathbf{p}-\mathbf{k})\right]A_+(p)\,A'_+(|\mathbf{k}-\mathbf{p}|)\;. \tag{7.62}$$

We write the second term making a change in the integration variable, $\mathbf{k}\to\mathbf{q}-\mathbf{k}$, so that it becomes:

$$\int\frac{\mathrm{d}^3\mathbf{p}}{(2\pi)^{3/2}}\frac{1}{k^2}\left[k_j\varepsilon_j(\mathbf{p})\,\varepsilon_i(\mathbf{k}-\mathbf{p})\,k_i\right]\left[\hat{a}(\mathbf{k}-\mathbf{p})+\hat{a}^\dagger(\mathbf{p}-\mathbf{k})\right]\cdot \cdot\left[\hat{a}(\mathbf{p})+\hat{a}^\dagger(-\mathbf{p})\right]A(|\mathbf{k}-\mathbf{p}|)\,A'(p) \tag{7.63}$$

since $k_i\varepsilon_i(k)=0$. Then, performing a further change of variable $\mathbf{k}\to\mathbf{q}-\mathbf{k}$, we recover the same arguments of A and A' of the first term in (7.62):

$$\int\frac{d^3\mathbf{p}}{(2\pi)^{3/2}}\frac{1}{k^2}\left[k_j\varepsilon_j(\mathbf{k}-\mathbf{p})\,\varepsilon_i(\mathbf{p})\,k_i\right]\left[\hat{a}(\mathbf{p})+\hat{a}^\dagger(-\mathbf{p})\right]\cdot \cdot\left[\hat{a}(\mathbf{k}-\mathbf{p})+\hat{a}^\dagger(\mathbf{p}-\mathbf{k})\right]A(p)\,A'(|\mathbf{k}-\mathbf{p}|) \tag{7.64}$$

By using the relation (c.f. Eq. (C3) of [62])

$$k_i\,k_j\,\varepsilon_i^+(\mathbf{p})\,\varepsilon_j^+(\mathbf{k}-\mathbf{p}) = \left[p\,|\mathbf{k}-\mathbf{p}| + (\mathbf{k}-\mathbf{p})\cdot\mathbf{p}\right]\varepsilon_i^+(\mathbf{p})\,\varepsilon_i^+(\mathbf{k}-\mathbf{p})\;, \tag{7.65}$$

to arrange eq.(7.64), the full expression (7.62) turns out to be:

$$S^{(3)}(k) = \frac{iI^2}{2a^2M_{pl}^2}\int\frac{d^3\mathbf{p}}{(2\pi)^{3/2}}\frac{1}{k^2}\left[\varepsilon_i(\mathbf{k}-\mathbf{p})\,\varepsilon_i(\mathbf{p})\right]\left[k_jp_j - p\,|\mathbf{k}-\mathbf{p}| + (\mathbf{k}-\mathbf{p})\cdot\mathbf{p}\right]\cdot \cdot\left[\hat{a}(\mathbf{p})+\hat{a}^\dagger(-\mathbf{p})\right]\left[\hat{a}(\mathbf{k}-\mathbf{p})+\hat{a}^\dagger(\mathbf{p}-\mathbf{k})\right]A(p)\,A'(|\mathbf{k}-\mathbf{p}|)\;, \tag{7.66}$$

where $p_ik_i - k\,|\mathbf{k}-\mathbf{p}| - (\mathbf{k}-\mathbf{p})\cdot\mathbf{p} = p^2 - p\,|\mathbf{k}-\mathbf{p}|$, so that:

$$S^{(3)}(\mathbf{k}) = \frac{I^2}{2\,a^2\,M_{pl}^2}\int\frac{d^3\mathbf{p}}{(2\pi)^{3/2}}\frac{1}{k^2}\left[\varepsilon_i^+(\mathbf{k}-\mathbf{p})\,\varepsilon_i^+(\mathbf{p})\right]\left[p^2 - p\,|\mathbf{k}-\mathbf{p}|\right]\cdot \left[\hat{a}(\mathbf{p})+\hat{a}^\dagger(-\mathbf{p})\right]\left[\hat{a}(\mathbf{k}-\mathbf{p})+\hat{a}^\dagger(\mathbf{p}-\mathbf{k})\right]A_+(p)\,A'_+(|\mathbf{k}-\mathbf{p}|)\;. \tag{7.67}$$

From the previous expression, and exploiting the commutation rules of $\hat{a}$ and $\hat{a}^\dagger$, the power spectrum of the $S^{(3)}/(\mathcal{H}\epsilon)$ term can be written as

$$P_{S^{(3)}}(k) = \frac{I^4\,\mathcal{H}^2}{2\pi^2\,a^4(\tau)\,(\varphi_0')^4}\int\frac{d^3\mathbf{p}}{(2\pi)^3}\frac{p\,|\mathbf{p}-\mathbf{k}|}{k}\left(p-|\mathbf{k}-\mathbf{p}|\right)^2\cdot \varepsilon_j^+(\mathbf{p})\,\varepsilon_j^+(\mathbf{k}-\mathbf{p})\;\varepsilon_i^+(\mathbf{p}-\mathbf{k})\,\varepsilon_i^+(-\mathbf{p})\;A_+(p)\,A'_+(|\mathbf{k}-\mathbf{p}|)\,A_+(|\mathbf{p}-\mathbf{k}|)\,A'_+(-p)\;. \tag{7.68}$$

We are interested in the behaviour at large scales, so we perform the limit $k \to 0$, where

$$\frac{p\,|\mathbf{p}-\mathbf{k}|}{k}\,(p-|\mathbf{k}-\mathbf{p}|)^2 \sim k\,p^2\,. \tag{7.69}$$

Then, in this limit the spectrum of $S^{(3)}/(\mathcal{H}\epsilon)$ behaves as:

$$P_{S^{(3)}}(k) \sim \frac{I^4\,\mathcal{H}^2}{a^4\,(\tau)\,(\varphi_0')^4}\,k\int \mathrm{d}p\,p^4\,A_+^2\,(p)\,{A'_+}^2\,(p)\,. \tag{7.70}$$

The contribution to the curvature power spectrum due to the spectrum of $S^{(3)}/(\mathcal{H}\epsilon)$ is therefore blue, with a spectral index equal to one. We will see that the contribution to the curvature power spectrum due to the term proportional to $\delta\varphi_{\rm flat}$ is instead scale invariant. The former contribution is therefore largely suppressed at large scales with respect to latter. Notice also that, from this result, we can say that also the contributions due to the correlation between the term $S^{(3)}/(\mathcal{H}\epsilon)$ and that proportional to $\delta\varphi_{\rm flat}$ are suppressed at large scales and can be neglected. For the same reason, we can safely neglect this term also in the calculation of the curvature bispectrum.
In conclusion, in the rest of the paper for the calculation of the curvature power spectrum and bispectrum we use

$$\mathcal{R} \simeq -\frac{\mathcal{H}}{\varphi_0'}\delta\varphi_{\rm flat}\,. \tag{7.71}$$

7.4 Sourced power spectrum and bispectrum

In this section we compute the contributions to the sourced scalar spectrum and bispectrum.

7.4.1 Curvature power spectrum

Since a source term is present in the equation of motion of $\delta\varphi$, one has

$$\delta\varphi = \delta\varphi_{\rm vacuum} + \delta\varphi_{\rm sourced} \tag{7.72}$$

where $\delta\varphi_{\rm vacuum}$ is given by the solution to the homogeneous part of eq. (7.48) with Bunch-Davies boundary condition. Since these two components are uncorrelated, the power spectrum $\langle\delta\varphi\,\delta\varphi\rangle$ receives two contributions:

$$\langle\delta\varphi\,\delta\varphi\rangle = \langle\delta\varphi_{\rm vacuum}\,\delta\varphi_{\rm vacuum}\rangle + \langle\delta\varphi_{\rm sourced}\,\delta\varphi_{\rm sourced}\rangle\,. \tag{7.73}$$

Here we calculate the contribution due to the presence of the source term.

In appendix D we simplified the expression of the source, so that we have:

$$2\,\varphi_0'\,S^{(3)} + \frac{\varphi_0'}{\mathcal{H}}\,S'^{(3)} + \frac{\varphi_0'}{\mathcal{H}}\,S^{(2)} \simeq \frac{I^2\,\varphi_0'\,a^2}{2\,\mathcal{H}\,M_P^2}\,\frac{\mathbf{k}_i\,\mathbf{k}_j}{k^2}\int\frac{d\mathbf{q}}{(2\pi)^3}E_i(\mathbf{k}-\mathbf{q})\,E_j(\mathbf{q})\,, \tag{7.74}$$

The gravitationally induced part of the source term of eq. (7.48), finally turns out to be:

$$2\,\varphi_0'\,S^{(3)}+\frac{\varphi_0'}{\mathcal{H}}\,S'^{(3)}+\frac{\varphi_0'}{\mathcal{H}}\,S^{(2)}\simeq\frac{I^2\,\varphi_0'\,a^2}{2\,\mathcal{H}\,M_{pl}^2}\,\hat{k}_i\,\hat{k}_j\,E_i*E_j\,, \tag{7.75}$$

where the $\simeq$ sign is due to the fact that we neglected terms proportional to B^2 that, as we have seen above in Eq. (7.46), are subdominant with respect to those proportional to E^2 in the regime $\xi\gg 1$ that we are considering.
In terms of $u_\varphi=a\,\delta\varphi_{\rm flat}$, the equation of motion (7.48) takes then the form

$$u_\varphi''+\left(k^2-\frac{2}{\tau^2}\right)u_\varphi=\frac{I^2\,\varphi_0'\,a^3}{2\,\mathcal{H}\,M_{pl}^2}\left[2\,N_\sigma\,n\,(E_i*E_i+2\,\gamma\,E_i*B_i)+\hat{k}_i\,\hat{k}_j\,E_i*E_j\right]\,, \tag{7.76}$$

where we have used $I_\sigma=n\,\mathcal{H}\,I/\sigma_0'$. Reference [62] considered only the second term on the right hand side of eq. (7.76), whereas [235] effectively considered only the first one. The first term indeed dominates, as we show in the following. Notice that those analyses were performed in the case in which only the $\tilde{F}\,F$ term was coupled to σ, that corresponds to the case $n\to 0$, $\xi=$constant. Here we perform the full analysis of eq. (7.76) in our model that allows for all values of $-2<n<0$.
Now we quantize the gauge field according to eq. (7.61) so that the source term above,

$$J_{\mathbf{k}}\,(\tau)\equiv\frac{I^2\,\varphi_0'\,a^3}{2\,\mathcal{H}\,M_{pl}^2}\left[2\,N_\sigma\,n\,(E_i*E_i+2\,\gamma\,E_i*B_i)+\hat{k}_i\,\hat{k}_j\,E_i*E_j\right] \tag{7.77}$$

takes the form

$$\begin{aligned}J_{\mathbf{k}}\,(\tau)=&\frac{I^2\,\varphi_0'}{2\,\mathcal{H}\,M_{pl}^2\,a}\int\frac{{\rm d}^3\mathbf{p}}{(2\pi)^{3/2}}\varepsilon_i^+\,(\mathbf{p})\,\varepsilon_i^+\,(\mathbf{k}-\mathbf{p})\left[\hat{a}_+\,(\mathbf{p})+\hat{a}_+^\dagger\,(-\mathbf{p})\right]\left[\hat{a}_+\,(\mathbf{k}-\mathbf{p})+\hat{a}_+^\dagger\,(\mathbf{p}-\mathbf{k})\right]\\&\cdot\left\{\left[2\,n\,N_\sigma-\frac{1}{k^2}\,[p\,|\mathbf{k}-\mathbf{p}|+(\mathbf{k}-\mathbf{p})\cdot\mathbf{p}]\right]A_+'\,(p,\tau)\,A_+'\,(|\mathbf{k}-\mathbf{p}|\,,\tau)\right.\\&\left.+\,4\,N_\sigma\,\xi\,|\mathbf{k}-\mathbf{p}|\,A_+'\,(p,\tau)\,A_+\,(|\mathbf{k}-\mathbf{p}|\,,\tau)\right\},\end{aligned} \tag{7.78}$$

where we used the relation (7.65) and in the last line we exchanged $\mathbf{k}-\mathbf{p}$ with $\mathbf{p}$, since the integral is symmetric under this exchange. We are now in position to evaluate the sourced scalar spectrum:

$$\begin{aligned}&\langle\delta\varphi_{\rm sourced}\,(\mathbf{k}_1,\,\tau)\;\delta\varphi_{\rm sourced}\,(\mathbf{k}_2,\,\tau)\rangle=\\&\quad\frac{1}{a^2\,(\tau)}\int_{\tau_0}^{\tau}d\tau' G_{\mathbf{k}_1}\,(\tau,\tau')\int_{\tau_0}^{\tau}d\tau'' G_{\mathbf{k}_2}\,(\tau,\tau'')\,\langle J_{\mathbf{k}_1}\,(\tau')\,J_{\mathbf{k}_2}\,(\tau'')\rangle\,,\end{aligned} \tag{7.79}$$

where the Green function $G_{\mathbf{k}}\,(\tau,\tau')$, for $|k\,\tau|<|k\,\tau'|\ll 1$ is well approximated by (c.f. Eq. (7.36))

$$G_k\,(\tau,\tau')\simeq-\frac{1}{3}\frac{\tau'^2}{\tau}\,. \tag{7.80}$$

Applying the commutation rules for the operators $\hat{a}_+$ and $\hat{a}_+^\dagger$, and exploiting the equality

$$\left|\varepsilon_i^+\left(\mathbf{k}+\mathbf{p}\right)\varepsilon_i^+\left(-\mathbf{p}\right)\right|^2 = \frac{1}{4}\left(1+\frac{\left|\mathbf{p}\right|^2+\mathbf{p}\cdot\mathbf{k}}{\left|\mathbf{p}\right|\cdot\left|\mathbf{k}+\mathbf{p}\right|}\right)^2 , \tag{7.81}$$

recalling definition (1.17), we obtain:

$$\begin{aligned} P_{\delta\varphi}^{\text{sourced}}(k) =& \frac{k^3}{2\,\pi^2}\,\frac{\epsilon}{32\,H^2\,M_P^2}\int\frac{\mathrm{d}^3\mathbf{p}}{(2\pi)^3}\,\left[1-\frac{\mathbf{p}\cdot(\mathbf{k}-\mathbf{p})}{p\,|\mathbf{k}-\mathbf{p}|}\right]^2\,\left|\int_{\tau_0}^{\tau}\mathrm{d}\tau'\,(-H\tau')^{-2n+3}\right. \\ &\cdot\left\{\left[2\,N_\sigma\,n-\frac{1}{k^2}\left[p\,|\mathbf{k}-\mathbf{p}|+(\mathbf{k}-\mathbf{p})\cdot\mathbf{p}\right]\right]\,A_+'\left(p,\tau'\right)\,A_+'\left(|\mathbf{k}-\mathbf{p}|\,,\tau'\right)\right. \\ &\left.\left.+\,4\,N_\sigma\,\xi\,|\mathbf{k}-\mathbf{p}|\,A_+'\left(p,\tau'\right)\,A_+\left(|\mathbf{k}-\mathbf{p}|\,,\tau'\right)\right\}\right|^2 . \end{aligned} \tag{7.82}$$

We are interested in the power spectrum evaluated at the end of inflation, so we set $\tau = 0$. The integrand is dominated by modes for which the particle creation is relevant, i.e. $|k\,\tau'| \sim 1/\xi$. Therefore, as long as σ is rolling for these values of τ', we can safely set $\tau_0 \to -\infty$ since this does not include extra relevant contributions to the integral. This puts us in the position to use the explicit expressions for the mode functions of the gauge field

$$\begin{aligned} A_+(k,\,\tau) &\simeq (-H\,\tau)^n\,\sqrt{-\frac{2\,\tau}{\pi}}\,e^{\pi\xi}\,K_{-2n-1}\left(\sqrt{-8\,\xi\,k\,\tau}\right)\,, \\ A_+(k,\,\tau)' &\simeq (-H\,\tau)^n\,\sqrt{\frac{4\,\xi\,k}{\pi}}\,e^{\pi\xi}\,K_{-2n}\left(\sqrt{-8\,\xi\,k\,\tau}\right)\,, \end{aligned} \tag{7.83}$$

and insert them into eq. (7.82). We then change variables to $y = \sqrt{-8\,\xi\,k\,\tau}$, choose a reference frame where the z-axis is parallel to $\mathbf{k}$, and define $Q \equiv p/k$, $\mu \equiv \cos\alpha$, where α is the angle between $\mathbf{k}$ and $\mathbf{p}$. The power spectrum then reads

$$\begin{aligned} P_{\delta\varphi}^{\text{sourced}}(k) =& \,\epsilon\,\frac{e^{4\pi\xi}}{\xi^6}\,\frac{H^4}{9\times 2^{23}\,\pi^6\,M_{pl}^2}\int_0^\infty dQ\,Q^3\int_{-1}^1 d\mu\,P\left(1-\frac{\mu-Q}{P}\right)^2 \\ &\cdot\left|\int_0^\infty dy\,y^7\left\{\left[2\,N_\sigma n-Q\,\left(P+\mu-Q\right)\right]\left[K_{-2n}\left(y\,\sqrt{Q}\right)\,K_{-2n}\left(y\,\sqrt{P}\right)\right]\right.\right. \\ &\left.\left.+\,N_\sigma\,\sqrt{P}\,\left[y\,K_{-2n-1}\left(y\sqrt{P}\right)\,K_{-2n}\left(y\,\sqrt{Q}\right)\right]\right\}\right|^2 , \end{aligned} \tag{7.84}$$

where $P \equiv \sqrt{1+Q^2-2\,Q\,\mu}$. The first term proportional to N_σ is the one due to the first term in (7.76), the term proportional to $Q\,(P+\mu-Q)$ corresponds to the part of the source proportional to $\hat{k}_i\hat{k}_j E_i * E_j$, and the last term to the part of the source proportional to $\gamma\,E_i * B_i$.

In figure 7.1, we show the relative contributions to the power spectrum due to each term in (7.84), collecting in a unique quantity the two terms proportional to N_σ^2. Contributions are shown up to a common factor. As visible, contributions which are not proportional to N_σ^2 are at least one order of magnitude smaller than the others. This is true also in the case in which $N_\sigma = 1$. For $N_\sigma > 1$, which corresponds to more

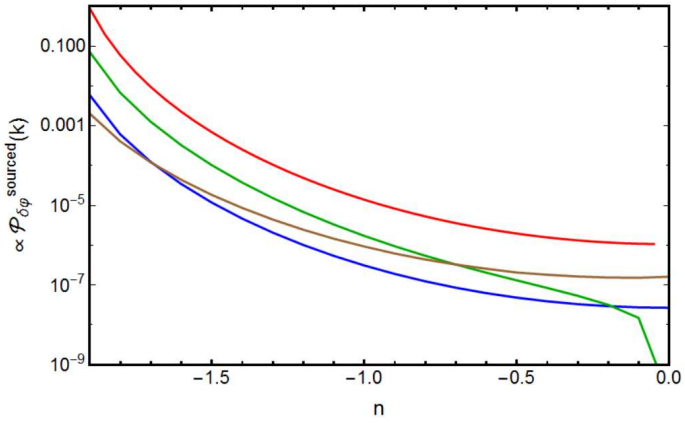

Figure 7.1: Relative contributions to the curvature power spectrum given in eq.(7.84), where we have fixed $N_\sigma = 1$. Contributions are shown up to the common factor $\epsilon \left(n \frac{e^{2\pi\xi}}{\xi^3} \frac{H^2}{\pi M_{pl}}\right)^2$. The red curve shows the power spectrum due to the sum of the two terms proportional to N_σ^2; in green the contribution to the power spectrum due to the cross-correlation between the term proportional to $N_\sigma E_i * E_i$ and the gravitationally induced term proportional to $\hat{k}_i \hat{k}_j E_i * E_j$; in brown the contribution due to the cross-correlation between the term proportional to $N_\sigma \gamma E_i * B_i$ and the gravitationally induced term; in blue the power spectrum due to the gravitationally induced term.

natural models, the amplitude of such terms become even smaller. Therefore for a comparison of the curvature power spectrum of our model with current observations, we can safely approximate the source of the inflaton perturbations by the first two terms in eq.(7.48), so that the curvature power spectrum is well approximated by:

$$
\begin{aligned}
P_{\delta\varphi}^{\rm sourced}(k) = & \epsilon \, \frac{e^{4\pi\xi}}{\xi^6} \frac{H^4}{9 \times 2^{23} \, \pi^6 \, M_{pl}^2} \int_0^\infty dQ \, Q^3 \int_{-1}^1 d\mu \, P \left(1 - \frac{\mu - Q}{P}\right)^2 \\
& \cdot \left| \int_0^\infty dy \, y^7 \Big\{ 2 \, N_\sigma n \left[K_{-2n}\left(y\sqrt{Q}\right) \, K_{-2n}\left(y\sqrt{P}\right) \right] \right. \\
& \left. + N_\sigma \sqrt{P} \left[y \, K_{-2n-1}\left(y\sqrt{P}\right) \, K_{-2n}\left(y\sqrt{Q}\right) \right] \Big\} \right|^2 . \qquad (7.85)
\end{aligned}
$$

7.4.2 Curvature bispectrum

For the calculation of the curvature bispectrum we proceed in an analogous manner as for the power spectrum. As before, the overall amplitude of the bispectrum is given by one contribution related to the homogeneous solution of the equation of motion for the inflaton perturbations, and one due to the presence of the sources. The former is well known to be very small, here we calculate the latter.
As before, we refer to the equation of motion for u_φ, eq.(7.76). Starting from the

definition of the curvature bispetrum we have:

$$\langle \delta\varphi_{\mathbf{k}_1}(\tau)\,\delta\varphi_{\mathbf{k}_2}(\tau)\,\delta\varphi_{\mathbf{k}_3}(\tau)\rangle = \frac{1}{a^3(\tau)}\int_{\tau_0}^{\tau} d\tau' G_{\mathbf{k}_1}(\tau,\tau')\int_{\tau_0}^{\tau} d\tau'' G_{\mathbf{k}_2}(\tau,\tau'') \int_{\tau_0}^{\tau} d\tau''' G_{\mathbf{k}_3}(\tau,\tau''')\langle J_{\mathbf{k}_1}(\tau')\,J_{\mathbf{k}_2}(\tau'')\,J_{\mathbf{k}_3}(\tau''')\rangle\ . \quad (7.86)$$

Using the expression for the source term (7.78) where we suppress the subdominant, gravitationally induced term not proportional to N_σ, and the Green function (7.80), the three point function of $\delta\varphi_{\rm sourced}$ takes the form

$$\begin{aligned}\langle \delta\varphi_{\mathbf{k}_1}\delta\varphi_{\mathbf{k}_2}\delta\varphi_{\mathbf{k}_3}\rangle =& \frac{n^3}{a^3}\frac{N_\sigma^3\epsilon^3}{\dot\varphi^3}\frac{e^{6\pi\xi}}{\xi^9}\frac{1}{9\times 2^{24}\pi^3}\delta(\mathbf{k}_1+\mathbf{k}_2+\mathbf{k}_3)\cdot\int\frac{\mathrm{d}^3\mathbf{p}}{(2\pi)^{9/2}}\\ &\cdot\left[\varepsilon_i^+(\mathbf{p})\,\varepsilon_i^+(\mathbf{p}-\mathbf{k}_1)\right]\left[\varepsilon_j^+(\mathbf{p}-\mathbf{k}_1)\,\varepsilon_j^+(-\mathbf{k}_3-\mathbf{p})\right]\left[\varepsilon_l^+(\mathbf{p}+\mathbf{k}_3)\,\varepsilon_l^+(-\mathbf{p})\right]\\ &\int_0^\infty \mathrm{d}x' h(|\mathbf{p}|,|\mathbf{k}_1-\mathbf{p}|;x')\int_0^\infty \mathrm{d}x'' h(|\mathbf{p}-\mathbf{k}_1|,|\mathbf{k}_3+\mathbf{p}|;x'')\\ &\int_0^\infty \mathrm{d}x''' h(|\mathbf{p}+\mathbf{k}_3|,|\mathbf{p}|;x''')\ , \end{aligned} \quad (7.87)$$

where we have defined

$$\begin{aligned}h(|\mathbf{p}|,|\mathbf{k}_1-\mathbf{p}|;x) =& \frac{\sqrt{|\mathbf{p}|\cdot|\mathbf{k}_1-\mathbf{p}|}}{H}x^7\left[K_{-2n}\left(x\sqrt{\frac{|\mathbf{k}_1-\mathbf{p}|}{H}}\right)K_{-2n}\left(x\sqrt{\frac{|\mathbf{p}|}{H}}\right)\right.\\ &\left.-\frac{x}{2n}\frac{\sqrt{|\mathbf{k}_1-\mathbf{p}|}}{\sqrt{H}}K_{-2n}\left(x\sqrt{\frac{|\mathbf{p}|}{H}}\right)K_{-2n-1}\left(x\sqrt{\frac{|\mathbf{k}_1-\mathbf{p}|}{H}}\right)\right].\end{aligned} \quad (7.88)$$

Exploiting the relation (7.81), the products of the polarization vectors in the second line of eq. (7.87) can be written as

$$\begin{aligned}[\varepsilon\text{ product}] \equiv \frac{1}{8}\big[&(\hat q_1\cdot\hat q_3)^2+(\hat p\cdot\hat q_3)^2+(\hat p\cdot\hat q_1)^2+(\hat p_1\cdot\hat q_3)+(\hat p\cdot\hat q_3)+(\hat p_1\cdot\hat p)+\\ &(\hat q_1\cdot\hat p)(\hat p\cdot\hat q_3)+(\hat p\cdot\hat q_1)(\hat q_1\cdot\hat q_3)+(\hat p\cdot\hat q_3)(\hat q_1\cdot\hat q_3)-(\hat p\cdot\hat q_1)(\hat p\cdot\hat q_3)(\hat q_1\cdot\hat q_3)\big]\end{aligned} \quad (7.89)$$

where $\mathbf{q}_1=\mathbf{p}-\mathbf{k}_1$ and $\mathbf{q}_3=\mathbf{p}+\mathbf{k}_3$.
We choose a reference system such that the vector $\mathbf{k}_1$ is along the z-axes and we decompose the integral in $\mathrm{d}^3\mathbf{p}$ in the following variables: $P\equiv p/k_1$, $\bar\Theta$ the angle between $\mathbf{p}$ and $\mathbf{k}_1$ and $\bar\Phi$ the angle between $\mathbf{p}$ and the x-direction. Moreover we call Φ the angle between the z-axes and $\mathbf{k}_3$. As it is usual for scenarios where non-gaussianities are generated by subhorizon dynamics, we expect the bispectrum to be maximized in the equilateral configuration $k\equiv|\mathbf{k}_1|=|\mathbf{k}_2|=|\mathbf{k}_3|$. In this case we obtain

$$\langle \delta\varphi_{\mathbf{k}_1}\delta\varphi_{\mathbf{k}_2}\delta\varphi_{\mathbf{k}_3}\rangle_{equil} = \frac{\delta(\mathbf{k}_1+\mathbf{k}_2+\mathbf{k}_3)}{k^6}\frac{H^6}{M_{pl}^3}\frac{e^{6\pi\xi}}{\xi^9}\left(N_\sigma\sqrt{2\epsilon}\right)^3 f(n)\ , \quad (7.90)$$

where

$$f(n) = \frac{n^3}{9\times 2^{27}\,\pi^3}\frac{1}{(2\pi)^{9/2}}\int_0^\infty dP\,P^3\int_{-1}^{1} d\cos\bar{\Theta}\,Q\,R\cdot[\varepsilon\ \text{product}]\cdot$$
$$\cdot\int_0^\infty dy_1\,y_1^7\left[K_{-2n}\left(y_1\sqrt{Q}\right)K_{-2n}\left(y_1\sqrt{P}\right)-\frac{y_1}{2n}\sqrt{Q}K_{-2n}\left(y_1\sqrt{P}\right)K_{-2n-1}\left(y_1\sqrt{Q}\right)\right]$$
$$\cdot\int_0^\infty dy_2\,y_2^7\left[K_{-2n}\left(y_2\sqrt{Q}\right)K_{-2n}\left(y_2\sqrt{R}\right)-\frac{y_2}{2n}\sqrt{R}K_{-2n}\left(y_2\sqrt{Q}\right)K_{-2n-1}\left(y_2\sqrt{R}\right)\right]$$
$$\cdot\int_0^\infty dy_3\,y_3^7\left[K_{-2n}\left(y_3\sqrt{R}\right)K_{-2n}\left(y_3\sqrt{P}\right)-\frac{y_3}{2n}\sqrt{P}K_{-2n}\left(y_3\sqrt{R}\right)K_{-2n-1}\left(y_3\sqrt{P}\right)\right], \tag{7.91}$$

where we have aligned $\mathbf{k}_1$ along the third axis, and we have defined $P\equiv p/k_1$, $\bar{\Theta}$ is the angle between $\mathbf{p}$ and $\mathbf{k}_1$, $\bar{\Phi}$ the angle between $\mathbf{p}$ and the x-direction, and

$$Q\equiv\sqrt{1-P^2-2P\cos\bar{\Theta}}\,,\qquad R\equiv\sqrt{1+P^2+2P\left(-\frac{1}{2}\cos\bar{\Theta}+\frac{\sqrt{3}}{4}\sin\bar{\Theta}\right)}\,. \tag{7.92}$$

Since other configurations are too complicated to evaluate, we are going to consider only the result of the equilateral configuration and compare it with current upper limits on curvature non-gaussianities in terms of $f_{\rm NL}^{equil}$. In principle this is not exhaustive, but, since the non-gaussian component is generated by sub-horizon dynamics, we expect the shape of the bispectrum to be close to equilateral, and our analysis to provide a robust picture of the current status of the model with respect to observations.

7.5 Constraints on the magnetic field production from inflationary perturbations

We obtained the tensor power spectrum and the curvature power spectrum and bispectrum as functions of the inflationary parameters. We want to compare them with the constraints provided by observations in order to obtain current bounds on the parameter space of our model. At the same time we require that the current lower bound on magnetic fields on cosmological scales is satisfied, see e.g. [11–13]. We will see that the combinations of these two requirements still leave available a large region in the parameter space, i.e. our model can explain the presence of magnetic fields on cosmological scales, satisfying at the same time current constraints on curvature and tensor perturbations.

Current cosmological observations provides an estimation of the curvature power spectrum amplitude of $A_s = 2.21\cdot 10^{-9}$ at $k = 0.05\text{Mpc}^{-1}$ at 68% of CL [2]. Moreover, the curvature power spectrum is constrained to be almost scale-invariant [2]. In order to satisfy the estimation for the power spectrum amplitude, we ask the contribution due to the presence of the gauge field, i.e (7.85) to be much less (one order of magnitude) than that due to vacuum fluctuations of the inflaton. We could have asked for the

sum of the contribution due to vacuum fluctuation and that due to the presence of the gauge field to be equal to the value estimated by the observations. However, if the field σ slows down its rolling while observed scales leave the horizon, a feature in the power spectrum is expected to appear (similarly to the case considered in [64]). Such a kind of feature is not observed in CMB data. In order to avoid such a phenomenon, N_σ to be sufficiently large would be required. In order to avoid such a problem, we impose the stricter constraint of requiring the contribution due to the gauge field to be much smaller, by a factor 10, than the vacuum one. Imposing this restrictive condition is sufficient, even if not necessary, and in any case it does not change our results: they are dominated by constraints from non-gaussianities, as we now show.

Cosmological observations provide also strict constraints on curvature non-gaussianities. In particular, for the equilateral configuration, [46] finds the following bound: $f_{\rm NL}^{equil} = -16 \pm 70$ from temperature data, $f_{\rm NL}^{equil} = -3.7 \pm 43$ for $T+E$ data, at 68% of CL [46]. As usual, we parametrize the bispectrum by $f_{\rm NL}^{equil}$, defined as

$$\langle \mathcal{R}(\mathbf{k}_1)\,\mathcal{R}(\mathbf{k}_2)\,\mathcal{R}(\mathbf{k}_3)\rangle = \frac{3}{10}(2\pi)^{5/2} f_{\rm NL}^{equil} P_{\mathcal{R}}^2 \delta(\mathbf{k}_1+\mathbf{k}_2+\mathbf{k}_3)\frac{\sum k_i^3}{\Pi k_i^3}\,, \tag{7.93}$$

where $P_{\mathcal{R}}$ is the total curvature power spectrum. From the expression of the bispectrum (7.90), using the relation (7.71), we have

$$f_{\rm NL}^{equil} = \frac{10}{9}\frac{1}{(2\pi)^{5/2}}\frac{1}{\mathcal{P}_{\mathcal{R}}^2}\frac{H^6}{M_{pl}^6}\frac{e^{6\pi\xi}}{\xi^9}N_\sigma^3 f(n)\,, \tag{7.94}$$

where we used $\dot{\varphi}_0 = \sqrt{2\epsilon}\,M_{pl}\,H$. We require $f_{\rm NL}^{equil}$ of our model to be equal or smaller than the current upper bound. At the same time we ask the lower bound on magnetic field on cosmological scales to be achived by the magnetic field production of our model.
Finally, we will also consider current upper bound on tensor perturbations, and we will check that they provide weaker constraints with respect to the scalar sector.

7.5.1 Constraints on inflationary parameters from scalar perturbations

The lower bound on magnetic fields on cosmological scales from [11–13], including the correction arising from the dependence on the magnetic field spectral index found in [227], reads

$$B_0\sqrt{\frac{L_0}{D_e}}\,\Pi\left(\frac{D_e}{L_0}, n_B\right) \geq B^{NV}\,, \tag{7.95}$$

where $B^{NV} \simeq 10^{-18} \div 10^{-16}$ G. Since in this context $D_e \simeq 80$ kpc [226], in the above equation we have selected the appropriate case $L_0 \ll D_e$ [1]. The function $\Pi\left(\frac{D_e}{L_0}, n_B\right)$ takes a particularly simple form if $n_B > 1/2$ (corresponding to $n_G > -2$, where $n_G = 2n_B - 3$ is the spectral index as defined in [227]), which is always the case for the range of values $-2 < n < 0$. Given the conditions $L_0 \ll D_e$ and $-2 < n < 0$, it

is therefore enough to require that our model leads to a present time magnetic field satisfying the (in-)equality

$$B_0 \sqrt{\frac{L_0}{D_e}} \sqrt{\frac{2n_B}{20n_B - 10}} \geq B^{NV} \,, \tag{7.96}$$

with $B^{NV} = 10^{-17}$ G: this guarantees that the model provides a strong enough intergalactic magnetic field. We have to express B_0 in eq.(7.95) as a function of the inflationary parameters of our model. We consider the present time magnetic field and related correlation length that we found in (7.14). We write B_0 in (7.95) as in (7.14), and substitute $B_{\rm reh}$ and $L_{\rm reh}$ as written in (7.8)-(7.9). Furthermore, in order to write the factor $a_{\rm reh}/a_0$ as a function of the inflationary parameters, we exploit the following relation:

$$\frac{a_0}{a_{\rm reh}} = \frac{g_*^{reh\,1/3} T_{\rm reh}}{g_*^{0\,1/3} T_0} \,, \tag{7.97}$$

where $g_*^0 = 3.36$ and $g_*^{\rm reh} = 106.75$ are the effective number of relativistic degrees of freedom at the respective temperatures, $T_0 = 2 \times 10^{-13}$ GeV, and the reheating temperature $T_{\rm reh}$ is obtained assuming instantaneous reheating:

$$\frac{g_*^{\rm reh}\,\pi^2}{30}\, T_{\rm reh}^4 = 3\, M_{pl}^2\, H^2 \,. \tag{7.98}$$

The factor $a_0/a_{\rm reh}$ then results:

$$\frac{a_0}{a_{\rm reh}} \simeq 2 \times 10^{31} \sqrt{\frac{H}{M_{pl}}} \,. \tag{7.99}$$

Therefore, from (7.95), finally we have:

$$\frac{e^{\pi\xi}}{\xi^2} = 60 \left(\frac{M_{pl}}{H}\right)^{3/4} \frac{B_{-17}^{NV}(n_B)}{b_n \sqrt{l_n}} \,, \tag{7.100}$$

where

$$B_{-17}^{NV}(n_B) = \sqrt{\frac{D_e}{\rm Mpc}} \sqrt{\frac{20n_B - 10}{2n_B}} \frac{B^{NV}}{10^{-17}\ {\rm G}} \,. \tag{7.101}$$

Inserting $D_e \simeq 80$ kpc and using the relation between n_B and n to express n_B as a function of n, this relation gives us the parameter ξ as a function of the two parameters $\xi = \xi\,(H, n)$. On the other hand, we require that the bispectrum of the curvature perturbations does not exceed the observational constraints provided by Planck. We fix the value of $f_{\rm NL}^{equil}$ to the allowed upper limit. From equation (7.94), imposing $P_{\mathcal{R}} = 2.21 \cdot 10^{-9}$, the latter requirement returns the Hubble parameter as a function of ξ, n and N_σ, i.e. $H = H\,(\xi, n, N_\sigma)$. Inserting the expression $\xi = \xi\,(H, n)$ found before in the expression for $H = H\,(\xi, n, N_\sigma)$, we obtain H as a function of n and N_σ. The latter identifies those inflationary models which provide a magnetogenesis accounting for the Neronov-Vovk limit, and at the same time a generation of curvature perturbations which equals the upper bound on $f_{\rm NL}$ provided by Planck.

For what concerns the parameter N_σ: in order to neglect the term proportional to $\delta\sigma$ in the expression of curvature perturbation (7.56), we supposed $N_\sigma < N_\varphi$, where with N_φ we indicate the e-folds number of inflation. The minimum value of N_φ is given as a function of H by

$$N_\varphi^{\rm min} = {\rm Log}\left[\left(\frac{g_*^{\rm reh}}{g_*^0}\right)^{1/3}\frac{M_{pl}}{T_0}\left(\frac{g_*^{\rm reh}\pi^2}{30}\right)^{1/4}\sqrt{\frac{H}{M_{pl}}}\right] . \tag{7.102}$$

As a good estimation we can take $N_\sigma = N_\varphi^{\rm min}$, so that we can write the parameter N_σ as a function of H, and then have $H = H(n)$. We show such curve in figure 7.2 in terms of $\rho_{\rm inf}^{1/4} = \left(3M_{pl}^2H^2\right)^{1/4}$. In the same plot we show the analogous curve obtained imposing the curvature power spectrum (7.85) to be negligible with respect to the current estimation of the amplitude provided by Planck. As visible, the bispectrum put stronger constraints on the parameter space with respect to the curvature power spectrum. On the other hand, we can also consider situations in which $N_\sigma \ll N_\varphi^{\rm min}$ choosing a value for N_σ by hand. In particular, lowering the value of N_σ leads to weaker constraints on $\rho_{\rm infl}^{1/4}$, since $f_{\rm NL}^{equil} \propto N_\sigma^2$. The energy scale of inflation spans a

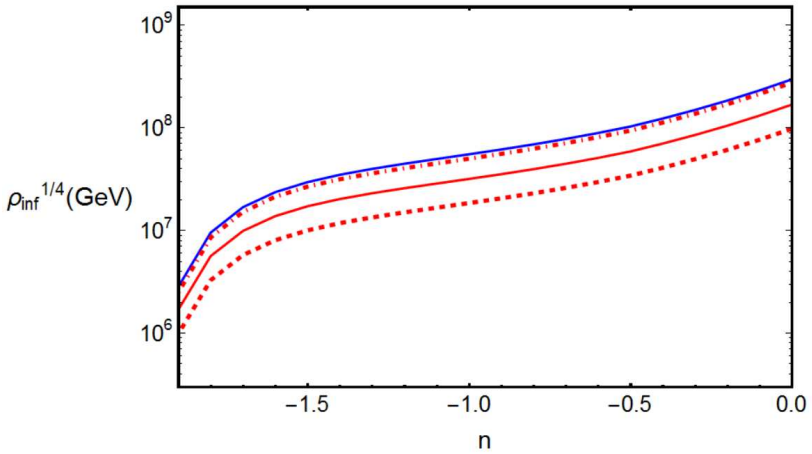

Figure 7.2: Constraints on the inflationary energy density due to scalar perturbations as a function of the inflationary parameter n. We imposed the magnetic field intensity today to satisfy eq.(7.95) with $B^{NV} = 10^{-17}$ G. The region below each curve is the allowed parameter space. The blue curve is obtained by fixing the curvature power spectrum to one tenth of the measured Planck value, and setting $N_\sigma = N_\varphi^{\rm min}$. Red curves are obtained by imposing that the sourced bispectrum in the equilateral configuration to fill the Plank upper limit on $f_{\rm NL}^{equil}$. The solid red curve is obtained for $f_{\rm NL}^{equil} = 50$ and $N_\sigma = N_\varphi^{\rm min}$, the dashed red curve for $f_{\rm NL}^{equil} = 10$ and $N_\sigma = N_\varphi^{\rm min}$, and the dot-dashed red curve for $f_{\rm NL}^{equil} = 50$ and $N_\sigma = 30$.

couple of orders of magnitude $10^6 \lesssim \rho_{\rm inf}^{1/4} \lesssim 10^8$ GeV as n varies from -2 to 0. We conclude that the model (7.1) is a possible explanation for the observed presence of magnetic fields on cosmological scales, which at the same time agrees with current observational constraints on scalar modes.

7.5.2 Constraints from sourced tensor modes

We calculate the values of the tensor-to-scalar ratio in correspondence of the parameter values identified by the curves on plot 7.2. The results are shown in figure 7.3.
We evaluate r for the values of $H(n)$ corresponding to the constraints obtained above. i.e. for $f_{\rm NL}^{equil} = 50$, 10 and $N_\sigma = N_\varphi^{\rm min}$, or in the case $f_{\rm NL}^{equil} = 50$ and $N_\sigma = 30$. The value of ξ is found, as before, from Eq. (7.100). We use again $P_\mathcal{R} = 2.21 \cdot 10^{-9}$. The results are shown in figure 7.3: the tensor-to-scalar ratio is too small to be detected both by future Earth- and space-based dedicated missions. However notice that it is not hugely below the projected sensitivity $r \sim 10^{-3}$ of the CMB-S4 experiment [180]. As explained in section 7.2.1, tensor modes due to vacuum fluctuations of the gravitational field are negligible with respect to those generated by the presence of the gauge field: our model would therefore be further constrained by a future detection of CMB B-polarisation of primordial origin.

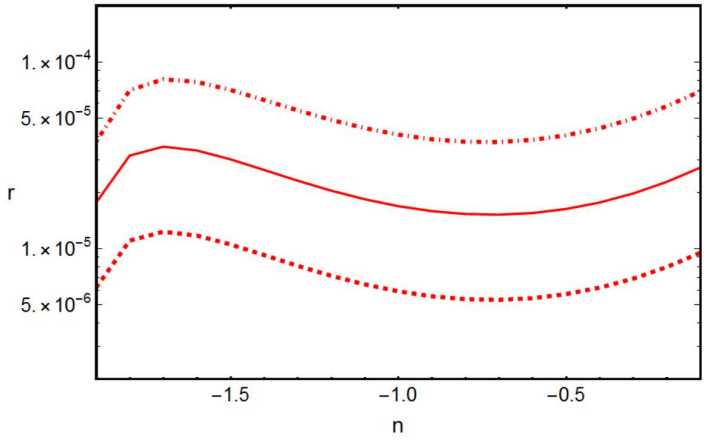

Figure 7.3: The tensor to scalar ratio as a function of the inflationary parameter n. The curves are found imposing the magnetic field intensity today to satisfy Eq. (7.95) with $B^{NV} = 10^{-17}$ G. The solid red curve corresponds to $H(n)$ that satisfies the bound from non-gaussianity when $f_{\rm NL}^{equil} = 50$ and $N_\sigma = N_\varphi^{\rm min}$; the dashed red curve when $f_{\rm NL}^{equil} = 10$ and $N_\sigma = N_\varphi^{\rm min}$; the dot-dashed red curve when $f_{\rm NL}^{equil} = 50$ and $N_\sigma = 30$.

7.5.3 Possible seeds for galactic dynamo process

At galactic scales, magnetic fields of the order of 10^6G are observed. It is believed that such magnetic fields are the result of the amplification by a dynamo mechanism of earlier seeds. There are large uncertainties on the evolution of such seeds after their generation, but estimations point out that the original magnetic fields should be at least of the order of $10^{-21} \div 10^{-23}$G at a comoving scale of 1Mpc in order to explain the observed amplitude [14]. Moreover, notice that such seeds, according to [240], could also justify the presence of magnetic field in clusters, which are observed to have an amplitude of 10^{-6}G at the cluster scale.
Other mechanisms, alternative to the amplification by a dynamo process, have been

proposed, see e.g. [241], as the ejection of magnetic fields from stars or by astrophysical mechanisms based on charge separation. On the other hand, the indirect observations of magnetic fields in the intergalactic medium is a clue of their primordial origin, since concern voids regions among structures where astrophysical process are difficult to be supposed.
A primordial generation mechanism able to provide magnetic fields that fulfil the bound on the intergalactic magnetic field, and at the same time have high enough amplitude at large scales $\mathcal{O}$(Mpc) to initiate the galactic dynamo, can in principle explain all present observations of magnetic fields in the intergalactic medium, galaxies and clusters.
In [1] it was obtained that our inflationary model is able to provide seeds larger than $10^{-21} \div 10^{-23}$G at 1Mpc, for a certain range of values of n, satisfying, at the same time, the lower bound on magnetic fields at cosmological scales. Here we show that this statement is still true also when the strict constraints on scalar non-gaussianities are taken into account. More precisely we consider the set of inflationary parameters H and ξ for which the bound on $f_{\rm NL}^{equil}$ is saturate and the limit (7.95) is matched, i.e. the points of the red-solid curve in figure 7.2, and we wonder if for those parameters values, the intensity of the magnetic field can explain also the lower bounds on the seeds in galaxies.
In order to do that, we impose the magnetic field to satisfy the lower bound we have on cosmological scales, i.e. the equality in the relation (7.95). The latter gives a relation between B_0 and L_0, which combined with the first equation in (7.12), provides the value of the magnetic field intensity B_0 and of the correlation length L_0 as function of n_B, independently on the mechanism that generated them.
From the expression for the spectral index, the amplitude of the magnetic field at a generic scale ℓ is given by:

$$B_0(\ell) = B_0 \cdot \left(\frac{L_0}{\ell}\right)^{(5-|2n+1|)/2} , \tag{7.103}$$

then, using the obtained values for B_0 and L_0, we calculate $B(\ell)$ for $\ell = 1$Mpc as a function of n. We compare the result with two indicative values of the required amplitude of magnetic seeds in galaxies on such scale, i.e. 10^{-21}G and 10^{-23}G. The situations is shown in figure 7.4. For $n = 0$, i.e. for the case in which only the term $F_{\mu\nu}\tilde{F}^{\mu\nu}$ is active, the amplitude of the generated magnetic field is too small to justify galactic seeds. On the other side, for $n \neq 0$ and sufficiently negative values, the inflationary magnetogenesis is able to generate magnetic fields at 1Mpc scale larger than the minimal amplitude required to explain current observations. Therefore, notice that the presence of the term $\sim F_{\mu\nu}F^{\mu\nu}$ in the lagrangian (7.1), that corresponds to the scenarios in which $n \neq 0$, is crucial to generate magnetic fields able to justify seeds in galaxies.

Inflationary model with the gauge field coupled to the inflaton. We considered also the scenario in which the gauge field A_μ is coupled to the inflaton, without

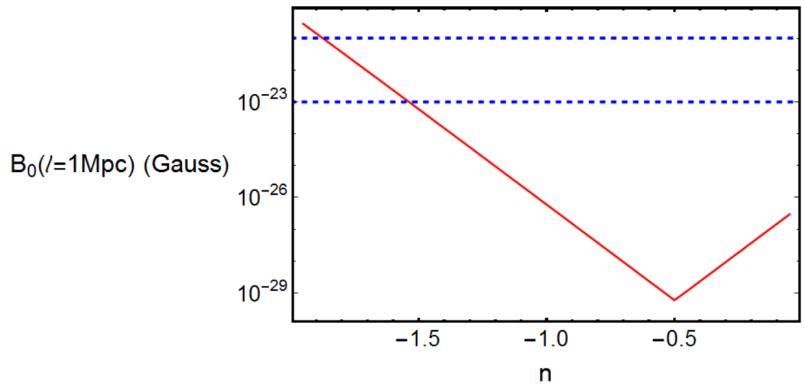

Figure 7.4: Magnetic field intensity at a scale of 1Mpc. In red the value of B_0 at 1Mpc obtained for the inflationary parameters which saturate current upper bound for scalar non-gaussianities (red curve in plot 7.2). In blue we show estimations of the amplitude of magnetic fields seeds required in order to explain current observation by introducing a dynamo mechanism: $10^{-21}G$ and 10^{-23}G.

the presence of an auxiliary field, i.e.:

$$L = -\frac{1}{2}\nabla_\mu\varphi\nabla^\mu\varphi - V(\varphi) + I^2(\varphi)\left(-\frac{1}{4}F_{\mu\nu}F^{\mu\nu} + \frac{\gamma}{8}\epsilon_{\mu\nu\rho\lambda}F^{\mu\nu}F^{\rho\lambda}\right). \tag{7.104}$$

In this case, the non-minimal coupling between the inflaton and the gauge field leads to a source in the equation of motion of the inflaton perturbations which dominates with respect to the sources due to the gravitational coupling (see e.g. [234]). More precisely, the equation of motion for the inflaton perturbations $\delta\varphi$ turns out to be

$$\delta\varphi''_{\rm flat} + 2\mathcal{H}\delta\varphi'_{\rm flat} - k^2\delta\varphi_{\rm flat} = II_\varphi\left[E_i * E_i + 2\gamma\ (E_i * B_i)\right] + 2\varphi'_0 S^{(3)} + \frac{\varphi'_0}{\mathcal{H}}S'^{(3)} + \frac{\varphi'_0}{\mathcal{H}}S^{(2)}, \tag{7.105}$$

where $S^{(3)}$ and $S^{(2)}$ have the same expressions as before, but $I = I(\varphi)$. Differently from the model (7.1), now the source is no more suppressed by the slow-roll parameter ϵ. Notice also that the expression (7.71) is still valid for this scenario. We checked that with such a kind of source current constraints on scalar perturbations do not allow for a magnetogenesis which satisfy the current lower bounds on cosmological scales.

7.6 Summary of the results

We showed that the mechanism of magnetogenesis with added helicity proposed in [1] is able to account for the magnetic fields at cosmological scales inferred in [11–13] while keeping the extra production of scalar and tensor perturbations under control and with reasonably high energy scales of inflation, i.e. of the order of $5 \cdot 10^5 \div 10^8$ GeV. In particular, if the field σ rolls for a few tens of e-folds, then magnetogenesis with added helicity can account for the observed magnetic fields while satisfying the observational bounds on equilateral non-gaussianities. We concluded that the model of [1] provides a possible explanation for magnetic fields observed at cosmological scales

and of the presence of sufficiently large primordial seeds to start the galactic dynamo process, even once the stringent constraints from non-gaussianities are accounted for. Moreover, we found that when the bound on non-gaussianities is saturated, the model leads to tensor modes with $r = 10^{-5} \div 10^{-4}$. An interesting signature of this kind of inflationary magnetogenesis is represented by the chirality of the associated GWs and then the appearing of non-vanishing cross-correlations between temperature and polarization CMB power spectra. Finally, we obtained that for a certain range of the model parameters the scenario would be able also to provide the seeds at the Mpc scales required in order to explain the presence of magnetic field at galactic scales by the dynamo mechanism.

It should be noted, however, that the constraints from CMB are only valid if the gauge field was already excited when CMB scales were leaving the horizon. Since the correlation length L_0 of the produced gauge field is well below the Mpc [1], one can think of a scenario where σ starts rolling after CMB scales, but before L_0, have left the horizon. In this (finely tuned) situation the constraints from CMB will not hold, and the mechanism can be effective even at higher energy scales for inflation.

Part IV

Conclusions

Outlook and Conclusions

Current cosmological observations strongly support the hypothesis that the universe underwent an inflationary period in its early stages [2]. To deeply investigate such an epoch, many efforts has been made both from a theoretical and a an observational point of view. Especially, in last years a particular attention has been devoted to CMB experiments with extremely successful results [162, 242]. Nevertheless, an unequivocal probe of the inflationary mechanism is still lacking and several questions about such a physics are still open and unsolved. In this scenario, the new era of direct GW detection opened by laser interferometer experiments [3], appears as a promising way to address such open issues, besides the opportunities offered by CMB polarization experiments. At the same time investigations on the inflationary mechanism continue to disclose new and fascinating aspects able to explain controversial cosmological observations. Recently, it has been noticed that some inflationary scenarios are able to account for current observations of magnetic fields in the intergalactic medium.

In the first part of the thesis, we considered the inflationary GW signal, both from a theoretical and an observational point of view. In particular, we presented in details the general mechanisms of GW production during inflation, showing the specific results for a few selected models and highlighting the possibility of exploiting the gravitational signal as a source of unique information about the early universe and to constrain the physics enclosed in the inflationary mechanism. We also showed how the inflationary consistency relation which involves tensor modes represents a way of probing the inflationary mechanism itself and a promising tool for testing specific inflationary models. In such a direction, a dedicated analysis on the realistic chance of extracting information from testing such consistency relation by current and upcoming experiments, may unveil new directions which future efforts should focus on.

In light of the outlined importance of searching for inflationary GWs, we concentrated on the exciting opportunity offered by current and upcoming experiments of direct GW detection. In particular, because of its high sensitivity to the GW spectral energy density, we focused on the project of the space-borne laser interferometer LISA. We performed a forecast analysis for a generic primordial power-law GW background and for the GW signal associated to a number of selected inflationary models, obtaining the capabilities of LISA in constraining the related primordial parameters. In particular, we studied inflationary models with events of particle production and scenarios in which scalar spectator fields are present. Moreover, we investigated inflationary mod-

els built on modified gravity theories. We presented also comparisons with bounds provided by other experiments and observations. We found that LISA offers a new efficient manner of probing inflationary physics. Moreover, the obtained results represent a validation of the significant science that can be done by such an experiment.

Anyhow, we are at the beginning of the path. The opportunity offered by LISA and other experiments of direct GW detection does not concerns only the measurement of the power spectrum GW amplitude, as we considered here. Studying of the capabilities of LISA in testing more advanced features of a GW background, such as the non-gaussianity level, the chirality and the isotropy, could unveil other exciting tools for probing inflationary physics and not only. In the same direction, accounting for the complementarity between space-borne, ground-based laser interferometers and CMB experiments could point out new channels for constraining the physics of the early universe.

In the second part of the thesis, we considered another fascinating aspect of the inflationary mechanism. Current gamma-ray observations highlight the presence of magnetic fields at cosmological scales. The origin of such fields is still under debate, however their presence in voids regions, where no charged plasma is present, suggests a process of primordial magnetogenesis. Interestingly, the inflationary mechanism provides a natural setting to explain such observations. On the other hand, several restrictions on this kind of models arise in order to keep under control the perturbation theory and to do not exceed current bounds on associated physical quantities. Typically, as a counterpart of such a process, an overproduction of curvature perturbations takes place with respect to the amount predicted by single-field slow-roll inflation. The same is true for tensor perturbations.

We considered a specific model of inflation, in which a magnetogenesis able to account for current observations in the intergalactic medium takes place.
Since CMB measurements provides strict constraints on curvature perturbations, we calculated their power spectrum and the non-gaussianities for the selected inflationary model and we verified that a magnetogenesis able to explain current observations at cosmological scales can be obtained preserving at the same time current bounds on scalar and tensor perturbations. Furthermore we found that for a range of the parameter values, the inflationary model we considered is also able to account for the primordial seeds on galactic scales required to start the dynamo mechanism leading to the present time magnetic fields observed at such scales.
In light of these results, we concluded that the investigated scenario represents a robust and attracting inflationary model, able to account for current observations of magnetic fields at cosmological scales, preserving at the same time CMB observations. Moreover, we found that, as a peculiar feature of such a model, a production of chiral GWs is predicted.
Clearly this analysis represents only a step towards solving the puzzle disclosed by gamma-ray observations. In order to disentangle the origin of magnetic fields at cosmological scales, deeper investigations are required. To address such an issue, from an

observational point of view, methods which allow for measurements of the magnetic field amplitude and a separate measurements of the correlation length would help in disentangling their origin. From a theoretical point of view, it would be interesting to investigate the presence of peculiar features in the physical observables associated to this kind of inflationary models, in order to recognize the origin of the observed fields, and to better investigate some approximations usually assumed in this context, such as instantaneous reheating after inflation.

In last decades an impressive contour of the physics of the early universe has been drown. However, various issues and open questions still remain, making the search for the physics of the early universe still fascinating.

Surely the new era opened by GW detectors offers a great opportunity to renovate our attitude as scientists opening our minds to possible surprises and to a sincere curiosity.

Part V

Appendix

Appendix A

Transverse and traceless gauge

General Relativity is invariant under coordinate transformations:

$$x^\mu \to x'^\mu \tag{A.1}$$

where x'^μ is a diffeomorphism with respect to x^μ. Under such a transformation, tensor objects transform as

$$g_{\mu\nu}(x) \to g'_{\mu\nu}(x') = \frac{\partial x^\sigma}{\partial x'^\mu}\frac{\partial x^\rho}{\partial x'^\nu} g_{\sigma\rho}(x) \ . \tag{A.2}$$

We consider the linearized theory of gravity, i.e. we suppose small perturbations h_{ij} on a flat spacetime. The perturbation h_{ij} has ten degrees of freedom, due to its symmetry. Asking for the theory to be linear breaks the invariance of the theory under all the coordinate transformations of eq.(A.1), leaving a residual gauge symmetry:

$$x^\mu \to x'^\mu = x^\mu + \xi^\mu(x) \ , \tag{A.3}$$

where ξ^μ is so that $\partial_\mu \xi_\nu$ are at most of the same order of $|h_{\mu\nu}|$. Under this transformation, according to (A.2), the tensor perturbation transform as

$$h_{\mu\nu}(x) \to h'_{\mu\nu}(x') = h_{\mu\nu}(x) - (\partial_\mu \xi_\nu + \partial_\nu \xi_\mu) \ . \tag{A.4}$$

Under this transformation, for $\partial_\mu \xi_\nu$ at most smaller as $|h_{\mu\nu}|$, the theory still remains linear. Equation (A.4), then unveils a residual gauge freedom encoded in $h_{\mu\nu}$. More precisely, the transformation (A.4) gives a gauge freedom that we can fix imposing the following condition:

$$\partial^\nu \bar{h}_{\mu\nu} = 0 \, , \tag{A.5}$$

where

$$\bar{h}_{\mu\nu} = h_{\mu\nu} - \frac{1}{2}\eta_{\mu\nu} h \, . \tag{A.6}$$

The condition (A.5) is called *harmonic gauge*. Notice however that such a condition does not fix completely the gauge freedom, more precisely from ten degrees of freedom we moved to six degrees of freedom, since eq.(A.5) provides four conditions. The choice of the harmonic gauge is allowed since we can always find ξ_μ, with $\partial_\mu \xi_\nu$ of the same

order of smallness of $|h_{\mu\nu}|$, so that $\partial^\nu \bar{h}'_{\mu\nu} = 0$.
Considering a vacuum spacetime, i.e. $T_{\mu\nu} = 0$, the equation of motion for the linear perturbations $h_{\mu\nu}$ reads:

$$\Box \bar{h}_{\mu\nu} + \eta_{\mu\nu}\partial^\rho\partial^\sigma \bar{h}_{\rho\sigma} - \partial^\rho\partial_\nu \bar{h} h_{\nu\rho} - \partial^\rho\partial_\mu \bar{h}_{\nu\rho} = 0\,, \tag{A.7}$$

where

$$h = \eta^{\mu\nu} h_{\mu\nu}\,. \tag{A.8}$$

Imposing the harmonic gauge, the equation of motion (A.7) turns out to be

$$\Box \bar{h}_{\mu\nu} = 0\,. \tag{A.9}$$

The gauge freedom (A.4) is not completely fixed by the harmonic gauge, indeed in case of vacuum spacetime, we can also impose the following condition:

$$\bar{h} = 0\,, \qquad h^{i0}\,(x) = 0\,. \tag{A.10}$$

The first condition corresponds to ask for $h_{\mu\nu}$ being traceless. Notice also that as a consequence of such a request it holds $\bar{h}_{\mu\nu} = h_{\mu\nu}$. The combination of the conditions of the harmonic gauge (A.5) and of eq.(A.10), is equivalent to the following requests:

$$\begin{aligned} &h_{\mu\nu} \to h_{ij} \\ &\partial^i h_{ij} = 0 \\ &h = 0\,, \end{aligned} \tag{A.11}$$

i.e. the so-called transverse and traceless gauge (TT gauge). Previous conditions fix all the gauge freedom, leading from the initial ten degrees of freedom to two gauge invariant degrees of freedom (the two polarizations).

Notice that in a non-vacuum spacetime, tensor perturbations cannot be written in the TT gauge, only the harmonic gauge can be considered. However, among the degrees of freedom left by such a gauge, only the two transverse and traceless degrees of freedom are radiative.

In cosmology people use a different point of view, they decompose the spatial tensor perturbation h_{ij} into irreducible parts with definite properties under spatial rotations as we did in eq.(1.32), i.e.:

$$h_{ij} = D_{ij} h^{\parallel} + \partial_i h^{\perp}_j + \partial_j h^{\perp}_i + h^{\mathrm{TT}}_{ij}\,. \tag{A.12}$$

This decomposition is unique, and the transverse and traceless part h^{TT}_{ij} corresponds to the radiative degrees of freedom we were describing before. In the calculations we performed in chapter 2, tensor perturbations refers to h^{TT}_{ij}.

Appendix B

Present time GW spectral energy density

The general solution of eq.(2.2) in terms of Fourier modes can be written as:

$$h_k(\tau) \equiv h_{k,\mathrm{prim}} T_{\mathrm{h}}(\tau, k) \ , \tag{B.1}$$

where $h_{k,\mathrm{prim}}$ is the amplitude at horizon crossing, and the transfer function $T_{\mathrm{h}}(\tau, k)$ describes the evolution of the GW mode after the time they enter the horizon during later stages after inflation. Let us now consider a GW at a generic time τ after inflation, i.e. $h_{ij}(\mathbf{x}, \tau)$.
We start recalling some preliminary definitions. We take the tensor power spectrum defined in (2.25), which follows the general definition (1.18):

$$\langle h_{ij,\mathrm{prim}}(\tau, \mathbf{x})\, h^{ij}_{\mathrm{prim}}(\tau, \mathbf{x})\rangle = \int \frac{dk}{k} P_{\mathrm{T}}(k, \tau) \ , \tag{B.2}$$

where, to be clear, we have specified that P_{T}, according to eq.(2.25), refers to the power spectrum of the primordial GWs, i.e. to the amplitude appearing in eq.(B.1). Recall also the equality (2.26), in which we specify the two polarization components:

$$\sum_{\lambda} \left| h^{(\lambda)}_{\mathbf{k},\mathrm{prim}}(\tau) \right|^2 = \frac{2\pi^2}{k^3} P_{\mathrm{T}}(k, \tau) \ . \tag{B.3}$$

First we consider the GW energy density, and then we will move to the spectral-energy density. From eq.(2.89) we have:

$$\rho_{\mathrm{GW}}(\tau) = \frac{1}{32\pi G a^2} \langle \left[h'^{(+)}(\tau, \mathbf{x}) \right]^2 + \left[h'^{(\times)}(\tau, \mathbf{x}) \right]^2 \rangle \, . \tag{B.4}$$

Decomposing $h^{(+)}(\tau, \mathbf{x})$ and $h^{(\times)}(\tau, \mathbf{x})$ in the Fourier space, it reads:

$$\rho_{\mathrm{GW}}(\tau) = \frac{1}{32\pi G a^2} \int \frac{d^3\mathbf{k}}{(2\pi)^{3/2}} \int \frac{d^3\mathbf{k'}}{(2\pi)^{3/2}} \langle h'^{(+)}_{\mathbf{k}}(\tau)\, h'^{(+)}_{\mathbf{k}}(\tau) + h'^{(\times)}_{\mathbf{k}}(\tau)\, h'^{(\times)}_{\mathbf{k}}(\tau) \rangle e^{i(\mathbf{k}+\mathbf{k'})\cdot\mathbf{x}} \, . \tag{B.5}$$

In (1.22) we obtained that (notice that here we are referring to the conformal time):

$$\langle h_{\mathbf{k}}^{\prime(+)}(\tau)\, h_{\mathbf{k}}^{\prime(+)}(\tau)\rangle = \delta(\mathbf{k}+\mathbf{k'})\left|h_{\mathbf{k}}^{\prime(+)}(\tau)\right|^2 , \tag{B.6}$$

and analogously for the other polarization. So that, considering the independence of the two polarizations:

$$\begin{aligned}\rho_{\mathrm{GW}}(\tau) =& \frac{1}{32\pi G a^2}\int \frac{d^3\mathbf{k}}{(2\pi)^{3/2}}\int \frac{d^3\mathbf{k'}}{(2\pi)^{3/2}}\delta(\mathbf{k}+\mathbf{k'})\left[\left|h_{\mathbf{k}}^{\prime(+)}(\tau)\right|^2+\left|h_{\mathbf{k}}^{\prime(\times)}(\tau)\right|^2\right]e^{i(\mathbf{k}+\mathbf{k'})\cdot\mathbf{x}} = \\ =& \frac{1}{32\pi G a^2}\int \frac{d^3\mathbf{k}}{(2\pi)^3}\left[\left|h_{\mathbf{k}}^{\prime(+)}(\tau)\right|^2+\left|h_{\mathbf{k}}^{\prime(\times)}(\tau)\right|^2\right] = \\ =& \frac{1}{32\pi G a^2}\int \frac{d^3\mathbf{k}}{(2\pi)^3}\left|T_{\mathrm{h}}'(\tau,\mathbf{k})\right|^2\left[\left|h_{\mathbf{k},\mathrm{prim}}^{(+)}\right|^2+\left|h_{\mathbf{k},\mathrm{prim}}^{(\times)}\right|^2\right] .\end{aligned} \tag{B.7}$$

Substituting eq.(B.3) in this expression, and using (B.1), then we have:

$$\begin{aligned}\rho_{\mathrm{GW}}(\tau) =& \frac{1}{32\pi G a^2}\int \frac{d^3\mathbf{k}}{(2\pi)^3}\frac{2\pi^2}{k^3}\left|T_{\mathrm{h}}'(\tau,\mathbf{k})\right|^2 P_T(k) = \\ =& \frac{1}{32\pi G a^2}\int \frac{dk}{k}\left|T_{\mathrm{h}}'(\tau,\mathbf{k})\right|^2 P_{\mathrm{T}}(k) .\end{aligned} \tag{B.8}$$

From eq.(2.91), the GW spectral energy density at a generic time τ, turns out to be:

$$\Omega_{\mathrm{GW}}(k,\tau) = \frac{1}{\rho_{\mathrm{c}}}\frac{\mathrm{d}\rho_{\mathrm{gw}}}{\mathrm{dlog}k} = \frac{1}{12}\left(\frac{1}{aH}\right)^2 T_{\mathrm{h}}'^2(k,\tau)\, P_T(k) . \tag{B.9}$$

For modes well inside the horizon, the previous formula can be approximated as [105]:

$$\Omega_{\mathrm{GW}}(k,\tau) = \frac{1}{12}\left(\frac{k}{aH}\right)^2 T_{\mathrm{h}}^2(k,\tau)\, P_T(k) . \tag{B.10}$$

Appendix C

Strain and energy density of gravitational waves

We present some useful formula which connect different quantities used to describe GWs [135, 212].
In this appendix we use the definition of the Fourier transformation commonly used in this context, which is different of that we used in the main text. We define the Fourier transformation as

$$\tilde{h}\left(f\right)=\int_{-\infty}^{+\infty}dt\,h\left(t\right)e^{-2\pi ift}\,. \tag{C.1}$$

Let us also recall the definition of the GW energy density and of the GW spectral energy density, where we restore the speed of light c:

$$\rho_{\mathrm{GW}}\equiv\frac{c^{2}}{32\pi G}\langle\dot{h}_{ij}\left(t,\mathbf{x}\right)\dot{h}^{ij}\left(t,.\mathbf{x}\right)\rangle\,,\qquad\Omega_{\mathrm{GW}}\left(f\right)\equiv\frac{1}{\rho_{c}}\frac{d\,\rho_{\mathrm{GW}}}{d\log f}\,. \tag{C.2}$$

First we look for the expression of the GW spectral energy density in terms of the GW strain. In case of a polarized GW propagating in a given direction $\hat{\Omega}$, such an expression can be found explicitly. In this case:

$$h_{ij}^{(\lambda)}\left(t,\mathbf{x}\right)=\int_{-\infty}^{+\infty}df\,\tilde{h}\left(f,\mathbf{x}\right)e_{ij}^{(\lambda)}\left(\hat{\Omega}\right)e^{-2\pi ift}\,, \tag{C.3}$$

where $e_{ij}^{(\lambda)}\left(\hat{\Omega}\right)$ is the polarization vector. We define the quantity $g\left(f\right)$ by

$$\langle\tilde{h}\left(f\right)\tilde{h}\left(f'\right)\rangle=\delta\left(f-f'\right)g\left(f\right)\,, \tag{C.4}$$

from which follows:

$$g\left(f\right)=2\tilde{h}^{2}\left(f\right)\,. \tag{C.5}$$

Differentiating the expression (C.3), the ensemble average in the definition of ρ_{GW} turns out to be:

$$\langle\dot{h}_{ij}\left(t,\mathbf{x}\right)\dot{h}^{ij}\left(t,.\mathbf{x}\right)\rangle=8\pi^{2}\int_{0}^{\infty}df\,f^{2}g\left(f\right)\,, \tag{C.6}$$

and then:

$$\rho_{\mathrm{GW}} = \frac{\pi c^2}{4G} \int_0^\infty df\, f^2 g\left(f\right) . \tag{C.7}$$

We finally obtain the sought expression:

$$\Omega_{\mathrm{GW}}\left(f\right) = \frac{2\pi^2}{3H_0^2} f^3 g\left(f\right) = \frac{4\pi^2}{3H_0^2} f^4 \left|\tilde{h}\left(f\right)\right|^2 . \tag{C.8}$$

We know consider a generalization of the previous case, which is useful when considering the incoming signal on a pair of GW detectors, required in order to detect a GW background. Consider an isotropic stochastic GW background, unpolarized and stationary, incoming in the point $\mathbf{x}$ at time t. In this situation, the GW signal is given by:

$$h_{ij}\left(t, \mathbf{x}\right) = \sum_{\lambda=\times,+} \int_{-\infty}^{+\infty} df \int_{S^2} d\hat{\Omega}\, \tilde{h}_\lambda\left(f, \hat{\Omega}\right) e^{\hat{}}_{ij}\left(\hat{\Omega}\right) e^{i2\pi t\left(t - \hat{\Omega}\cdot\frac{\mathbf{x}}{c}\right)} , \tag{C.9}$$

where S^2 is the unitary two-sphere surrounding the detector and $\hat{\Omega}$ is a unit vector which specifies the direction on such a sphere. We define $H\left(f\right)$ by:

$$\langle \tilde{h}_\lambda\left(f, \hat{\Omega}\right) \tilde{h}_{\lambda'}\left(f', \hat{\Omega}'\right)\rangle = \delta\left(\hat{\Omega}, \hat{\Omega}'\right) \delta_{\lambda\lambda'} \delta\left(f - f'\right) H\left(f\right) , \tag{C.10}$$

where now the direction and the polarization are specified. The expression of Ω_{GW} in terms of $H\left(f\right)$ is obtained as follows. From (C.9), the ensemble average appearing in ρ_{GW} reads:

$$\langle \dot{h}_{ij}\left(t, \mathbf{x}\right) \dot{h}^{ij}\left(t, .\mathbf{x}\right)\rangle = 128\pi^3 \int_0^\infty df\, f^2 H\left(f\right) . \tag{C.11}$$

Substituting this expression in the definition of the GW energy density, then we have:

$$\rho_{\mathrm{GW}} = \frac{4\pi c^2}{G} \int_0^\infty df\, f^2 H\left(f\right) , \tag{C.12}$$

and for the GW spectral energy density:

$$\Omega_{\mathrm{GW}}\left(f\right) = \frac{32\pi^3}{3H_0^2} f^3 H\left(f\right) . \tag{C.13}$$

We calculate the expression for $\langle h^2\left(t\right)\rangle$ in case of a pair of coaligned and coincident detectors, which is useful for obtaining the SNR. The GW strain is defined by:

$$h\left(t\right) \equiv h_{ij}\left(t, \mathbf{x}\right) Y^{ij} , \tag{C.14}$$

where Y^{ij} encodes the response of the detector to the different directions, and in general it is a function of time and of the orientations of the arms of the detector. Since we are assuming coaligned and colocated detectors, the function Y^{ij} is the same for the two observatories. We define also:

$$F_\lambda\left(\hat{\Omega}\right) \equiv e^{(\lambda)}_{ij}\left(\hat{\Omega}\right) Y^{ij} . \tag{C.15}$$

Then $\langle h^2(t)\rangle$ turns out to be:

$$\langle h^2(t)\rangle = \sum_{\lambda,\lambda'} \int_{S^2} d\hat{\Omega} \int_{S^2} d\hat{\Omega}' \int_{-\infty}^{+\infty} df \int_{-\infty}^{+\infty} df'\, e^{-i2\pi f\left(t-\hat{\Omega}\cdot\frac{\mathbf{x}}{c}\right)} e^{i2\pi f'\left(t-\hat{\Omega}'\cdot\frac{\mathbf{x}}{c}\right)} \cdot \langle \tilde{h}_\lambda\left(f,\hat{\Omega}\right)\tilde{h}\left(f',\hat{\Omega}'\right)\rangle F_\lambda\left(\hat{\Omega}\right) F_{\lambda'}\left(\hat{\Omega}'\right). \tag{C.16}$$

Using (C.10) and then substituting the expression of $H(f)$ with eq.(C.13), we have:

$$\langle h^2(t)\rangle = \frac{3H_0^2}{20\pi^2} \int_{-\infty}^{+\infty} df\, \frac{\Omega_{\mathrm{GW}}(f)}{f^3}, \tag{C.17}$$

where we used

$$\sum_\lambda \int_{S^2} d\hat{\Omega} F_\lambda^2\left(\hat{\Omega}\right) = \frac{8\pi}{5}. \tag{C.18}$$

The previous expression becomes more complicated in case of a general network of detectors. In such a situation each observatory is associated to a specific Y^{ij}, and the whole response to a GW signal is given by a combination of such functions.
Notice that the GW strain used here, i.e. $h(t)$, is the perturbation appearing in the metric, while what people usually call *characteristic strain* is defined as $h_c(t) = h(t)/f$.

Appendix D

Simplification of the gravitationally induced source terms for $\delta\varphi_{\rm flat}$

The equations of motion for the gauge field

$$\partial^\mu \left[I^2 \left(F_{\mu\nu} - \frac{\gamma}{2} \eta_{\mu\nu\rho\lambda} F^{\rho\lambda} \right) \right] = 0 \tag{D.1}$$

can be written in terms of the electric and magnetic fields defined in eq. (7.7), along with the Bianchi identities, as

$$\begin{aligned} &\nabla \cdot \mathbf{E} = \nabla \cdot \mathbf{B} = 0 \,, \qquad \mathbf{B}' + 2\,\mathcal{H}\,\mathbf{B} + \nabla \times \mathbf{E} = 0 \,, \\ &\mathbf{E}' + 2\frac{I'}{I}\,\mathbf{E} + 2\,\frac{a'}{a}\,\mathbf{E} + 2\,\gamma\,\frac{I'}{I}\,\mathbf{B} - \nabla \times \mathbf{B} = 0 \,. \end{aligned} \tag{D.2}$$

Now, in coordinate space,

$$S^{(3)} = -\frac{I^2\,a^2}{2\,M_P^2}\,\frac{\partial_j}{\nabla^2}\epsilon_{ijk}\,B_k\,E_i = \frac{I^2\,a^2}{2\,M_P^2\,\nabla^2}\nabla \cdot (\mathbf{E} \times \mathbf{B}) \,, \tag{D.3}$$

so that

$$2\,\varphi_0'\,S^{(3)} + \frac{\varphi_0'}{\mathcal{H}}\,S'^{(3)} = \frac{\varphi_0'}{\mathcal{H}\,a^2}\left(a^2\,S^{(3)}\right)' = -\frac{I^2\,\varphi_0'\,a^2}{2\,\mathcal{H}\,M_P^2\,\nabla^2}\,\nabla \cdot [\mathbf{E} \times (\nabla \times \mathbf{E}) + \mathbf{B} \times (\nabla \times \mathbf{B})] \,, \tag{D.4}$$

with

$$\nabla \cdot [\mathbf{E} \times (\nabla \times \mathbf{E})]\,(\mathbf{k}) = k_i \int \frac{d\mathbf{q}}{(2\pi)^3} E_i(\mathbf{k}-\mathbf{q})\,k_j\,E_j(\mathbf{q}) - k_i \int \frac{d\mathbf{q}}{(2\pi)^3}(\mathbf{k}-\mathbf{q})_i\,E_j(\mathbf{q})\,E_j(\mathbf{k}-\mathbf{q}) \,. \tag{D.5}$$

The latter term can be simplified by noticing that

$$\int d\mathbf{q}\,\mathbf{q}_i\,E_j(\mathbf{q})\,E_j(\mathbf{k}-\mathbf{q}) = \int d\mathbf{p}\,(\mathbf{k}-\mathbf{p})_i\,E_j(\mathbf{k}-\mathbf{p})\,E_j(\mathbf{p}) \,, \tag{D.6}$$

which implies

$$\int d\mathbf{q}\, \mathbf{q}_i\, E_j(\mathbf{q})\, E_j(\mathbf{k}-\mathbf{q}) = \frac{\mathbf{k}_i}{2} \int d\mathbf{q}\, E_j(\mathbf{k}-\mathbf{q})\, E_j(\mathbf{q})\,. \tag{D.7}$$

To sum up, we obtain

$$\nabla \cdot [\mathbf{E} \times (\nabla \times \mathbf{E})]\,(\mathbf{k}) = \mathbf{k}_i\, \mathbf{k}_j \int \frac{d\mathbf{q}}{(2\pi)^3} E_i(\mathbf{k}-\mathbf{q})\, E_j(\mathbf{q}) - \frac{k^2}{2} \int \frac{d\mathbf{q}}{(2\pi)^{3/2}}\, E_j(\mathbf{q})\, E_j(\mathbf{k}-\mathbf{q})\,. \tag{D.8}$$

Acknowledgments

Desidero ringraziare i miei relatori prof. Nicola Bartolo e prof. Sabino Matarrese, per avermi guidato con pazienza e attenzione in questi tre anni. Vi ringrazio per avermi subito inserito in importanti progetti scientifici, avendo fiducia e stima nei miei confronti, e per aver sempre valorizzato il mio lavoro. Vi sono grata anche per aver accolto con sensibilità e rispetto la mia decisione di lasciare il mondo della ricerca. Sono sinceramente contenta di aver lavorato con voi in questi anni.
In particolare, ringrazio Nicola per come ha modellato il progetto di dottorato sulle mie capacità e per la pazienza e delicatezza con cui mi ha sempre trattato. Ringrazio Sabino per avermi sostenuto e indirizzato nel muovere i miei passi nel mondo della ricerca e per la lungimiranza e la passione con cui guida il gruppo di cosmologia di Padova.
Ringrazio Chiara Caprini per avermi accolto e seguito nei mesi trascorsi a Parigi.
Ringrazio il gruppo di cosmologia di Padova, per la vivacità scientifica e allo stesso tempo per la cordialità e familiarità che lo caratterizzano (aspetti non scontati per un gruppo di ricerca).
I would like to thank the theory group of the APC institute for hosting me for some months during my PhD.
I am also grateful to the Cosmology Working Group of the LISA mission for several opportunities of stimulating discussions.
Tra le numerose altre persone con cui ho interagito lungo questo percorso, un particolare ringraziamento va ad Angelo Ricciardone, per i suoi consigli e incoraggiamenti e per la sua cordialità e gratuità. Ringrazio anche prof. Lorenzo Sorbo, per la curiosità sincera con cui affronta la ricerca scientifica.
A number of research activities along my PhD have been supported by founds of the INFN project "InDark". My PhD has been founded by a Cariparo Foundation grant.

Infine desidero ringraziare i numerosi amici, vecchi e nuovi, che mi hanno fatto compagnia in questi anni.
Innanzitutto ringrazio gli amici a cui ho voluto dedicare questo lavoro, Stefano, Davide A., Davide M., e Paolo, che più estesamente o a tratti, mi hanno accompagnato in modo decisivo in questi anni. Vi ringrazio per come mi volete bene gratuitamente, per come guardate al mio cuore e al suo desiderio di pienezza, e per come vivete.
Ringrazio gli amici incontrati a Padova, che mi hanno accolto in una città che per me era nuova e che ora sento un po' come una casa, in particolare Elena, Elisa, Marco, Samir e tanti altri, per la compagnia vera e leale che mi hanno fatto in questi anni.

Grazie anche ai miei carissimi compagni di ufficio, e amici, Amedeo, Andrea, William e Niccolò. Vi ringrazio per avermi voluto bene, e per la compagnia sconclusionata, ma in fondo sincera, che mi avete fatto... e per la vostra simpatia, con cui avete allietato le giornate in ufficio. Ringrazio anche gli altri amici dottorandi (e non), la cui amicizia mi ha accompagnato e sostenuto, in particolare Andrea, Giampaolo, Purnendu, Marco, Raj e Roberto.
Ringrazio gli amici incontrati a Parigi, in particolare Francesco, per la serietà e profondità con cui vivi e per la tua bontà, Luca ed Emanuele, per come mi avete accolto, e l'Aumonerie des Grands Moulins, regalo completamente inaspettato che ha segnato profondamente la mia strada.
Ringrazio anche gli amici sparsi per il mondo, che nei più dei casi ho incrociato solo poche volte in questi anni, ma il cui volto e sguardo, ridona un cuore vivo e la grazia della letizia.
Infine, sono grata alla mia famiglia, per avermi sostenuto in questi anni, per avermi aiutato nelle piccole cose, e per come mi vuole bene. Ringrazio in particolare Caterina per la gratuità con cui mi vuole bene e per la semplicità del suo cuore.

Bibliography

[1] C. Caprini and L. Sorbo, JCAP 1410 (2014) 056, 1407.2809.

[2] Planck, P.A.R. Ade et al., (2015), 1502.02114.

[3] Virgo, LIGO Scientific, B.P. Abbott et al., Phys. Rev. Lett. 116 (2016) 061102, 1602.03837.

[4] A.A. Starobinsky, JETP Lett. 30 (1979) 682, [Pisma Zh. Eksp. Teor. Fiz.30,719(1979)].

[5] A. Kosowsky, M.S. Turner and R. Watkins, Phys. Rev. D45 (1992) 4514.

[6] S.Yu. Khlebnikov and I.I. Tkachev, Phys. Rev. Lett. 77 (1996) 219, hep-ph/9603378.

[7] https://www.elisascience.org/files/publications/.

[8] C. Caprini et al., JCAP 1604 (2016) 001, 1512.06239.

[9] N. Bartolo et al., JCAP 1612 (2016) 026, 1610.06481.

[10] N. Tamanini et al., JCAP 1604 (2016) 002, 1601.07112.

[11] A. Neronov and I. Vovk, Science 328 (2010) 73, 1006.3504.

[12] A.M. Taylor, I. Vovk and A. Neronov, Astron. Astrophys. 529 (2011) A144, 1101.0932.

[13] I. Vovk et al., Astrophys. J. 747 (2012) L14, 1112.2534.

[14] A. Brandenburg and K. Subramanian, Phys. Rept. 417 (2005) 1, astro-ph/0405052.

[15] S. Dodelson, Modern Cosmology (Academic Press, Amsterdam, 2003).

[16] A.H. Guth, Phys. Rev. D23 (1981) 347.

[17] Planck, P.A.R. Ade et al., (2015), 1502.01589.

[18] C. Guzzetti, M. et al., Riv. Nuovo Cim. 39 (2016) 399, 1605.01615.

[19] J.E. Lidsey et al., Rev. Mod. Phys. 69 (1997) 373, astro-ph/9508078.

[20] A.R. Liddle, P. Parsons and J.D. Barrow, Phys. Rev. D50 (1994) 7222, astro-ph/9408015.

[21] D.H. Lyth and A. Riotto, Phys. Rept. 314 (1999) 1, hep-ph/9807278.

[22] A.H. Guth and S.Y. Pi, Phys. Rev. Lett. 49 (1982) 1110.

[23] A.D. Linde, Phys. Lett. B116 (1982) 335.

[24] J. Martin, V. Vennin and P. Peter, Phys. Rev. D86 (2012) 103524, 1207.2086.

[25] L.P. Grishchuk and Yu.V. Sidorov, Phys. Rev. D42 (1990) 3413.

[26] P.M. Pearle, Phys. Rev. A39 (1989) 2277.

[27] A. Bassi et al., Rev. Mod. Phys. 85 (2013) 471, 1204.4325.

[28] M. Bruni et al., Class. Quant. Grav. 14 (1997) 2585, gr-qc/9609040.

[29] S. Matarrese, S. Mollerach and M. Bruni, Phys. Rev. D58 (1998) 043504, astro-ph/9707278.

[30] V. Acquaviva et al., Nucl. Phys. B667 (2003) 119, astro-ph/0209156.

[31] J.M. Bardeen, Phys. Rev. D22 (1980) 1882.

[32] H. Kodama and M. Sasaki, Prog. Theor. Phys. Suppl. 78 (1984) 1.

[33] V.F. Mukhanov, H.A. Feldman and R.H. Brandenberger, Phys. Rept. 215 (1992) 203.

[34] A. Taruya and Y. Nambu, Phys. Lett. B428 (1998) 37, gr-qc/9709035.

[35] K.A. Malik and D. Wands, Phys. Rept. 475 (2009) 1, 0809.4944.

[36] A. Albrecht et al., Phys. Rev. Lett. 48 (1982) 1437.

[37] A.D. Linde, Phys. Lett. B108 (1982) 389.

[38] L.F. Abbott, E. Farhi and M.B. Wise, Phys. Lett. B117 (1982) 29.

[39] A.D. Dolgov and A.D. Linde, Phys. Lett. B116 (1982) 329.

[40] L.P. Grishchuk, Annals N. Y. Acad. Sci. 302 (1977) 439.

[41] L.P. Grishchuk, Sov. Phys. JETP 40 (1975) 409, [Zh. Eksp. Teor. Fiz.67,825(1974)].

[42] C.W. Misner, K.S. Thorne and J.A. Wheeler, Gravitation (W. H. Freeman, San Francisco, 1973).

[43] T.S. Bunch and P.C.W. Davies, Proc. Roy. Soc. Lond. A360 (1978) 117.

[44] L.F. Abbott and M.B. Wise, Nucl. Phys. B244 (1984) 541.

[45] S. Mollerach, S. Matarrese and F. Lucchin, Phys. Rev. D50 (1994) 4835, astro-ph/9309054.

[46] Planck, P.A.R. Ade et al., (2015), 1502.01592.

[47] K. Tomita, Prog. Theor. Phys. 37 (1967) 831.

[48] M. Maggiore, Gravitational Waves. Vol. 1: Theory and ExperimentsOxford Master Series in Physics (Oxford University Press, 2007).

[49] E. Pajer and M. Peloso, Class. Quant. Grav. 30 (2013) 214002, 1305.3557.

[50] M.M. Anber and L. Sorbo, JCAP 0610 (2006) 018, astro-ph/0606534.

[51] N. Barnaby and M. Peloso, Phys. Rev. Lett. 106 (2011) 181301, 1011.1500.

[52] N. Barnaby, R. Namba and M. Peloso, JCAP 1104 (2011) 009, 1102.4333.

[53] N. Barnaby, E. Pajer and M. Peloso, Phys. Rev. D85 (2012) 023525, 1110.3327.

[54] M.M. Anber and L. Sorbo, Phys. Rev. D85 (2012) 123537, 1203.5849.

[55] M. Peloso, L. Sorbo and C. Unal, JCAP 1609 (2016) 001, 1606.00459.

[56] M.M. Anber and L. Sorbo, Phys. Rev. D81 (2010) 043534, 0908.4089.

[57] L. Sorbo, JCAP 1106 (2011) 003, 1101.1525.

[58] A. Lue, L.M. Wang and M. Kamionkowski, Phys. Rev. Lett. 83 (1999) 1506, astro-ph/9812088.

[59] J.L. Cook and L. Sorbo, JCAP 1311 (2013) 047, 1307.7077.

[60] M. Shiraishi, A. Ricciardone and S. Saga, JCAP 1311 (2013) 051, 1308.6769.

[61] N. Bartolo et al., JCAP 1501 (2015) 027, 1411.2521.

[62] N. Barnaby et al., Phys. Rev. D86 (2012) 103508, 1206.6117.

[63] S. Mukohyama et al., JCAP 1408 (2014) 036, 1405.0346.

[64] R. Namba et al., JCAP 1601 (2016) 041, 1509.07521.

[65] J.L. Cook and L. Sorbo, Phys. Rev. D85 (2012) 023534, 1109.0022, [Erratum: Phys. Rev.D86,069901(2012)].

[66] L. Pearce, M. Peloso and L. Sorbo, (2016), 1603.08021.

[67] T. Fujita, J. Yokoyama and S. Yokoyama, PTEP 2015 (2015) 043E01, 1411.3658.

[68] M. Biagetti, M. Fasiello and A. Riotto, Phys. Rev. D88 (2013) 103518, 1305.7241.

[69] M. Biagetti et al., JCAP 1504 (2015) 011, 1411.3029.

[70] J.M. Hyde, Phys. Rev. D92 (2015) 044026, 1502.07660.

[71] J.H. Traschen and R.H. Brandenberger, Phys. Rev. D42 (1990) 2491.

[72] L. Kofman, A.D. Linde and A.A. Starobinsky, Phys. Rev. Lett. 73 (1994) 3195, hep-th/9405187.

[73] L. Kofman, A.D. Linde and A.A. Starobinsky, Phys. Rev. D56 (1997) 3258, hep-ph/9704452.

[74] G.N. Felder and L. Kofman, Phys. Rev. D75 (2007) 043518, hep-ph/0606256.

[75] J.F. Dufaux et al., JCAP 0903 (2009) 001, 0812.2917.

[76] J.F. Dufaux et al., Phys. Rev. D76 (2007) 123517, 0707.0875.

[77] G.W. Horndeski, Int. J. Theor. Phys. 10 (1974) 363.

[78] C. Deffayet et al., JCAP 1010 (2010) 026, 1008.0048.

[79] T. Kobayashi, M. Yamaguchi and J. Yokoyama, Phys. Rev. Lett. 105 (2010) 231302, 1008.0603.

[80] C. Deffayet et al., Phys. Rev. D84 (2011) 064039, 1103.3260.

[81] T. Kobayashi, M. Yamaguchi and J. Yokoyama, Prog. Theor. Phys. 126 (2011) 511, 1105.5723.

[82] Y. Cai, Y.T. Wang and Y.S. Piao, Phys. Rev. D94 (2016) 043002, 1602.05431.

[83] J. Sakstein and B. Jain, Phys. Rev. Lett. 119 (2017) 251303, 1710.05893.

[84] P. Creminelli and F. Vernizzi, Phys. Rev. Lett. 119 (2017) 251302, 1710.05877.

[85] J.M. Ezquiaga and M. Zumalacárregui, Phys. Rev. Lett. 119 (2017) 251304, 1710.05901.

[86] N. Bartolo et al., JCAP 1603 (2016) 044, 1511.07414.

[87] S. Endlich et al., Phys. Rev. D90 (2014) 063506, 1307.8114.

[88] A. Ricciardone and G. Tasinato, Phys. Rev. D96 (2017) 023508, 1611.04516.

[89] C. Cheung et al., JHEP 03 (2008) 014, 0709.0293.

[90] D. Cannone, J.O. Gong and G. Tasinato, JCAP 1508 (2015) 003, 1505.05773.

[91] D. Cannone, G. Tasinato and D. Wands, JCAP 1501 (2015) 029, 1409.6568.

[92] J. Khoury et al., Phys. Rev. D64 (2001) 123522, hep-th/0103239.

[93] Y.F. Cai et al., JHEP 10 (2007) 071, 0704.1090.

[94] P. Peter and N. Pinto-Neto, Phys. Rev. D78 (2008) 063506, 0809.2022.

[95] P. Creminelli, A. Nicolis and E. Trincherini, JCAP 1011 (2010) 021, 1007.0027.

[96] D.H. Lyth, Phys. Lett. B147 (1984) 403, [Erratum: Phys. Lett.B150,465(1985)].

[97] BICEP2, Keck Array, P.A.R. Ade et al., Phys. Rev. Lett. 116 (2016) 031302, 1510.09217.

[98] D.H. Lyth, Phys. Rev. Lett. 78 (1997) 1861, hep-ph/9606387.

[99] L. Boubekeur and D. Lyth, JCAP 0507 (2005) 010, hep-ph/0502047.

[100] L. Boubekeur, Phys. Rev. D87 (2013) 061301, 1208.0210.

[101] G. Efstathiou and K.J. Mack, JCAP 0505 (2005) 008, astro-ph/0503360.

[102] J. Garcia-Bellido et al., JCAP 1409 (2014) 006, 1405.7399.

[103] J. Garcia-Bellido et al., Phys. Rev. D90 (2014) 123539, 1408.6839.

[104] R. Easther, W.H. Kinney and B.A. Powell, JCAP 0608 (2006) 004, astro-ph/0601276.

[105] Y. Watanabe and E. Komatsu, Phys. Rev. D73 (2006) 123515, astro-ph/0604176.

[106] W. Zhao and Y. Zhang, Phys. Rev. D74 (2006) 043503, astro-ph/0604458.

[107] K. Nakayama et al., JCAP 0806 (2008) 020, 0804.1827.

[108] M.S. Turner, M.J. White and J.E. Lidsey, Phys. Rev. D48 (1993) 4613, astro-ph/9306029.

[109] L.A. Boyle and P.J. Steinhardt, Phys. Rev. D77 (2008) 063504, astro-ph/0512014.

[110] S. Mollerach, D. Harari and S. Matarrese, Phys. Rev. D69 (2004) 063002, astro-ph/0310711.

[111] K.N. Ananda, C. Clarkson and D. Wands, Phys. Rev. D75 (2007) 123518, gr-qc/0612013.

[112] D. Baumann et al., Phys. Rev. D76 (2007) 084019, hep-th/0703290.

[113] H. Assadullahi and D. Wands, Phys. Rev. D81 (2010) 023527, 0907.4073.

[114] G. Mangano et al., Phys. Lett. B534 (2002) 8, astro-ph/0111408.

[115] T.L. Smith, E. Pierpaoli and M. Kamionkowski, Phys. Rev. Lett. 97 (2006) 021301, astro-ph/0603144.

[116] S. Weinberg, Cosmology (Oxford, UK: Oxford Univ. Pr., 2008).

[117] Z. Hou et al., Phys. Rev. D87 (2013) 083008, 1104.2333.

[118] L. Pagano, L. Salvati and A. Melchiorri, Phys. Lett. B760 (2016) 823, 1508.02393.

[119] M. Kamionkowski and A. Kosowsky, Ann. Rev. Nucl. Part. Sci. 49 (1999) 77, astro-ph/9904108.

[120] W. Hu and S. Dodelson, Ann. Rev. Astron. Astrophys. 40 (2002) 171, astro-ph/0110414.

[121] A.R. Liddle and D.H. Lyth, Cosmological inflation and large scale structure (Cambridge, UK: Univ. Pr., 2000).

[122] W. Hu and M.J. White, New Astron. 2 (1997) 323, astro-ph/9706147.

[123] M.J. Rees, ApJ 153 (1968) 1.

[124] A. Kosowsky, Annals Phys. 246 (1996) 49, astro-ph/9501045.

[125] S. Bashinsky and U. Seljak, Phys. Rev. D69 (2004) 083002, astro-ph/0310198.

[126] A. Ota et al., JCAP 1410 (2014) 029, 1406.0451.

[127] J. Chluba et al., Mon. Not. Roy. Astron. Soc. 446 (2015) 2871, 1407.3653.

[128] K.W. Masui and U.L. Pen, Phys. Rev. Lett. 105 (2010) 161302, 1006.4181.

[129] F. Schmidt and D. Jeong, Phys. Rev. D86 (2012) 083513, 1205.1514.

[130] L. Dai, D. Jeong and M. Kamionkowski, Phys. Rev. D88 (2013) 043507, 1306.3985.

[131] F. Schmidt, E. Pajer and M. Zaldarriaga, Phys. Rev. D89 (2014) 083507, 1312.5616.

[132] S. Dodelson, E. Rozo and A. Stebbins, Phys. Rev. Lett. 91 (2003) 021301, astro-ph/0301177.

[133] S. Dodelson, Phys. Rev. D82 (2010) 023522, 1001.5012.

[134] D. Jeong and F. Schmidt, Phys. Rev. D86 (2012) 083512, 1205.1512.

[135] C.J. Moore, R.H. Cole and C.P.L. Berry, Class. Quant. Grav. 32 (2015) 015014, 1408.0740.

[136] E. Dimastrogiovanni et al., JCAP 1412 (2014) 050, 1407.8204.

[137] E. Dimastrogiovanni, M. Fasiello and M. Kamionkowski, (2015), 1504.05993.

[138] J. Garcia-Bellido, A.D. Linde and D. Wands, Phys. Rev. D54 (1996) 6040, astro-ph/9605094.

[139] S. Clesse and J. García-Bellido, Phys. Rev. D92 (2015) 023524, 1501.07565.

[140] S. Clesse and J. García-Bellido, (2016), 1610.08479.

[141] T. Nakama and T. Suyama, Phys. Rev. D92 (2015) 121304, 1506.05228.

[142] T. Nakama and T. Suyama, Phys. Rev. D94 (2016) 043507, 1605.04482.

[143] J. García-Bellido, J. Phys. Conf. Ser. 840 (2017) 012032, 1702.08275.

[144] S. Bird et al., Phys. Rev. Lett. 116 (2016) 201301, 1603.00464.

[145] B.C. Joshi, Int. J. Mod. Phys. D22 (2013) 1341008, 1301.5730.

[146] R.M. Shannon et al., Science 349 (2015) 1522, 1509.07320.

[147] C.R. Contaldi, Phys. Lett. B771 (2017) 9, 1609.08168.

[148] D. Bertacca et al., (2017), 1702.01750.

[149] LIGO Scientific, B.P. Abbott et al., Rept. Prog. Phys. 72 (2009) 076901, 0711.3041.

[150] R. Ballantini et al., Class. Quant. Grav. 20 (2003) 3505.

[151] C. Sabin et al., New J. Phys. 16 (2014) 085003, 1402.7009.
[152] L. Ju, D.G. Blair and C. Zhao, Rept. Prog. Phys. 63 (2000) 1317.
[153] S. Singh et al., New J. Phys. 19 (2017) 073023, 1606.04980.
[154] S. Dimopoulos et al., Phys. Lett. B678 (2009) 37, 0712.1250.
[155] M.R. Adams and N.J. Cornish, Phys. Rev. D82 (2010) 022002, 1002.1291.
[156] M.R. Adams and N.J. Cornish, Phys. Rev. D89 (2014) 022001, 1307.4116.
[157] P.D. Meerburg et al., Phys. Rev. D91 (2015) 103505, 1502.00302.
[158] P.D. Lasky et al., Phys. Rev. X6 (2016) 011035, 1511.05994.
[159] M. C. Guzzetti, Nuovo Cim. C40 (2017) 94.
[160] LIGO Scientific, J. Aasi et al., Class. Quant. Grav. 32 (2015) 074001, 1411.4547.
[161] Virgo, LIGO Scientific, B.P. Abbott et al., Phys. Rev. Lett. 118 (2017) 121101, 1612.02029, [Erratum: Phys. Rev. Lett.119,no.2,029901(2017)].
[162] BICEP2, Planck, P. Ade et al., Phys. Rev. Lett. 114 (2015) 101301, 1502.00612.
[163] G. Cabass et al., Phys. Rev. D93 (2016) 063508, 1511.05146.
[164] Q.G. Huang and S. Wang, JCAP 1506 (2015) 021, 1502.02541.
[165] Y.T. Wang et al., JCAP 1701 (2017) 010, 1612.05088.
[166] VIRGO, LIGO Scientific, J. Aasi et al., Phys. Rev. Lett. 113 (2014) 231101, 1406.4556.
[167] R.N. Manchester et al., Publ. Astron. Soc. Austral. 30 (2013) 17, 1210.6130.
[168] Virgo, LIGO Scientific, B.P. Abbott et al., Phys. Rev. Lett. 116 (2016) 131102, 1602.03847.
[169] L. Lentati et al., Mon. Not. Roy. Astron. Soc. 453 (2015) 2576, 1504.03692.
[170] NANOGrav, Z. Arzoumanian et al., Astrophys. J. 821 (2016) 13, 1508.03024.
[171] J. Crowder and N.J. Cornish, Phys. Rev. D72 (2005) 083005, gr-qc/0506015.
[172] E. Thrane and J.D. Romano, Phys. Rev. D88 (2013) 124032, 1310.5300.
[173] A. Petiteau, to appear.
[174] B. Sathyaprakash et al., Class. Quant. Grav. 29 (2012) 124013, 1206.0331, [Erratum: Class. Quant. Grav.30,079501(2013)].
[175] E. Calabrese et al., JCAP 1408 (2014) 010, 1406.4794.
[176] POLARBEAR, P.A.R. Ade et al., Astrophys. J. 794 (2014) 171, 1403.2369.
[177] J.R. Eimer et al., Proc. SPIE Int. Soc. Opt. Eng. 8452 (2012) 845220, 1211.0041.
[178] PIPER, N.N. Gandilo et al., 2016, 1607.06172.
[179] B.P. Crill et al., Proc. SPIE Int. Soc. Opt. Eng. 7010 (2008) 2P, 0807.1548.
[180] CMB-S4, K.N. Abazajian et al., (2016), 1610.02743.
[181] http://www.cosmosnet.it/.
[182] CORE, E. Di Valentino et al., (2016), 1612.00021.
[183] PRISM, P. Andrè et al., JCAP 1402 (2014) 006, 1310.1554.
[184] T. Matsumura et al., (2013), 1311.2847, [astro-ph.IM] [J. Low. Temp. Phys.176,733(2014)].

[185] M.A. McLaughlin, Class. Quant. Grav. 30 (2013) 224008, 1310.0758.
[186] G. Janssen et al., PoS AASKA14 (2015) 037, 1501.00127.
[187] J.D. Romano and N.J. Cornish, Living Rev. Rel. 20 (2017) 2, 1608.06889.
[188] W. Zhao et al., Phys. Rev. D87 (2013) 124012, 1303.6718.
[189] C.S. Unnikrishnan, Int. J. Mod. Phys. D22 (2013) 1341010, 1510.06059.
[190] KAGRA, Y. Aso et al., Phys. Rev. D88 (2013) 043007, 1306.6747.
[191] S. Kawamura et al., Class. Quant. Grav. 28 (2011) 094011.
[192] R.H. Brandenberger et al., Phys. Rev. Lett. 98 (2007) 231302, hep-th/0604126.
[193] Y.F. Cai, D.A. Easson and R. Brandenberger, JCAP 1208 (2012) 020, 1206.2382.
[194] Y.F. Cai et al., JCAP 1310 (2013) 024, 1305.5259.
[195] D. Wands et al., Phys. Rev. D66 (2002) 043520, astro-ph/0205253.
[196] C. Armendariz-Picon, T. Damour and V.F. Mukhanov, Phys. Lett. B458 (1999) 209, hep-th/9904075.
[197] X. Chen et al., JCAP 0701 (2007) 002, hep-th/0605045.
[198] S. Matarrese and A. Riotto, JCAP 0308 (2003) 007, astro-ph/0306416.
[199] S. Das et al., Phys. Rev. D90 (2014) 043503, 1404.5740.
[200] Y. Wang and W. Xue, JCAP 1410 (2014) 075, 1403.5817.
[201] A. Ashoorioon et al., Phys. Lett. B737 (2014) 98, 1403.6099.
[202] Y.F. Cai and Y. Wang, Phys. Lett. B735 (2014) 108, 1404.6672.
[203] K. Kamada et al., Phys. Rev. D83 (2011) 083515, 1012.4238.
[204] S. Unnikrishnan and S. Shankaranarayanan, JCAP 1407 (2014) 003, 1311.0177.
[205] LISA Pathfinder, K. Danzmann et al., (2007).
[206] M. Armano et al., Phys. Rev. Lett. 116 (2016) 231101.
[207] A. Klein et al., Phys. Rev. D93 (2016) 024003, 1511.05581.
[208] A. Sesana, Phys. Rev. Lett. 116 (2016) 231102, 1602.06951.
[209] W. Del Pozzo, A. Sesana and A. Klein, (2017), 1703.01300.
[210] S. Babak et al., Phys. Rev. D95 (2017) 103012, 1703.09722.
[211] B. Allen, Relativistic gravitation and gravitational radiation. Proceedings, School of Physics, Les Houches, France, September 26-October 6, 1995, 1996, gr-qc/9604033.
[212] B. Allen and J.D. Romano, Phys. Rev. D59 (1999) 102001, gr-qc/9710117.
[213] Planck, P.A.R. Ade et al., Astron. Astrophys. 571 (2014) A16, 1303.5076.
[214] J. Garcia-Bellido, M. Peloso and C. Unal, JCAP 1612 (2016) 031, 1610.03763.
[215] R. Durrer and A. Neronov, Astron. Astrophys. Rev. 21 (2013) 62, 1303.7121.
[216] R. Banerjee and K. Jedamzik, Phys. Rev. D70 (2004) 123003, astro-ph/0410032.
[217] D.T. Son, Phys. Rev. D59 (1999) 063008, hep-ph/9803412.
[218] G.B. Field and S.M. Carroll, Phys. Rev. D62 (2000) 103008, astro-ph/9811206.
[219] T. Vachaspati, Phys. Rev. Lett. 87 (2001) 251302, astro-ph/0101261.

[220] G. Sigl, Phys. Rev. D66 (2002) 123002, astro-ph/0202424.

[221] M. Christensson, M. Hindmarsh and A. Brandenburg, Phys. Rev. E64 (2001) 056405, astro-ph/0011321.

[222] L. Campanelli, Phys. Rev. Lett. 98 (2007) 251302, 0705.2308.

[223] L. Campanelli, Eur. Phys. J. C74 (2014) 2690, 1304.4044.

[224] Planck, P.A.R. Ade et al., (2015), 1502.01594.

[225] C. Caprini, R. Durrer and T. Kahniashvili, Phys. Rev. D69 (2004) 063006, astro-ph/0304556.

[226] A. Neronov and D.V. Semikoz, Phys. Rev. D80 (2009) 123012, 0910.1920.

[227] C. Caprini and S. Gabici, Phys. Rev. D91 (2015) 123514, 1504.00383.

[228] M.S. Turner and L.M. Widrow, Phys. Rev. D37 (1988) 2743.

[229] V. Demozzi, V. Mukhanov and H. Rubinstein, JCAP 0908 (2009) 025, 0907.1030.

[230] J. Martin and J. Yokoyama, JCAP 0801 (2008) 025, 0711.4307.

[231] B. Ratra, Astrophys. J. 391 (1992) L1.

[232] W.D. Garretson, G.B. Field and S.M. Carroll, Phys. Rev. D46 (1992) 5346, hep-ph/9209238.

[233] C. Bonvin, C. Caprini and R. Durrer, Phys. Rev. D86 (2012) 023519, 1112.3901.

[234] N. Barnaby, R. Namba and M. Peloso, Phys. Rev. D85 (2012) 123523, 1202.1469.

[235] R.Z. Ferreira and M.S. Sloth, JHEP 12 (2014) 139, 1409.5799.

[236] C. Caprini, M.C. Guzzetti and L. Sorbo, (2017), 1707.09750.

[237] N. Bartolo et al., Phys. Rev. D87 (2013) 023504, 1210.3257.

[238] S. Kanno, J. Soda and M.a. Watanabe, JCAP 0912 (2009) 009, 0908.3509.

[239] R. Durrer, L. Hollenstein and R.K. Jain, JCAP 1103 (2011) 037, 1005.5322.

[240] J. Donnert et al., Mon. Not. Roy. Astron. Soc. 392 (2009) 1008, 0808.0919.

[241] R.M. Kulsrud and E.G. Zweibel, Rept. Prog. Phys. 71 (2008) 0046091, 0707.2783.

[242] Planck, R. Adam et al., Astron. Astrophys. 594 (2016) A1, 1502.01582.